WATER POLLUTION CONTROL RESEARCH SERIES • 16130FDQ03/71

HEATED SURFACE JET DISCHARGED INTO A FLOWING AMBIENT STREAM

U.S. ENVIRONMENTAL PROTECTION AGENCY

WATER POLLUTION CONTROL RESEARCH SERIES

The Water Pollution Control Research Series describes the results and progress in the control and abatement of pollution in our Nation's waters. They provide a central source of information on the research, development and demonstration activities in the Environmental Protection Agency, through inhouse research and grants and contracts with Federal, State, and local agencies, research institutions, and industrial organizations.

Inquiries pertaining to Water Pollution Control Research Reports should be directed to the Chief, Publications Branch (Water), Research Information Division, R&M, Environmental Protection Agency, Washington, D.C. 20460.

HEATED SURFACE JET DISCHARGED INTO A FLOWING AMBIENT STREAM

by

Louis H. Motz
Barry A. Benedict

National Center for Research and Training in
the Hydrologic and Hydraulic Aspects of
Water Pollution Control

Vanderbilt University
Nashville, Tennessee

for the

Environmental Protection Agency

Grant # 16130 FDQ

March, 1971

EPA Review Notice

This report has been reviewed by the Environmental Protection Agency and approved for publication. Approval does not signify that the contents necessarily reflect the views and policies of the Environmental Protection Agency nor does mention of trade names or commercial products constitute endorsement or recommendation for use.

For sale by the Superintendent of Documents, U.S. Government Printing Office, Washington, D.C. 20402 - Price $1.75

ABSTRACT

The temperature distribution in the water body due to a discharge of waste heat from a thermal-electrical plant is a function of the hydrodynamic variables of the discharge and the receiving water body. The temperature distribution can be described in terms of a surface jet discharging at some initial angle to the ambient flow and being deflected downstream by the momentum of the ambient velocity. It is assumed that in the vicinity of the surface jet, heat loss to the atmosphere is negligible. It is concluded that the application of the two dimensional surface jet model is dependent on the velocity ratio and the initial angle of discharge, and the value of the initial Richardson number, as low as 0.22. Both laboratory and field data are used for verification of the model which has been developed. Laboratory data is used to evaluate the two needed coefficients, a drag coefficient and an entrainment coefficient, as well as the length of the zone of flow establishment and the angle at the end of that zone. The drag coefficient and characteristics of the establishment zone are found to be functions of the velocity ratio (ambient velocity/jet velocity), while the entrainment coefficient is primarily a function of geometry.

This report was submitted as a portion of the work under Grant No. 16130 FDQ between the Federal Water Quality Administration, now in the Environmental Protection Agency, and Vanderbilt University.

KEY WORDS

Cooling Water, Thermal Pollution, Jets, Turbulent Flow, Heated Water, Thermal Power Plants, Thermal Stratification, Diffusion, Water Temperature, Heat Exchange, Temperature

ACKNOWLEDGMENTS

Special thanks are extended to Mr. E. M. Polk, Jr., who directed the Vanderbilt University field surveys and made available much of the field data used in this report.

Major thanks are also due to Dr. F. L. Parker for general technical report guidance, to Mmes. Beverly Laird and Peggie Bush for typing the report, and to the laboratory staff personnel for their outstanding cooperation.

The investigations described herein were supported by the Federal Water Quality Administration, of the Environmental Protection Agency, through its establishment of the National Center for Research and Training in the Hydrologic and Hydraulic Aspects of Water Pollution Control, contract number 16130 FDQ. This support took the form of a research assistantship, equipment, and computer time. During a portion of the work, the senior author held a traineeship grant from the National Aeronautics and Space Administration. Grateful acknowledgment is made for the financial support from these groups.

Appreciation is also extended to the Tennessee Valley Authority for their cooperation in conducting field surveys, supervised by Mr. Polk.

TABLE OF CONTENTS

TABLE OF CONTENTS (Continued)

LIST OF TABLES

LIST OF ILLUSTRATIONS

LIST OF ILLUSTRATIONS (Continued)

LIST OF ILLUSTRATIONS (Continued)

LIST OF ILLUSTRATIONS (Continued)

CHAPTER I

INTRODUCTION

The determination of the temperature distribution of power plant condenser cooling water discharges is of immediate interest. Almost one half of all the water used in the United States is utilized for cooling and condensing by the power and manufacturing industries. In 1964, the cooling water intake was 50 x 10^{12} gallons, of which 80% was used by the electric power generating industry, according to the Federal Water Pollution Control Administration (FWPCA) (23). Presently, power is generated by hydro- and steam-electric plants, with the latter requiring the cooling water for dissipation of waste heat. Since the remaining sites which are suitable for hydro-electric plants are limited, steam-electric plants will have to be increasingly relied on for future needs. Of these, fossil-fueled plants operate at about 40% thermal efficiency, and nuclear plants operate at about 33% efficiency. These low efficiencies result in a large part of the heat produced by a steam-electric plant being wasted to the atmosphere or into water bodies. Based on the projected need for electric power, heat rejection from fossil- and nuclear-fueled plants is expected to increase almost ninefold by the year 2000. Thus, based on the present and future requirements for cooling water, the effects of heated discharges should be examined.

Effects of Heated Discharges

The addition of heated discharges to a water body can have chemical, biological, and physical effects. The chemical and biological effects of increased temperature on water quality, aquatic life, and waste assimilative capacity have been noted by several authors. According to the FWPCA (23), which has defined the addition of waste heat as thermal pollution, the dissolved oxygen may be reduced, chemical reactions increased, tastes and odors made more noticeable, and the rate of oxygen depletion by organic wastes increased. According to Clark (15), fish are particularly sensitive to changes in the thermal environment because, as cold-blooded animals, they are unable to regulate their body temperature and can be harmed by an increase or decrease in their metabolic rate. Cairns (11) has stated that large quantities of heat added to a stream will cause all but the very tolerant forms of fish and other aquatic life to disappear and may seriously impair the stream. Krenkel, Thackston, and Parker (32) have cited evidence that an increase in stream temperature due to an electric generating plant's heated discharge has the same end result in terms of reduced waste assimilative capacity as adding an equivalent amount of sewage or other organic waste to the river. Since chemical and biological effects are a function of the temperature distribution, the physical effects of heated discharges should be examined

Temperature Distribution

The physical effect, or the temperature distribution, is a function of hydrodynamic and meteorological variables. The temperature distribution problem can be divided into two parts which are analyzed almost

separately. According to Edinger (17), the first part is the initial mixing, or dilution, of the discharge, and the second is atmospheric cooling. Edinger has stated that these two parts have different length and time scales: mixing takes place in the immediate vicinity of the discharge and affects a small portion of a water body, while atmospheric cooling is relied on after mixing takes place and affects a larger portion of a water body farther downstream.

Atmospheric Cooling

Heat transfer across the air-water interface requires a large surface area and/or long time periods. Calculations, using standard heat transfer rates and based on the work of Edinger and Geyer (19), indicate that, for many water bodies, the downstream distance required for cooling is on the order of miles. The distance is particularly large for a relatively narrow stream whose width does not exceed 1000 feet or so, and, thus, whose surface area is small. Edinger and Polk (20) have described the initial mixing of heated discharges and have presented data which tend to validate the assumption that atmospheric cooling can be neglected in the vicinity of the discharge, at least as a first approximation.

Mixing

The temperature distribution in the immediate vicinity of the discharge can take several forms. Brooks (9) has noted two extremes: surface spreading of hot water with minimal mixing, and extensive jet mixing of the effluent with the receiving water. Churchill (14) has mentioned that at several large Tennessee Valley Authority (TVA) steam plants, the

stream velocity is not sufficiently high to mix the heated discharge, and the discharge flows out across the receiving water as a density overflow. Harleman and Elder (27) have noted that thermal stratification can develop where part of the heated water intrudes upstream as a heated layer and may be recirculated through the power plant unless a skimmer wall is built at the intake channel. Bata (5) and Harleman (26) have analytically described the formation of the upstream stratified layer. Harleman (26) has also described the design of horizontal diffusers placed across the bottom of the stream which completely mix the heated discharge by entraining river water. Edinger and Polk (20) have studied the lateral and vertical mixing in a uniform current from the point of surface discharge to a completely mixed condition downstream. In most literature dealing with mixing of surface discharges, it is assumed that the mixing, if it occurs, is due to the velocity and associated turbulence of the receiving water body. Also, most temperature distribution models based on the basic conservation of heat equation consider only a uniform velocity field in the receiving water body.

Surface Jets

In some cases, the spatial distribution of temperature is a function of the velocity of the discharge as well as the velocity of the ambient stream. The velocity field of the ambient stream is no longer uniform but is influenced by the velocity field of the cooling water in the immediate vicinity of the discharge. In these cases, cooling water discharged at the surface can have the characteristics of a surface jet if the discharge flow possesses sufficient momentum. Some work on the

problem of surface jets has already been done by Jen, Wiegel, and Mobarek (29), Zeller (48), Carter (12), and others. However, this problem needs more study in order to better analyze and predict the spatial distribution of temperature in the vicinity of thermal-electric generating plants.

Description of the Problem

When waste heat from a thermal-electric power plant is discharged into a receiving water body, the temperature distribution in the water body is a function of the hydrodynamic variables of the discharge and the receiving water body. When the velocity field of the water body is influenced by the velocity of the heated discharge, and the heat is initially advected almost perpendicularly to the river flow, then the temperature distribution can be described in terms of a surface jet discharging at some initial angle to the ambient flow and being deflected downstream by the momentum of the ambient velocity. The decrease in temperature rise along the jet axis is due to the entrainment of colder ambient water into the jet as the jet spreads laterally and, to some extent, vertically.

Complete solution of the temperature distribution problem will not be attempted in this study. The present investigation will consider only the problem of surface jets. At some distance downstream from the discharge, the jet velocity will have been decreased until it is equal to the ambient velocity. The decrease in the remaining temperature excess from this point could be determined from the temperature distribution models which consider only the ambient, or river, velocity and ambient

turbulence. However, the complexity of the two phenomena, neither of which is at present completely understood, precludes immediate combination of the two in a model. At some farther distance downstream, after mixing takes place, surface exchange of heat becomes important, but it is assumed that, in the vicinity of the surface jet, heat loss to the atmosphere is negligible.

CHAPTER II

PREVIOUS WORK

A literature review by Krenkel and Parker (31) describing the many aspects of the mechanisms and modeling of heated discharges is readily available and will not be duplicated here. Instead, the previous work done on submerged and surface jets will be examined in detail to provide a basis for the development of an analytical model describing surface jet discharges.

Submerged Jets

Schlichting (41) has presented solutions for submerged plane and axi-symmetric jets. These solutions require assumptions based on the mixing length theories of Prandtl, von Kármán, and Taylor.

Abramovich (2) has discussed solutions for simple jets and for jets in a parallel ambient stream. For jets deflected by a cross-flow, references are made to empirical relations, to superimposing the stream functions of the jet and the external flow, and to a method which balances the force caused by the pressure difference at the forward and back surface of the jet by a centrifugal force.

Albertson, Dai, Jensen, and Rouse (4) have presented a model which describes the behavior of a simple air-in-air jet. Analytic expressions for the distributions of velocity, volume flux, and energy flux were developed for the patterns of mean flow within submerged jets from both

slots and orifices. A single experimentally-determined coefficient was evaluated.

Entrainment

Taylor (44) made a simple transfer assumption of entrainment which relates the inflow into the edge of a plume to a characteristic velocity in the plume. This assumption retains the broad outline of the mechanics of a rising, buoyant plume without the necessity for understanding in detail how the turbulent eddies mix the heated and the ambient air. This concept of entrainment has made possible the solution to many problems describing buoyant and momentum jets which are difficult, if not impossible, at present, to solve by other means.

Entrainment of a Buoyant Plume

Morton, Taylor, and Turner (34) used the concept of entrainment to develop relations predicting the behavior of a buoyant plume rising through a fluid with a linear density gradient. Three main assumptions were made in deriving the prediction equations:

(1) The profiles of vertical velocity and buoyancy are similar at all heights and are Gaussian, or, as shown in Equations 1 and 2,

$$u(x,r) = u(x)\ \exp(-r^2/b^2) \tag{1}$$

and

$$\frac{g[\rho_o - \rho(x,r)]}{\rho_1} = \frac{g[\rho_o - \rho(x)]}{\rho_1}\ \exp\ (-r^2/b^2) \tag{2}$$

where [1] $u(x,r)$ = the vertical velocity;

$u(x)$ = the centerline velocity;

[1]Notation used in this chapter is unique to this chapter.

x,r = the cylindrical coordinates with the x axis vertical;

b = the width of the plume;

ρ_o = the ambient density;

$\rho(x,r)$ = the plume density;

$\rho(x)$ = the centerline plume density; and

ρ_1 = a reference density.

(2) The rate of entrainment of fluid at any height is proportional to a characteristic velocity at that height, or, as shown in Equation 3,

$$\frac{dQ}{dx} = 2\pi b\alpha u \tag{3}$$

where Q = the plume flowrate; and α = the experimentally-determined entrainment coefficient.

(3) The fluids are incompressible, and local variations in density are small compared to a reference density.

Based on the conservation of volume, momentum, and heat energy, a system of ordinary differential equations was developed. The conservation equations were written as shown in Equations 4-6,

Volume:

$$\frac{d}{dx}\ (\pi b^2 u) = 2\pi b\alpha u \tag{4}$$

Momentum:

$$\frac{d}{dx}\ (\pi b^2 u^2) = 2\pi b^2 g(\rho_0 - \rho) \tag{5}$$

Density Deficiency:

$$\frac{d}{dx}\ [\pi b^2 u(\rho_1 - \rho)] = 2\pi b\alpha u(\rho_1 - \rho_0) \tag{6}$$

Morton et al. (34) wrote the heat energy equation in terms of the density difference instead of the temperature rise for a more unified treatment of all types of convection problems. The temperature field is expressed

indirectly in terms of the equivalent density deficiency.

Jets, Plumes, and Wakes

Morton (33) showed that jets, plumes, and wakes could be related by means of a momentum-mass flux diagram. Using a simple model based on the concept of entrainment, the relation was found from the solution of a single, ordinary differential equation.

Morton's treatment was based on a common set of assumptions applied to jets, plumes, and wakes. Mean cross-sectional profiles of velocity were assumed similar along the axis. Longitudinal dispersion was assumed negligible compared to lateral dispersion, making possible the usual boundary layer assumptions for free turbulent shear flows. The flow was assumed to be affected by density differences only in the form of buoyancy forces. Entrainment, or turbulent mixing of the jet and the ambient fluid, was represented by an inflow velocity across the jet boundary, and this inflow was assumed to be proportional to the difference between a characteristic velocity along the axis and the velocity of the ambient fluid.

Equations representing the conservation of mass, momentum, and density deficiency, similar to those used by Morton et al. (34), were written. The non-dimensional variables, volume flux and momentum flux, and the density deficiency were defined, and then solutions representing a simple jet, a jet in a uniform current, a buoyant jet, a simple plume in a stratified environment, a buoyant jet projected along a uniform stream, a simple wake, a forced wake, and a buoyant forced wake were presented in which the momentum flux, M, was a function of the volume flux, V. Morton (33) called this M vs. V curve a momentum-mass diagram.

Jet Trajectory

Bosanquet, Horn, and Thring (7) studied a negatively buoyant, submerged jet flowing into a lighter, non-flowing ambient fluid. The jet trajectory was predicted in terms of the initial angle of the discharge, the initial velocity, the density ratio, and the nozzle diameter. The predicted axis was shown to compare favorably with values obtained from the water-in-water model.

Cross Flows

Keffer and Baines (30) studied the flow of a vertical air-in-air jet directed normally to a uniform, steady ambient current for velocity ratios (jet/ambient velocity) of 2, 4, 6, 8, and 10. The integrated equations of continuity and motion along the deflected jet axis were made non-dimensional after the general method of Morton (33). Entrainment was defined in terms of an inflow velocity, v_i, which was assumed proportional to the difference between the centerline jet velocity, U, and the ambient velocity, U_a. The entrainment relation was written as shown in Equation 7,

$$v_i = E(U - U_a) \tag{7}$$

Keffer and Baines observed that the ambient flow was decelerated at the upstream surface of the jet, creating a positive pressure region, and that separation occurred at the rear, creating a negative pressure region.

They also studied the effects of the velocity ratio on the zone of flow establishment, which is defined as the region in which the velocity distribution changes from a uniform distribution at the jet nozzle to a

fully developed Gaussian distribution at the beginning of the zone of established jet flow. They observed that at low velocity ratios (2 and 4) the establishment zone was deflected downstream by the pressure field, and the beginning of the established flow region was at an angle less than 90° to the ambient current. At these low ratios, the jet was observed to cling to the wall, and entrainment may have been restricted by the proximity of a solid surface. For velocity ratios greater than 4, the beginning of the established flow region was observed to be approximately above the center of the jet orifice. For these larger ratios, the effect of the pressure field was mainly to change the cross-section from a circular shape at the orifice to a distorted kidney shape at the end of the zone of flow establishment. In all of the cases studied, a pair of vortices was observed along the jet axis. Keffer and Baines felt that the vortices were caused by the separation of the ambient flow.

Keffer and Baines observed that the velocity excess for the jet in an ambient current decreased much more rapidly than that reported by Albertson et al. (4) for a simple jet where the ambient velocity is zero, and that the rate of decrease increased with distance from the source. They felt that the entrainment was augmented by the twin vortices, which do not exist in the free jet where the ambient velocity is zero. Also, they observed that the lateral spreading did not appear to be affected by the vortices. They reported that the entrainment coefficient, E, which was determined by fitting the observed velocities measured with a hot-wire anemometer to the predicted values, varied along the jet axis from 0.3 to 1.6 and also varied as a function of the velocity ratio.

Buoyant Jet in a Cross Flow

Fan (22) used Morton's work (33) as a basis for studying an inclined, round buoyant jet in a stagnant environment with linear density-stratification and for studying a round buoyant jet in a uniform cross stream of homogeneous density. Extending the integral technique of analysis, for the case of a uniform cross stream, Fan included the effect of an initial angle of discharge at the end of the zone of flow establishment that was not 90° to the ambient flow, presented empirical relations describing the zone of flow establishment, assumed an entrainment mechanism based on the vector difference between a characteristic jet velocity and the ambient velocity, and approximated the effect of the pressure gradient across the jet parallel to ambient current by a drag coefficient. From laboratory experiments in which the jet Froude Number was varied from 10 to 80 and the velocity ratio (jet/current) varied from 4 to 16, the entrainment coefficient and the drag coefficient were found to vary from 0.4 to 0.5 and from 1.7 to 0.1, respectively. Fan determined the entrainment coefficient from the jet centerline dilution ratios and noted that the cross-sectional concentration profiles were horse-shoe shaped with the maximum concentration at two sides of the plane of symmetry. The maximum concentrations were from 1.60 to 1.80 times greater than the values at the jet axis, or centerline.

Surface Jets

Jets discharged at the surface of a heavier fluid have been studied by several authors. The jet fluid, usually water, was the same as the ambient fluid except that its density was less. This was accomplished

by heating the jet fluid or by increasing the density of the ambient water by adding salt.

Vertical Entrainment and the Richardson Number

Ellison and Turner (21) studied the entrainment process in stratified flows and found that vertical entrainment could be expressed as a function of the Richardson Number. In the case of a surface jet with the ambient velocity zero, the inflow velocity into the turbulent jet region was assumed to be proportional to the velocity of the surface jet. The constant of proportionality was called the entrainment coefficient, E.

Ellison and Turner performed a series of laboratory experiments using a salt solution to increase the density of the ambient fluid. With no density difference, the flow formed a simple, two-dimensional half-jet, the depth of which increased nearly linearly with distance. When the ambient fluid was heavier than the jet fluid, the rate of increase of depth became smaller and at some distance downstream, depending on the density difference and the rate of flow, the jet depth changed very little with distance. These experiments also demonstrated that, in most practical cases, the surface layer will attain an equilibrium state in which the Ri Number does not vary with distance downstream. The observed relation between E and the Ri Number is shown in Figure 1.

Small Richardson Numbers

Jen, Wiegel, and Mobarek (29) performed laboratory studies on the mixing of heated, buoyant jets discharging horizontally at the surface of a large body of initially quiescent receiving water. The

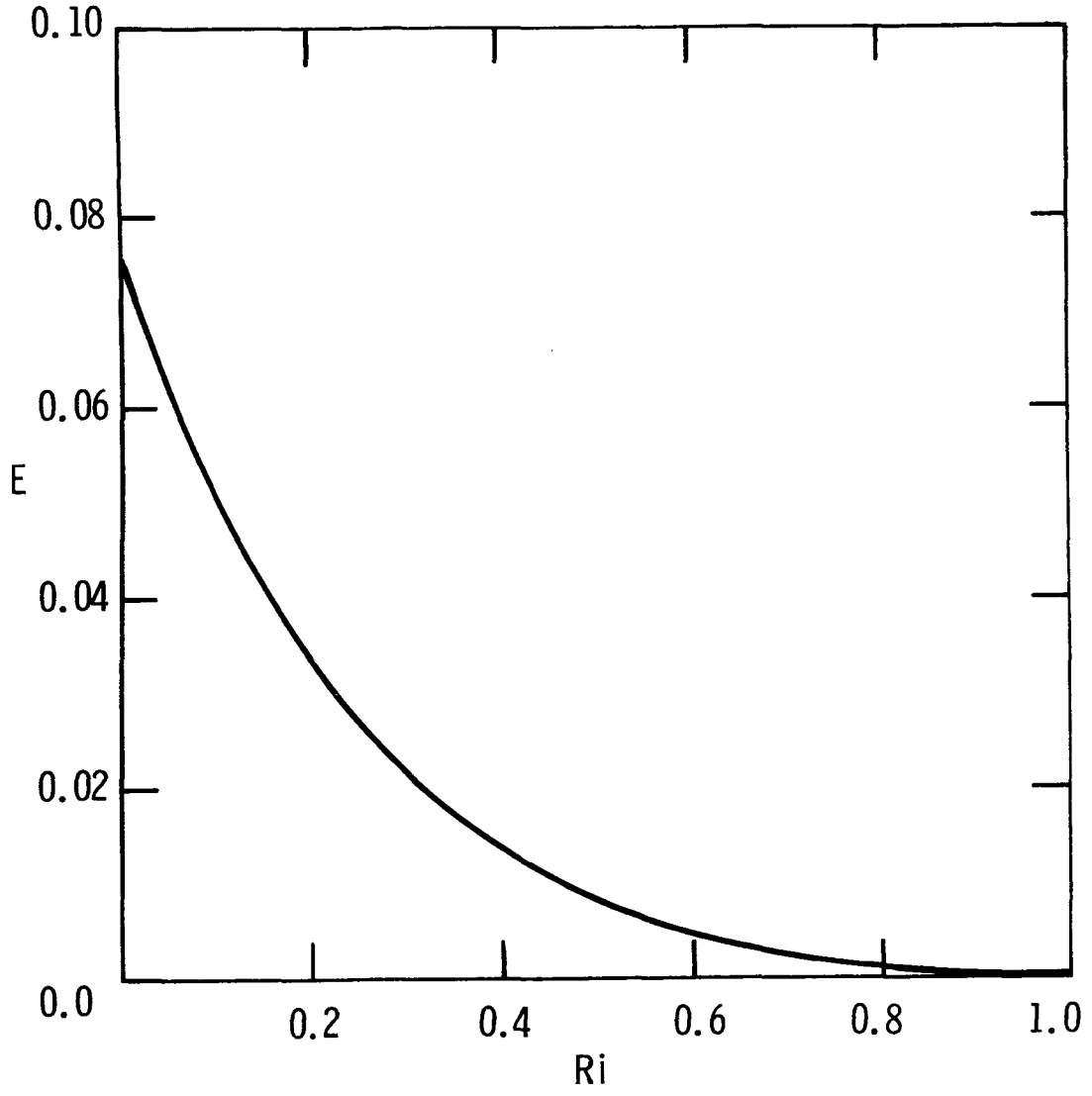

FIGURE 1.--VERTICAL ENTRAINMENT VERSUS RICHARDSON NUMBER
[After Ellison and Turner (21)]

initial Ri Number of the jets was defined as shown in Equation 8,

$$Ri_o = \frac{\Delta\rho g d'_o}{\rho U_o^2} \tag{8}$$

where $\Delta\rho$ = the density difference;

g = the acceleration of gravity;

ρ = the ambient density;

d'_o = the jet diameter; and

U_o = the initial jet velocity.

In these studies, the Ri_o Number was small, i.e., $5.0 \times 10^{-5} \leq Ri_o \leq 3.0 \times 10^{-3}$.

Jen et al. observed that the jet mixed less with depth than it did laterally by a factor of about two. They attributed this difference to the buoyancy force, which they felt inhibits the vertical component of the turbulent velocity fluctuations but does not inhibit the lateral component. An empirically-determined equation for the temperature along the jet axis was presented.

Larger Richardson Numbers

Tamai, Wiegel, and Tornberg (43) studied the same type of buoyant jets as Jen et al. (29) except that the Ri_o Number was larger, i.e., $1.0 \times 10^{-2} \leq Ri_o \leq 2.0 \times 10^{-1}$. A comparison of the data taken at these higher Richardson Numbers with the empirical equation of Jen et al., plotted in Figure 2, showed that the temperature rise along the jet centerline was generally greater than predicted for values of Ri_o approaching 2×10^{-1}.

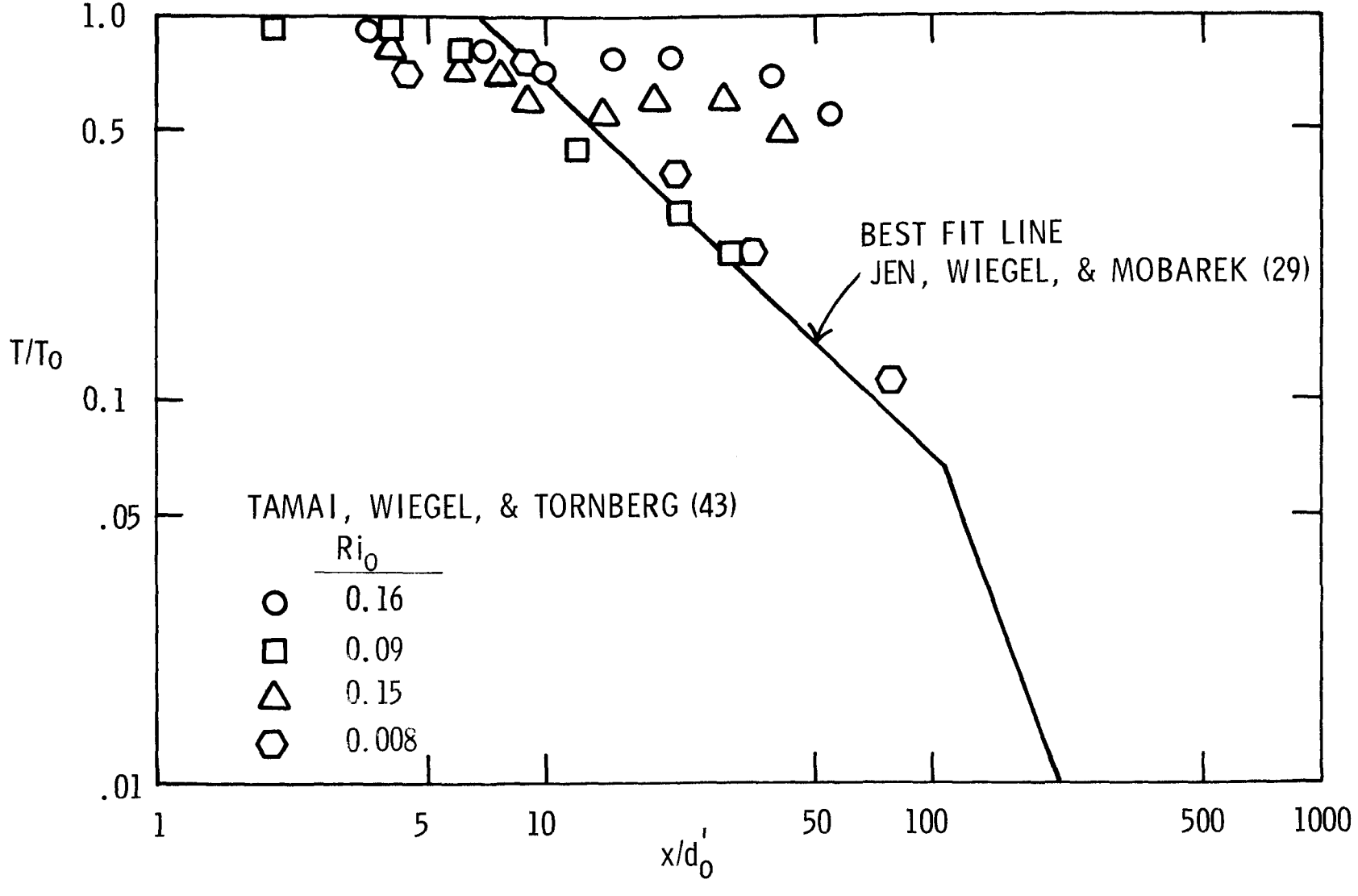

FIGURE 2.--TEMPERATURE RISE ALONG JET AXIS AT WATER SURFACE
[After Tamai, Wiegel, and Tornberg (43)]

Approximate Theory

Hayashi and Shuto (28) also studied the diffusion of warm water jets discharged horizontally at the surface of an initially quiescent water body. The initial temperature was from 0.2°C to 28°C higher than the receiving water, and the Ri_o Number of the jets varied from 0.004 to 0.54. An approximate theory was developed in which the non-linear inertial terms representing the square of the jet velocity in the equation of motion were neglected, and an approximate solution was presented for the case of no vertical entrainment. The experimental results were compared with the approximate theory, and the effect of the Richardson Number on vertical entrainment was in agreement with the work of Ellison and Turner (21). Figure 3 shows a comparison between the approximate theory and one set of experimental data of Hayashi and Shuto.

Similarity Criteria

Stefan (42), using the dimensionless equation of motion, continuity, and heat transfer, presented similarity criteria for the flow of heated water over a stagnant and colder body of water. He felt that turbulent flow in the model, matching of reduced gravitational forces and surface heat losses as well as sufficient size of the model were the most essential modeling requirements.

Integral Technique

Zeller (48) developed a two-dimensional mathematical model based on the work of Morton (33) and Fan (22) to describe the observed temperature distribution offshore from a steam-electric generating plant which discharged heated water through two outfalls 640 feet apart. According

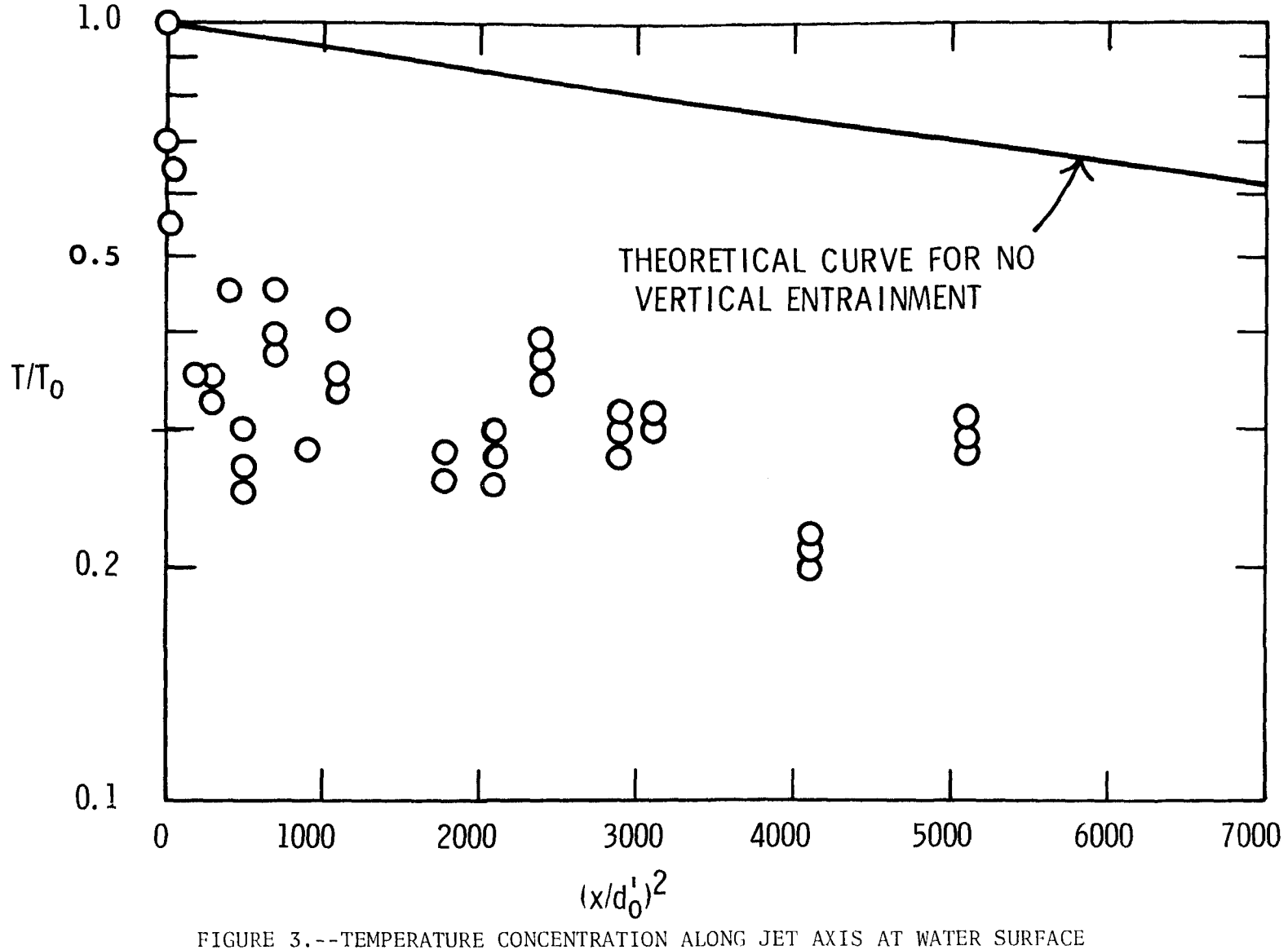

FIGURE 3.--TEMPERATURE CONCENTRATION ALONG JET AXIS AT WATER SURFACE
[After Hayashi and Shuto (28)]

to Zeller, field surveys indicated that, beyond a region close to shore, the warm water from each outfall spread as a two-dimensional surface jet about 3 feet thick and could be followed for several thousand feet out into the lake. Measurements of the temperature distribution were made by traversing the jets in a boat, and jet velocities were determined by tracking the paths of drogues.

Zeller developed a system of two-dimensional mass, momentum, and heat energy conservation equations. Based on the work of Ellison and Turner (21), vertical entrainment was assumed negligible because of the stability of the surface jet at high Richardson Numbers. Lateral entrainment was assumed to be represented by the expression shown in Equation 9,

$$\frac{dQ}{ds} = EzU \tag{9}$$

which equates the increase in flow rate along the jet axis to the product of the entrainment coefficient, E, the depth, z, and the jet velocity, U. Zeller reported that the value of the entrainment coefficient varied from 0.127 to 0.993 for 22 field surveys.

Slot Jet

Carter (12) developed a mathematical model to describe the behavior of a two-dimensional slot jet discharged perpendicularly into a flowing ambient stream. Equations representing the change in momentum along the jet axis were developed, and the decrease in temperature rise along the axis was described in terms of an empirically-measured dilution. The solution to the equations predicted the location of the jet trajectory in terms of empirically-determined coefficients and the dilution. The

zone of flow establishment and the pressure gradient that exists across the jet parallel to the ambient flow were both considered in the mathematical model.

Justification for Present Study

A survey of the literature indicates that further study on surface jets is justified. Previous work does not contain a completely suitable method for analyzing and predicting the spatial temperature distribution in the vicinity of power plants located on rivers when the discharge velocity is important.

Laboratory Studies

The results of laboratory studies by Jen, et al. (29), and Tamai, et al. (43) are applicable primarily to jets discharging into ambient water bodies that have no appreciable velocity. The effect of a cross flow on a submerged jet has been discussed by Keffer and Baines (30), and this effect must be considered in the present case of a surface jet.

Theory

None of the theoretical models examined is completely satisfactory. The model of Hayashi and Shuto (28) neglects the inertial terms in the equation of motion, which is permissible only for velocities much less than those normally encountered at a power plant discharge. Also, their model is applicable only to a quiescent water body.

Zeller's (48) definition of entrainment, shown in Equation 9,

$$\frac{dQ}{ds} = EzU \tag{9}$$

is different from that used by Morton (33), Fan (22), and Keffer and Baines (30), all of whom have defined the entrainment in terms of the difference between some characteristic jet velocity and the velocity of the moving ambient current. Also, Zeller's model does not consider the effect of the pressure gradient that exists across the surface jet parallel to the ambient current in predicting the trajectory of the jet, nor does it consider the zone of flow establishment.

The theoretical model developed by Carter (12) differs from others in several respects. The decrease in temperature along the jet axis is described in terms of an empirically-measured dilution, but the entrainment mechanism causing the dilution is not specifically considered. The equation of volume continuity is not used, and its integrated form, the volume flux equation, does not appear. Since the continuity equation is not used, in order to integrate the combined momentum equation which contains two dependent variables and one independent variable, an assumption has to be made concerning one of the dependent variables. In order to graphically integrate the momentum equation, it is assumed that the component of the jet velocity in the same direction as the ambient velocity is equal to the ambient velocity everywhere in the zone of established jet flow. The validity of this assumption, according to Carter, is "...it appears from the data that the pressure field, the length of the zone of flow establishment, and the velocity field may adjust themselves so that at (x_e, y_e) [the beginning of the zone of established jet flow] the x-component of the jet velocity is equal to the u_a [the ambient velocity]." In addition, the length of the zone of flow establishment is assumed constant with respect to the velocity

ratio, which differs from the results reported by Fan (22), Keffer and Baines (30), Pratte and Baines (36), and others. Finally, the increase in the width of the jet cannot be predicted by the solution presented by Carter.

Present Study

Therefore, using the work of Morton (33), Fan (22), and Zeller (48) as a base, a more refined model of surface jets has been developed which is able to describe certain cases of heated power plant discharges.

CHAPTER III

ANALYTIC DEVELOPMENT

The present study, which is based on the Morton technique of integral analysis, develops a system of ordinary differential equations, which, when solved numerically, predicts the jet trajectory, width, velocity, and temperature distribution for the case of a two-dimensional surface jet.

Assumptions

Certain assumptions are made in the development of the mathematical model:

(1) The jet is assumed to be two-dimensional.

(2) Profiles of velocity and temperature normal to the jet axis are similar along the length of the jet axis.

(3) The flow regime is completely turbulent, which means that molecular diffusion can be neglected, and that the flow is independent of the Reynolds Number.

(4) Changes in density are small compared to a reference density. Thus, inertial forces due to density gradients are negligible, and mass flux terms can be replaced by volume flux terms. This is commonly called the Boussinesq assumption.

(5) Turbulent mixing into the jet can be represented by entrainment, or an inflow velocity across the jet boundary.

(6) Separation of the ambient flow around the jet can be represented by a drag force.

(7) Temperature losses in the region of the jet are small compared to losses farther downstream and can be neglected.

Shape of the Surface Jet

Observation of warm water surface jets indicates that a surface jet may be either two- or three-dimensional. For a jet to be two-dimensional, only the width should increase, and the change in depth along the axis should be zero. For a jet to be three-dimensional, both the depth and the width should increase along the jet axis. Primarily, two forces determine the extent of vertical spreading. The inertial force, or the difference between the axial velocity of the jet and the ambient velocity, creates the shearing force which entrains ambient fluid, causing the jet boundary to spread laterally and vertically. The buoyancy force due to the density difference between the heated surface jet and the heavier ambient fluid opposes the vertical spreading of the jet. When the inertial forces dominate, the jet will spread equally in the vertical and lateral directions. However, when the buoyancy is large, vertical spreading is suppressed.

Richardson Number

Quantitatively, vertical spreading, or vertical entrainment, is an inverse function of the Richardson Number of the jet. When the ambient velocity is not zero, the Richardson Number can be defined as shown in Equation 10, or

$$Ri = \frac{\Delta\rho g d_o'}{\rho (U - U_a)^2} \tag{10}$$

where ρ = density of the jet;

$\Delta\rho$ = density difference between the jet and the ambient flow;

g = acceleration of gravity;

d_o' = the diameter of the jet;

U = axial velocity of the jet; and

U_a = ambient velocity.

When the inertial force is large, or the Richardson Number much less than 1.0, vertical entrainment takes place. However, when the buoyancy force is large, or the Richardson Number approximately 1.0 or greater, vertical entrainment is small.

Field Cases

In many field cases, the density difference due to a heated discharge is relatively large, and the square of the velocity difference is relatively small, particularly when the initial jet velocity is not much greater than the ambient velocity. Thus, the initial Richardson Number of the jet is 1.0, or very close to 1.0. Theory and laboratory experiments by Ellison and Turner (21) and field observations by Zeller (48) indicate that the Richardson Number along the jet axis changes rapidly from an initial value less than 1.0 to a value equal to or greater than 1.0, and that vertical entrainment decreases rapidly almost to zero along the axis.

Thus, if the initial Richardson Number of the jet is 1.0, or close to 1.0, vertical entrainment can be neglected, and the decrease in

temperature along the jet axis can be approximately described in terms of a two-dimensional surface jet deflected downstream by the ambient velocity.

Conservation Equations

The differential equations for conservation of volume flux, momentum flux, and heat energy can be integrated over the cross-sectional area of a two-dimensional momentum jet to obtain integral equations based on the method of Morton (33). A definition sketch is shown in Figure 4.

Conservation of Volume Flux

Integrating the volume continuity equation over the cross-section gives the relation between the rate of change of volume flux along the jet axis and the flow entrained into the jet across the outer edge as shown in Equation 11,

$$\frac{d}{ds}\left[\int_A u \, dA\right] = \int_C v_i dC \tag{11}$$

where u = the jet velocity directed along the s axis;

v_i = the inflow velocity;

dA = the differential area; and

C = the circumference through which entrainment takes place.

The inflow, or entrainment, velocity is assumed in this study to be proportional to the magnitude of the difference between a characteristic velocity along the jet and the parallel component of the ambient velocity. If this entrainment is expressed as an equality, then the inflow velocity can be written as shown in Equation 12,

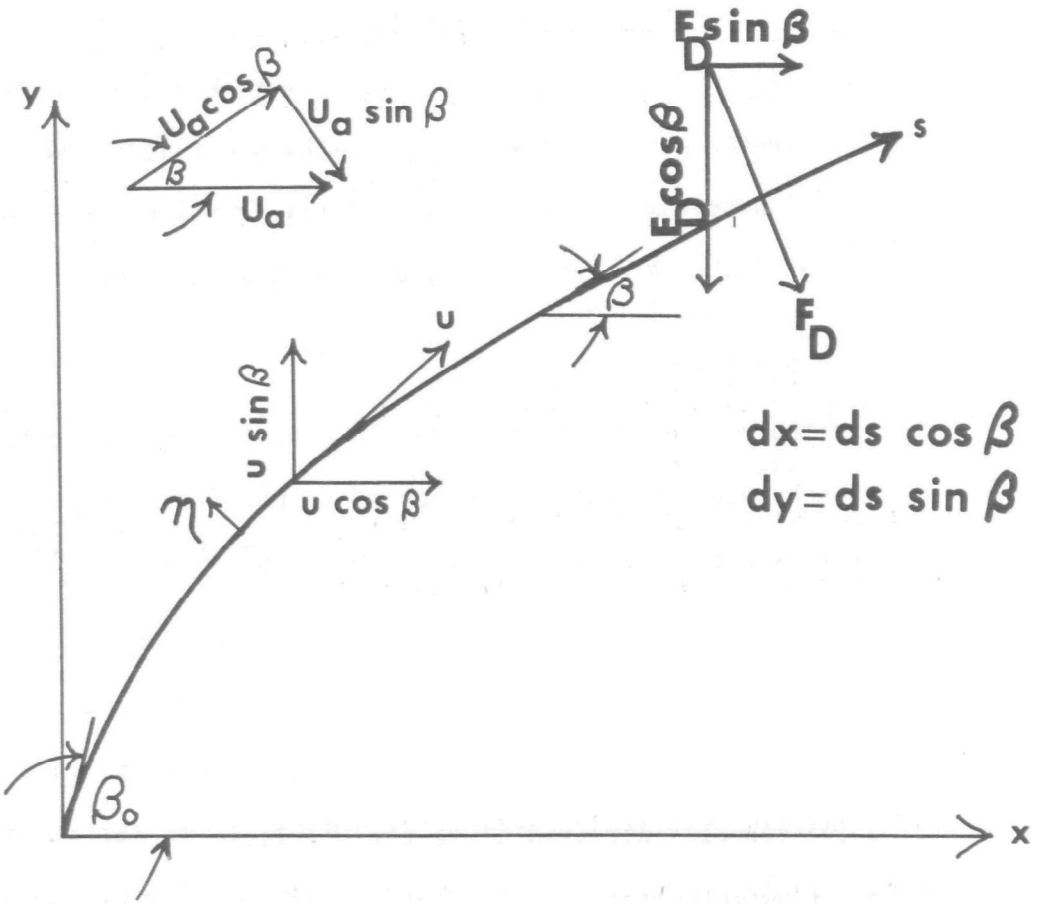

FIGURE 4.--DEFINITION SKETCH

$$v_i = E(U - U_a \cos \beta) \tag{12}$$

where U = the centerline velocity;

$U_a \cos \beta$ = the parallel component of the ambient velocity, U_a;

β = the angle between the jet and the ambient current; and

E = the experimentally-determined entrainment coefficient.

Substituting this expression for entrainment, Equation 12, into the continuity relation, Equation 11, gives the integral form of the volume continuity equation, Equation 13,

$$\frac{d}{ds}\left[\int_A u \, dA\right] = CE(U - U_a \cos \beta) \tag{13}$$

This definition of entrainment is different from the definition used by Zeller (48), who assumed that entrainment was related to only the jet velocity, as shown in Equation 9,

$$\frac{dQ}{ds} = EzU \tag{9}$$

Zeller's definition is really applicable only when the jet is at 90° to the ambient flow, or when the jet velocity is an order of magnitude greater than the ambient velocity. Realistically, as the jet is deflected, the parallel component of the ambient velocity becomes more and more important. When the jet and ambient velocities are nearly equal and parallel, mixing due to entrainment becomes quite small, because the velocity field is nearly uniform. Zeller's model does not take this into account.

Conservation of Momentum

The momentum equation along the jet axis can be integrated over the cross-section to give the relation between the rate of change of jet momentum flux, the rate of entrainment of ambient momentum flux, and the force exerted by the pressure gradient across the jet. For convenience, the resulting momentum equation is resolved into its longitudinal and lateral components along the x and y axes, respectively. The pressure gradient, due to the separation of the ambient flow, is assumed to be represented by a drag force.

In the x-direction, the rate of change of momentum flux is equal to the rate of entrainment of ambient momentum flux and to the x-component of the drag term, or as in Equation 14,

$$\frac{d}{ds}\left[\int u^2 dA \cos\beta\right] = CE(U - U_a\cos\beta)\,U_a + F_D \sin\beta \qquad (14)$$

where the drag term, F_D, is assumed to be related to the ambient velocity, U_a, as shown in Equation 15,

$$F_D = \frac{C_D U_a^2\, z \sin\beta}{2} \qquad (15)$$

and where C_D is defined as the experimentally-determined drag coefficient.

In the y-direction, since all the ambient flow is oriented along the x axis, the rate of change of momentum flux decreases due to the y-component of the drag term, or as in Equation 16,

$$\frac{d}{ds}\left[\int u^2 dA \sin\beta\right] = -F_D \cos\beta \qquad (16)$$

To compare the drag term used in the present study with the drag terms used by Carter (12) for a two-dimensional slot jet and by Fan (22)

for a submerged axi-symmetric jet, Equation 15 can be written in terms of the drag force normal to the jet axis as shown in Equation 17,

$$(\rho_a F_D ds) = \frac{C_D \rho_a U_a^2 (zds) \sin \beta}{2} \tag{17}$$

Carter defined the drag force, dP, normal to the jet axis in terms of the ambient density, a drag coefficient, the ambient velocity, and the projected area of the jet as shown in Equation 18,

$$dP = \frac{C_D \rho_a U_a^2 zds}{2} \tag{18}$$

Upon examining the definition sketch, Figure 4, it can be seen that at distances downstream, where β approaches zero, the y-component of Equation 18, or dP cos β, would continue to deflect the jet by continuing to change the y-momentum flux. Thus, the trajectory of the jet would be an ellipse. This is not realistic, since all the ambient momentum is in the x-direction, and, as β approaches zero, all the jet momentum is also in the x-direction. Thus, the y-momentum of the jet could not continue to change, and the jet should remain parallel to the ambient flow.

In comparison, the y-component of Equation 17, or $(\rho_a F_D ds)$ cos β, becomes zero as the jet becomes parallel to the ambient flow, because the projected area normal to the ambient current, or (zds sin β) in Equation 17, goes to zero. The addition of the sin β term makes the drag force representation in this study more realistic, since the jet remains parallel to the ambient flow as β goes to zero.

Fan used a $\sin^2\beta$ term in his formulation of the drag force normal to the jet axis as shown in Equation 19,

$$(F_D ds) = \frac{C_D \rho_a U_a^2 \sin^2\beta \ (2\sqrt{2}\ r ds)}{2} \tag{19}$$

where r = radius of the axi-symmetric jet. The $U_a^2 \sin^2\beta$ term is the square of the ambient velocity component normal to the projected area. This formulation differs from Equation 17, in which the component of the projected area normal to the ambient velocity is considered. According to Prandtl and Tietjens (35), pressure drag depends more on the form of the body and on separation at the rear of the body than on conditions at the front of the body. Thus, it is felt that the sin β term used in the present study is adequate to describe the conditions at the front of the jet, and that Fan's $\sin^2\beta$ term may be an unnecessary refinement.

Conservation of Temperature

If the temperature can be treated as a conservative property, which is reasonable considering the relatively small size of the jet surface area, then the integrated temperature equation can be written as in Equation 20,

$$\frac{d}{ds}\left[\int uT' \, dA\right] = 0 \tag{20}$$

where T' is the temperature rise at any point in the cross-section. The temperature rise is the difference between the jet and the ambient temperatures.

Equations 13, 14, and 20 represent the general integrated forms of the equations of volume, momentum, and heat flux.

Velocity and Temperature Profiles

Profile Shape

The Morton technique of integral analysis requires an assumption regarding the lateral distribution of velocity and temperature. According to Morton (33), the result of assuming similar profiles and the form of the inflow velocity is to suppress analytic solution of the details of the lateral structure of the jet. Thus, any reasonable profile shape can be assumed in the theoretical model. One such shape assumed by Morton is the laterally-averaged, or top-hat, profile in which the temperature and velocity have constant values across the entire width of the jet. However, the top-hat profile is not the most realistic assumption, since profiles almost Gaussian in shape in turbulent jets have been reported by Wiegel, Mobarek, and Jen (46), Cederwall (13), and Samai (40) among others. Thus, the Gaussian profile seems to more accurately describe the details of the lateral distribution and is the shape assumed in this study.

This study also assumes that the lateral spreading of heat is the same as the lateral spreading of momentum. For some cases of jets, detailed velocity and temperature measurements indicate that the assumption is not completely valid. Rouse, Yih, and Humphreys (39) report that the spread of temperature is greater than the spread of velocity by a factor of 1.16 for the case of a vertical buoyant jet. However, for other cases, detailed velocity and temperature measurements are lacking. For example, Fan (22) assumes that the spreading ratio is unity for the case of a jet discharged into a flowing stream. Since no detailed velocity measurements

were made in the present study, the same assumption --that the spreading ratio is unity --is made here.

Continuity Equation

If the velocity distribution of the jet is approximated by a Gaussian profile, then the velocity, u, at any point in the cross-section can be related to the centerline velocity, U, by Equation 21, or

$$u = U \exp(-\eta^2/2\sigma^2) \tag{21}$$

where σ = the standard deviation; and

η = distance along the axis perpendicular to the s axis.

Substituting Equation 21 into the integral on the left side of the continuity equation, Equation 13, gives Equation 22,

$$\int_{-b}^{+b} U \exp(-\eta^2/2\sigma^2)\, z\,d\eta \simeq Uz \int_{-\infty}^{+\infty} \exp(-\eta^2/2\sigma^2)\, d\eta \tag{22}$$

where b = the jet half-width;

dA = $z d\eta$; and

z = jet depth.

The integral on the right side of Equation 22 is a definite integral whose value is $\sigma\sqrt{2\pi}$. Equating this result to the right side of the continuity equation, Equation 13, gives, for the continuity equation, Equation 23,

$$\frac{d}{ds}(Uz\sigma\sqrt{2\pi}) = 2zE(U - U_a \cos\beta) \tag{23}$$

where 2z = C, the circumference through which entrainment takes place.

If the half-width b is defined as in Equation 24,

$$b = \sigma\sqrt{2} \tag{24}$$

and this relation, Equation 24, substituted into equation 23, then the continuity equation can be written in terms of the centerline velocity and jet width as in Equation 25,

$$\frac{d}{ds}(Ub) = \frac{2E}{\sqrt{\pi}}(U - U_a \cos \beta) \tag{25}$$

after dividing both sides by z.

Momentum Equations

The square of the velocity, U, is approximated using Equation 21 and is written as in Equation 26,

$$u^2 = U^2 \exp(-\eta^2/\sigma^2) \tag{26}$$

Upon substituting this relation, Equation 26, into the general form of the x-momentum equation, Equation 14, and using the relations $dA = zd\eta$ and $C = 2z$; the definition of the drag term, Equation 15; and the definition of the half-width, Equation 24; then the x-momentum equation can be written in terms of the centerline velocity and the jet width as in Equation 27,

$$\frac{d}{ds}(U^2 b \cos \beta) = \sqrt{2}\,\frac{2E}{\sqrt{\pi}}(U - U_a \cos \beta)\,U_a + \frac{\sqrt{2}}{\sqrt{\pi}}\,\frac{C_D U_a^2 \sin^2 \beta}{2} \tag{27}$$

after dividing both sides by z.

Similarly, the y-momentum equation, Equation 16, can be written in terms of U and b as in Equation 28,

$$\frac{d}{ds}(U^2 b \sin \beta) = -\frac{\sqrt{2}}{\sqrt{\pi}}\,\frac{C_D U_a \sin \beta \cos \beta}{2} \tag{28}$$

Temperature Equation

If the temperature rise distribution is approximated by a Gaussian profile, then the temperature rise, T', in the cross-section is related to the centerline temperature rise, T, by Equation 29,

$$T' = T \exp(-\eta^2/2\sigma^2) \tag{29}$$

Substituting Equations 21 and 29 into the general form of the temperature equation, Equation 20, gives the conservation of temperature equation in terms of U, T, and b, or Equation 30,

$$\frac{d}{ds}(UTb) = 0 \tag{30}$$

Summary of the Equations

The integrated mass, momentum, and temperature rise equations give a system of 4 equations and 4 unknowns:

Four equations:

continuity:

$$\frac{d}{ds}(Ub) = \frac{2E}{\sqrt{\pi}}(U - U_a \cos\beta) \tag{25}$$

x-component momentum:

$$\frac{d}{ds}(U^2 b \cos\beta) = \sqrt{2}\,\frac{2E}{\sqrt{\pi}}(U - U_a \cos\beta)\,U_a + \frac{\sqrt{2}}{\sqrt{\pi}}\,\frac{C_D U_a^2 \sin^2\beta}{2} \tag{27}$$

y-component momentum:

$$\frac{d}{ds}(U^2 b \sin\beta) = -\frac{\sqrt{2}}{\sqrt{\pi}}\,\frac{C_D U_a^2 \sin\beta\cos\beta}{2} \tag{28}$$

temperature rise:

$$\frac{d}{ds}(UTb) = 0 \tag{30}$$

Four unknowns:

U, T, b, β

The geometry of the jet trajectory as shown in Figure 4 gives two additional equations and unknowns,

Two geometry equations:

$$\frac{dx}{ds} = \cos \beta \tag{31}$$

$$\frac{dy}{ds} = \sin \beta \tag{32}$$

Two unknowns:

x, y

Thus, there are six unknowns--U, T, b, β, x and y--and six equations, all functions of the jet axis distance, s. In addition, there are two experimentally-determined coefficients--C_D and E.

Solution of the Equations

Non-Dimensional Volume Flux and Momentum Flux

The volume continuity equation and the two momentum equations are made non-dimensional by defining V as the non-dimensional volume flux and M as the non-dimensional momentum flux as shown in Equation 33,

$$V = \frac{Ub}{U_o b_o} \quad ; \quad M = \frac{U^2 b}{U_o^2 b_o} \tag{33}$$

Using Equation 33, then Equations 25, 27, and 28 take the respective forms:

volume continuity:

$$\frac{dV}{dS} = \frac{M}{V} - A \cos \beta \tag{34}$$

x-component of momentum flux:

$$\frac{d(M \cos \beta)}{dS} = \sqrt{2}\, A \left[\frac{M}{V} - A \cos \beta + A\, C_D' \sin^2\beta\right] \tag{35}$$

y-component of momentum flux:

$$\frac{d(M \sin \beta)}{dS} = -\sqrt{2}\ A\ (A\, C_D' \sin \beta \cos \beta) \tag{36}$$

where S = the non-dimensional jet axis distance;

$$S = (2E/\sqrt{\pi}\, b_o)s \tag{37}$$

A = the ratio of the ambient velocity to the initial jet velocity;

$$A = U_a/U_o \tag{38}$$

and C_D' = the reduced drag coefficient;

$$C_D' = C_D/4E \tag{39}$$

Geometry Equations

The geometry equations, Equations 31 and 32, can be written in non-dimensional form as shown in Equations 40 and 41,

$$\frac{dX}{dS} = \cos \beta \tag{40}$$

$$\frac{dY}{dS} = \sin \beta \tag{41}$$

where

$$X = (2E/\sqrt{\pi}\, b_o)x \quad ; \quad Y = (2E/\sqrt{\pi}\, b_o)y \tag{42}$$

Temperature Equation

The temperature equation, Equation 30, can be integrated immediately to give Equation 43,

$$\frac{UTb}{U_o T_o b_o} = 1 \tag{43}$$

where U_o, T_o, and b_o = the initial values of the velocity, temperature rise, and jet half-width, respectively.

Solution in Terms of S, and X and Y

There are now five differential equations, Equations 34, 35, 36, 40, and 41, and five unknowns, or V, M, β, X, and Y, all functions of the jet axis distance, S. By solving this set of differential equations for M and V, then the velocity ratio, U/U_o, the temperature rise ratio, T/T_o, and the half-width ratio, b/b_o, can be solved as functions of S.

Using the definition of the volume flux and the momentum flux, or Equation 33, the ratio U/U_o is related to M and V as shown in Equation 44,

$$U/U_o = M/V \tag{44}$$

Using the definition of V, Equation 34, and the integrated temperature equation, Equation 43, the ratio T/T_o is related to V as shown in Equation 45,

$$T/T_o = 1/V \tag{45}$$

Using Equation 34, the ratio b/b_o is related to V and M as in Equation 46,

$$b/b_o = V^2/M \tag{46}$$

The ratios U/U_o, T/T_o, and b/b_o are functions of S, since M and V are functions of S.

Next, by solving the set of differential equations for β, then U/U_o, T/T_o, and b/b_o can also be expressed as functions of the rectangular coordinates, X and Y. As shown in Equation 47 and 48, these coordinates

can be located by integrating Equations 40 and 41 along the jet axis, S, or

$$X = \int_0^S \cos \beta \, dS \tag{47}$$

$$Y = \int_0^S \sin \beta \, dS \tag{48}$$

Numerical Solution

A numerical integration method was used to solve the five equations for the five unknowns--V, M, β, X, and Y -- as functions of S. Then, at each step of the integration, values of U/U_o, T/T_o, and b/b_o were calculated from the values of M and V and expressed as functions of S, and X and Y.

The system of differential equations was solved using General Electric's FORTRAN subprogram RKPBX$, which is available in the time-sharing service program library. This subprogram integrates a system of first-order differential equations by the fourth-order Runge-Kutta method.

The five equations — the volume flux equation, the two momentum flux equations, and the two geometry equations — were rewritten in a form suitable for the subprogram. Equations 34, 35, 36, 40, and 41 became, respectively,

continuity:

$$\frac{dV}{dS} = \frac{(L^2 + F^2)^{1/2}}{V} - \frac{AL}{(L^2 + F^2)^{1/2}} \tag{49}$$

x-component of momentum:

$$\frac{dL}{dS} = \sqrt{2}\ A \left[\frac{(L^2 + F^2)^{1/2}}{V} - \frac{AL}{(L^2 + F^2)^{1/2}} + \frac{AC_D' F^2}{(L^2 + F^2)} \right] \quad (50)$$

y-component of momentum:

$$\frac{dF}{dS} = -\sqrt{2}\ A \left[\frac{AC_D' FL}{(L^2 + F^2)} \right] \quad (51)$$

geometry equations:

$$\frac{dX}{dS} = \frac{L}{(L^2 + F^2)^{1/2}} \quad (52)$$

$$\frac{dY}{dS} = \frac{F}{(L^2 + F^2)^{1/2}} \quad (53)$$

where $L = M \cos \beta$; (54)

$F = M \sin \beta$; (55)

$M = (L^2 + F^2)^{1/2}$; and (56)

$\beta = \arctan (F/L)$ (57)

Example Solution

The numerical solution was used to solve for values of V, L, F, X, and Y and then M, T/T_o, U/U_o, and b/b_o at each increment of $dS = 0.1$ along the jet axis, S, for given values of the coefficients A and C_D'.

For example, consider a surface jet discharging into an ambient stream at an initial angle of $\beta_o = 60.0^o$. The initial value of the volume flux is $V_o = 1.0$ from Equation 33. The initial value of $L_o = 0.50$ from Equation 54, and the initial value of $F_o = 0.86603$ from Equation 55, since the initial value of the momentum flux is $M_o = 1.0$ from Equation 33. The initial values of the rectangular coordinates are $X_o = 0.0$ and $Y_o = 0.0$. For this example, the value of the initial jet velocity is assumed to be four times greater than the ambient velocity, or $A = 0.25$ from Equation 38. The reduced drag coefficient, C_D, is assigned the values 0.0, 0.5, and 1.0 to illustrate its effect on the location of the jet trajectory.

After integrating the system of equations, the result can be shown graphically. The volume flux, V, and the momentum flux, M, are plotted as functions of the jet axis distance, S, in Figure 5. The temperature rise, velocity, and width ratios -- T/T_o, U/U_o, and b/b_o -- are plotted as functions of S in Figure 6. The location of the jet trajectory as a function of the reduced drag coefficient, C_D', is plotted in Figure 7. The value of T/T_o along the jet trajectory is not significantly changed by the different values of C_D'. For example, at $S = 100.0$, the value of the temperature rise is $T/T_o = 0.0597$, 0.0582, and 0.0572 for the respective values of $C_D' = 0.0$, 0.5, and 1.0.

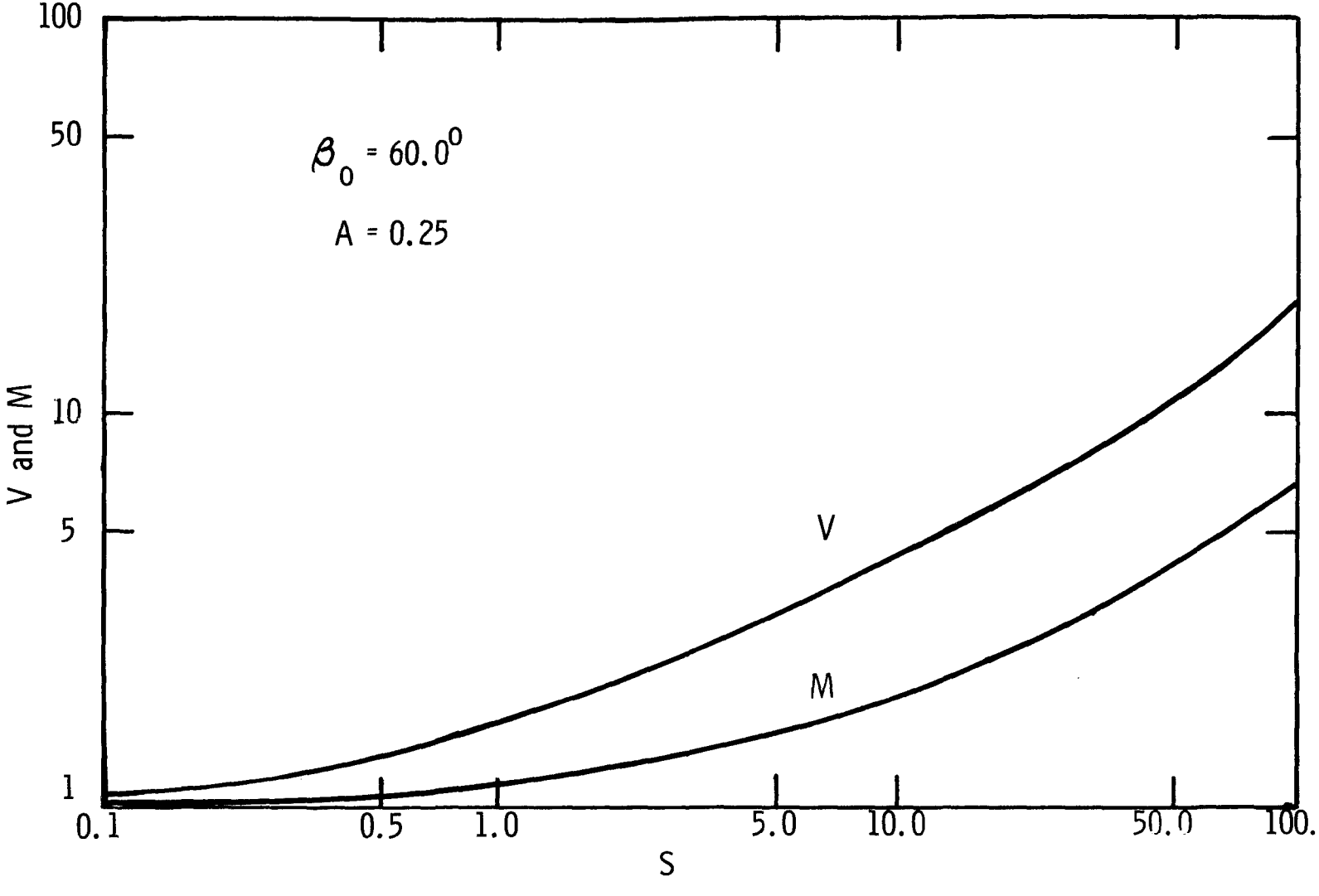

FIGURE 5.--VOLUME FLUX AND MOMENTUM FLUX VERSUS NON-DIMENSIONAL JET AXIS DISTANCE

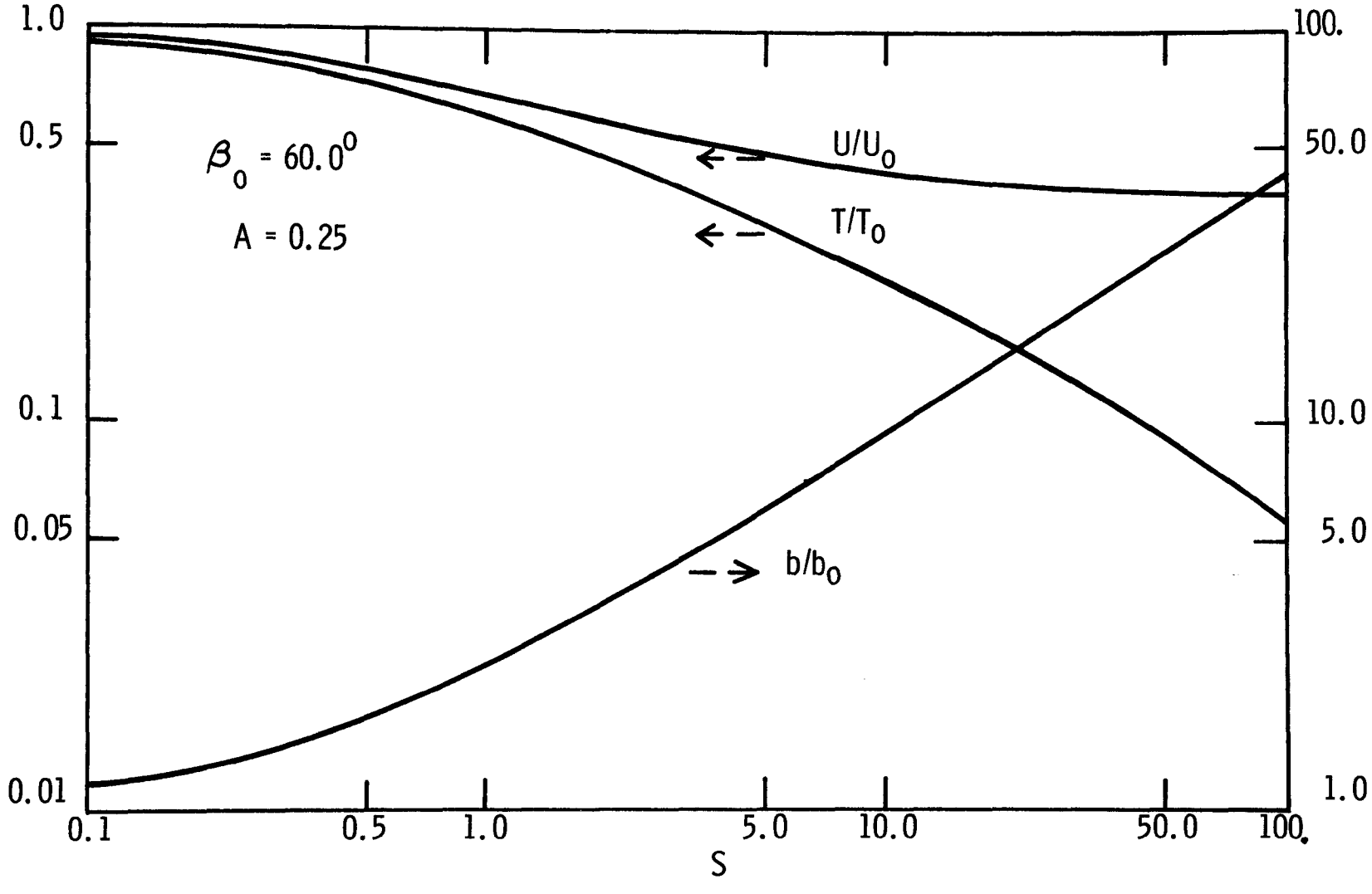

FIGURE 6.--TEMPERATURE, VELOCITY, AND WIDTH RATIOS VERSUS NON-DIMENSIONAL JET AXIS DISTANCE

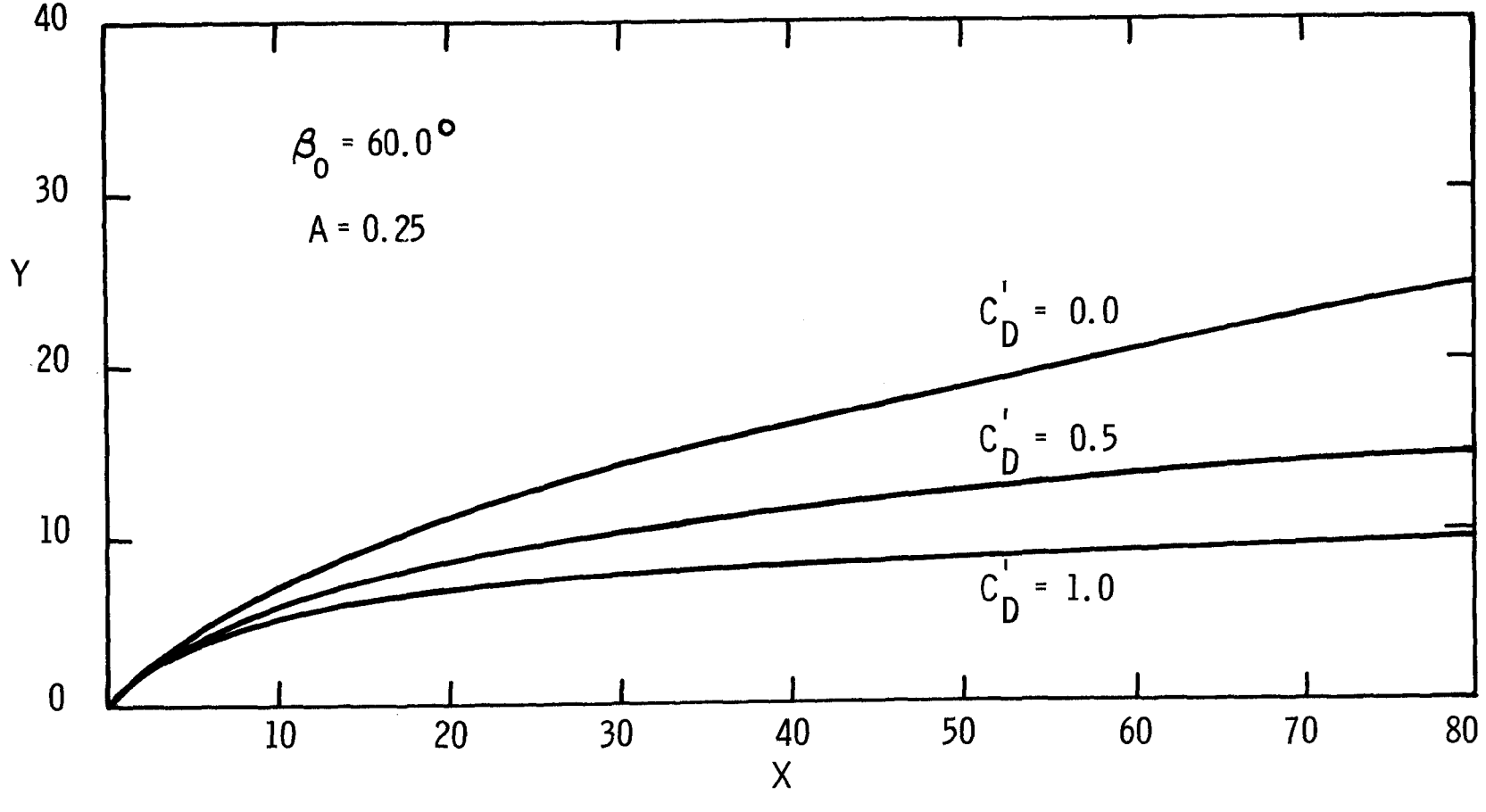

FIGURE 7.--EFFECT OF REDUCED DRAG COEFFICIENT ON LOCATION OF JET TRAJECTORY

Zone of Flow Establishment

In practical applications, the zone of flow establishment of the jet, illustrated in Figure 8, must be determined. This zone is a mixing region in which turbulent mixing changes the uniform temperature and velocity profiles at the jet origin to fully-developed turbulent profiles which are Gaussian in shape at the beginning of the established flow region.

Previously, when the zone of establishment has been determined for jets in a flowing stream, it has been done by measuring the length, s'_e, and the initial angle, β_o, at the end of the zone of establishment. Fan (22), for example, empirically related the length of the establishment zone and the initial angle, β_o, to the ratio of the ambient velocity and the initial jet velocity, or $A = U_a/U_o$. Based upon Gordier's data (25), the length of the establishment zone was found by Fan to be related to A as shown in Equation 58,

$$\frac{s'_e}{d'_o} = 6.2 \exp(-3.32\, A) \tag{58}$$

The initial angle at the end of the zone, β_o, was found to be related to A as shown in Equation 59,

$$\beta_o = 90° - 110°\, A \tag{59}$$

Unfortunately, Fan's results in Equations 58 and 59 are not directly applicable to the present study. In cases where the initial angle of the discharge is 60° or even 45°, Fan's results can not be used directly since the initial angle, β'_o, in Equation 59 is 90°. In cases

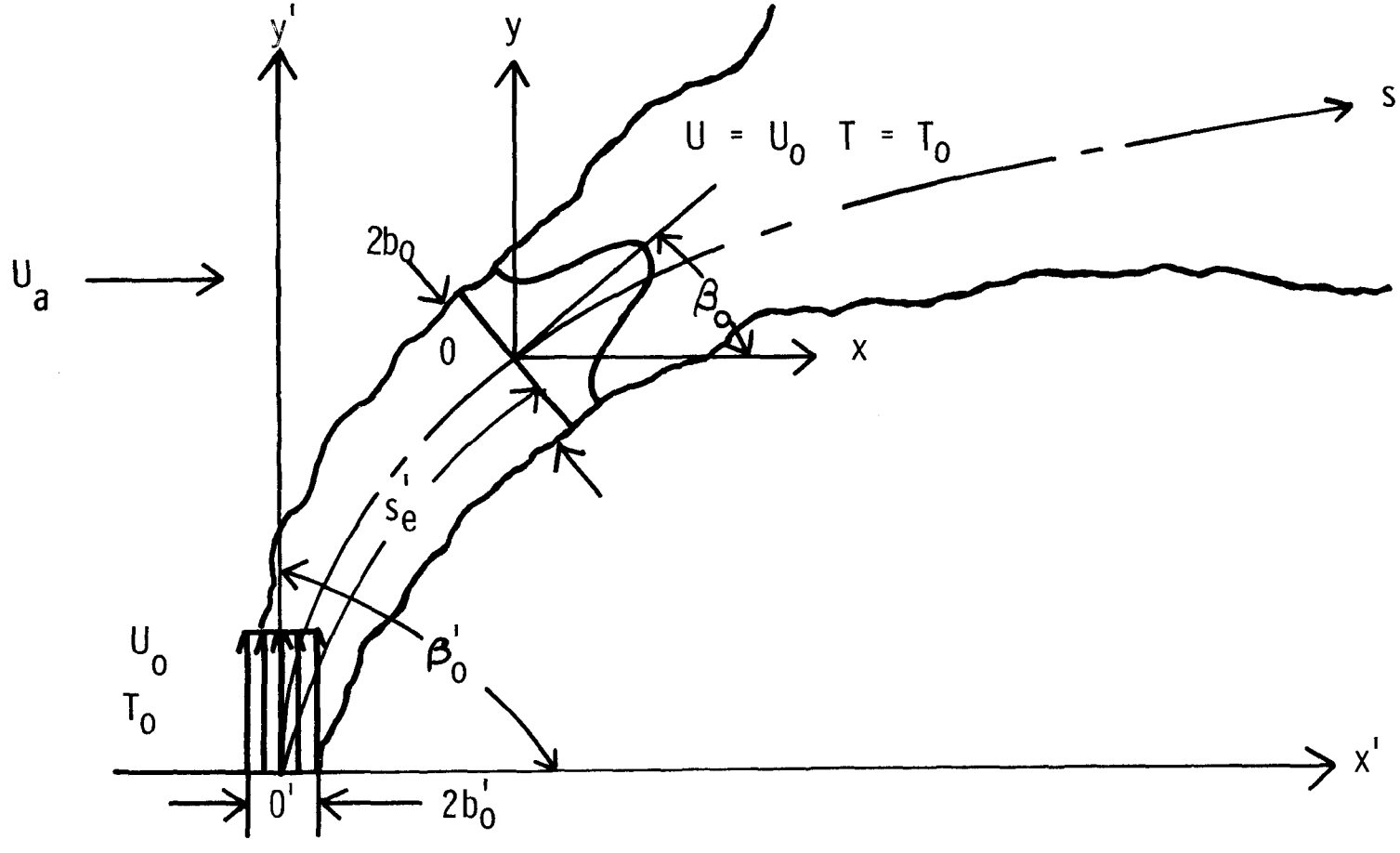

FIGURE 8.--ZONE OF FLOW ESTABLISHMENT

of two-dimensional surface jets where the range of the velocity ratio, A, is anticipated to be $0.20 \leq A \leq 0.80$ or higher, Fan's results should not be directly applied even when $\beta_o' = 90°$ since his results were developed for a different range of A, or $0.125 \leq A \leq 0.25$. Therefore, it will be necessary to extend Fan's work by empirically determining how the length of the zone of flow establishment, s_e', and how the initial angle at the end of the zone of establishment, β_o, are related to the velocity ratio, $A = U_a/U_o$, for cases in the range of $0.20 \leq A \leq 0.80$ and at the same time for cases where the initial angle of the discharge, β_o', is not 90° to the ambient flow.

Summary of Analytical Development

By considering the basic volume, momentum, and heat equations, a model has been developed describing a two-dimensional surface jet deflected downstream by a flowing ambient current. By using a numerical solution, values of temperature rise, velocity, and width can be predicted as functions of a non-dimensional jet axis distance. The location of the jet trajectory can be predicted in terms of non-dimensional rectangular coordinates. The model contains two experimentally-determined coefficients, the entrainment coefficient and the drag coefficient. Since the non-dimensional coordinates S, X, and Y are defined as functions of the entrainment coefficient, E, in Equations 37 and 42, and since the location of the jet trajectory depends on the drag coefficient, C_D, these coefficients must be evaluated by laboratory experiments before the model can be used to predict temperature distributions at field sites. Also, the zone of flow establishment of the jet must be determined from laboratory

experiments before the mathematical model can be used in practical situations.

CHAPTER IV

LABORATORY EXPERIMENTS

The laboratory experiments were designed to functionally relate the entrainment and drag coefficients and the zone of flow establishment to the velocity ratio, A, and the initial angle of discharge, β_o'.

Modeling

The complete modeling of a heated discharge would require modeling several phenomena: the inertial mixing due to the jet velocity, the buoyancy due to the temperature difference between the jet and the ambient current, the advection of the heat by the ambient current, the turbulent diffusion in the ambient stream, and the evaporative heat loss across the air-water interface. According to Ackers (3) and other investigators, it is impossible to accurately reproduce all the phenomena in the same model. Thus, it is necessary to identify the dominant forces present in a given situation.

Dominant Forces in a Surface Jet

As assumed in the development of the mathematical model, the three dominant forces involved in a surface jet are the inertial, viscous, and buoyancy forces. The ratio of the difference between the inertial force of the jet and the ambient current to the buoyancy force due to the temperature difference between the jet and the ambient current is the Richardson Number and can be written as in Equation 10. The ratio of

the inertial force of the jet to the viscous force is the jet Reynolds Number. In addition, the ratio of the inertial to the viscous forces in the stream, or the ambient Reynolds Number, must be considered.

Jet Reynolds and Richardson Numbers

Two of the criteria considered in modeling a surface jet are the equivalence of the model and prototype jet Reynolds and Richardson Numbers. Unfortunately, exact equivalence cannot be achieved in the laboratory.

Equivalence of the initial Richardson Numbers (Ri_o Number) can be achieved by reducing the velocity and velocity differences in the model. This is shown in Equation 60,

$$Ri_o = \left[\frac{\Delta\rho g d_o'}{\rho (U_o - U_a)^2}\right]_m = \left[\frac{\Delta\rho g d_o'}{\rho (U_o - U_a)^2}\right]_p \qquad (60)$$

where m and p refer to the model and prototype, respectively. The diameter, d_o', of the model is necessarily much smaller than that of the prototype, and the density and density difference of the model are approximately the same as that of the prototype unless an impractically large temperature rise is used in the model, since water is to be used as the model fluid.

However, equivalence of the jet Reynolds Numbers (Re_o Number) could only be achieved by increasing the model velocity to very large values. This is shown in Equation 61,

$$Re_o = \left[\frac{U_o d_o'}{\nu}\right]_m = \left[\frac{U_o d_o'}{\nu}\right]_p \qquad (61)$$

where ν = kinematic viscosity. This is because the diameter, d_o', of the model is still much smaller than that of the prototype, and the kinematic viscosity, ν, is approximately the same in both the model and the prototype.

Thus, approximate equivalence of the Ri_o Numbers can be achieved only at the expense of very small jet Re_o Numbers in the model. Other investigators, such as Abraham (1) and Burdick and Krenkel (10), have assumed that, if the model jet flow is turbulent, as in the prototype, i.e., if the Re_o Number is greater than some critical value, then the criterion for exact equivalence between model and prototype jet Re_o Numbers can be relaxed. Then, the criterion for similarity between model and prototype Ri_o Numbers can be achieved.

Ambient Reynolds Numbers

The third criterion, exact equivalence of prototype and model ambient Reynolds Numbers, also cannot be achieved in the laboratory. It is assumed that the requirements for exact equivalence can be relaxed if the flow regime in the laboratory flume is turbulent.

Model Surface Jet

The model surface jet is thus an approximation of the prototype. Equivalence of model and prototype Ri_o Numbers is chosen in preference to equivalence of Re_o Numbers. Prototype Ri_o Numbers can be calculated based on conditions representing typical field sites, and the model Ri_o Numbers should be on the same order of magnitude. Since prototype Re_o Numbers indicate a turbulent flow regime in the jet and in the ambient stream, the model Re_o Numbers should also indicate a turbulent flow regime.

Laboratory Equipment and Procedure

The laboratory experiments were performed in the hydraulics laboratory of the Department of Environmental and Water Resources Engineering at Vanderbilt University.

Flume

The flow system used was a rectangular flume 60 feet long, 2.0 feet wide, and 1.0 foot deep. The flume has glass sides and a painted steel bottom, and is mounted on a truss system so that the slope can easily be varied.

Jets

Circular jets were selected for laboratory use for two reasons -- convenience and the object of the experiments. Using circular jets required only a minimum of commercially-available fittings, while using square or rectangular orifices would have required extensive fabrication of special shapes and equipment. The object of the experiments -- relating the entrainment and drag coefficients and the zone of establishment to the velocity ratio, A, and the initial angle, β_o' -- was restricted to what were considered the significant factors influencing the spatial distribution of temperature. Understanding these factors, the influences of A and β_o', more fully was felt to be necessary before considering the many possible variations of orifice shape.

The design of the jets was based on the desire to maintain constant Re Numbers in the jet and in the flume. It was decided to maintain a constant jet velocity and jet Re_o Number and vary the velocity ratio, $A = U_a/U_o$, by varying the ambient velocity, U_a, in the flume.

Since it was decided to use the maximum flowrate, $Q_a \simeq 0.15$ cfs, this meant that the flume, or ambient, Reynolds Number could be kept constant by inversely changing the ambient depth, z_a, with changes in the flume velocity, U_a. The ambient Reynolds Number can be written as shown in Equation 62,

$$Re_a = \frac{U_a z_a}{\nu} \tag{62}$$

where Re_a = the ambient Re Number; and

z_a = the ambient depth.

Thus, for each desired value of the velocity ratio, $A = U_a/U_o$, a different value of U_a was indicated, since U_o was constant. For each value of U_a, then, a different value of z_a was indicated from Equation 62, since Re_a and Q_a were to be kept constant. This resulted in the jets being designed to enter the flume at different heights so that the top of the jet discharge for each jet when in use would coincide with the ambient water surface.

The 1.0-inch diameter jets were built using PVC pipe and Plexiglass. One of the glass panels near the upstream end of the flume was removed, and a Plexiglass panel with a circular opening approximately 0.7 feet in diameter was sealed in its place. Into this opening could be placed a Plexiglass "plug" drilled to hold a vertical row of four jets mounted so that they would be flush with the inside wall of the flume. The jets were designed so that each one could be sealed when not in use. Since it was decided to study the effect of three different jet angle orientations, or $\beta_o' = 90°$, 60°, and 45° to the ambient flow, three of these plugs were constructed, each containing a vertical row of jets oriented

at one of the angles, β_o', mentioned above. Figure 9 shows the three plugs with the jets offset horizontally for clearance, while Figure 10 shows one of the jets in use with the other three sealed off.

Temperature Determination

The temperature distribution was determined using probes small enough to produce minimum disturbance in the flow pattern, a manually-operated switchbox, and a digital thermometer. Point measurements were made by using a single Cole-Parmer No. 8432-1 probe mounted on a traveling point gauge apparatus. This probe had a length of 2 1/2 inches, and the temperature-sensitive bulb at the tip of the probe had a diameter of 1/8 inch. Lateral temperature measurements were determined using eleven Cole-Parmer No. 8434 stainless steel probes with a length of 4 1/2 inches and a diameter of 5/32 inches. These probes were spaced laterally on a movable platform which was suspended over the water surface. Preliminary investigation indicated that the thermal sensitivity of these probes was limited to the lower 1/2 inch or so of the tip. Thus, when the tips were immersed below the water surface, a vertically-averaged temperature could be read over this depth. A manually-operated YSI twelve-point switchbox was used to route the output of the probes to a Digitec Model 1515 digital thermometer. Preliminary investigation also indicated that the time-varying turbulent fluctuations of temperature along the centerline of the surface jets were sufficiently small to allow average centerline temperatures to be determined directly from the read-out scale of the digital thermometer, precluding the necessity of re-cording apparatus. Figure 11 shows the temperature probes, the switch-box, and the digital thermometer.

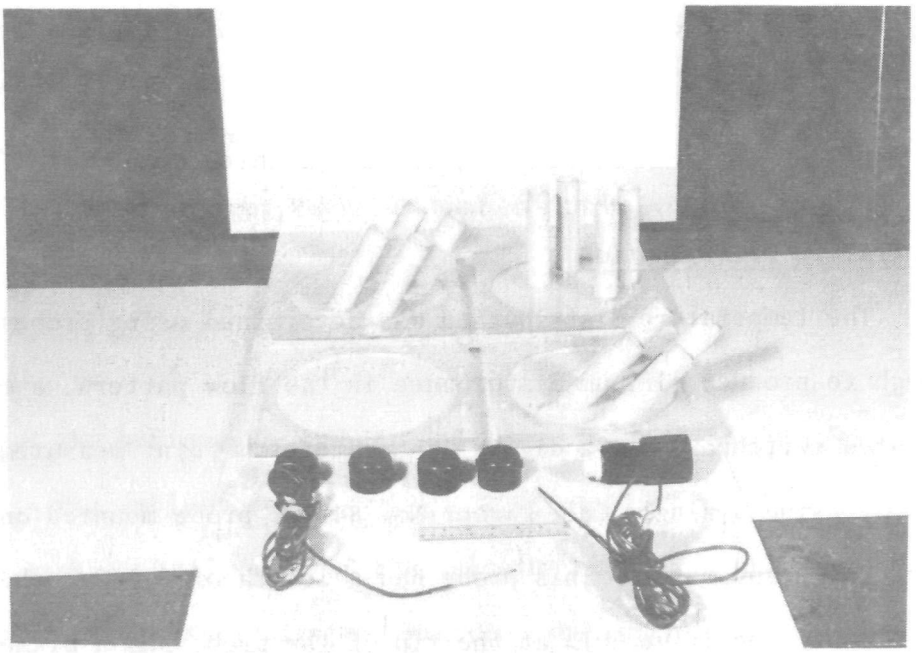

FIGURE 9.--JETS AND TEMPERATURE PROBES

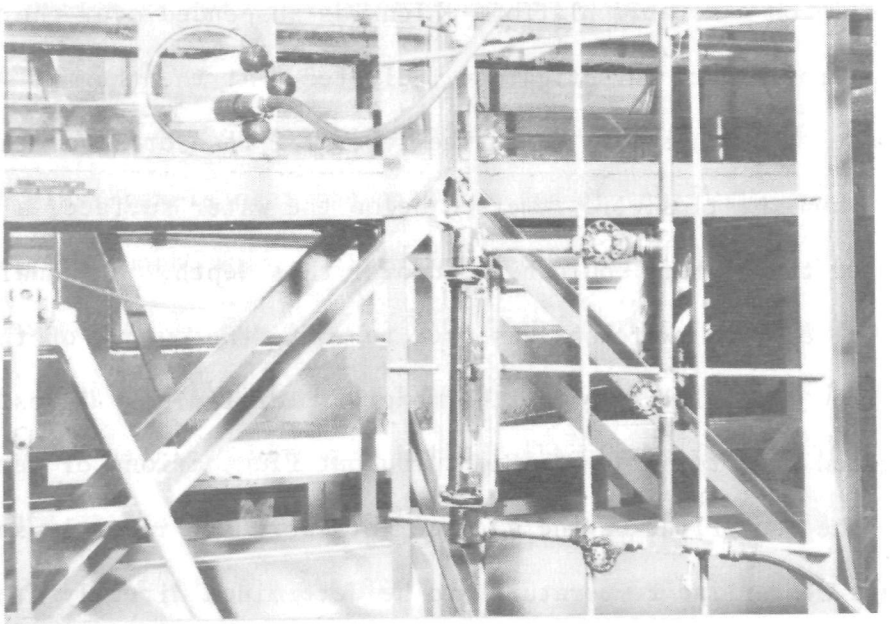

FIGURE 10.--SURFACE JET AND ROTAMETER

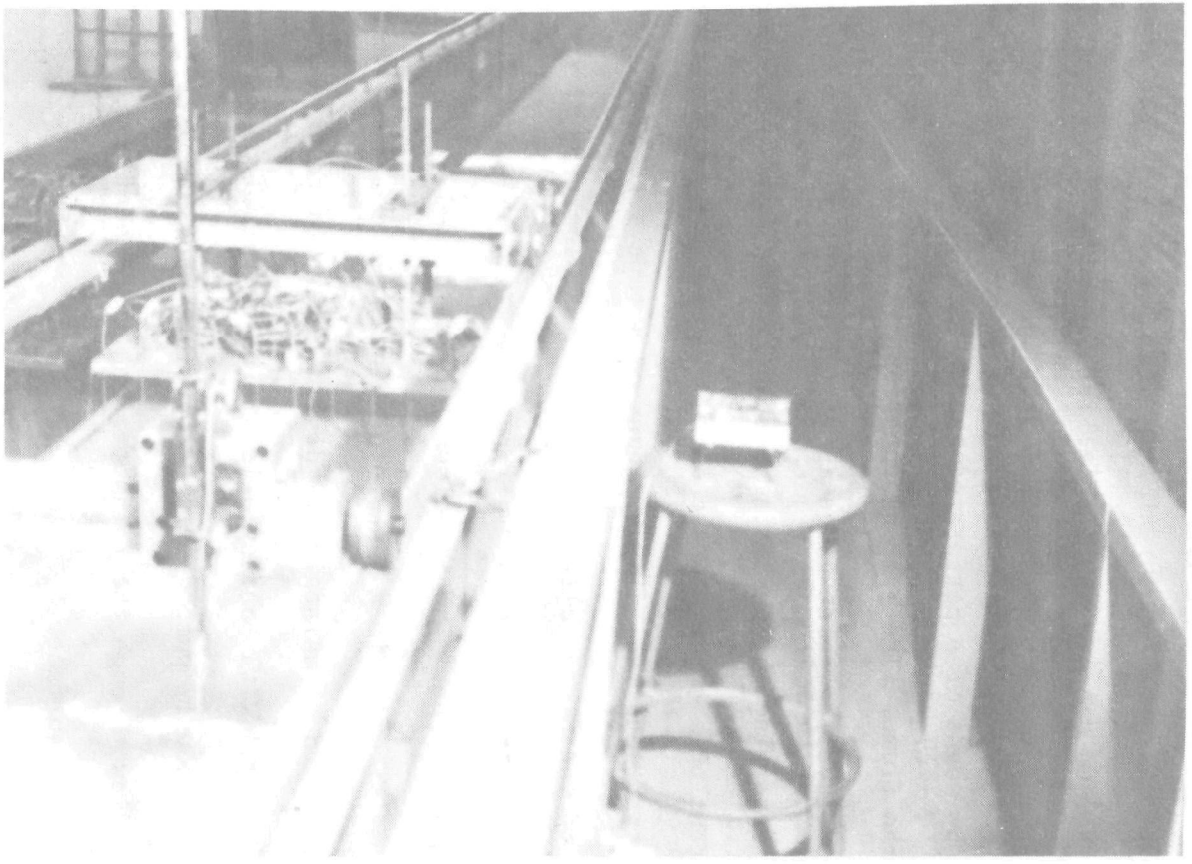

FIGURE 11.--TEMPERATURE PROBES AND OTHER LABORATORY EQUIPMENT

Other Equipment

Other laboratory equipment was also used in performing the experiments. A 60° V-notched weir installed at the upstream end of the flume was used to measure the ambient flowrate, Q_a. A 2.00-gpm capacity rotameter was used to measure the initial jet flowrate, Q_o. The traveling point gauge was used to measure the flume depth, z_a, which was controlled by means of a perforated baffle installed at the downstream end of the flume. The spatial location of the temperature probe attached to the traveling point gauge apparatus relative to the origin of the jet was determined by measuring vertically with the point gauge, laterally by means of a scale mounted on the lateral arm of the traveling cart, and longitudinally by means of a tape stretched along the upper edge of the flume wall. The longitudinal location of the platform containing the eleven laterally-spaced probes was determined by means of the same tape. The jet discharge was heated by mixing about 150 gallons of water in a tank into which steam could be admitted at a flowrate adjusted to maintain the desired elevated temperature. The heated water, dyed with Pontacyl Pink to allow visual observation of the jet, was continuously pumped into a 10.0-foot constant heat tank, then allowed to flow through the rotameter and into the flume, entering at the ambient water surface.

Procedure

The procedure followed in performing the laboratory experiments was similar for all the runs. Selection of parameters such as ambient depth, z_a, and the initial temperature of the heated discharge for each run was based on preliminary calculations of the desired value of the

velocity ratio, A, and the desired values of the Ri_o and Re Numbers. Uniform ambient flow was obtained by adjusting the slope of the flume before each run. Steady-state conditions were insured by allowing the jet to discharge into the ambient flow for at least 15 minutes before data were taken. Lateral temperature distributions were measured at predetermined intervals starting at the downstream end of the flume. Point temperature measurements were made to accurately locate the jet centerline, to determine the zone of flow establishment, and to measure vertical temperature distributions. The initial temperature of the jet was measured with the point probe in the mouth of the jet flush with the inside wall of the flume. The flume water was not recirculated, since preliminary calculations had indicated that the ambient temperature would be increased during the estimated time for each run by the heated jet by about 5°F, which was significant compared to the initial temperature rises planned.

CHAPTER V

RESULTS OF THE LABORATORY EXPERIMENTS

The results of the laboratory experiments were analyzed in terms of the parameters in the mathematical model.

Relation of Circular Jet to Half-Width b_o

The two-dimensional mathematical model predicts the temperature distribution along the jet axis in terms of the initial jet half-width, b_o, located at the end of the zone of flow establishment as seen in Equation 37,

$$S = (2E/\sqrt{\pi}\, b_o)s \tag{37}$$

In order to plot the observed trajectories and temperature data in terms of non-dimensional coordinates, it was necessary to calculate the value of b_o, which can be determined from the value of the diameter, d_o', and the value of the equivalent half-width at the origin of the jet, b_o'.

Circular and Square Orifices

According to Yevdjevich (47), the entrainment characteristics of a square jet approximate the entrainment characteristics of a circular jet if the cross-sectional areas of the two orifices are equal. If the circular orifice diameter is d_o', and the square orifice half-width is b_o', then equating the cross-sectional areas of the two shapes gives Equation 63,

$$d_o' = 2.26\, b_o' \tag{63}$$

This equation is established by Yevdjevich for a vertical three-dimensional jet but is assumed in this study to be applicable to a horizontal surface jet as well.

Relation of b_o' to b_o

The value of the initial jet half-width, b_o, at the end of the zone of flow establishment can be related to the half-width, b_o', at the origin by considering the conservation of heat flux between the two cross-sections at 0' and 0 shown in the definition sketch of the zone of flow establishment, Figure 8. Using the assumed Gaussian velocity and temperature profiles, Equations 21 and 29, and integrating the conservation of heat flux relation, Equation 30, at 0' and 0, and then equating the resulting heat flux at 0' to the flux at 0 gives Equation 64,

$$2\, U_o T_o z_o b_o' = UTzb_o\sqrt{\pi}/\sqrt{2} \tag{64}$$

Since the temperature rise, T_o, the jet velocity, U_o, and the depth, z_o, at 0' are equal to the respective centerline values of T and U and the value of z at 0 in Equation 64, then b_o can be related to b_o', as shown in Equation 65,

$$b_o = 1.60\, b_o' \tag{65}$$

Relation of b_o to d_o'

The two equations, Equations 63 and 65, express d_o' and b_o as functions of b_o'. Solving the equations to eliminate b_o' relates the initial half-width at the end of the zone of flow establishment, b_o, to the diameter, d_o', of a circular jet as shown in Equation 66,

$$b_o = 0.708\, d_o' \tag{66}$$

In the laboratory experiments the diameter, d_o', of the jets was equal to 1.0 inch. Therefore, from Equation 66, the value of the half-width was $b_o = 5.90 \times 10^{-2}$ feet.

Laboratory Measurements

A complete summary of the data is presented in Appendices A and B.

Velocities

The ambient velocity, U_a, and the initial jet velocity, U_o, for each run were calculated from the measured flowrates, since no attempt was made to directly measure the ambient velocities or the spatially-varied velocity distribution in the jet flow field. The value of the velocity ratio, $A = U_a/U_o$, was calculated from these values of U_a and U_o. Then the initial jet Reynolds Number was calculated using the diameter, d_o', and Equation 61, and the ambient Reynolds Number was calculated using measured values of the ambient depth, z_a, and Equation 62. These values are presented in Table 1.

Temperature

The initial jet Richardson Number was calculated from Equation 60, using the initial jet and ambient temperatures, which are presented in Table 1, and standard tables for the density of water. These values are presented in Table 1.

Geometry

The values of the initial angle of the discharge, β_o', are also presented in Table 1.

TABLE 1

LABORATORY MEASUREMENTS

Run	U_a ft/sec	U_o ft/sec	A Eq.38	Re_o Eq.61	Re_a Eq.62	z_a ft	Ambient Temp. °F	Initial Jet Temp. °F	β_o'	$(Ri_o)_m$ Eq.60	$(Ri_o)_p$ Eq.60
1-90	0.38	0.52	0.73	5240	5370	0.20	43.5	111.0	90.0	1.17	4.12
2-90	0.23	0.52	0.44	5240	5340	0.33	45.5	106.0	90.0	2.61×10^{-1}	3.55×10^{-1}
3-90	0.16	0.52	0.30	5240	5370	0.48	46.0	91.5	90.0	9.55×10^{-2}	1.11×10^{-1}
4-90	0.12	0.52	0.23	5240	5300	0.63	47.0	84.2	90.0	6.90×10^{-2}	5.07×10^{-2}
5-90	0.10	0.52	0.20	5240	4590	0.62	47.7	70.5	90.0	3.20×10^{-2}	3.57×10^{-2}
1-60	0.31	0.52	0.67	5240	5300	0.21	43.5	101.0	60.0	6.32×10^{-1}	2.51
2-60	0.23	0.52	0.44	5240	5340	0.33	45.6	106.0	60.0	2.65×10^{-1}	3.67×10^{-1}
3-60	0.16	0.52	0.30	5240	5370	0.49	46.2	93.0	60.0	1.05×10^{-1}	1.07×10^{-1}
3-60-1	0.17	0.52	0.32	5240	5400	0.46	43.9	93.0	60.0	8.74×10^{-2}	1.37×10^{-1}
4-60	0.12	0.51	0.23	5240	5300	0.64	47.1	83.0	60.0	6.15×10^{-2}	5.13×10^{-2}
5-60	0.10	0.52	0.19	5240	4300	0.63	46.8	74.5	60.0	3.88×10^{-2}	3.04×10^{-2}
1-45	0.34	0.52	0.66	5240	5370	0.22	44.7	101.0	45.0	5.92×10^{-1}	2.27
2-45	0.22	0.52	0.42	5240	5300	0.34	45.5	107.0	45.0	2.48×10^{-1}	3.16×10^{-1}
3-45	0.16	0.52	0.30	5240	5340	0.49	46.4	92.5	45.0	1.04×10^{-1}	1.05×10^{-1}
4-45	0.12	0.52	0.23	5240	5370	0.63	46.6	84.0	45.0	6.11×10^{-2}	5.32×10^{-2}
5-45	0.10	0.52	0.18	5240	4300	0.62	47.0	73.0	45.0	3.83×10^{-2}	2.82×10^{-2}

Analysis of Data

Reynolds Number

The Re Numbers of the jet and ambient flow, shown in Table 1, were all Re ≈ 5,000, which indicates that the Re Numbers were constant, and that the flow regime was almost fully turbulent.

Comparison of Model and Prototype Ri_o

The initial Richardson Number for each value of A in Table 1 can be compared to a representative prototype Ri_o Number calculated from Equation 60 by assuming a 15° temperature rise from 70°F to 85°F, a 10.0-foot discharge depth, and an ambient velocity of U_a = 1.0 ft/sec. These prototype values were based upon anticipated conditions at several Tennessee Valley Authority generating plants. The model and prototype Ri_o Numbers for corresponding values of $A = U_a/U_o$ in Table 1 are seen to all be of the same order of magnitude.

Gaussian and Two-Dimensional Assumptions

The temperature data were examined to determine the validity of the Gaussian and two-dimensional assumptions made in the mathematical model.

Gaussian Assumption.-- The assumption made in Equation 29 that the lateral temperature distribution perpendicular to the jet axis is Gaussian in shape was examined for a representative run. Surface temperature measurements were made with the point probe at a distance far enough downstream from the origin of the jet so that the cross-section, measured laterally across the flume, was perpendicular to the

axis of the jet. The surface temperature measurements were plotted, and then a Gaussian curve was fitted to the distribution as shown in Figure 12. The mean of this distribution is 0.56 feet, and the standard deviation of the sample is 0.27 feet. The correlation coefficient for the fitted Gaussian distribution is equal to 0.90, which indicates that the Gaussian distribution is adequate to describe the temperature profile. The bimodal distribution observed by Fan (22) for a submerged jet was not observed in this study of a surface jet.

Two-Dimensional Assumption.--The assumption that the surface jet spreads laterally much greater than it does vertically was examined by measuring cross-sectional and vertical temperature distributions. A cross-section drawn from measurements made with the point probe is shown in Figure 13. In terms of the 0.05 temperature rise contour in Figure 13, the jet has spread laterally from $y'/b_o = 1.25$ to $y'/b_o = 20.0$, while vertically the jet has spread from $z/b_o = 1.25$ to $z/b_o = 2.75$. Thus, for this representative cross-section, the rate of lateral mixing is 7.3 times greater than the rate of vertical mixing, which is approximately a full order of magnitude.

Vertical temperature profiles were measured with the point probe at several points along the jet centerline for each run. The representative profiles shown in Figure 14 indicate that vertical entrainment is small, since the jet does not spread vertically along the jet axis. If vertical entrainment were significant, then the temperature profiles shown in Figure 14 would indicate more and more vertical mixing with distance along the jet axis. Visual observation also indicated the limited extent of vertical mixing, as seen in Figure 15.

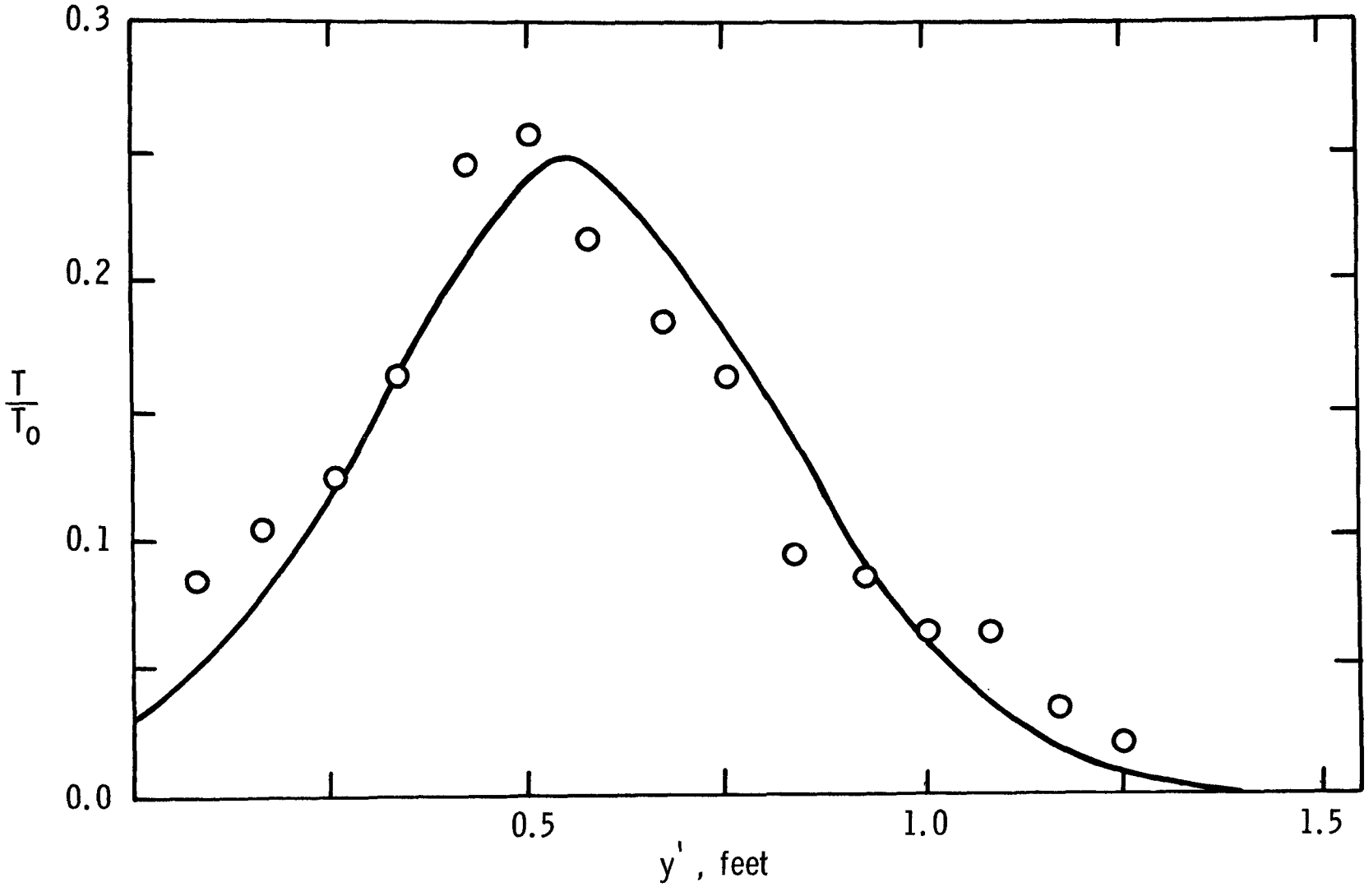

FIGURE 12.--OBSERVED TEMPERATURE DISTRIBUTION AND FITTED GAUSSIAN CURVE AT s'/b_o = 35.3, RUN 3-60-1

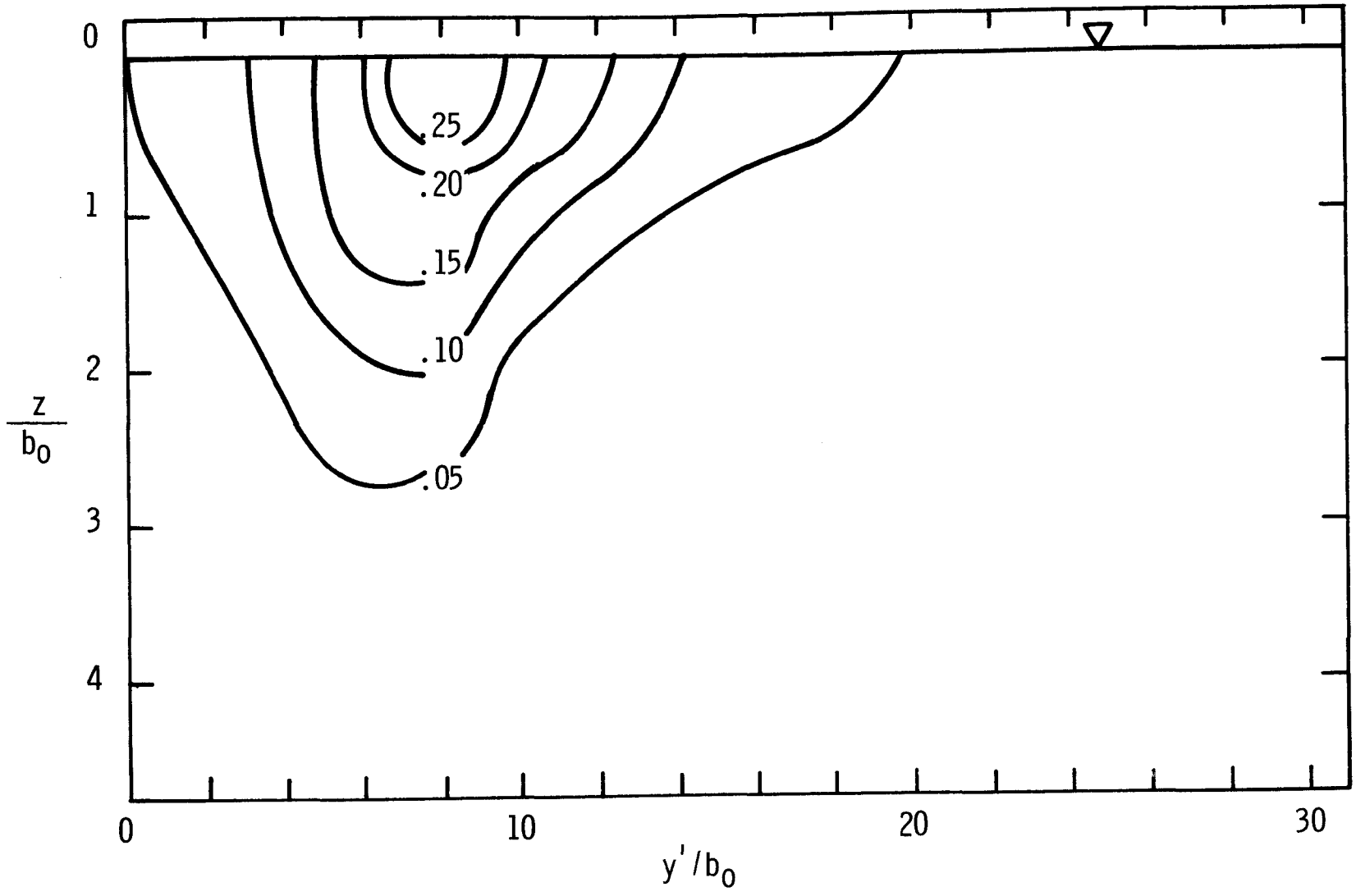

FIGURE 13.--TEMPERATURE DISTRIBUTION AT s'/b_o = 35.3, RUN 3-60-1, T/T_o

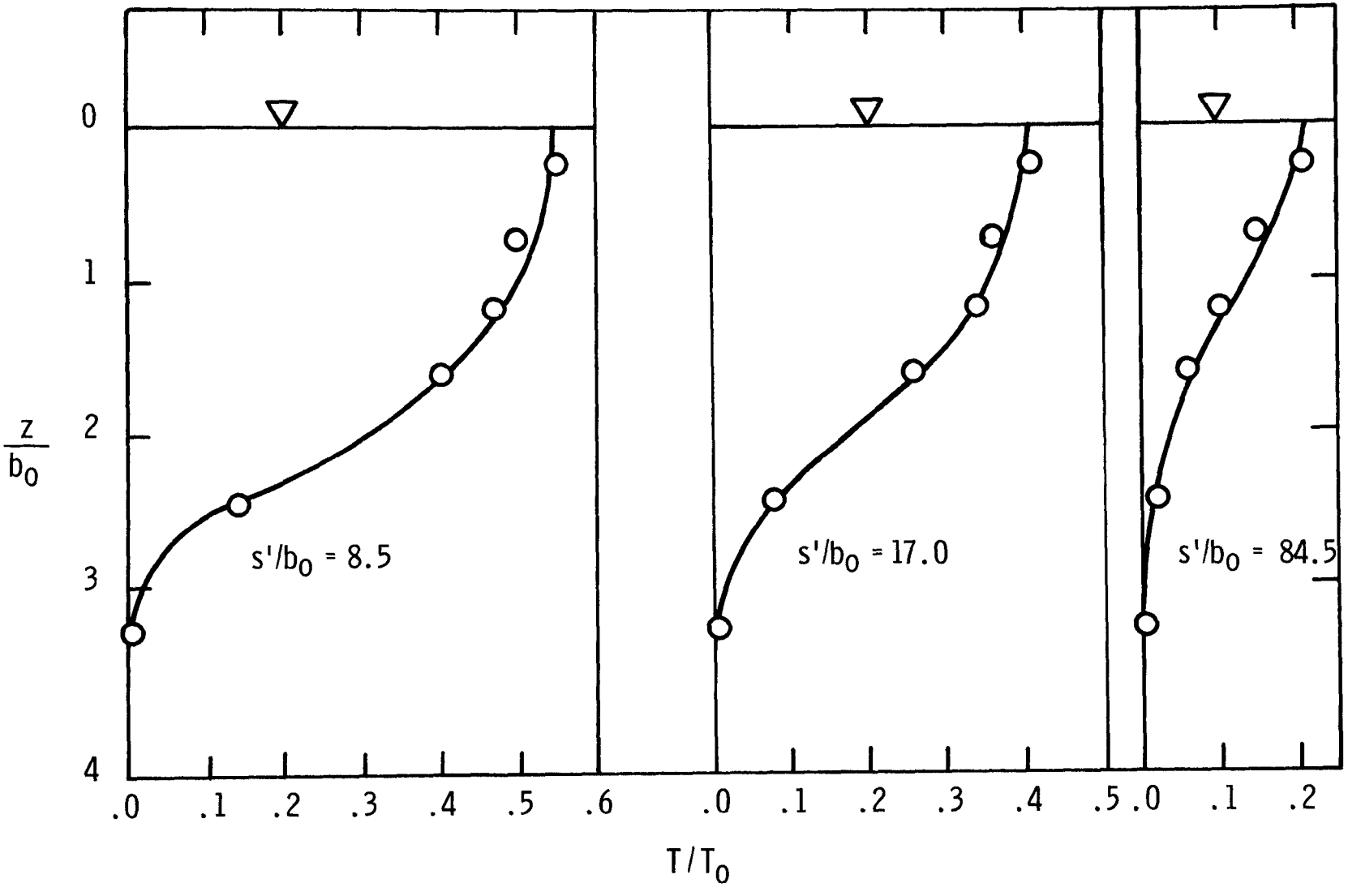

FIGURE 14.--VERTICAL TEMPERATURE PROFILES, RUN 1-60

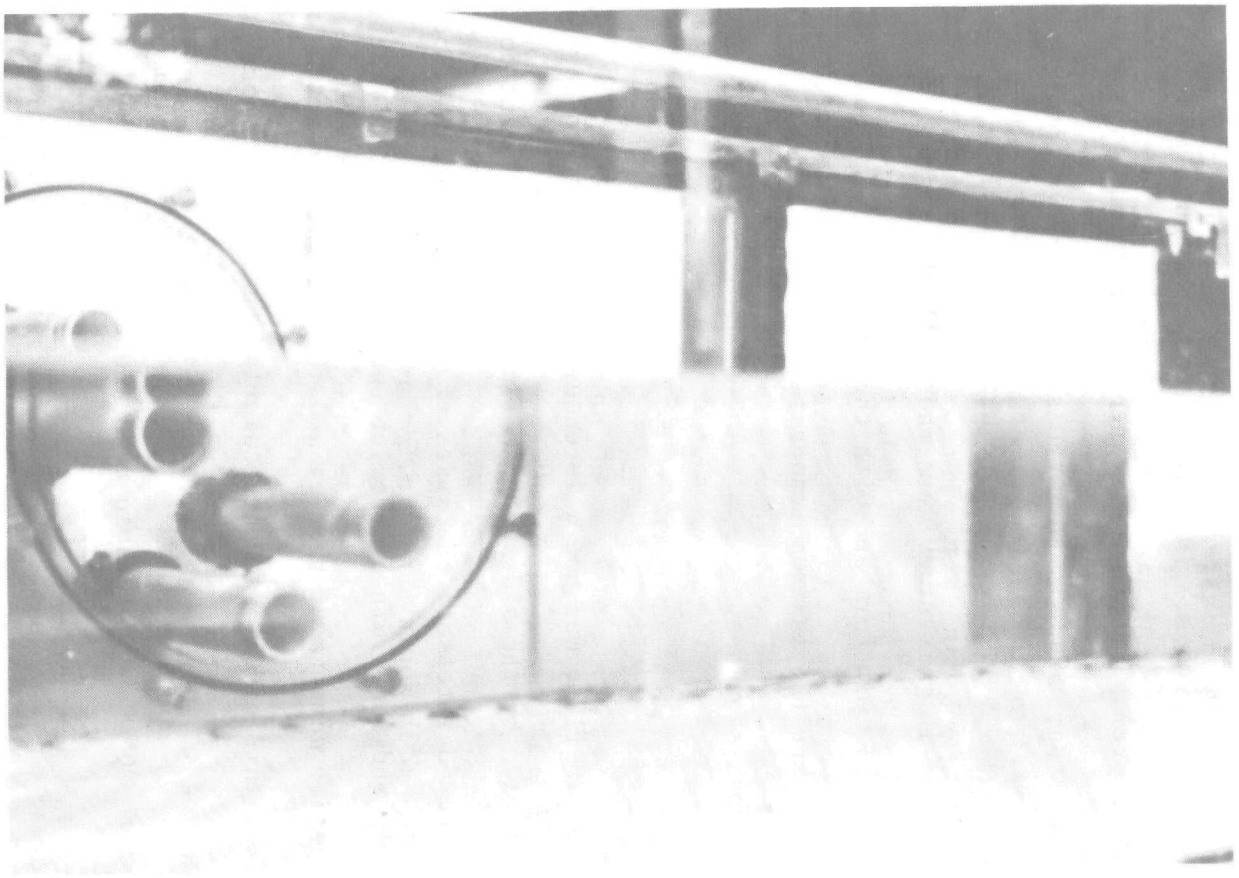

FIGURE 15.--TWO-DIMENSIONAL SURFACE JET, RUN 3-90

The vertical temperature profiles in Figure 14 also indicate that temperature measurements made just below the water surface with the point probe should agree with measurements taken just below the surface with the larger set of probes. The larger probes measure average temperature values over a vertical distance of approximately $z/b_o = 0.5$. The reason for this agreement is that the slope of the vertical profiles over this depth is almost zero. As a result, the centerline values of temperature reported in this study were made with the larger probes mounted on the movable platform and with the point probe. These centerline values, then, are the maximum temperatures, laterally and vertically, in each of the cross-sections.

Geometry Effects

The laboratory flume was not wide enough for the jet to spread completely unaffected by the sides of the flume. At some point downstream, the jet would intersect the sides of the flume, and the location of the trajectory and the width of the jet would no longer be functions of only the relative momenta of the jet and the ambient current. As had been anticipated, this effect was particularly apparent for those runs where the value of $A = U_a/U_o$ was relatively small and the angle β_o' of the discharge equal to 90°, and for those runs where A was relatively large and β_o' equal to 45°.

Temperature measurements taken with the larger probes mounted on the movable platform at $x'/b_o = 33.8$ ($x' = 2.0$ feet), $x'/b_o = 50.7$ ($x' = 3.0$ feet), and farther downstream showed a tendency for the trajectories to converge along the sides of the flume. Also, the exact

lateral location of the maximum temperature rise in the cross-sections from the measured lateral distributions was difficult to determine. As a result, data for the observed trajectories at $x'/b_o = 33.8$ and beyond were not used in locating the jet centerline or in determining the drag coefficient, C_D. However, the decrease in the temperature rise due to lateral mixing as far downstream as $x'/b_o = 84.5$ ($x' = 5.0$ feet) seemed to be relatively unaffected by the sides of the flume, and these data, taken with the larger probes, were used, along with values taken from $x'/b_o = 0.0$ to $x'/b_o = 16.9$ with the point probe, in determining the value of the entrainment coefficient, E.

Width Measurements

The width of the jet was determined from measurements made with the eleven probes mounted on the movable platform. At each of several points along the jet, measurements were made of the lateral temperature distribution, and then the standard deviation of the temperature rise in terms of T'/T_o was computed. Then, values of b/b_o were calculated using $b_o = 0.71$ inches and Equation 24,

$$b = \sqrt{2}\,\sigma \tag{24}$$

Determination of the Zone of Flow Establishment and the Entrainment and Drag Coefficients

Graphical methods were used to determine the parameters and coefficients from the laboratory data and from numerical solutions of the mathematical model.

Trajectories and Temperature Plots.-- The jet trajectory for each run was determined from the measured location of the maximum temperature in each cross-section taken along the jet axis. These data points were plotted relative to the jet origin in terms of x'/b_o and y'/b_o. A smooth curve was fitted through the observed points on the jet centerline by using an n-th order polynomial fitting routine. Next, the temperature data were plotted on log-log plots in terms of T/T_o vs. s'/b_o, where s'/b_o had been measured for each data point along the fitted y'/b_o vs. x'/b_o curves.

Zone of Flow Establishment.-- The length of the zone of flow establishment in terms of s'_e/b_o for each run was measured by examining the data points on the T/T_o vs. s'/b_o curve and interpolating to the largest value of s'/b_o where T/T_o was still equal to 1.0. This measured value of s'/b_o was the length of the zone of flow establishment, or s'_e/b_o.

The angle, β_o, at the end of the zone of flow establishment was determined for each run by using the value of s'_e/b_o from the T/T_o vs. s'/b_o plot and measuring this distance along the fitted trajectory curve from $x'/b_o = y'/b_o = 0.0$. The angle at this value of s'_e/b_o was measured, giving the value of the angle at the beginning of the established jet flow, or β_o, The rectangular coordinates x'_e/b_o and y'_e/b_o were also measured at this value of s'_e/b_o.

Entrainment Coefficient.-- To determine the value of the entrainment coefficient, numerical solutions of T/T_o vs. S were computed and plotted on a log-log scale for each observed value of A and β_o. A preliminary

value of E for each run was determined by over-laying the predicted T/T_o vs. S curve with the observed T/T_o vs. s'/b_o data plot. A set of corresponding values of S and s'/b_o was noted after sliding the T/T_o vs. s'/b_o plot horizontally until the best fit of the data and the theoretical curve was obtained. Then, Equation 37 was solved for E,

$$E = (\sqrt{\pi}\, S/2) \;/\; (s/b_o) \tag{37}$$

Next, the value of S'_e, which is the length of the establishment zone in non-dimensional form, was calculated from the observed value of s'_e/b_o, the preliminary value of E, and Equation 67,

$$S'_e = (2E/\sqrt{\pi}\, b_o)s'_e \; . \tag{67}$$

The T/T_o vs. S plot, which is referenced to the beginning of the jet flow region, was then redrawn as T/T_o vs. S', referenced to the jet origin, using the value of S'_e and Equation 68,

$$S' = S'_e + S \tag{68}$$

A set of corresponding values of S' and s'/b_o was noted after sliding the T/T_o vs. s'/b_o plot horizontally over the T/T_o vs. S' curve until the best fit of the data and the theoretical curve was obtained. Then, Equation 69 was solved for the final value of E,

$$E = (\sqrt{\pi}\, S'/2) \;/\; (s'/b_o) \tag{69}$$

Drag Coefficient.-- To determine the value of the drag coefficient, C_D, for each run, numerical solutions of X and Y were computed along

with the T/T_o solutions for each value of A and β_o. For each run, at least two numerical solutions for two different assumed values of the reduced drag coefficient, C_D', were computed. Each of the predicted trajectories was plotted in terms of x'/b_o and y'/b_o, using Equation 42 to calculate x/b_o and y/b_o,

$$X = (2E/\sqrt{\pi}\, b_o)x \quad ; \quad Y = (2E/\sqrt{\pi}\, b_o)y \tag{42}$$

and then using Equations 70 and 71 to calculate x'/b_o and y'/b_o,

$$x'/b_o = x/b_o + x_e'/b_o \tag{70}$$

$$y'/b_o = y/b_o + y_e'/b_o \tag{71}$$

This was possible since the value of E, and x_e'/b_o and y_e'/b_o had already been determined from the temperature plots.

The observed value of the reduced drag coefficient for each run was determined by over-laying the predicted trajectories with the observed jet trajectory. The value of C_D' was chosen by interpolating between the predicted trajectories to the observed trajectory. For example, if the values $C_D' = 0.5$ and 1.0 were assumed in obtaining two predicted trajectories, and if the observed trajectory were located exactly half-way between the two predicted trajectories, then the observed value would be $C_D' = 0.75$.

The value of the drag coefficient, C_D, for each run was obtained from the observed values of E and C_D' and Equation 39,

$$C_D' = C_D/4E \tag{39}$$

Width of the Jet

The predicted and observed values of b/b_o were then plotted. The numerical solution obtained for each run predicted b/b_o vs. S. Predicted values of b/b_o vs. s'/b_o were calculated and plotted as smooth curves by using the observed values of E and S'_e determined for each run from the centerline data and Equations 68 and 69,

$$S' = S'_e + S \tag{68}$$

$$S' = (2E/\sqrt{\pi}\, b_o)s' \tag{69}$$

Then, the observed values of b/b_o vs. s'/b_o were plotted on the same figure.

Presentation of Results

Trajectories, and Temperature and Width Plots

The trajectories and temperature plots, from which the values of C'_D and E were determined, and the width plots are presented in Figures 16 and 17 for a representative laboratory run and in Appendix C for the other cases. The data points which indicate the observed trajectory for each run are plotted on the same figure as the fitted trajectory computed from the numerical solution. The observed T/T_o vs. s'/b_o data for each run are plotted on the same figure as the fitted T/T_o curve computed from the numerical solution. The observed b/b_o vs. s'/b_o data for each run are plotted on the same figure as the predicted b/b_o curve also computed from the numerical solution.

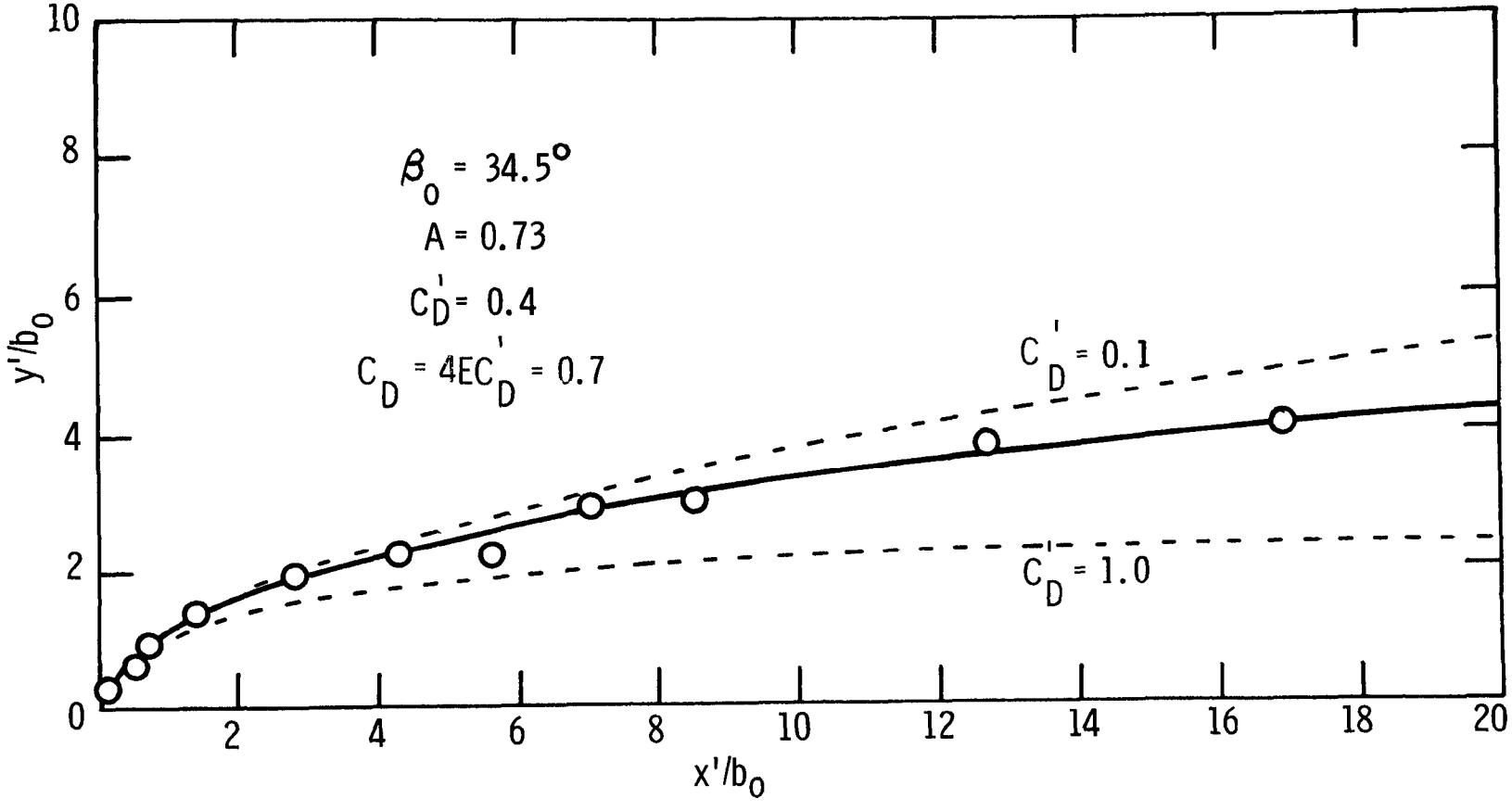

FIGURE 16.--OBSERVED AND FITTED TRAJECTORIES, RUN 1-90

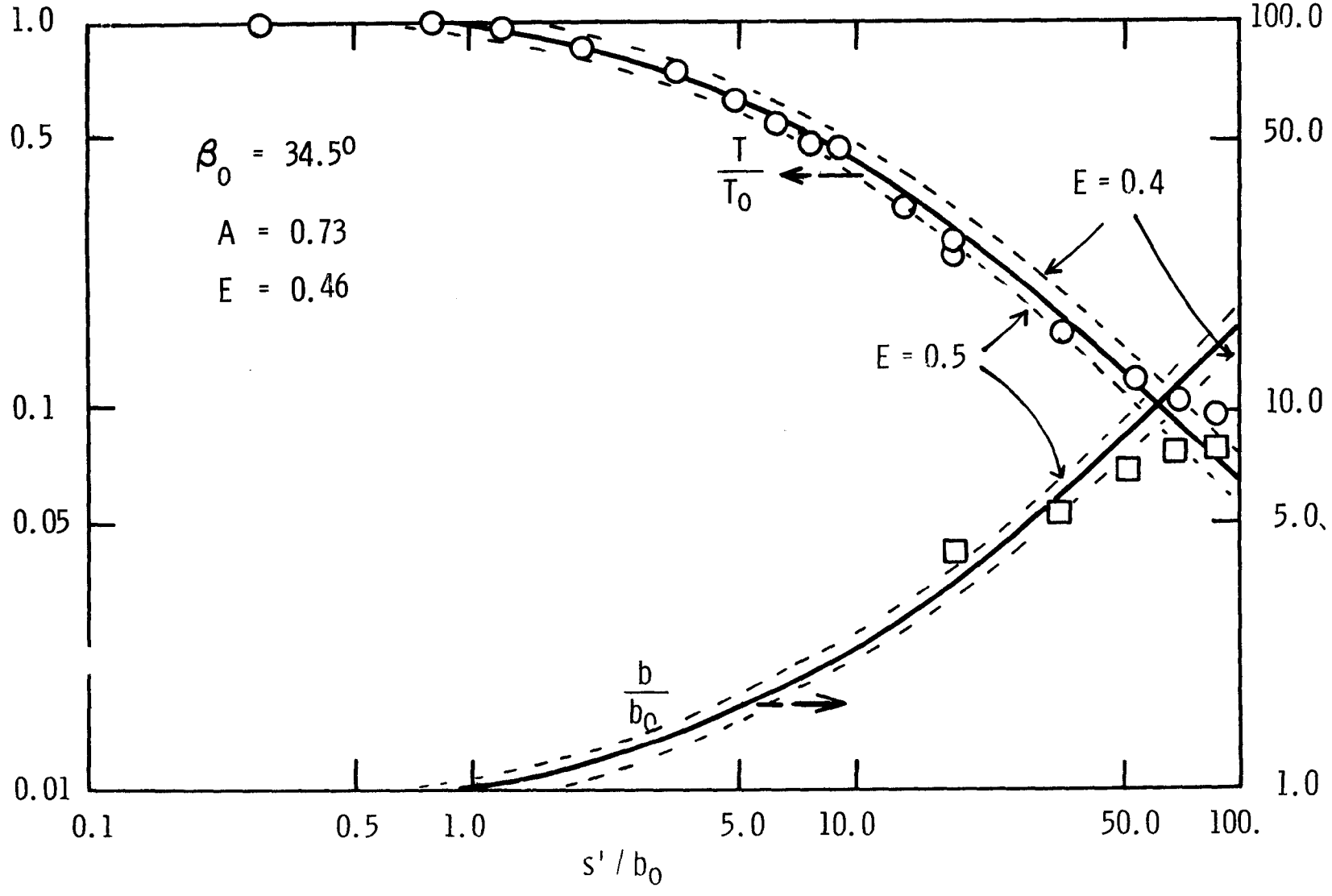

FIGURE 17.--OBSERVED VALUES AND FITTED CURVES FOR TEMPERATURE AND WIDTH, RUN 1-90

Parameters

The values of the various parameters as determined from the laboratory data are presented in tabular form. The values of A, β_o, s'_e/b_o, x'_e/b_o, and y'_e/b_o are presented in Table 2. The corresponding best-fit values of E and C'_D, the values of S'_e calculated from Equation 67 and X'_e and Y'_e calculated from Equation 72,

$$X'_e = (2E/\sqrt{\pi}\, b_o)x'_e \quad ; \quad Y'_e = (2E/\sqrt{\pi}\, b_o)y'_e \tag{72}$$

and values of C_D calculated from Equation 39 are also presented in Table 2.

Relation of Parameters to A and β'_o

The object of the laboratory experiments was to determine how the establishment zone and the entrainment and drag coefficients are related to the velocity ratio and to the discharge angle. The experimentally-determined values of s'_e/b_o and β_o/β'_o are related to A as shown in Figures 18 and 19, respectively. The values of C'_D are plotted as a function of A in Figure 20, and the values of the drag coefficient, C_D, are related to A as shown in Figure 21. The correlation coefficients of the relations and the correlation coefficient at the 1% level of significance are shown in Table 3. These correlation coefficients were obtained using a regression analysis routine, which gives the correlation coefficients and predicted values for assumed arithmetic, semi-log, and log-log relations between the dependent and independent variables. The assumed relation which gave the highest correlation is the relation presented in each of Figures 18, 19, and 21. The regression analysis

TABLE 2

LABORATORY RESULTS

A	β_o'	β_o	s_e'/b_o	x_e'/b_o	y_e'/b_o	E	S_e'	X_e'	Y_e'	C_D'	C_D
0.73	90.0	34.5	0.9	0.6	0.8	0.46	0.47	0.31	0.41	0.4	0.7
0.44	90.0	47.5	1.4	0.6	1.3	0.39	0.62	0.26	0.57	1.0	1.6
0.30	90.0	50.0	1.3	0.6	1.3	0.31	0.46	0.21	0.45	2.8	3.5
0.23	90.0	62.0	1.7	0.4	1.7	0.47	0.90	0.21	0.90	2.0	3.8
0.20	90.0	71.5	1.9	0.1	2.0	0.44	0.94	0.05	0.99	2.0	3.5
0.67	60.0	13.5	0.7	0.6	0.3	0.24	0.24	0.19	0.16	0.08	0.1
0.44	60.0	36.5	1.3	0.9	0.8	0.13	0.19	0.13	0.12	1.5	0.8
0.30	60.0	40.0	1.5	1.2	1.0	0.19	0.32	0.26	0.21	3.0	2.3
0.23	60.0	41.0	2.0	1.4	1.3	0.25	0.56	0.39	0.37	2.7	2.7
0.19	60.0	45.0	2.3	1.4	1.9	0.29	0.75	0.46	0.62	3.4	3.9
0.66	45.0	25.0	0.7	0.6	0.4	0.19	0.15	0.13	0.08	1.5	1.1
0.42	45.0	23.0	1.2	1.1	0.6	0.13	0.18	0.16	0.09	1.0	0.5
0.30	45.0	26.5	1.7	1.5	0.8	0.21	0.40	0.36	0.19	1.0	0.8
0.23	45.0	33.5	2.1	1.6	1.1	0.27	0.64	0.49	0.33	1.0	1.1
0.18	45.0	35.0	2.3	1.8	1.3	0.22	0.57	0.45	0.32	2.0	1.7

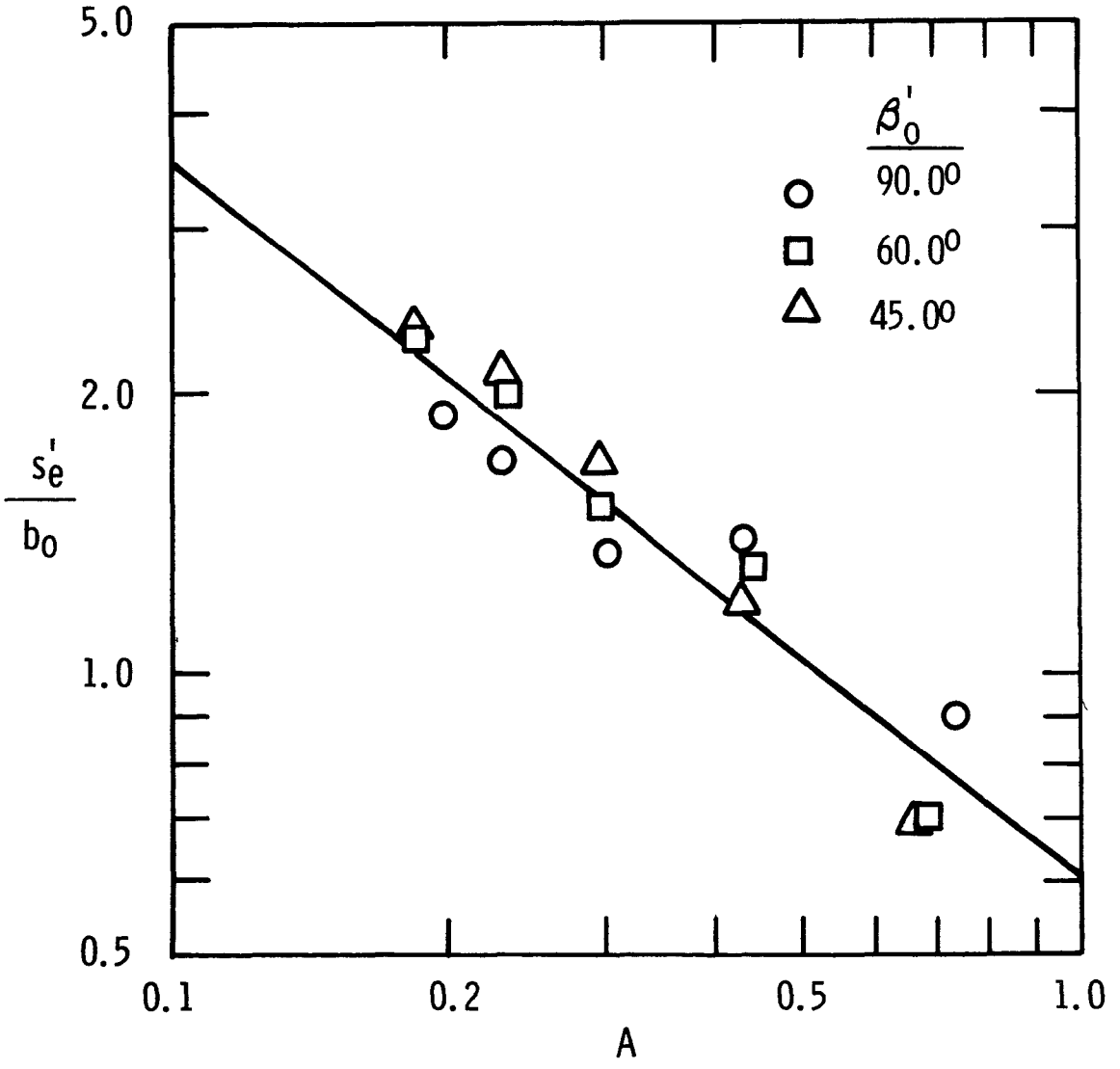

FIGURE 18.--OBSERVED VALUES AND FITTED CURVE FOR LENGTH OF ESTABLISHMENT ZONE VERSUS VELOCITY RATIO

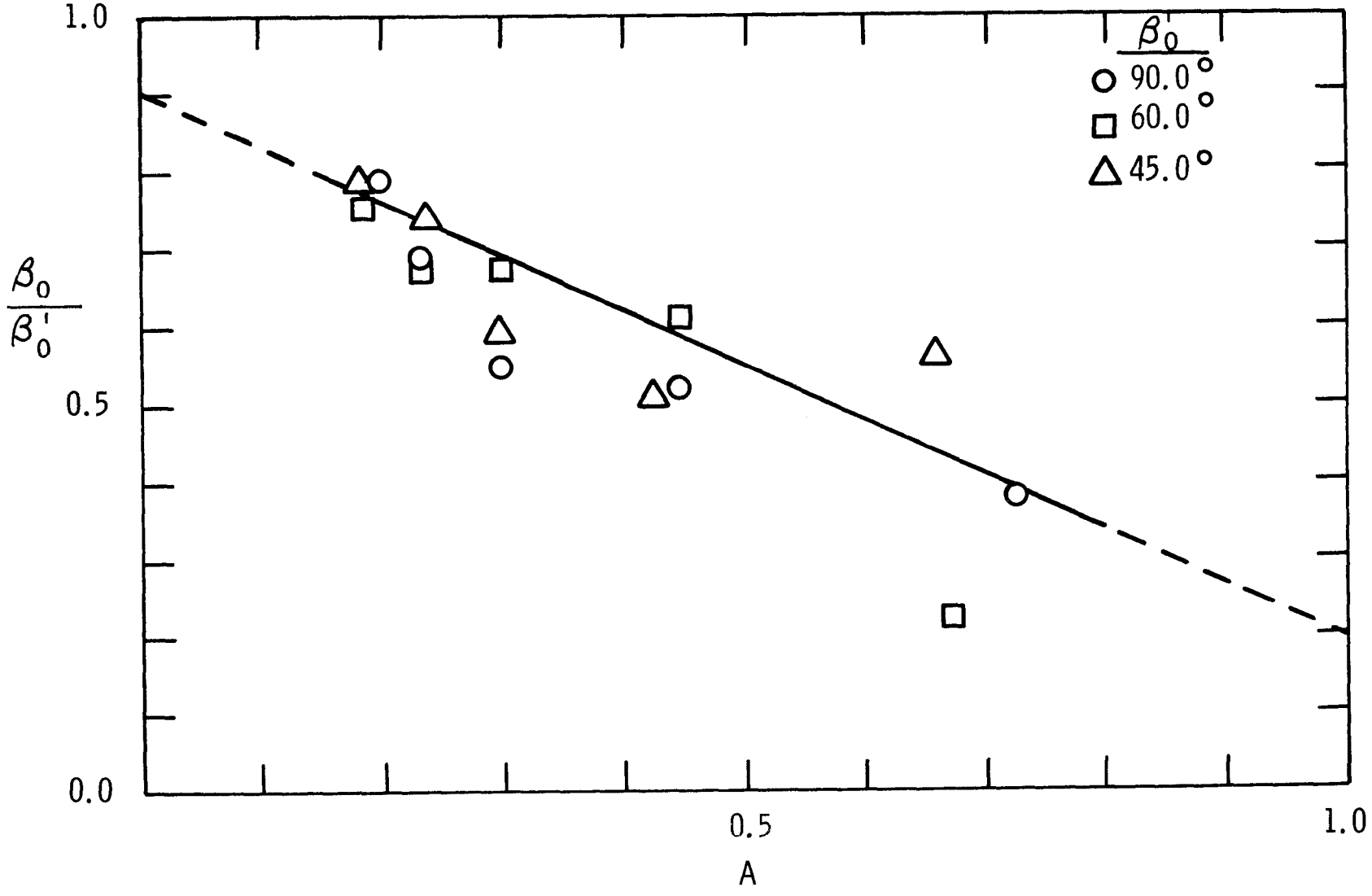

FIGURE 19.--OBSERVED VALUES AND FITTED CURVE FOR INITIAL ANGLE VERSUS VELOCITY RATIO

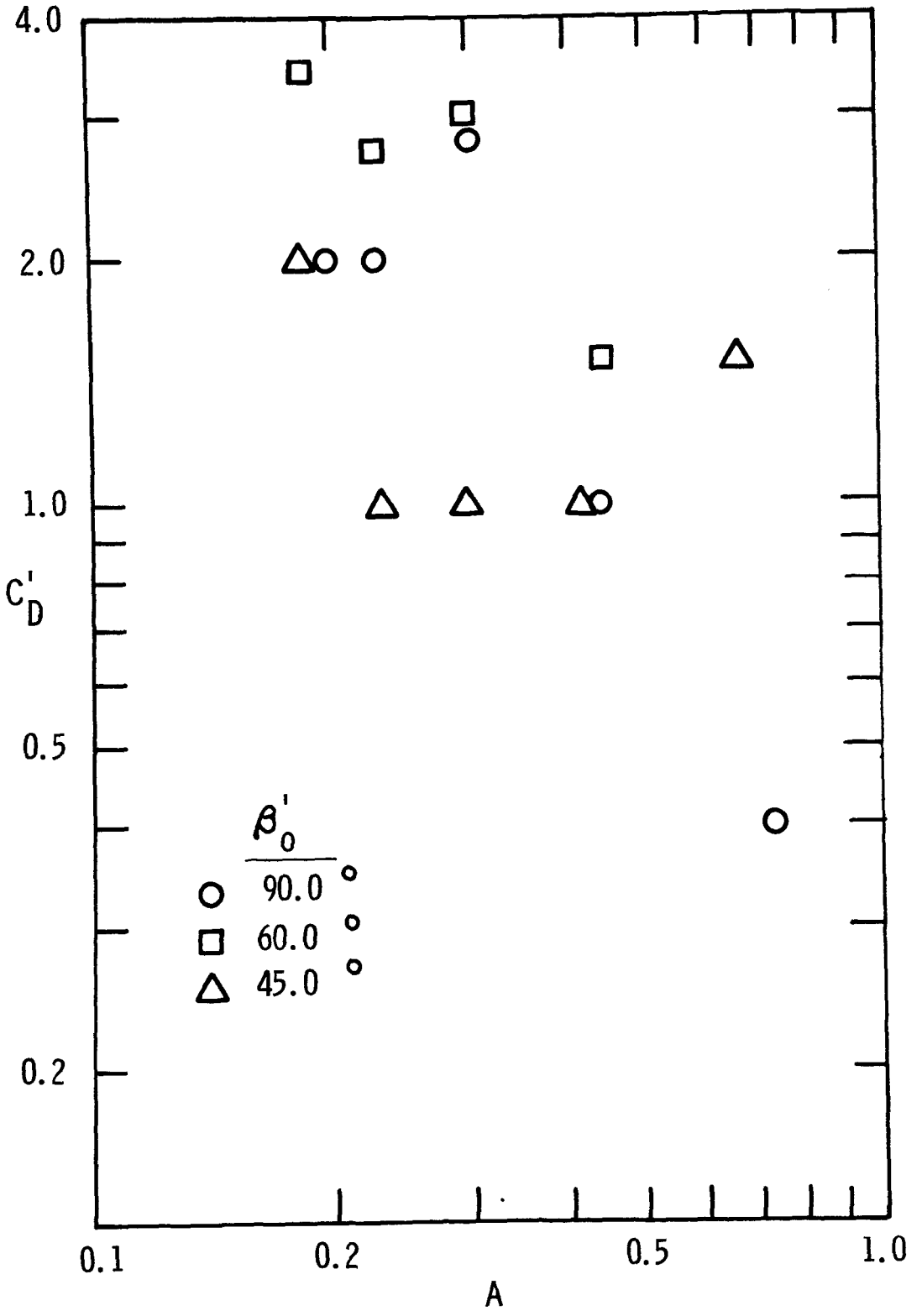

FIGURE 20.--OBSERVED VALUES OF REDUCED DRAG COEFFICIENT VERSUS VELOCITY RATIO

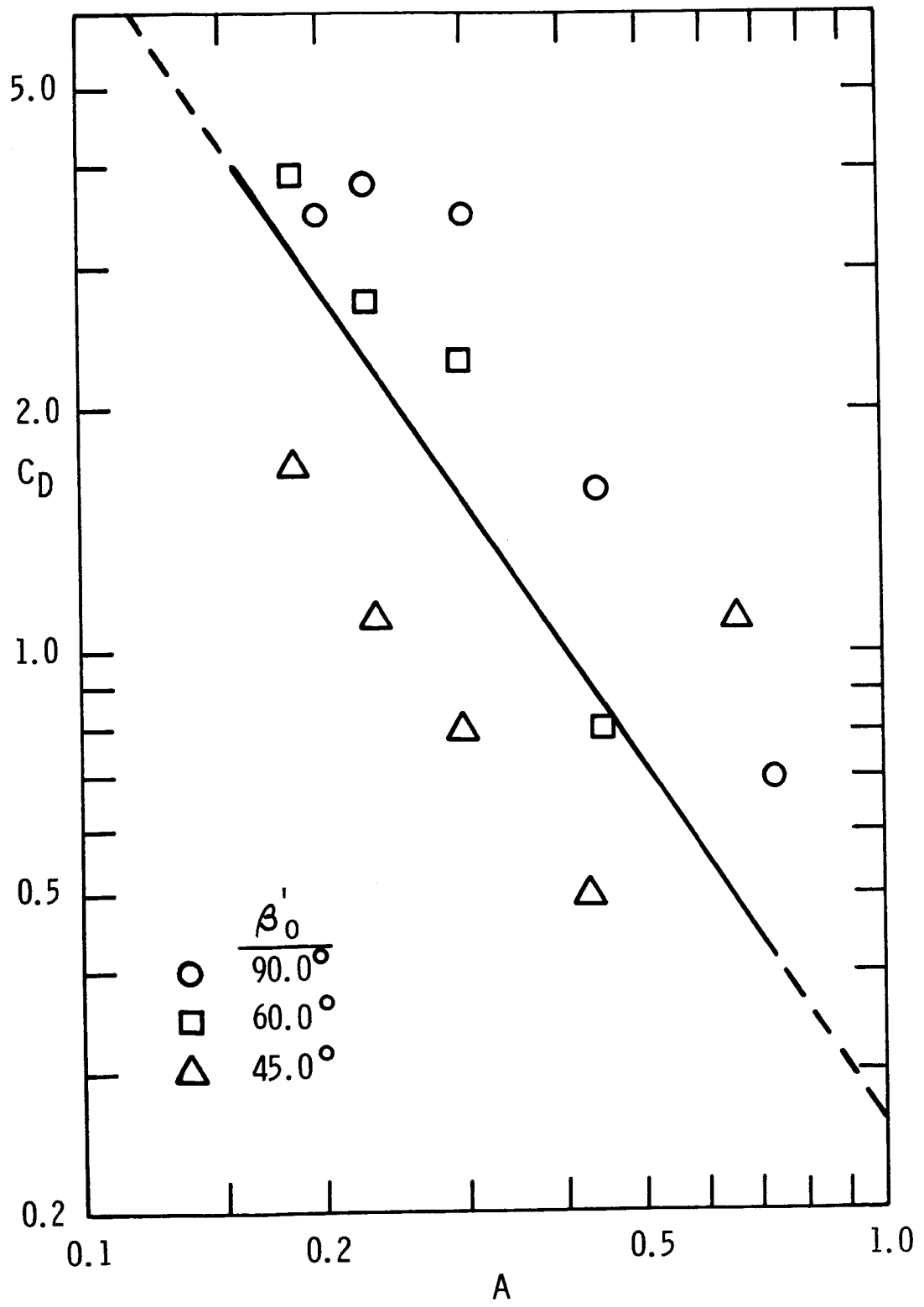

FIGURE 21.--OBSERVED VALUES AND FITTED CURVE FOR DRAG COEFFICIENT VERSUS VELOCITY RATIO

also indicated, as shown in Table 3, that the entrainment coefficient, E, does not appear to be a function of A over the range of A investigated in this study.

TABLE 3

RESULTS OF STATISTICAL TESTS ON PARAMETERS

Relation	Observed Correlation Coefficient	Correlation Coefficient at 1% Level of Significance
s'_e/b_o vs. A	0.95	0.64
β_o/β'_o vs. A	0.87	0.64
C_D vs. A	0.72	0.64
E vs. A	0.01	0.64
C_D vs. A ($\beta'_o = 90.0°$)	0.98	0.96
C_D vs. A ($\beta'_o = 60.0°$)	0.97	0.96
C_D vs. A ($\beta'_o = 45.0°$)	0.99	0.96

Examination of Figure 21 indicates that C_D may be a function of β'_o, the initial angle of discharge, as well as a function of A. This possible relation was tested, and the results are shown in Figure 22. The correlation coefficients, which are presented in Table 3, are good. However, because of the small number of data points, the confidence limits of each of the curves plotted in Figure 22 tend to overlap, and the relation of C_D to β'_o as well as to A cannot be conclusively established from this study.

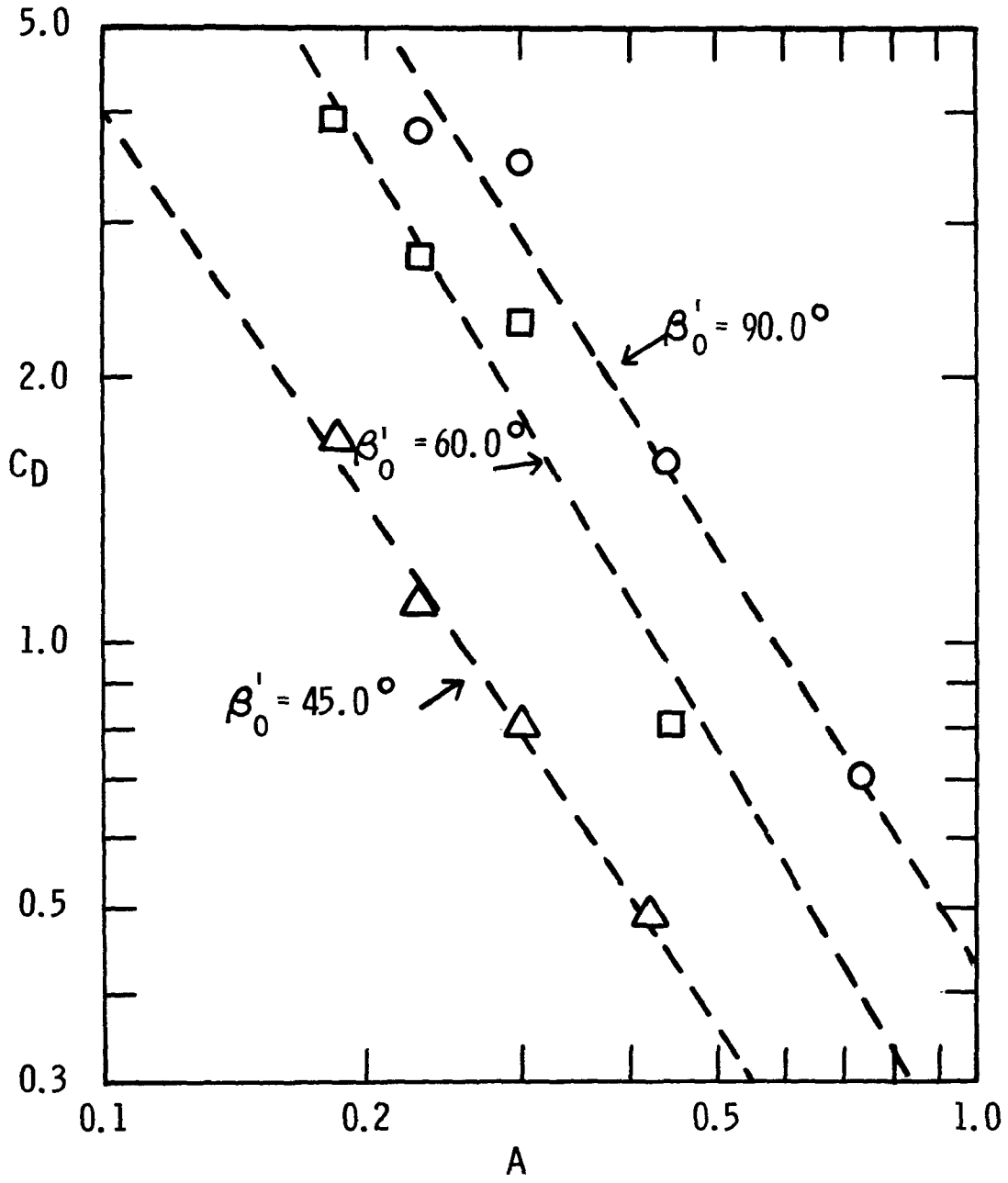

FIGURE 22.--OBSERVED VALUES AND FITTED CURVES FOR DRAG COEFFICIENT VERSUS VELOCITY RATIO AND DISCHARGE ANGLE

A dependence of E on the initial angle of discharge was indicated by an F test, which was used to compare the variances of the experimentally-determined values of E for each of the three discharge angles. The results of the F test are presented in Table 4, and they show that the mean value of E at $\beta_o' = 90°$ is significantly different from the mean of the values obtained at $\beta_o' = 60°$ and 45°. Thus, E appears to be a function of β_o'.

TABLE 4

RELATION OF E TO β_o'

β_o'	$\overline{E}$	F Ratio	Level of Significance
90°	0.41		
		23.1	0.1%
60°	0.22		
		0.20	None
45°	0.20		

CHAPTER VI

FIELD SURVEYS

Data were obtained from five surveys at three different steam-electric generating plants. Data from three of the surveys were collected by Vanderbilt University (VU) personnel (37), and data from the other two surveys were taken from reports written by Churchill (45) and Beer and Pipes (6).

Description of VU Surveys

Flowrates

The field surveys were made on regulated river systems over a period of time when plant discharge and river flowrate were maintained very near to steady-state conditions. Stream flowrates were not measured in the field but were determined from data provided by the regulating agency. Plant flowrates were determined from pumping records routinely kept by plant personnel.

Geometry

River and discharge channel geometries were determined from field measurements and from maps. Ground control was established using a transit and a stadia rod to lay out a base line which paralleled the river along one bank for a distance extending several thousand feet downstream. From this base line, stations were located which were perpendicular to the river centerline and, if possible, to the jet

centerline. At each of these stations, the cross-sectional area of the channel was determined using a Raytheon portable recording fathometer carried in one of the survey boats. From the base line measurements, the longitudinal location of each of the cross-sections could be plotted on a scale drawing traced from a U. S. Geological Survey (USGS) 1:24000 scale map of the area. In addition, the initial angle, β_o', of the discharge channel was measured from these maps.

Velocity Data

Measurements were made to determine the magnitude and direction of the initial jet velocity, U_o, and the ambient velocity, U_a.

The magnitudes of U_a and U_o were determined by two methods. By the first method, the magnitudes of the velocities were measured at a cross-section in the discharge channel and at a river cross-section just upstream from the discharge. The measurements were made with a Price current meter mounted on one of the survey boats. Lateral stations within each cross-section were located using anchored buoys whose lateral distance from the bank had been measured either with a transit on the bank and a stadia rod held in the boat or by means of timed runs from the bank in the boat. Vertical distances were measured using the cable to which the velocity meter was attached. Ideally, this first method should have given detailed velocity profiles from which spatially-averaged ambient and initial jet velocities could be determined.

By the second method, magnitudes of the velocities were calculated indirectly using the cross-sectional areas obtained from the depth-sounding records and the flowrates obtained from gauging station

and power plant records. This second method yielded average values of U_o and U_a which were in close agreement with the values obtained by the first method.

The directions of U_o and U_a were measured from the map of the area. This method was chosen because the velocity vectors could not be measured directly.

Temperature Distribution

Temperature measurements were made at each of the cross-sections using Whitney temperature probes carried in the survey boats. Lateral stations were located using the anchored buoys, while vertical measurements were made using the cable to which each of the probes was attached. Approximately 100 measurements were made in each of the cross-sections.

Procedure

The normal procedure for the field surveys involved most of two days spent on preliminary work and most of a third day spent obtaining the temperature and velocity data. The preliminary work involved laying out the base line, locating the cross-sections, making a depth-sounding record across the channel at each of the cross-sections, and setting out the buoys. The distance from the base line to each of the buoys was then measured. The temperature and velocity data were measured on the last day during the time when steady plant and river discharges were maintained. Normally, one boat and at least three men were required for the preliminary work, while three boats -- one to measure velocities and two to measure temperatures -- and as many as eight or nine men were required on the third day. The field surveys were quite extensive in scope

and recorded considerable data, which were used in other studies in addition to this present study.

Results of the Widows Creek Surveys

Introduction

Data were collected by VU and USGS personnel on November 20 and 21, 1968, and by TVA personnel on August 30, 1967, at TVA's Widows Creek Steam Plant. The data for the VU surveys were obtained from a report by Polk (37) and for the TVA survey from the report by Churchill (45). At this plant, cooling water from the condensers is discharged into a small coal-barge harbor and flows directly onto the river surface with a minimum of mixing. Velocity measurements taken at several stations in the river indicated that the velocity field of the receiving ambient water body was influenced by the discharge. Since the discharged heat was initially advected across the river almost perpendicularly to the river flow, its spatial distribution can be described in terms of a jet discharging at some initial angle to the ambient flow. Temperature measurements indicated that the rate of lateral spreading for the first 5000 feet downstream was approximately 10 times greater than the rate of vertical spreading due to the buoyancy of the heated discharge. Thus, the application of the two-dimensional surface jet theory to describe a large, initial portion of the mixing zone is considered reasonable.

VU Survey Number 1, November 20

Temperature Measurements.-- The results of the temperature measurements are shown in Figures 23-28. The temperature contours at the

1.0-foot depth and the location of the cross-sections are shown in Figure 23. The vertical temperature profiles along the jet centerline, which is assumed to be located at the point of the maximum temperature in each cross-section for a distance of about 7000 feet downstream, are shown in Figures 24 and 25. The temperature contours for three of the downstream cross-sections are shown in Figures 26-28. The jet spread laterally from an initial discharge width on the order of 100 feet to a width of approximately 1200 feet, while it spread vertically from an initial depth on the order of 10 feet to almost 15 feet. Thus, the rate of vertical spreading was almost an order of magnitude less than lateral spreading and can be considered negligible for the first five downstream cross-sections, which is approximately 5000 feet. Beyond this point, it appears that the ambient turbulence of the stream can no longer be neglected, because vertical mixing began to take place.

Determination of Ambient Velocity.-- The value of the ambient velocity, U_a, was determined from the ambient flowrate, cross-sectional areas, and velocity measurements. The river flowrate at Widows Creek was estimated to be 26,170 cfs, which was the average flowrate during the period of the survey at Nickajack Dam, located about 20 miles upstream. The minimum flowrate at Nickajack was 26,000 cfs and the maximum approximately 27,000 cfs. The flow at Guntersville Dam, located approximately 60 miles downstream, was also maintained steady during the period of the field survey. Thus, the value of Q_r = 26,170 cfs is considered a reasonable estimate of the river flowrate. The value of the ambient flowrate past the discharge was calculated to be Q_a = 23,800 cfs

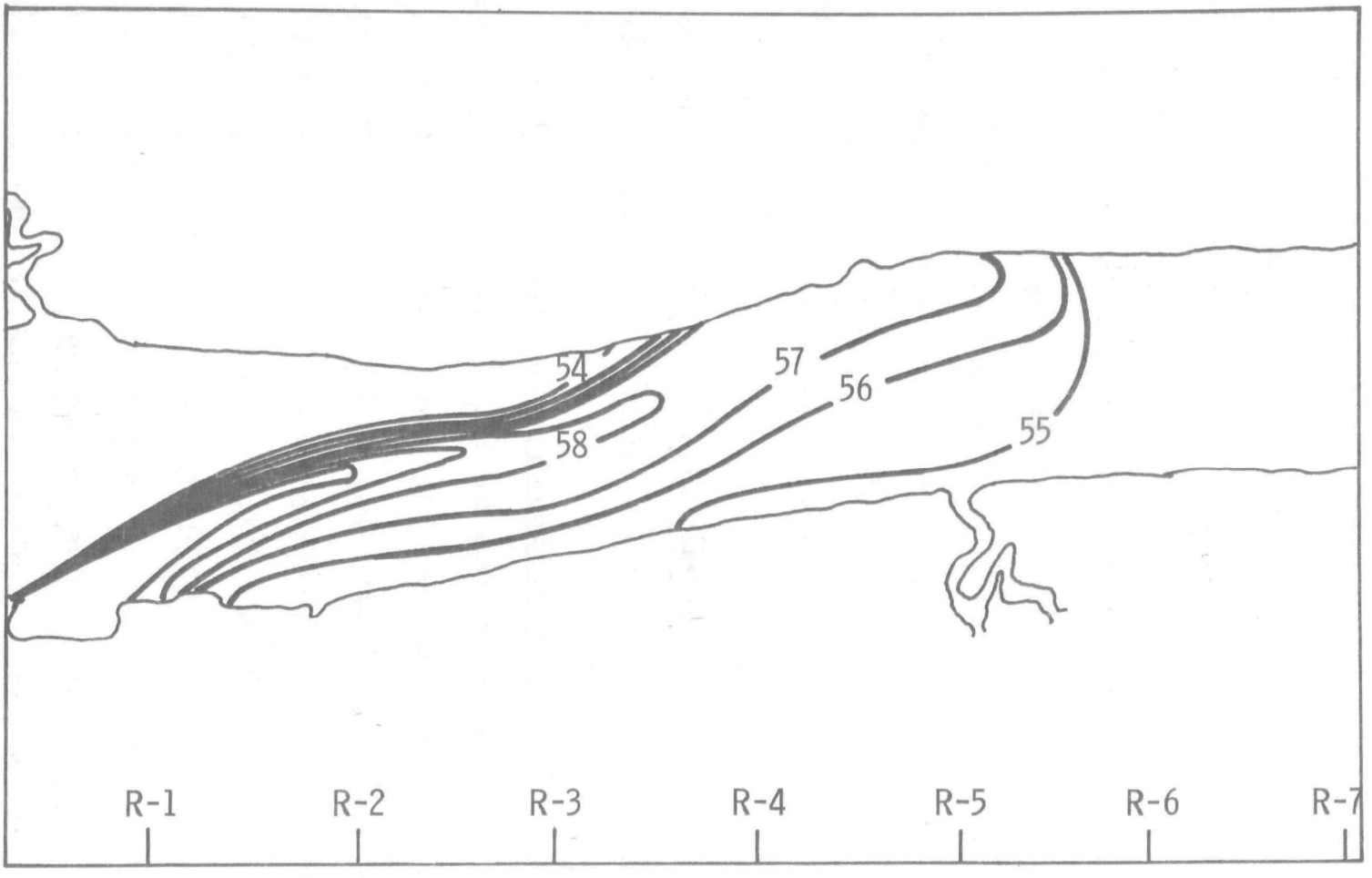

FIGURE 23.--TEMPERATURE DISTRIBUTION, °F, AT 1.0-FOOT DEPTH, WIDOWS CREEK, VU 1

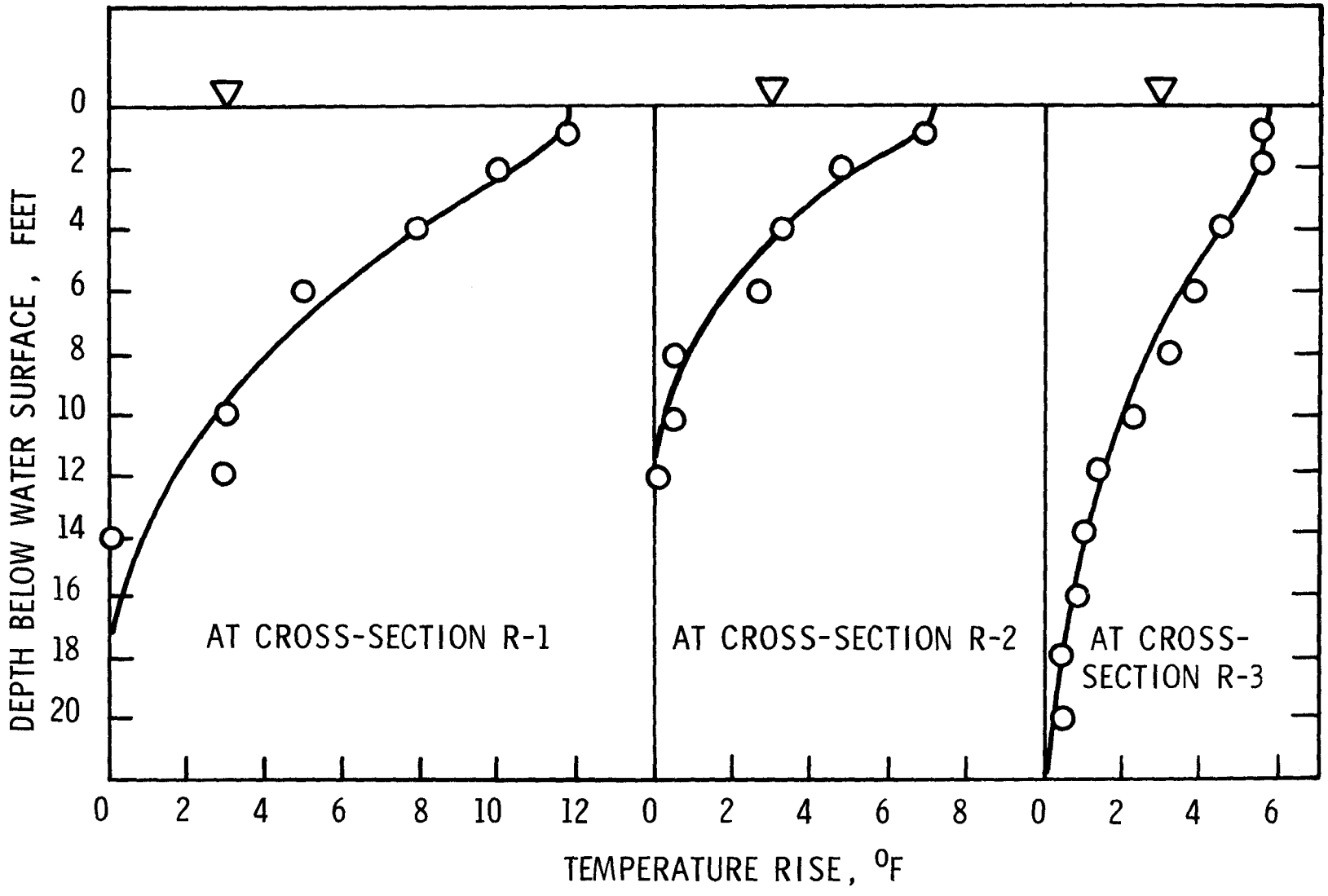

FIGURE 24.--TEMPERATURE RISE ALONG JET AXIS AT CROSS-SECTIONS R-1 TO R-3

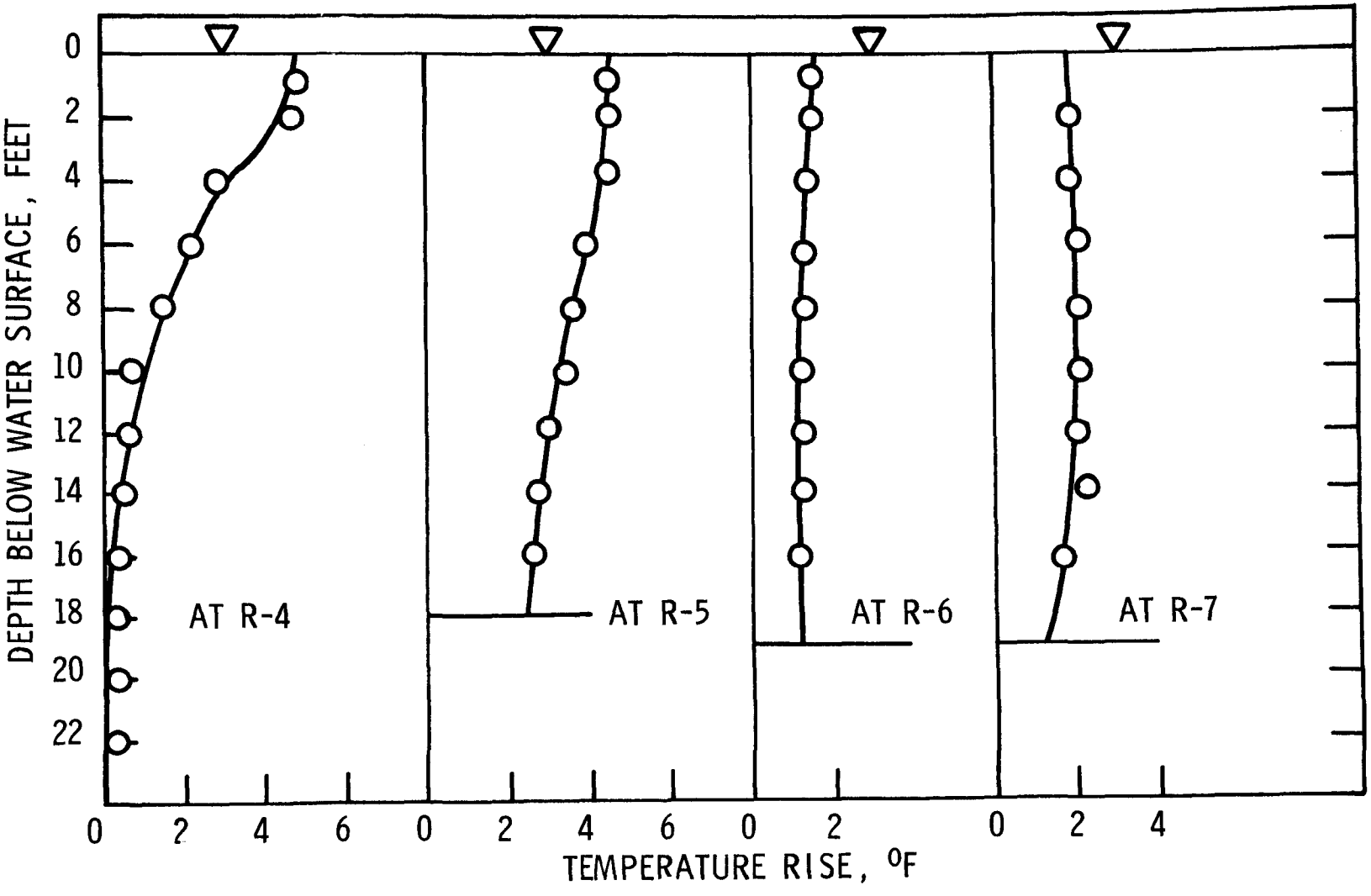

FIGURE 25.--TEMPERATURE RISE ALONG JET AXIS AT CROSS-SECTIONS R-4 TO R-7

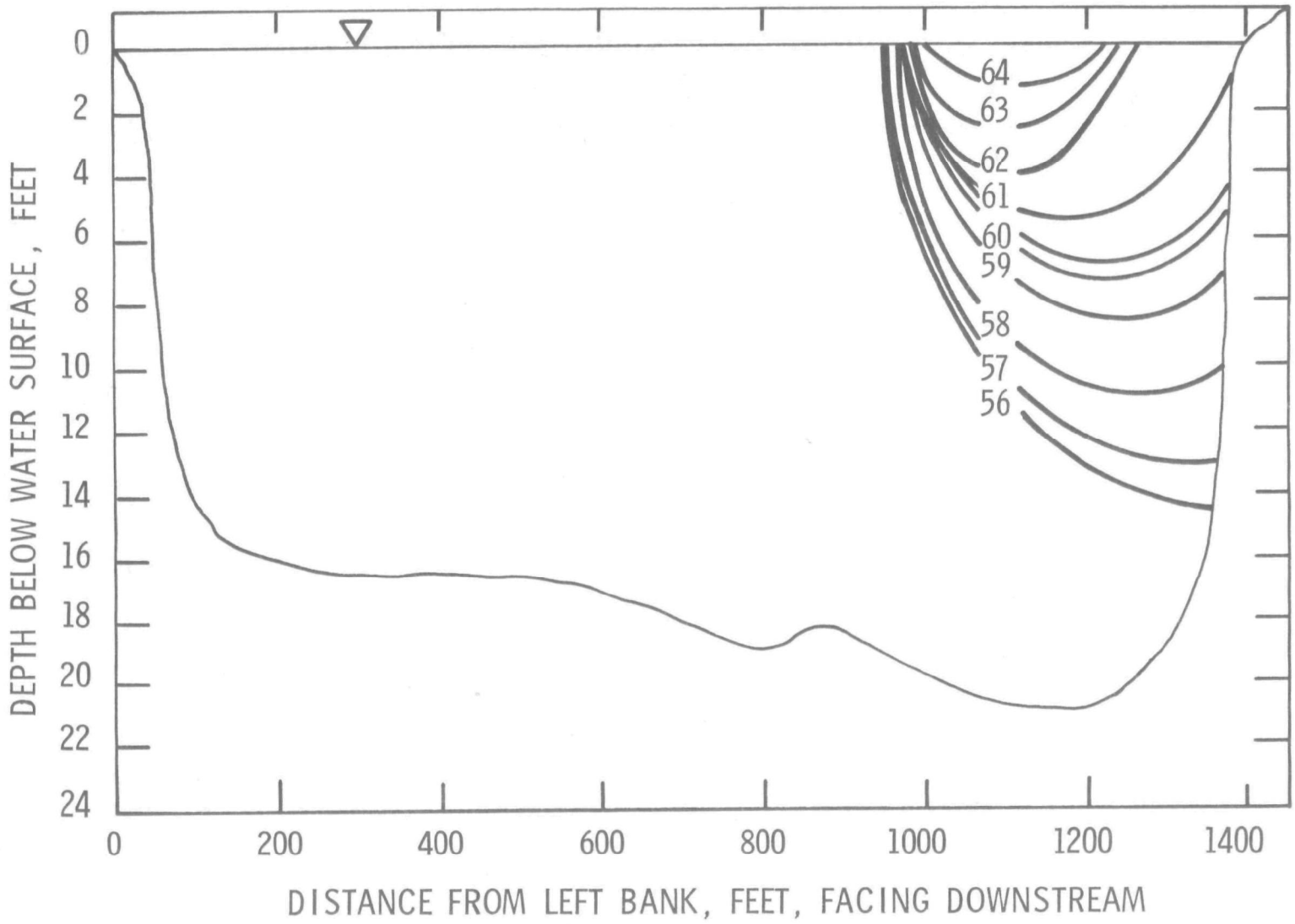

FIGURE 26.--TEMPERATURE DISTRIBUTION, °F, IN CROSS-SECTION R-1

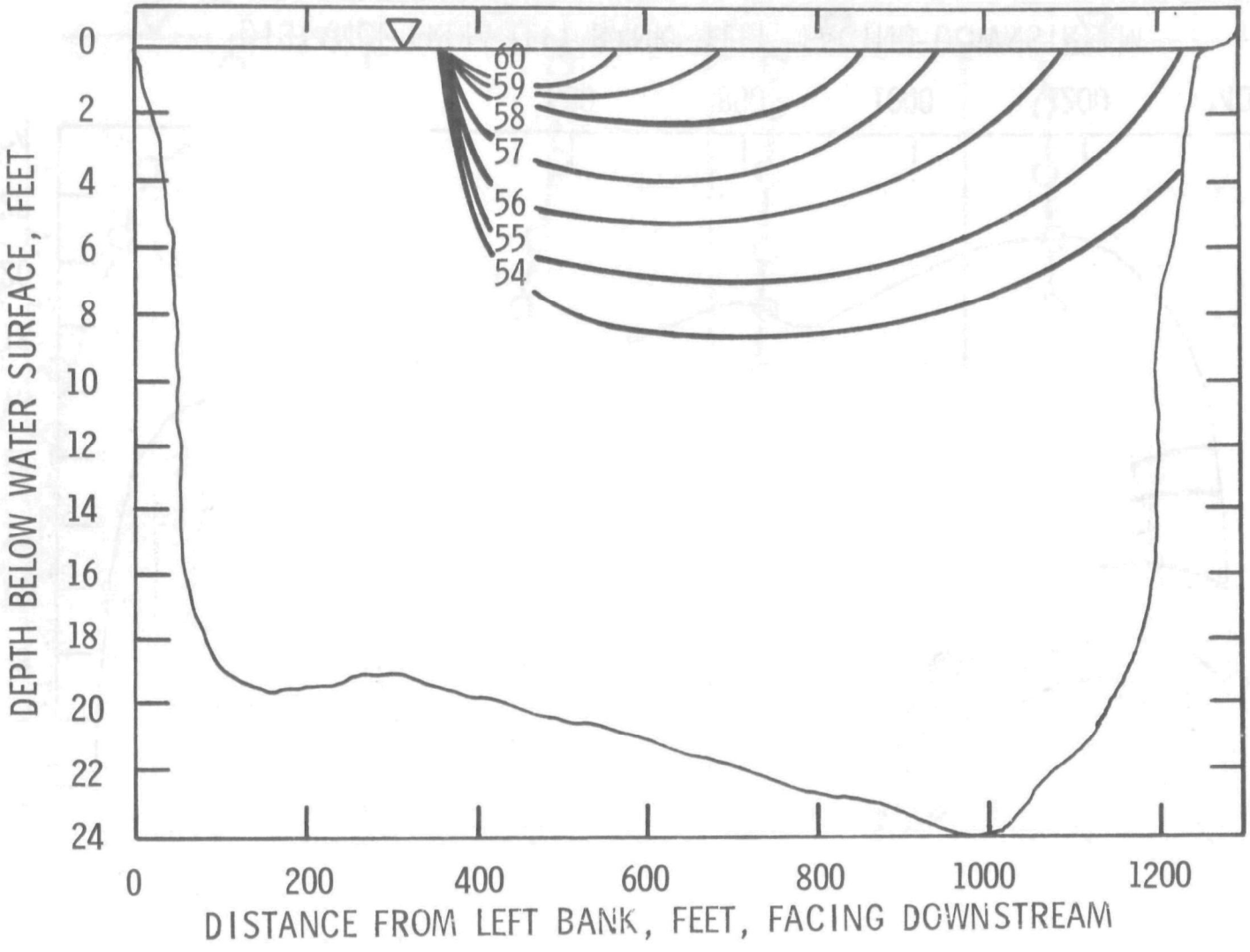

FIGURE 27.--TEMPERATURE DISTRIBUTION, °F, IN CROSS-SECTION R-2

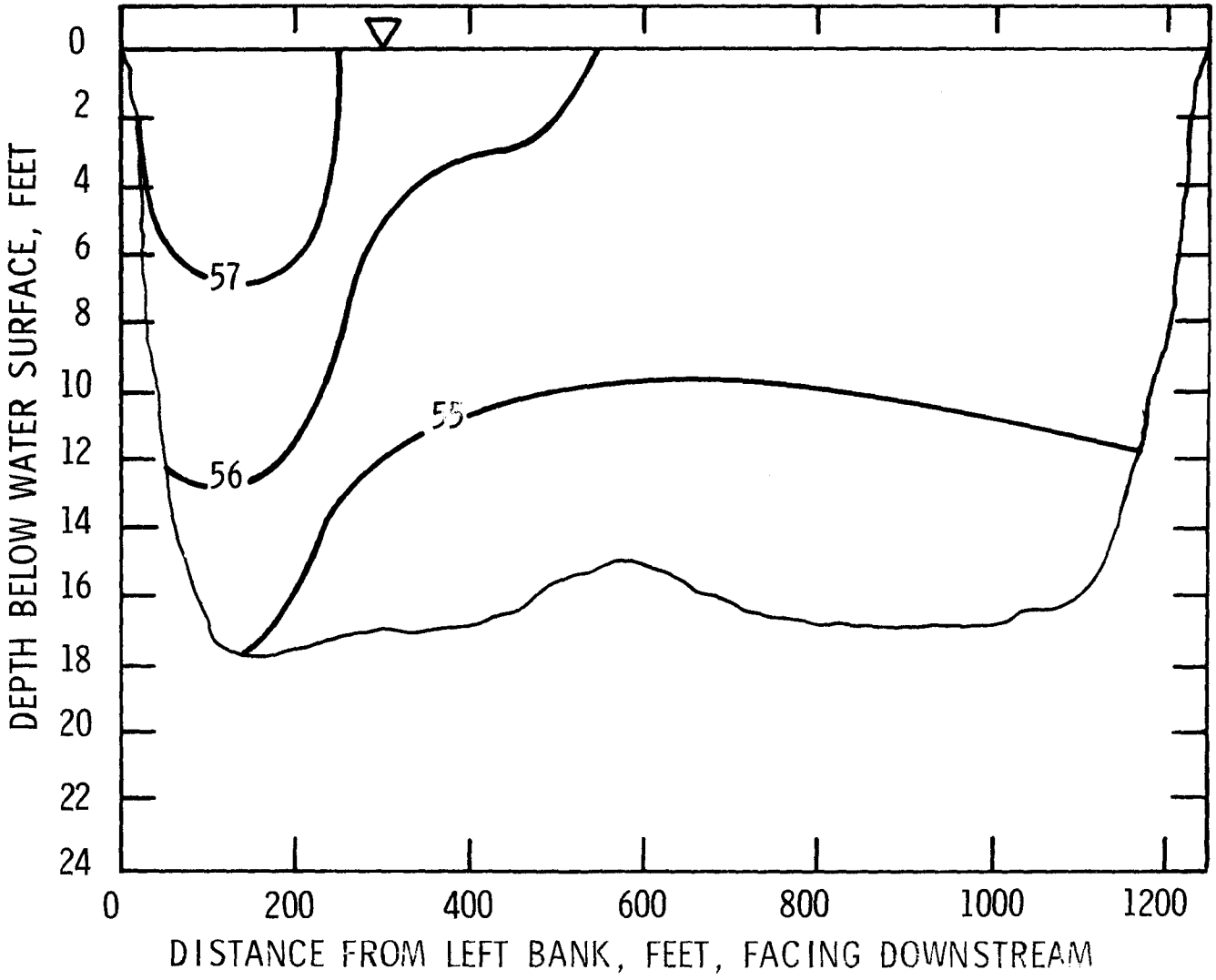

FIGURE 28.--TEMPERATURE DISTRIBUTION, °F, IN CROSS-SECTION R-5

by subtracting from Q_r = 26,170 cfs the value of the diverted plant flowrate, Q_o = 2370 cfs.

Cross-sectional areas were measured for each of the downstream cross-sections. The average value of the first five cross-sections was 22,400 ft^2. This downstream reach is considered to be the extent of the influence of the two-dimensional surface jet. The value of the ambient velocity was found to be U_a = 1.06 ft/sec by dividing the ambient flowrate by the average cross-sectional area.

To check this method of obtaining U_a, velocity measurements made during the survey by USGS personnel were used. Velocity measurements taken in the undisturbed ambient velocity field at cross-section R-1 are shown in Figure 29. The value of the velocity obtained after vertically averaging each of the profiles shown in Figure 29 using a planimeter and then averaging these values was equal to 1.05 ft/sec at cross-section R-1. Dividing the value of Q_a = 23,800 cfs by the value of the cross-sectional area at R-1, or 23,200 ft^2, gave a comparable value of U_a = 1.03 ft/sec. Thus, using the flowrate and the cross-sectional area gave the same value of ambient velocity as did detailed velocity measurements for cross-sections as well. Since the cross-sectional areas varied from 23,900 ft^2 to 18,800 ft^2, it is felt that using the flowrate Q_a = 23,800 cfs and the <u>average</u> value of the cross-sectional areas of the first five downstream stations gave the best determination of the ambient velocity along the reach of stream affected by the jet discharge.

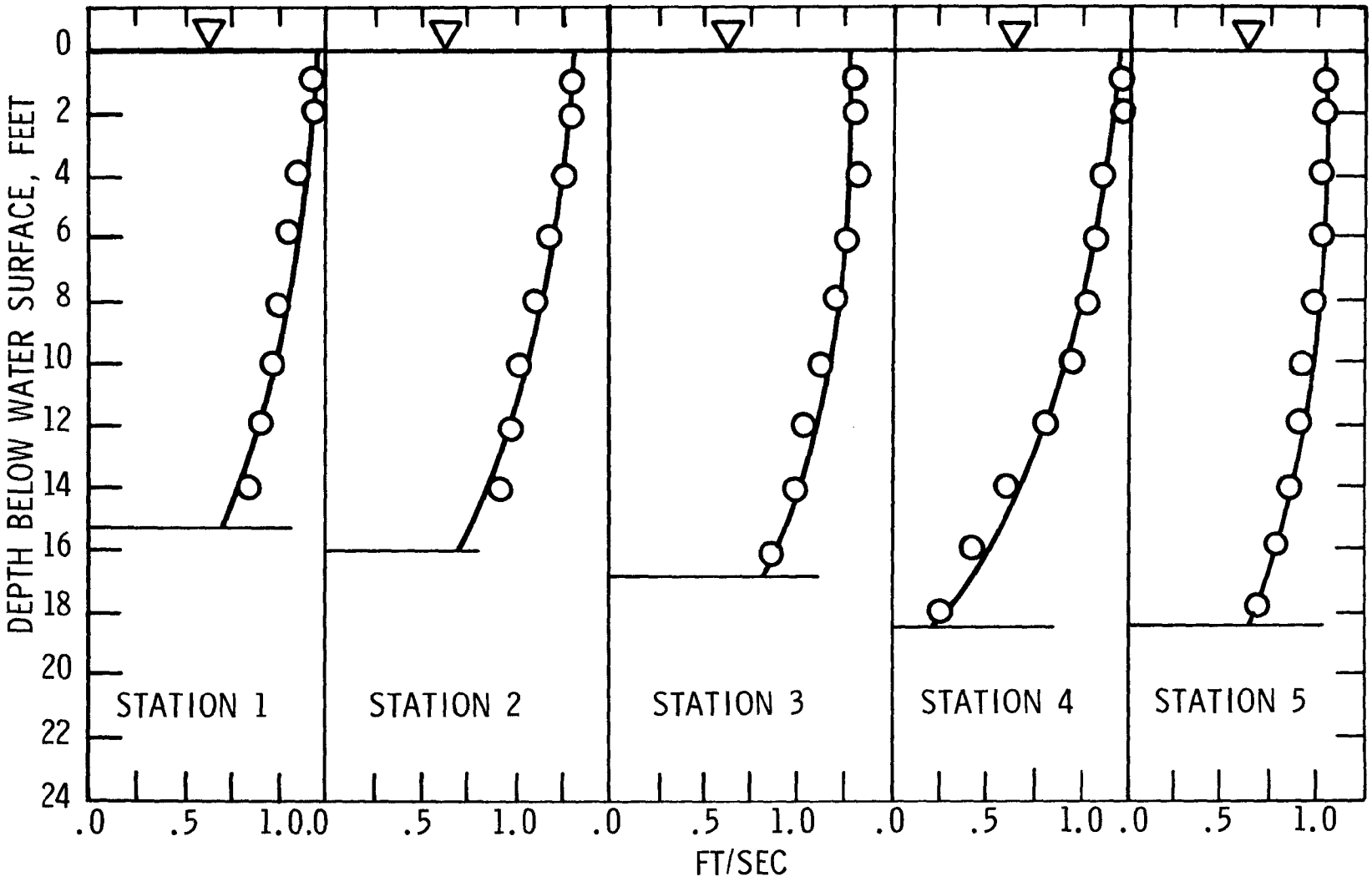

FIGURE 29.--VELOCITY PROFILES AT CROSS-SECTION R-1

Initial Jet Width.-- The value of the width of the discharge was estimated to be 187 feet from the scale drawing traced from the USGS map of the Widows Creek area. The value of the half-width at the origin was half of this, or $b_o' = 93.5$ feet. The value of b_o, the initial half-width at the beginning of the zone of established jet flow, was found to be $b_o = 150.0$ feet from Equation 65,

$$b_o = 1.60\ b_o' \tag{65}$$

Depth of the Jet.-- It was originally intended to theoretically calculate the depth of the jet at the mouth of the discharge channel. According to Harleman (26), when the density difference between the discharge water and river water is sufficiently great, the colder ambient water will intrude into the discharge channel under the lighter condenser water. The interface between the discharge water and ambient water can be described in terms of two-layer stratified flow theory. Upon assuming that a critical Froude Number occurs at the junction of the discharge channel and the river, the depth of the upper layer, or the depth of the jet, can be predicted based on Harleman's work in terms of the discharge flowrate, the channel width, and the density difference.

However, the predicted depth of the upper layer using the observed field values for the plant flowrate, the discharge width, and the density difference was on the order of 15.0 feet, or almost the entire depth of the ambient stream. The vertical temperature profiles in Figure 24 and 25 indicate that the average depth of the jet in the ambient stream was considerably less than 15.0 feet. Therefore, it was concluded that the conditions necessary to theoretically predict the jet depth were not

met at Widows Creek.

Therefore, the depth of the jet was empirically estimated from the field data in a manner which is consistent with the definition of the half-width, b, in Equation 24,

$$b = \sqrt{2}\,\sigma \tag{24}$$

The jet depth, which is assumed constant compared to the jet width, was estimated from the vertical temperature data shown in Figures 24 and 25 by using a similar definition, shown in Equation 73,

$$z_o = \sqrt{2}\,\sigma_z \tag{73}$$

where σ_z is the standard deviation of the vertical temperature data.

The standard deviation and sample variance for each of the first five sets of vertical temperature data are shown in Table 5. The estimated jet depth was found by calculating the standard deviation from the average of the variances. The standard deviation was 4.24 feet, and the jet depth was found to be z_o = 6.0 feet by using Equation 73.

TABLE 5

VERTICAL PROFILE STATISTICS
VU SURVEY NUMBER 1

Location	Standard Deviation	Sample Variance
R-1	3.71	13.7
R-2	3.07	9.4
R-3	5.07	25.7
R-4	4.31	18.6
R-5	4.75	22.6

Initial Jet Velocity.-- The value of the initial jet velocity was calculated to be U_o = 2.12 ft/sec from Equation 74,

$$Q_o = U_o z_o 2\, b'_o \tag{74}$$

where Q_o = 2370 cfs;

z_o = 6.0 feet; and

b'_o = 93.5 feet.

Velocity Ratio.-- The value of the velocity ratio was found to be A = 0.50 using U_a = 1.06 ft/sec and U_o = 2.12 ft/sec and Equation 38,

$$A = U_a/U_o \tag{38}$$

Initial Angle of Discharge.-- The initial angle, β'_o, of the discharge was found by assuming that the centerline axis of the river passed through the center of cross-sections R-1 and R-5, which are shown in Figure 23. This reach of the river between R-1 and R-5 was assumed to be a straight segment, with the direction of the ambient velocity along this axis. The x'-axis was parallel to this centerline axis. The origin of the x' and y' axes was assumed to be located, in terms of x', in the middle of the discharge channel, and, in terms of y', at the edge of the ambient stream. After locating the x' and y' axes in this way, the initial angle of the discharge was measured, giving β'_o = 85.0°.

Zone of Flow Establishment.-- From Figure 18, the length of the zone of flow establishment was estimated to be s'_e/b_o = 1.05, using A = 0.5. From Figure 19, the initial angle at the beginning of the

zone of established jet flow was estimated to be $\beta_o = 46.7°$, using $A = 0.5$ and $\beta_o' = 85.0°$.

Jet trajectory.-- The distance along the jet trajectory was found from Figure 23 by measuring the distance s'/b_o along a smooth curve from the origin to the location of the maximum temperature in each cross-section. Then, the value of T/T_o at each of the cross-sections was calculated.

Entrainment Coefficient.-- Numerical solutions for $A = 0.5$ and $\beta_o = 46.7°$ were used to determine the value of E. First, a preliminary value of $E = 0.2$ was determined by sliding the T/T_o vs. s'/b_o data plot horizontally over the T/T_o vs. S curve, which was computed from $S = 0.0$. When the best fit of the data and the theoretical curve was obtained, a corresponding set of values of s'/b_o and S was noted. Equation 37 was then solved for the preliminary value of E,

$$E = (\sqrt{\pi}\, S/2) \,/\, (s/b_o) \tag{37}$$

Next, Equation 67 was solved for S_e', using the value of $s_e'/b_o = 1.05$ and $E = 0.2$,

$$S_e' = (2E/\sqrt{\pi}\, b_o) s_e' \tag{67}$$

The T/T_o vs. S plot was then redrawn as T/T_o vs. S', referenced to the jet origin, using the value of S_e' and Equation 68,

$$S' = S_e' + S \tag{68}$$

A set of corresponding values of S' and s'/b_o was noted after sliding the T/T_o vs. s'/b_o plot horizontally over the T/T_o vs. s'/b_o curve until the best fit of the data and the theoretical curve was obtained. Then,

Equation 69 was solved for the final value of E,

$$E = (\sqrt{\pi}\, S'/2) \;/\; (s'/b_o) \tag{69}$$

Drag Coefficient.-- To determine the value of the drag coefficient, C_D, numerical solutions of X and Y were computed along with the T/T_o solutions with A = 0.50 and $\beta_o = 46.7°$. Two different values of the reduced drag coefficient, $C_D' = 0.5$ and 1.0, were assumed. Each of the predicted trajectories was plotted in terms of x'/b_o and y'/b_o,

$$X = (2E/\sqrt{\pi}\, b_o)x \quad ; \quad Y = (2E/\sqrt{\pi}\, b_o)y \tag{42}$$

In the field cases, the values of x_e'/b_o and y_e'/b_o were considered to be negligible compared to the values of x/b_o and y/b_o. Thus, it was assumed that $x'/b_o = x/b_o$, and $y'/b_o = y/b_o$.

The value of the reduced drag coefficient was determined by overlaying the predicted trajectories with the observed jet trajectory. For this field case, interpolation between the predicted trajectories to the observed trajectory was not necessary, because the assumed value of $C_D' = 1.0$ gave the best fit.

The value of the drag coefficient was found to be $C_D = 0.6$ from the observed values of E = 0.16 and $C_D' = 1.0$ and Equation 39,

$$C_D' = C_D/4E \tag{39}$$

Width Ratio.-- The observed values of the width ratio b/b_o were obtained by calculating the standard deviation of the temperature values at each of the cross-sections and then using Equation 24,

$$b = \sqrt{2}\, c \tag{24}$$

and the value of b_o = 150.0 feet.

Initial Ri_o Number.-- The value of the initial Richardson Number of the jet was calculated to be Ri_o = 0.22 using the values $\Delta\rho/\rho = 1.29 \times 10^{-3}$, U_o = 2.12 ft/sec, U_a = 1.06 ft/sec, z_o = 6.0 feet, and Equation 60.

Check of Initial Jet Velocity.-- The value of U_o = 2.12 ft/sec was obtained by using Equation 74,

$$Q_o = U_o z_o 2\, b'_o \tag{74}$$

To check this method of obtaining U_o, the velocity measurements made by USGS personnel were used. Since the velocity measurements made at the discharge near cross-section R-1 were inconsistent and scattered, presumably due to turbulence caused by the presence of several large piers used by coal barges, it was necessary to use the measurements taken at R-2. These velocity measurements, shown in Figure 30, indicated that the jet discharge created a non-uniform velocity field when compared to the unaffected, uniform part of the velocity field at R-1, shown in Figure 29.

The observed velocity and temperature rise at R-2 was examined to see if the values of U_o and A used in the numerical solution were consistent with the observed values. As seen in Figure 30, the maximum value of the velocity in cross-section R-2 was 1.7 ft/sec. At this same cross-section, the value of the temperature rise was T/T_o = 0.49. The numerical solution using A = 0.50 and β_o = 46.7° predicted that

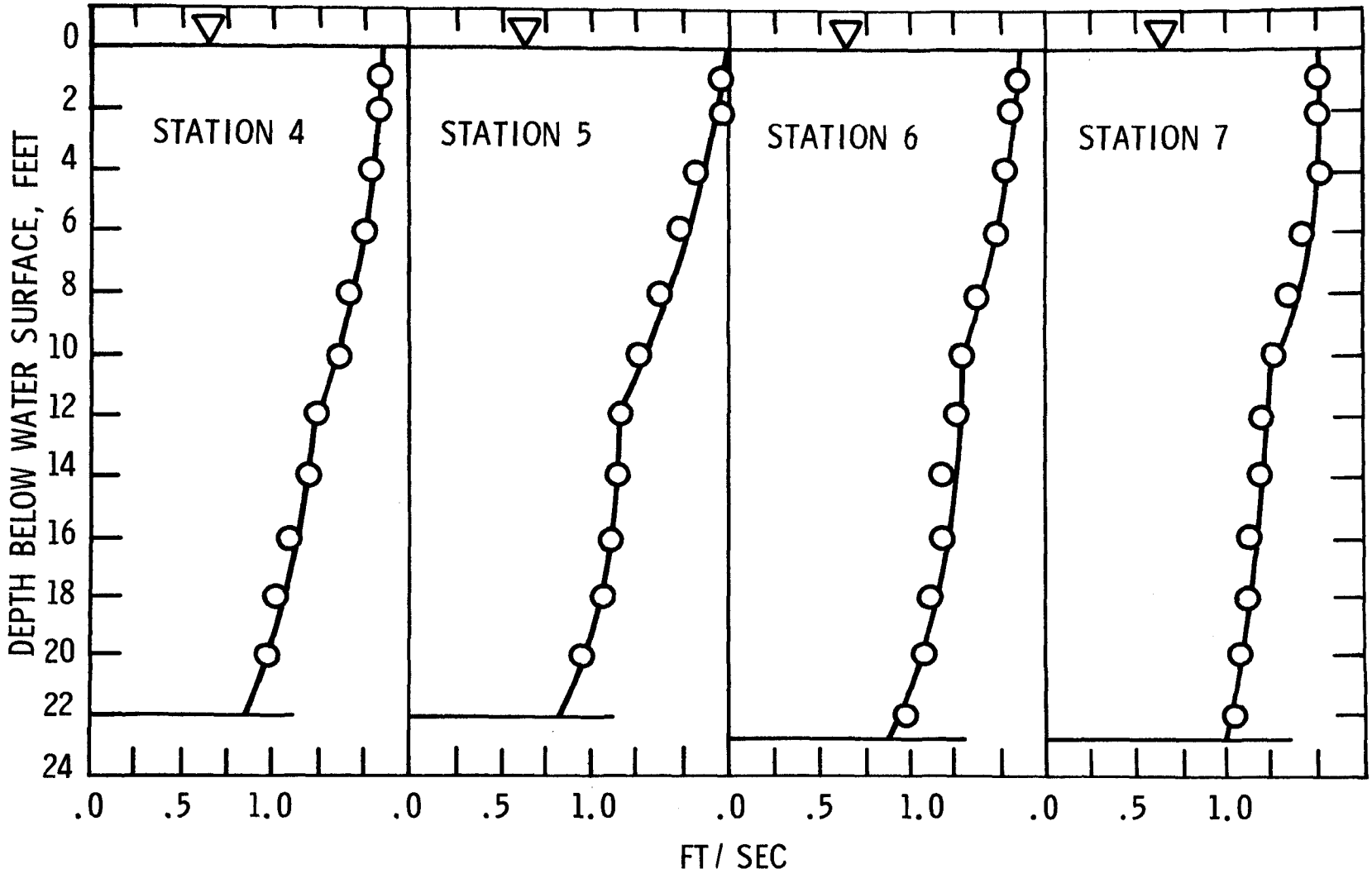

FIGURE 30.--VELOCITY PROFILES AT CROSS-SECTION R-2

T/T_o = 0.49 at S' = 28.0. At this same value of S', the numerical solution also predicted a value of U/U_o = 0.8. If U = 1.7 ft/sec, then the initial jet velocity based on data taken at this one cross-section should have been U_o = 2.13 ft/sec, which compares favorably with the value calculated from Equation 74, or U_o = 2.12 ft/sec, which is based on data taken at five cross-sections.

Presentation of Results.-- The data for the November 20 survey are presented in Table 6, and the parameters are presented in Table 7. The trajectory and temperature plots, from which the values of C_D' and E were determined, are presented in Figures 31 and 32. The data points which indicate the observed centerline of the jet are plotted on Figure 31, along with the fitted trajectory computed from the numerical solution. The observed T/T_o vs. s'/b_o data are plotted on Figure 32, along with the fitted T/T_o curve also computed from the numerical solution. The observed values of b/b_o are plotted on Figure 32 along with predicted b/b_o curve computed from the numerical solution. The observed value of E = 0.16 determined from the centerline temperature data was used to calculate the values of s'/b_o and from S, using Equations 68 and 69,

$$S' = S_e' + S \tag{68}$$

$$S' = (2E/\sqrt{\pi}\, b_o)s' \tag{69}$$

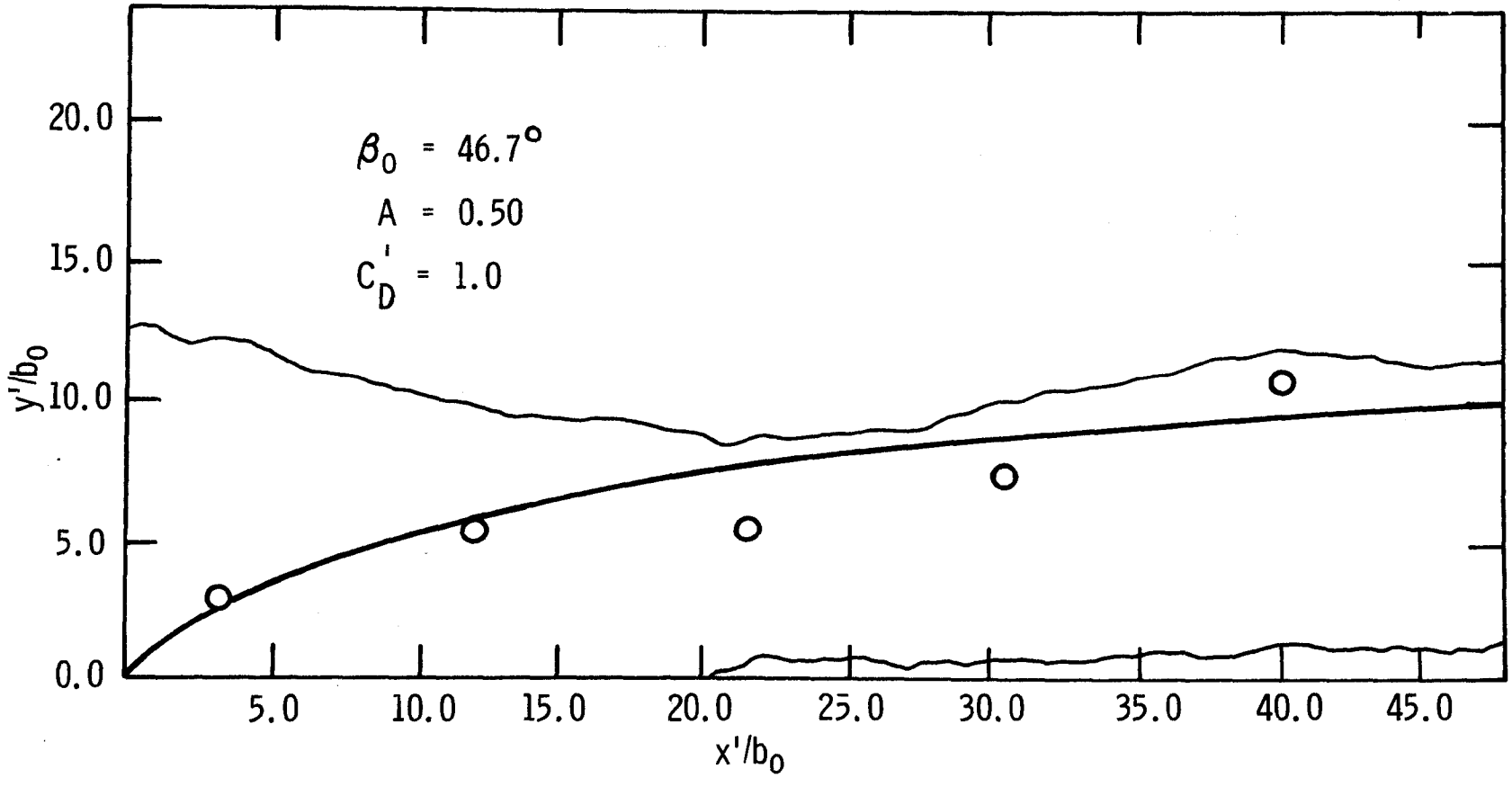

FIGURE 31.--OBSERVED AND FITTED TRAJECTORIES, WIDOWS CREEK, VU 1

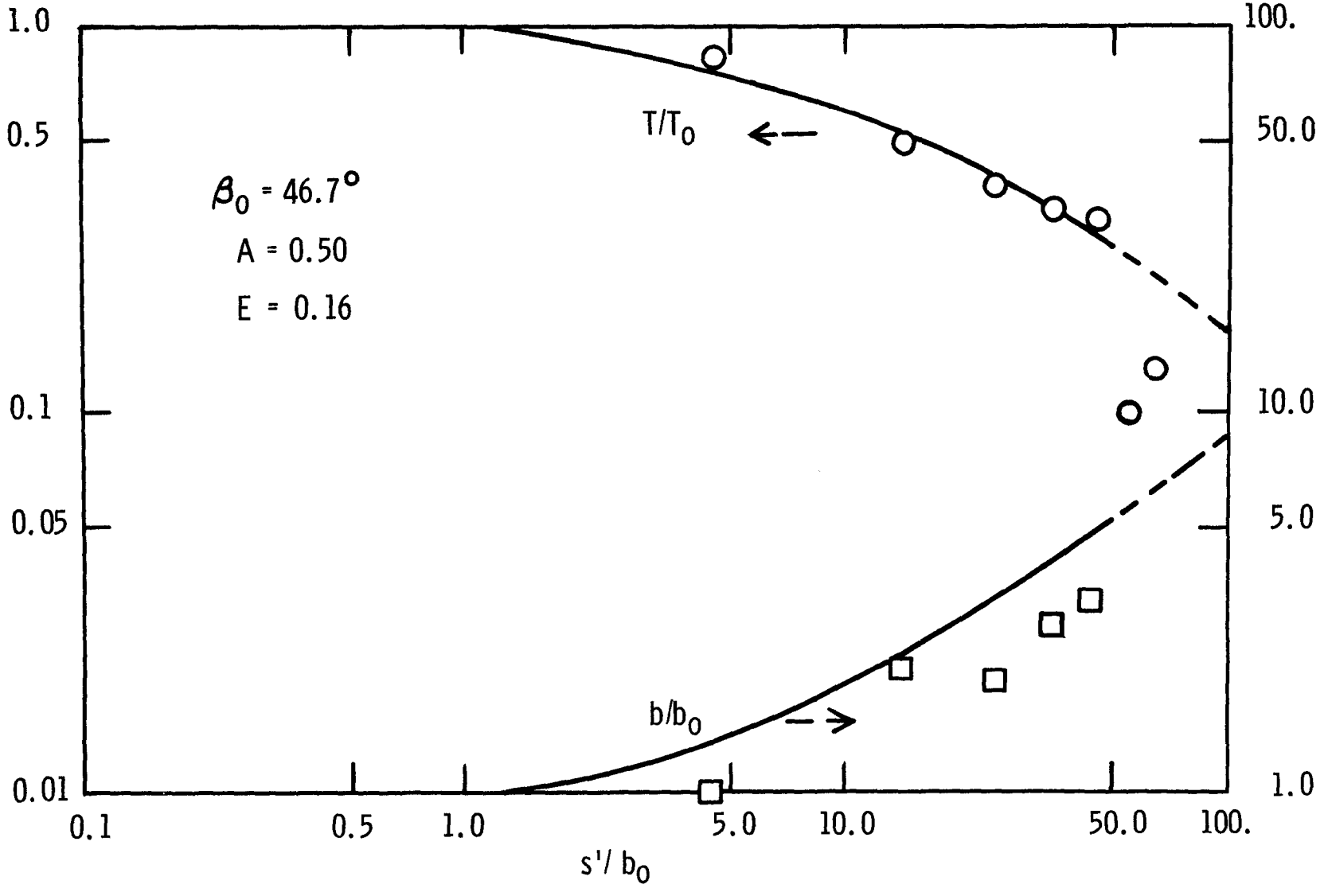

FIGURE 32.--OBSERVED VALUES AND FITTED CURVES FOR TEMPERATURE AND WIDTH, WIDOWS CREEK, VU 1

TABLE 6

DATA, VU SURVEY NUMBER 1

Cross-Section	s'/b_o	T/T_o	b/b_o
R-1	4.46	0.82	1.00
R-2	14.0	0.49	2.11
R-3	24.3	0.38	2.02
R-4	34.5	0.33	2.80
R-5	45.2	0.31	3.16
R-6	54.2	0.099	--
R-7	63.5	0.13	--

VU Survey Number 2 and TVA Survey

Temperature Measurements.-- The temperature measurements taken November 21 by VU personnel and August 30 by TVA personnel at Widows Creek showed that the temperature distribution could again be described in terms of a two-dimensional surface jet. The surface temperature contours for these two surveys are shown in Figures 33 and 34. The location of the cross-sections was the same as for the first survey.

Presentation of Results.-- The procedure for analyzing the data was the same as that used for the first survey. The numerical solution was used with different values of A and β_o since the velocity ratio, $A = U_a/U_o$, was different in each case from the first survey. The data

TABLE 7

PARAMETERS, VU SURVEY NUMBER 1

Observed Values	
T_o, Initial Temperature Rise, °F	14.2
Q_r, River Flowrate, ft^3/sec	26,170
Q_o, Plant Flowrate, ft^3/sec	2,370
b'_o, Discharge Half-Width, ft	93.5
β'_o, Discharge Angle, °	85.0
Calculated Values	
Q_a, Ambient Flowrate, ft^3/sec	23,800
Ri_o, Initial Ri Number	0.22
Average Cross-Sectional Area, ft^2	22,400
U_a, Ambient Velocity, ft/sec	1.06
b_o, Initial Jet Half-Width, ft	150
z_o, Jet Depth, ft	6.0
U_o, Initial Jet Velocity, ft/sec	2.12
A, Velocity Ratio	0.50
s'_e/b_o, Establishment Zone	1.05
β_o, Initial Jet Angle, °	46.7
Observed Results	
E, Entrainment Coefficient	0.16
C'_D, Reduced Drag Coefficient	1.0
C_D, Drag Coefficient	0.6

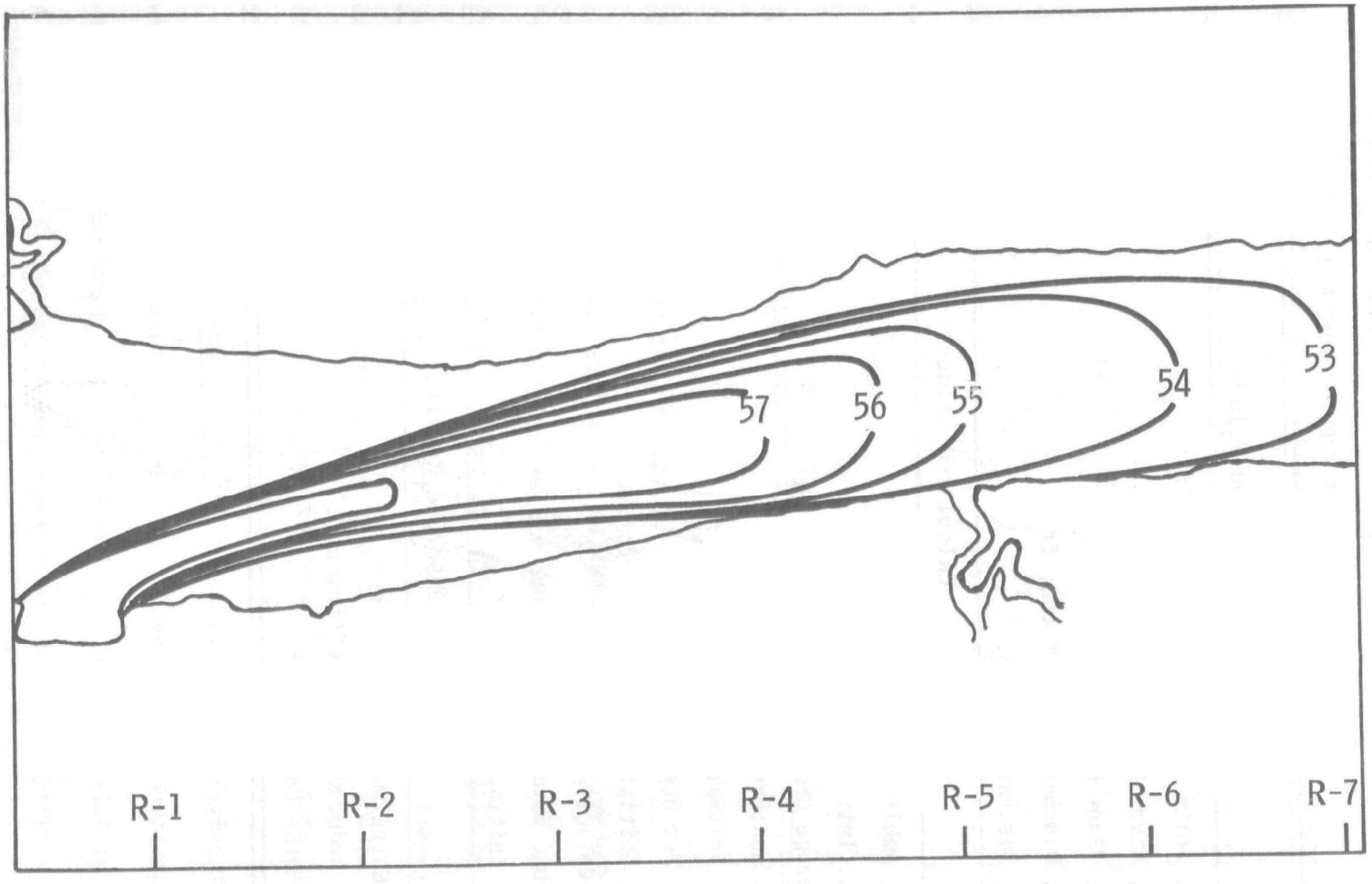

FIGURE 33.--TEMPERATURE DISTRIBUTION, °F, AT 1.0-FOOT DEPTH, WIDOWS CREEK, VU 2

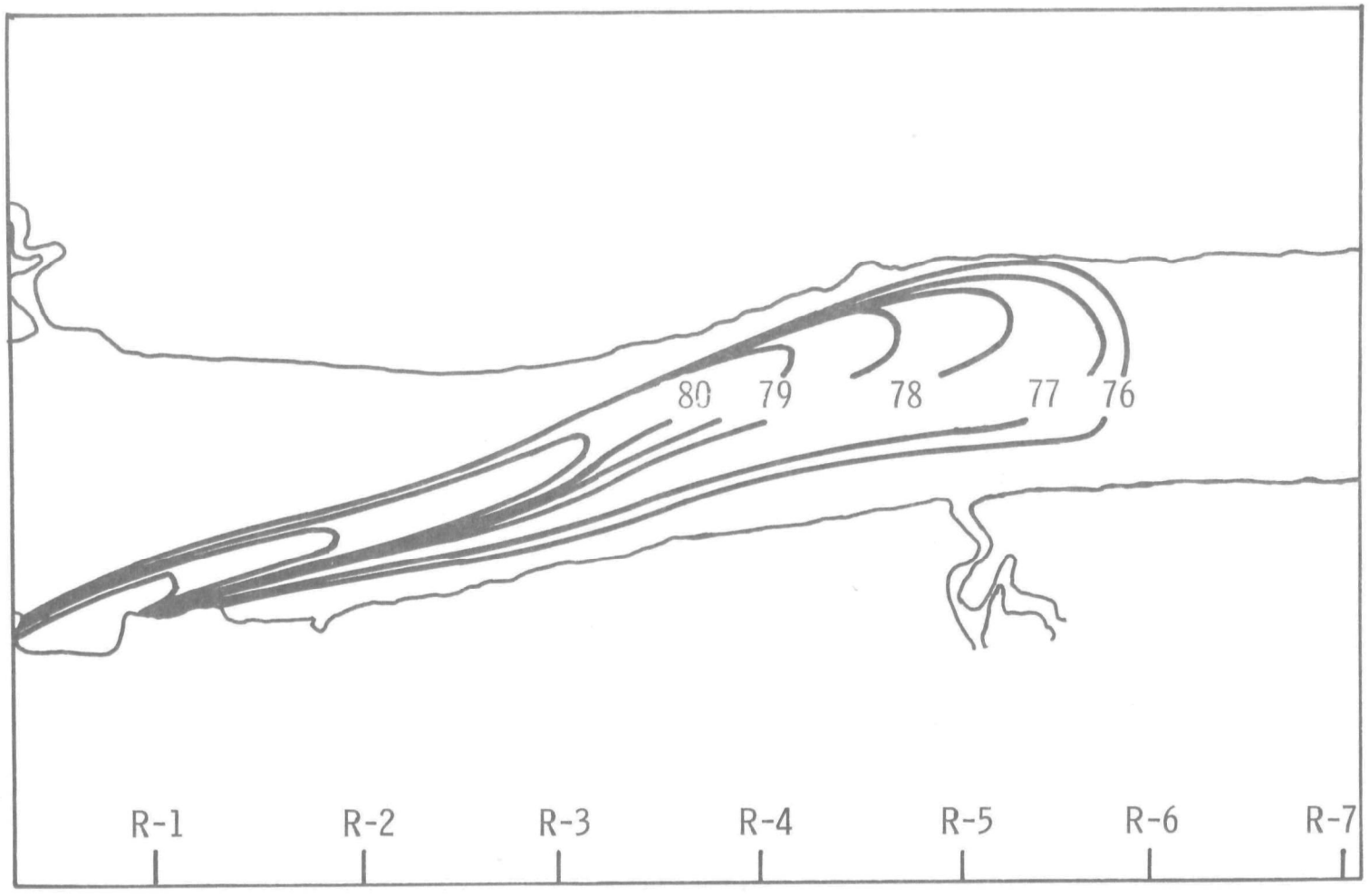

FIGURE 34.--TEMPERATURE CONTOURS, °F, AT 0.5-FOOT DEPTH, WIDOWS CREEK, TVA

for VU Number 2 and TVA surveys are presented in Table 8, and the parameters are presented in Table 9. The trajectories and temperature plots are presented in Figures 35-38. The observed and predicted values of b/b_o are presented in Figures 36 and 38. For the VU survey, the observed values were E = 0.16, $C_D' = 0.9$, and $C_D = 0.6$. For the TVA survey, the observed values were E = 0.16, $C_D' = 0.4$, and $C_D = 0.3$.

TABLE 8

DATA, VU SURVEY NUMBER 2 AND TVA SURVEY

Cross-Section	s'/b_o	VU No. 2		TVA	
		T/T_o	b/b_o	T/T_o	b/b_o
R-1	4.46	0.81	--	0.74	--
R-2	14.0	0.56	1.66	0.50	1.28
R-3	24.3	0.40	2.03	0.47	1.98
R-4	34.5	0.42	2.48	0.41	2.55
R-5	45.2	0.25	2.58	0.28	2.88
R-6	54.2	0.15	--	0.07	4.01
R-7	63.5	--	--	0.08	4.15

Results of the New Johnsonville Survey

Introduction

Data (37) were collected by VU personnel on May 29, 1969, at TVA's New Johnsonville Steam Plant located on Kentucky Lake. This plant is similar to Widows Creek in that condenser water is discharged into a small coal barge harbor and then flows onto the river surface. The spatial distribution of the discharged heat is again described in

TABLE 9

PARAMETERS, VU SURVEY NUMBER 2 AND TVA SURVEY

Observed Values

	VU No. 2	TVA
T_o, °F	13.0	14.2
Q_r, ft^3/sec	26,170	47,000
Q_o, ft^3/sec	1,840	2,200
b_o', ft	93.5	93.5
β_o', °	85.0	85.0

Calculated Values

	VU No. 2	TVA
Q_a, ft^3/sec	24,330	44,800
Ri_o	0.64	1.21
Average Cross-Sectional Area, ft^2	22,400	26,250
U_a, ft/sec	1.09	1.71
b_o, ft	150	150
z_o, ft	6.0	5.2
U_o, ft/sec	1.64	2.27
A	0.67	0.75
s_e'/b_o	0.84	0.75
β_o, °	36.5	32.3

Observed Results

	VU No. 2	TVA
E	0.16	0.16
C_D'	0.9	0.4
C_D	0.6	0.3

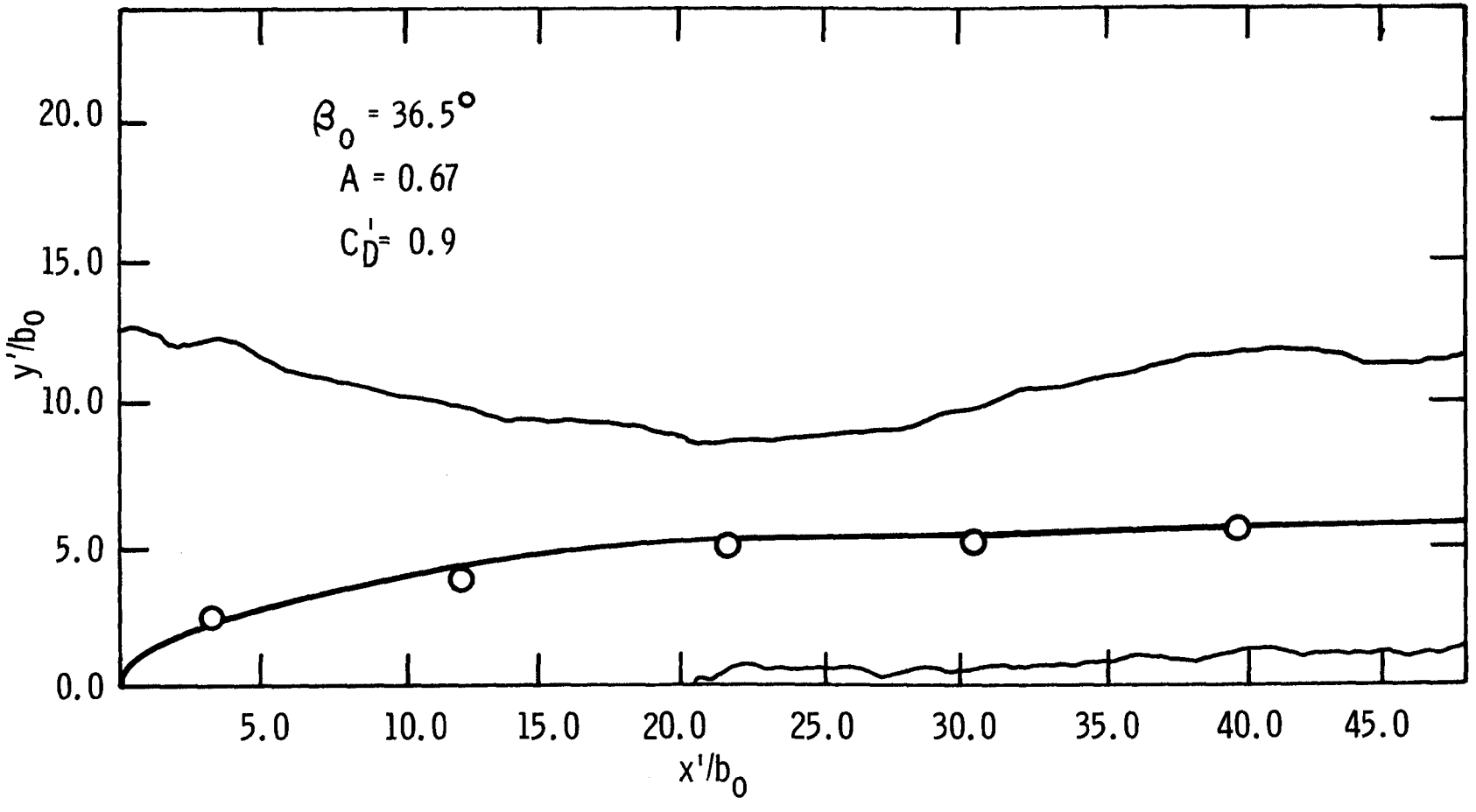

FIGURE 35.--OBSERVED AND FITTED TRAJECTORIES, WIDOWS CREEK, VU 2

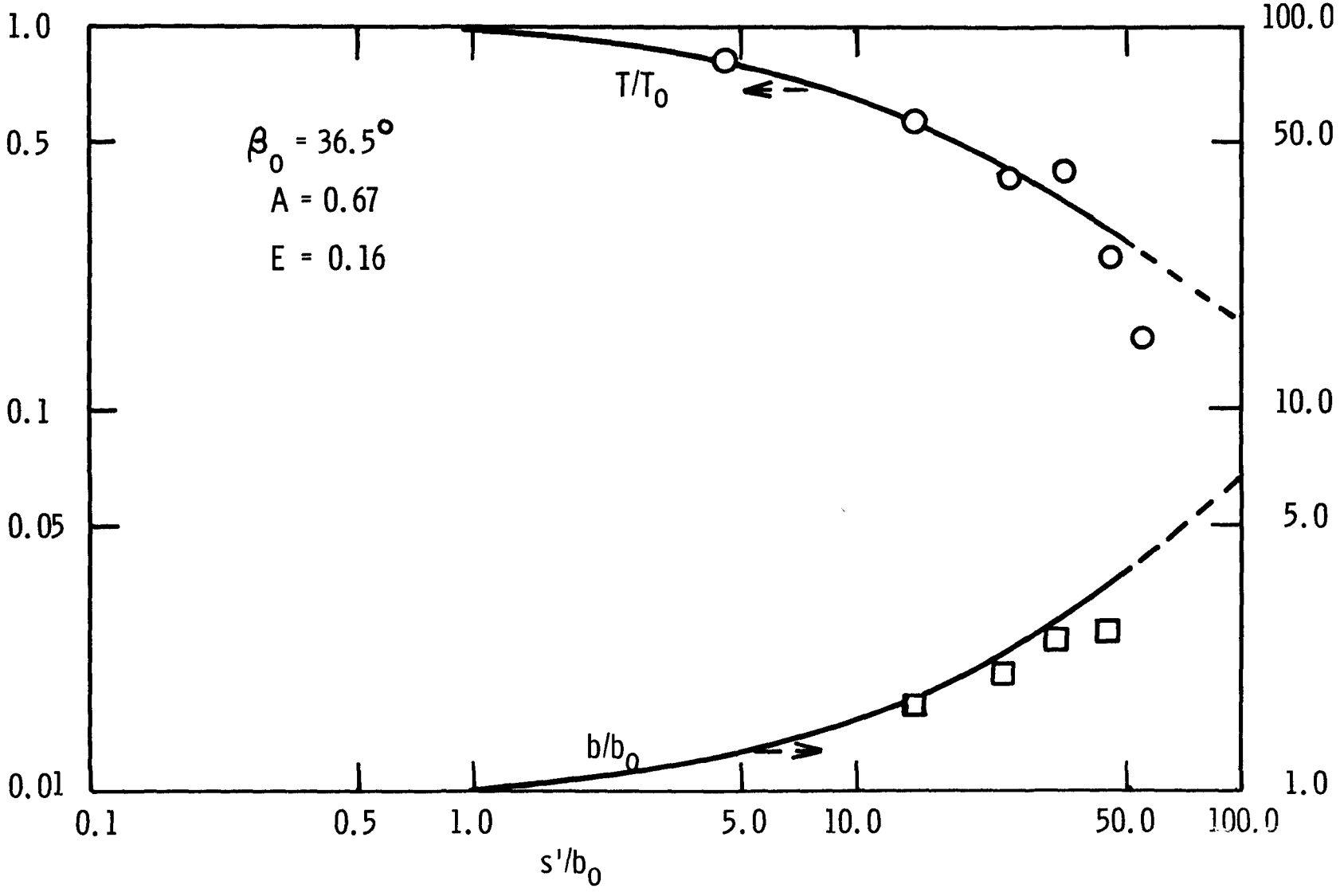

FIGURE 36.--OBSERVED VALUES AND FITTED CURVES FOR TEMPERATURE AND WIDTH, WIDOWS CREEK, VU 2

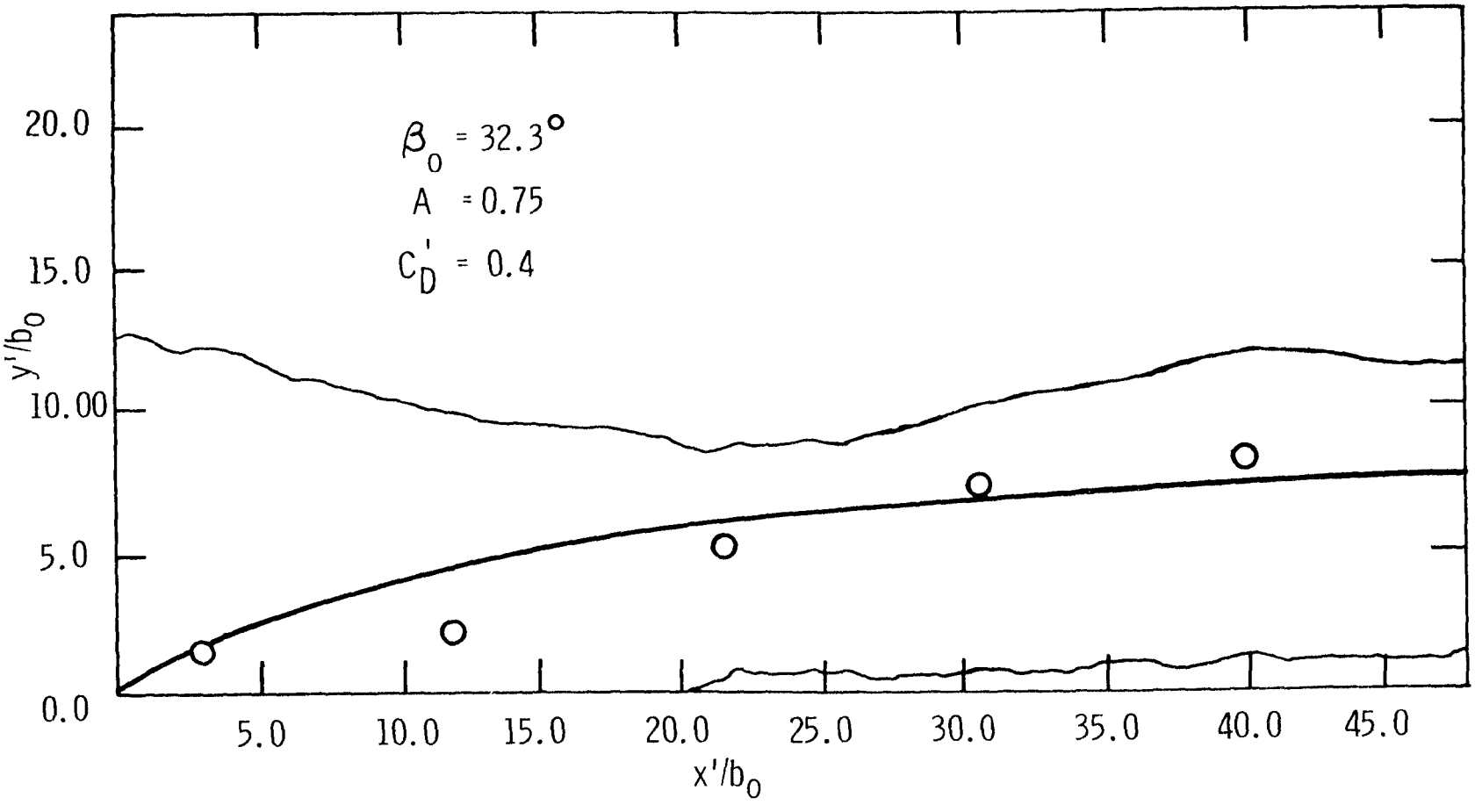

FIGURE 37.--OBSERVED AND FITTED TRAJECTORIES, WIDOWS CREEK, TVA

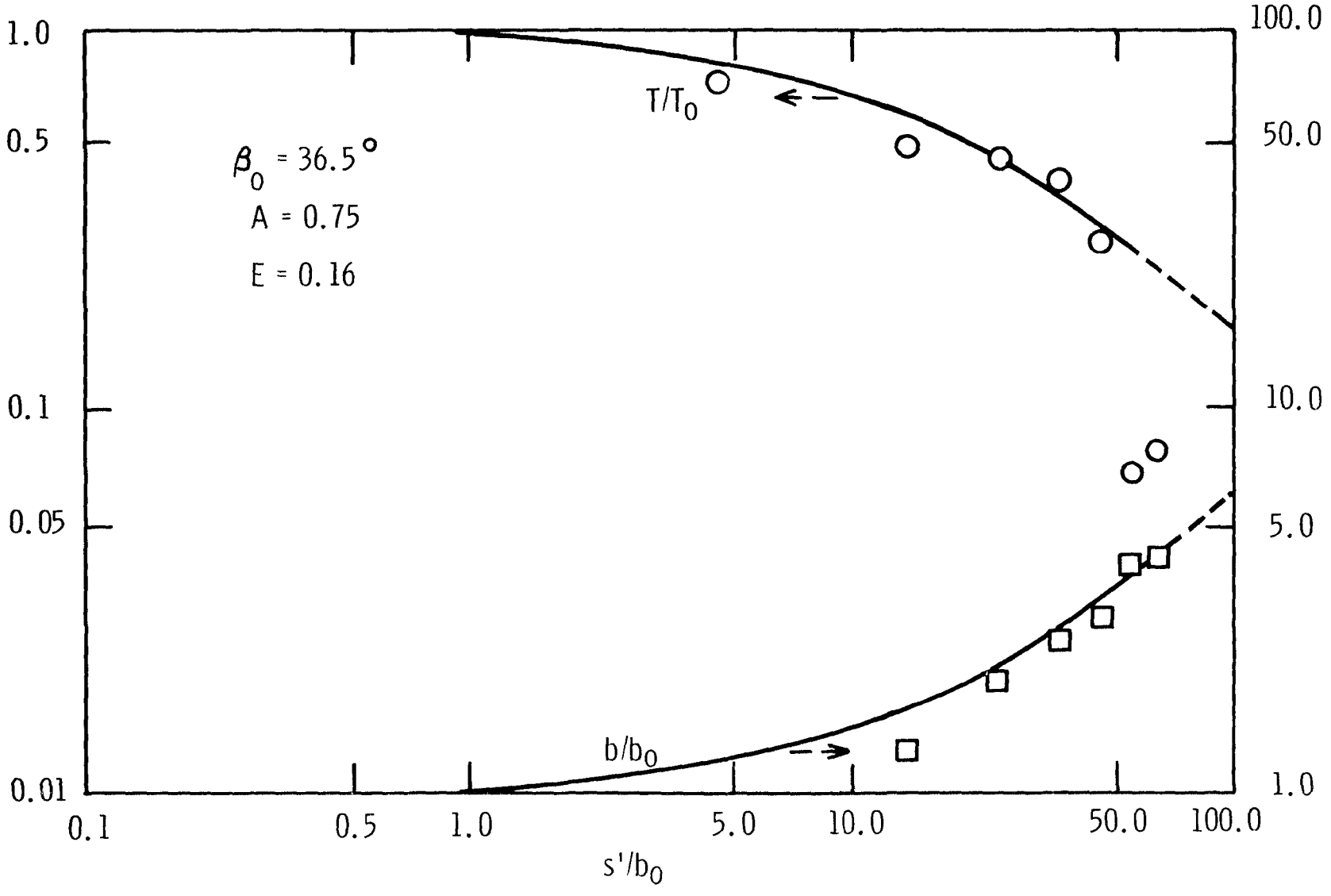

FIGURE 38.--OBSERVED VALUES AND FITTED CURVES FOR TEMPERATURE AND WIDTH, WIDOWS CREEK, TVA

terms of a two dimensional surface jet deflected by the ambient current. At the discharge, the width of the ambient water body is only four times larger than the width of the discharge. As a result, the entrainment characteristics and the spatial location of the jet were affected by the narrow boundaries. The surface temperature contours are shown in Figure 39.

Depth of the Jet

At New Johnsonville, detailed velocity measurements were made at the mouth of the discharge channel. These velocity measurements were used to estimate the depth of the jet at this field site. The sample standard deviation of the velocity data shown in Table 10 was calculated, and then the depth of the jet was found to be z_o = 5.95 feet, using Equation 73,

$$z_o = \sqrt{2}\,\sigma_z \tag{73}$$

TABLE 10

VELOCITY DATA, NEW JOHNSONVILLE SURVEY

Depth, ft	Velocity, ft/sec
1.0	0.99
2.5	0.93
5.0	0.73
7.5	0.10
10.0	0.14
12.5	0.01
15.0	0.10
17.5	0.14
20.0	0.0
22.0	0.0

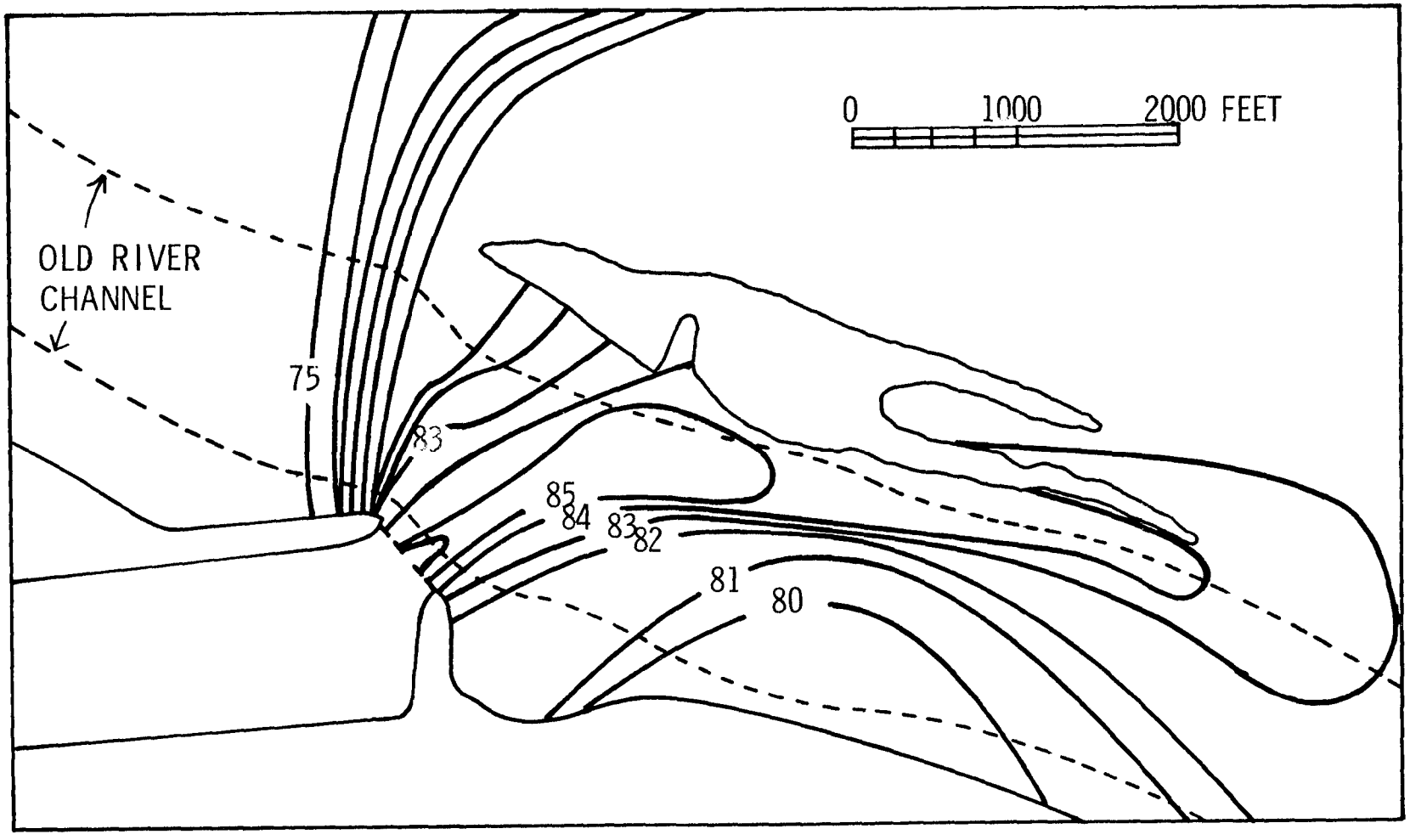

FIGURE 39.--OBSERVED TEMPERATURE DISTRIBUTION, °F, AT 1.0-FOOT DEPTH, NEW JOHNSONVILLE

Presentation of Results

Except for the depth determination discussed above, the procedure for analyzing the data was the same as for the Widows Creek surveys. The numerical solution was used with A = 0.57 and β_o = 30.0°. The temperature data are presented in Table 11 and the parameters in Table 12, while the trajectory and temperature plots are presented in Figures 40 and 41, respectively. The width ratio, b/b_o, is not calculated. The distortion caused by the narrow boundaries precluded measuring with any degree of accuracy the location of the lateral temperature rise perpendicular to the jet axis. The observed values of E = 0.04 and C_D' = 3.0 reflect the influence of the geometry.

TABLE 11

TEMPERATURE DATA, NEW JOHNSONVILLE SURVEY

s'/b_o	T/T_o
0.63	1.00
5.62	0.91
12.5	0.82
15.7	0.73

TABLE 12

PARAMETERS, NEW JOHNSONVILLE SURVEY

Observed Values	
T_o, °F	11.0
Q_r, ft^3/sec	26,500
Q_o, ft^3/sec	2,180
b_o', ft	250
β_o', °	60.0
Calculated Values	
Q_a, ft^3/sec	24,320
Ri_o	3.30
Average Cross-Sectional Area, ft	58,182
U_a, ft/sec	0.42
b_o, ft	400
z_o, ft	5.95
U_o, ft/sec	0.73
A	0.57
s_e'/b_o	0.93
β_o, °	30.0
Observed Results	
E	0.044
C_D'	3.0
C_D	0.5

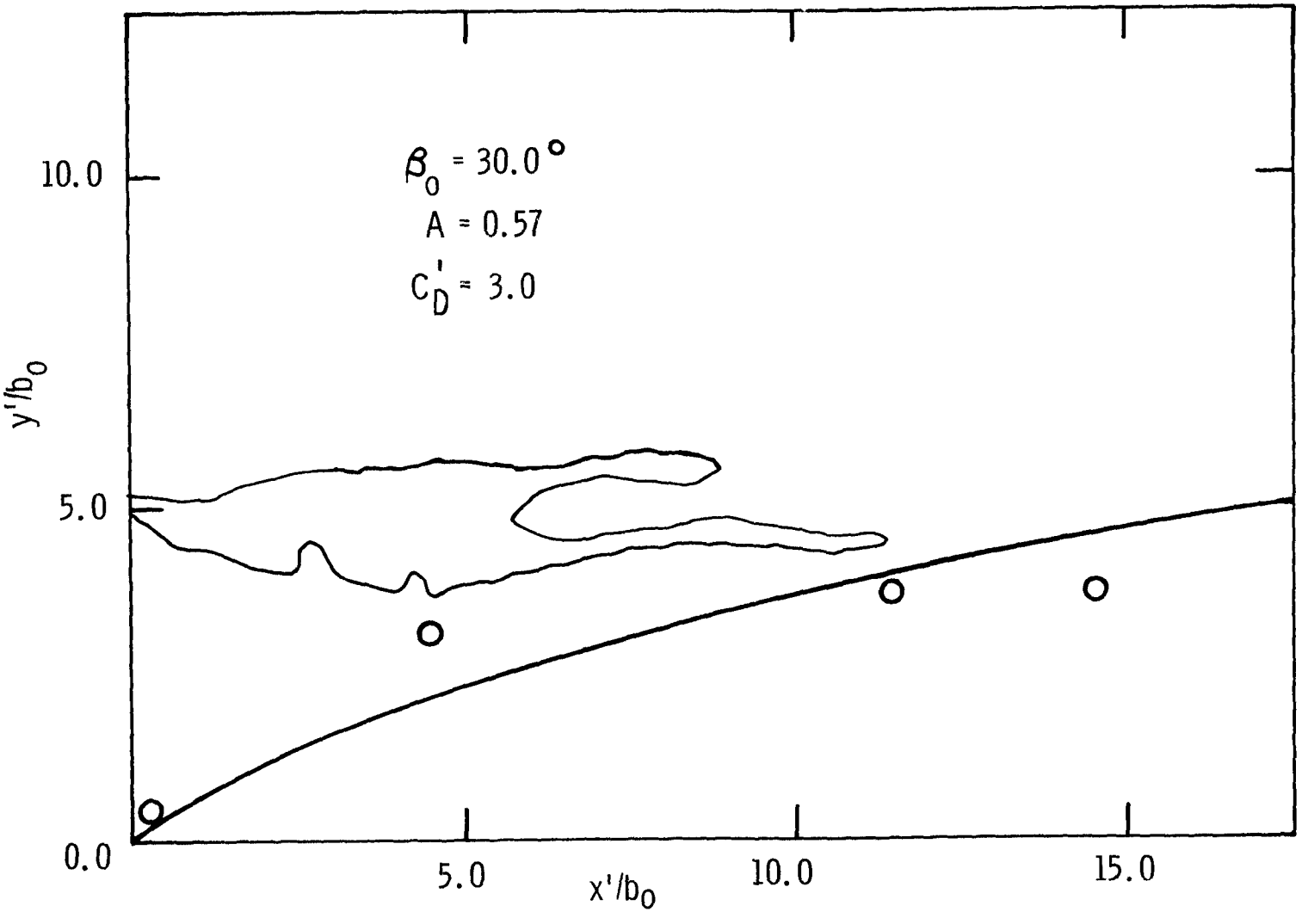

FIGURE 40.--OBSERVED AND FITTED TRAJECTORIES, NEW JOHNSONVILLE

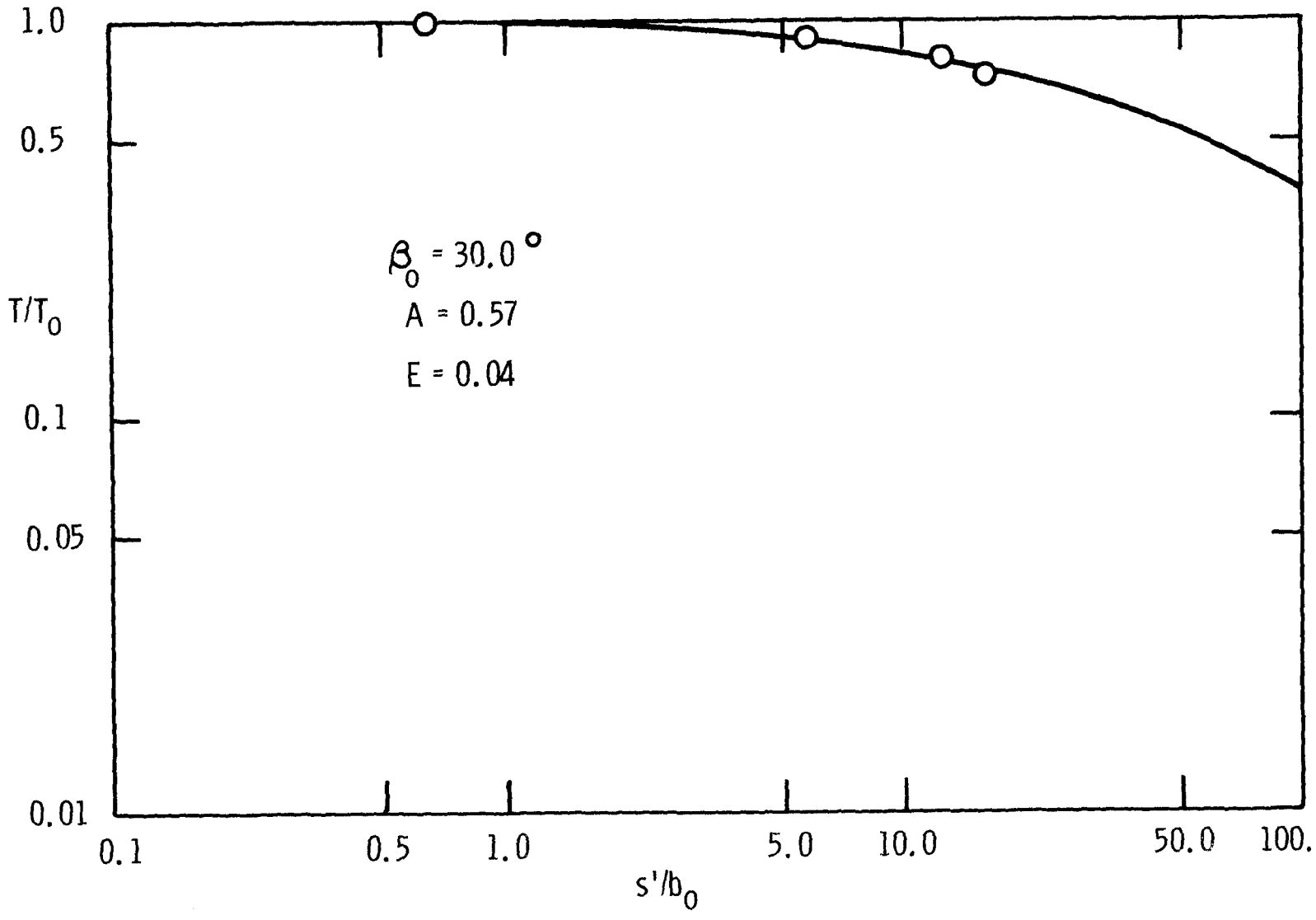

FIGURE 41.--OBSERVED VALUES AND FITTED CURVE FOR TEMPERATURE, NEW JOHNSONVILLE

Results of the Waukegan Survey

Introduction

Data obtained from a report by Beer and Pipes (6) at Waukegan generating station located on Lake Michigan were analyzed in terms of a two-dimensional surface jet. The cooling water from the plant was discharged into a 2000-foot long channel and then into the lake. There was no appreciable ambient velocity, and, therefore, the velocity ratio was equal to zero, or $A = U_a/U_o = 0.0$. This case of a jet discharging into a stagnant environment ordinarily could not be described as two-dimensional, since the Richardson Number is quite low, and vertical entrainment would be significant. However, the shallow depth of the lake near the shore inhibits vertical entrainment to some degree. Over a longitudinal distance of 3600 feet, the jet spread laterally from an initial width on the order of 250 feet to about 2500 feet and spread vertically from about 6 feet to a depth on the order of 15 feet. Thus, the rate of lateral mixing was approximately five times greater than vertical mixing. Even though the rate of lateral mixing was not a full order of magnitude greater than vertical mixing, it is felt that application of the two-dimensional model is reasonable, if only in order to examine a case in which the two-dimensional assumption is not fully met.

Temperature Measurements

The temperature contours at the 1.0-foot depth are shown in Figure 42.

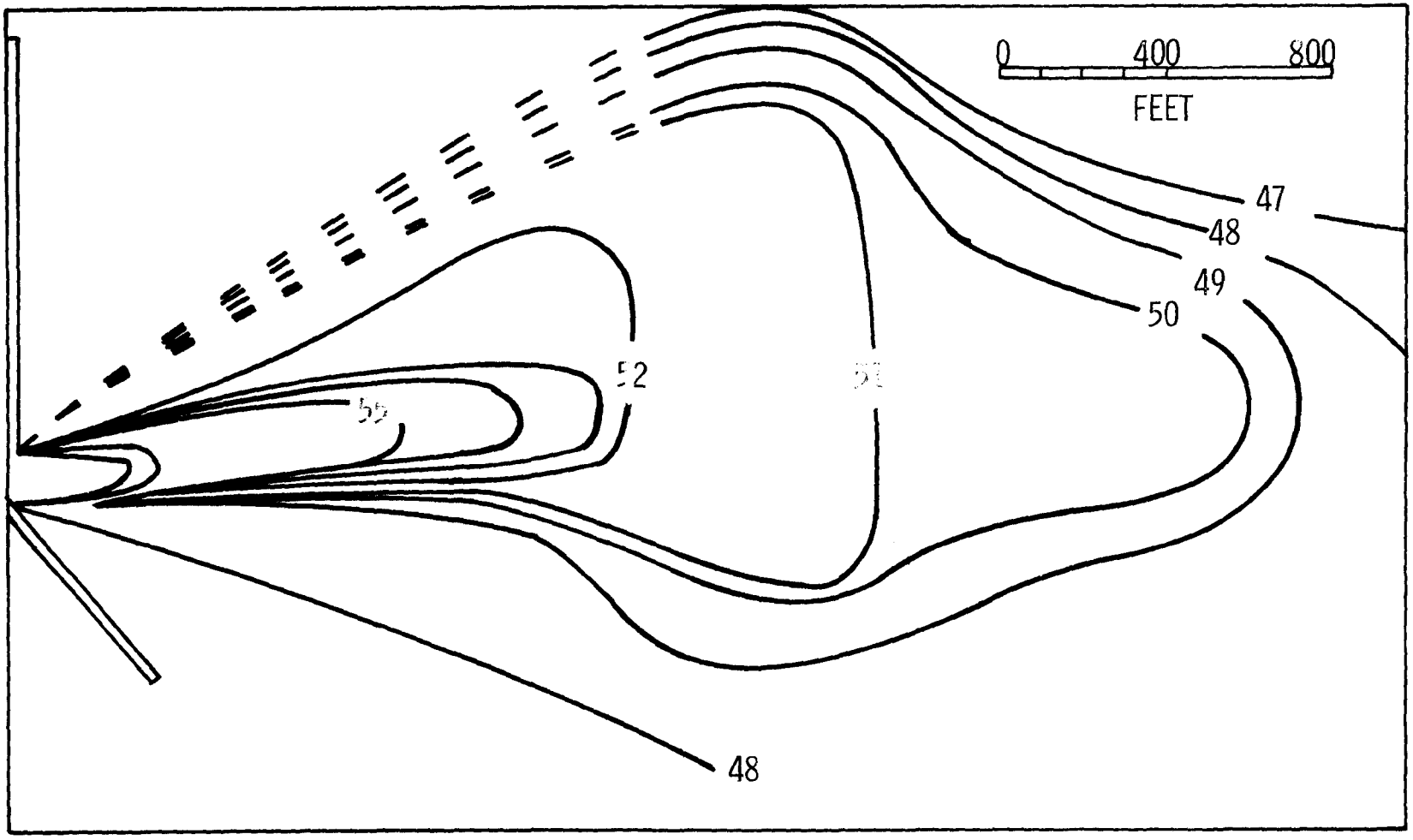

FIGURE 42.--TEMPERATURE DISTRIBUTION, °F, AT 1.0-FOOT DEPTH, WAUKEGAN
[AFTER BEER AND PIPES (6)]

Zone of Establishment

The length of the zone of establishment is not estimated from Figure 18 because the laboratory experiments did not include the case of A = 0.0. Instead, the length was taken to be $s'_e/d'_o = 6.2$ from the work of Albertson et al. (4). Expressed in terms of b_o, the length is found to be $s'_e/b_o = 4.4$ by using Equation 66,

$$b_o = 0.708d'_o \tag{66}$$

Results of Analysis

The procedure for analyzing the data was the same as for the other surveys. The numerical solution was used with A = 0.0. The temperature data are presented in Table 13 and the parameters in Table 14, while the temperature plot is presented in Figure 43. Values of b/b_o estimated from Figure 42 are also presented in Figure 43 along with the predicted b/b_o curve. The value of the entrainment coefficient was found to be E = 0.44.

The temperature and width plots, Figure 43, indicate that the two-dimensional model can be matched to the observed data reasonably well in the zone of established flow. However, in the zone of establishment, the predicted values are greater than the observed data. For a distance of $s'/b_o = 4.4$, the curve predicts $T/T_o = 1.0$, while over the same distance, the values of the data decrease from $T/T_o = 0.8$ to 0.7.

The initial temperature rise, $T_o = 15.0°F$, was computed from the difference of the reported condenser temperature, 60°F, and the lowest ambient temperature in the region of the jet, or 45°F. Examination of the surface contour plot, Figure 42, indicates that the temperature at

TABLE 13

DATA, WAUKEGAN SURVEY

s'/b_o	T/T_o	b/b_o
0.0	1.0	--
0.39	0.80	--
0.48	0.80	--
1.29	0.80	--
1.95	0.67	--
3.41	0.67	--
4.34	0.67	2.0
5.60	0.60	2.75
6.89	0.53	3.5
7.99	0.40	4.75
9.65	0.40	5.25
11.6	0.33	5.0
14.7	0.33	--
16.8	0.20	--

TABLE 14

PARAMETERS, WAUKEGAN SURVEY

Observed Values	
T_o, °F	15.0
Q_o, ft^3/sec	1,690
b_o', ft	125
Calculated Values	
Ri_o	0.01
b_o, ft	200
U_o, ft/sec	2.6
A	0.0
s_e'/b_o	4.4
Observed Results	
E	0.44

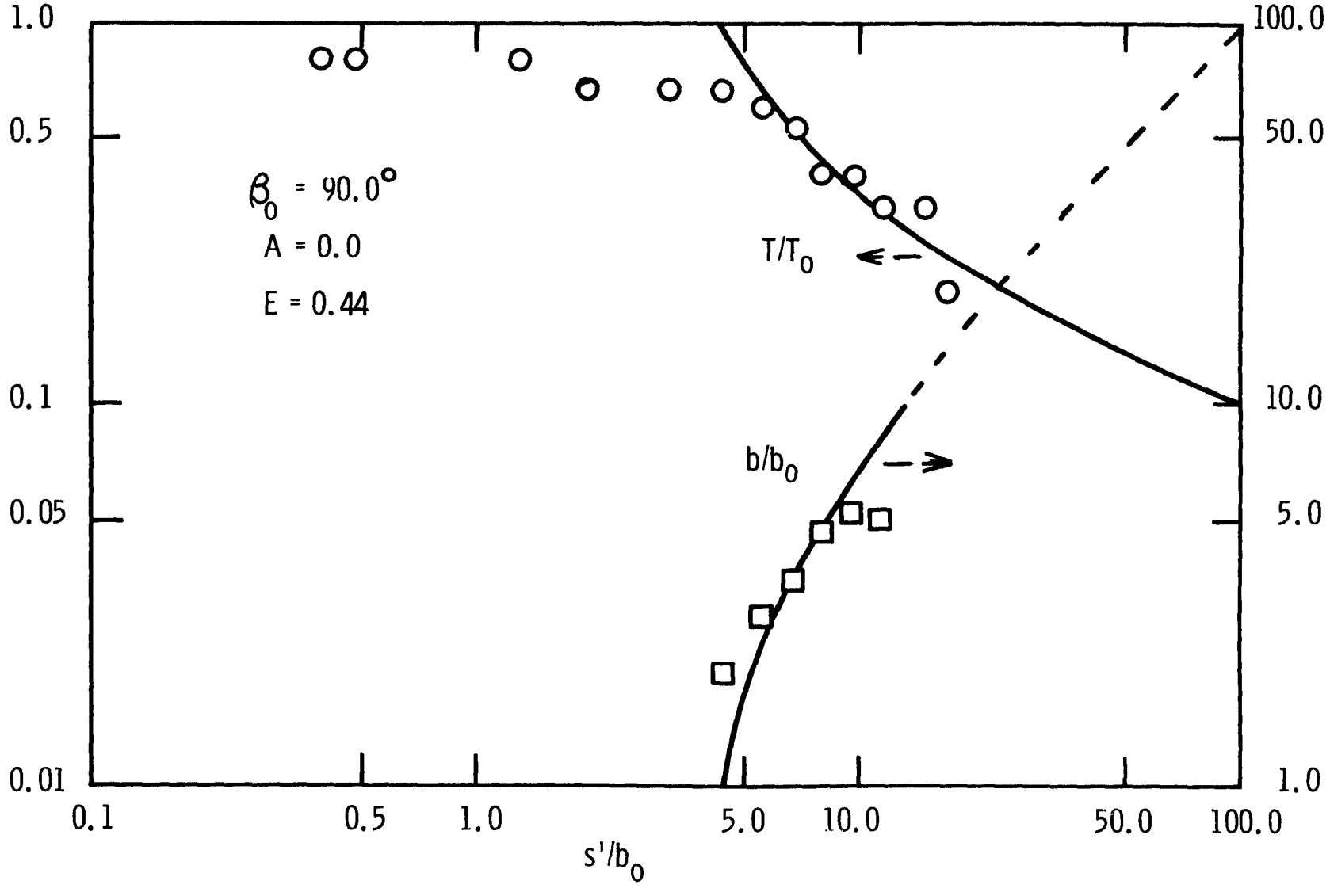

FIGURE 43.--OBSERVED VALUES AND FITTED CURVES FOR TEMPERATURE AND WIDTH, WAUKEGAN

the origin of the jet may have been on the order of 58°F, and that the initial temperature rise may have been 13°F, instead of 15°F. If an initial temperature rise of T_o = 13.0°F could be assumed, then all the points in the zone of establishment would be closer to the predicted value of T/T_o = 1.0.

Comparison of Results

The results from the three Widows Creek surveys, the New Johnsonville survey, and the Waukegan survey are summarized in Table 15. The values of the entrainment coefficient at Widows Creek were consistently E = 0.16 for three different field surveys with different values of $A = U_a/U_o$. The small value of E = 0.04 at New Johnsonville indicates the influence of the relatively narrow boundaries, which apparently greatly inhibited lateral entrainment. The value of E = 0.4 at Waukegan seems reasonable, since there were no boundaries to inhibit the lateral entrainment of colder water into the jet. However, this value may indicate the effects of vertical entrainment, since the rate of lateral mixing was not a full order of magnitude greater than vertical mixing at the Waukegan site. Because of the scatter of the data, it is difficult to determine the significance of this effect.

The values of the drag coefficient, C_D, ranged from 0.3 to 0.6, as A varied from 0.75 to 0.50. Over this narrow range of A, at least, it appears that C_D is a function of A under field conditions as well as under laboratory conditions.

TABLE 15

SUMMARY OF FIELD RESULTS

	A	ε'_o	Ri_o	E	C'_D	C_D
Widows Creek						
VU No. 1	0.50	85.0	0.22	0.16	1.0	0.6
VU No. 2	0.67	85.0	0.64	0.16	0.9	0.6
TVA	0.75	85.0	1.21	0.16	0.4	0.3
New Johnsonville	0.57	60.0	3.30	0.04	3.0	0.5
Waukegan	0.00	--	0.01	0.44	--	--

CHAPTER VII

DISCUSSION

Results of Laboratory and Field Investigations

Establishment Zone

Laboratory results describing how the zone of flow establishment is related to the velocity ratio are presented in Figures 18 and 19. These relations were used in analyzing the field data in order to obtain initial values of the jet axis distance and the initial angle, θ_o, from which to obtain the numerical solution. The laboratory results were used because detailed field measurements of the establishment zone could not be obtained due to time and equipment limitations. It is felt that the empirical curves in Figures 18 and 19 are adequate to describe the observed field conditions, as can be seen by examining the temperature and trajectory plots of the field data.

The length of the zone of flow establishment is, in general, slightly less than values found in the literature. A possible explanation is that the relations in this study were derived for the cases of the jet origin coinciding with the flume wall, while the relation used by Fan (22), for instance, was developed for a jet placed away from the boundary into a region of more nearly uniform flow. The effect of the velocity gradient near the boundary, it is felt, is to shorten the length of the establishment zone. Since the discharge coincides with

the boundary at most field sites, the relations derived in the present study are felt to be more realistic when applied to field sites.

Entrainment Coefficient

The entrainment mechanism, or the inflow velocity, is assumed to represent the turbulent mixing of the jet. The laboratory results presented in Tables 2, 3, and 4 indicate that $E = 0.4$ when $\beta_o = 90.0°$, and that $E = 0.2$ when $\beta_o' = 60.0°$ and $45.0°$. Thus, E appears to be a function of the initial angle of discharge of the jet. Apparently, as β_o' is decreased, the volume of colder water available for inflow and dilution of the heated jet on the side of the jet near the boundary is also decreased. Thus, the smaller values of E at $\beta_o' = 60.0°$ and $45.0°$ indicate the effect of the near boundary on entrainment.

The values of E at the two field sites located on rivers are lower than the laboratory results for comparable values of β_o'. These lower values apparently indicate the effect of the narrow boundaries on lateral inflow on both sides of the jet, since the ratios of the ambient width to the discharge width of 7.5 at Widows Creek and 3.5 at New Johnsonville are lower than the ratio of 24.0 used in the laboratory experiments.

The values of E at Widows Creek are consistently equal to 0.16 for three different field surveys with different values of $A = U_a/U_o$. Thus, it appears that, for a given site, the entrainment coefficient is reasonably constant.

For cases where $A = 0.0$, other investigators, such as Fan (22), have reported laboratory values of the entrainment coefficient on the order of 0.10. The value of $E = 0.44$ at the Waukegan field site is

greater and possibly indicates the effects of ambient turbulence and vertical mixing, the effects of which are not considered in the analytical model.

The entrainment coefficients determined in this study differ slightly from values found in the literature. Fan (22) has reported values on the order of 0.45 determined from measurements along the axis of a buoyant jet discharged vertically into a uniform, ambient current. However, his values would be smaller if a more realistic, bimodal profile had been assumed, since the maximum cross-sectional concentrations on both sides of the jet axis were 60 to 80% greater than concentrations along the jet axis. Keffer and Baines (30) have reported values of the entrainment coefficient which varied along the jet axis from 0.3 to 1.6 for air-in-air jets subject to a steady cross-wind. Zeller (48) presented values which varied from 0.127 to 0.993, not along the jet axis, but as determined from 22 sets of data for two surface jets at a field site. The values of E determined in the present study are not unreasonable, however, when the variation in the values of E reported by these other investigators is considered.

The entrainment coefficient appears to be a function of the assumed profile shape and other factors, the effects of which are not yet completely understood. For example, although some investigators suggest that E is a function of A, the results of the present study indicate that boundary geometry may be more significant when relatively narrow channels and discharge angles less than 90° are considered.

Drag Coefficient

The laboratory results presented in Tables 2 and 3, and in Figures 21 and 22 indicate that C_D varies with the velocity ratio and, possibly, with the angle of discharge. Values of C_D vs. A have also been reported by Fan (22) and Carter (12).

The range and magnitude of C_D from 0.1 to 3.8 are greater than would be expected based on the work of Fan, who reported a range of C_D from 0.1 to 1.7, and Carter, who reported values of C_D ranging from 0.74 to 1.36. However, as shown in Equations 17-19, the analytical form of the drag force used in this study is different from the forms used by Fan and Carter. Thus, a direct comparison of C_D values cannot be made.

The possible dependence of C_D on β_o' is indicated in Figure 22. The values of C_D are seen to decrease as β_o' decreases from 90° to 60° and 45°. In the analytical model, the drag force is assumed to represent the effects of the pressure gradient caused by the separation of the ambient flow behind the jet. At β_o' = 60.0° and 45.0°, the jet is closer and closer to the near boundary, the presence of which may inhibit the ambient flow and reduce the separation of the flow. Thus, the drag force may be reduced at β_o' = 60.0° and 45.0°, which would account for the smaller values of C_D observed at β_o' = 60.0° and 45.0°.

The field values of C_D are very close to the values that would have been predicted based on the laboratory results, as shown in Figure 44. In this figure, the observed field values of C_D vs. A, determined over the range of A from 0.5 to 0.75, are plotted along with the empirical laboratory curve, which was shown in Figure 21. Unfortunately, the lack of field values of C_D determined in the range of

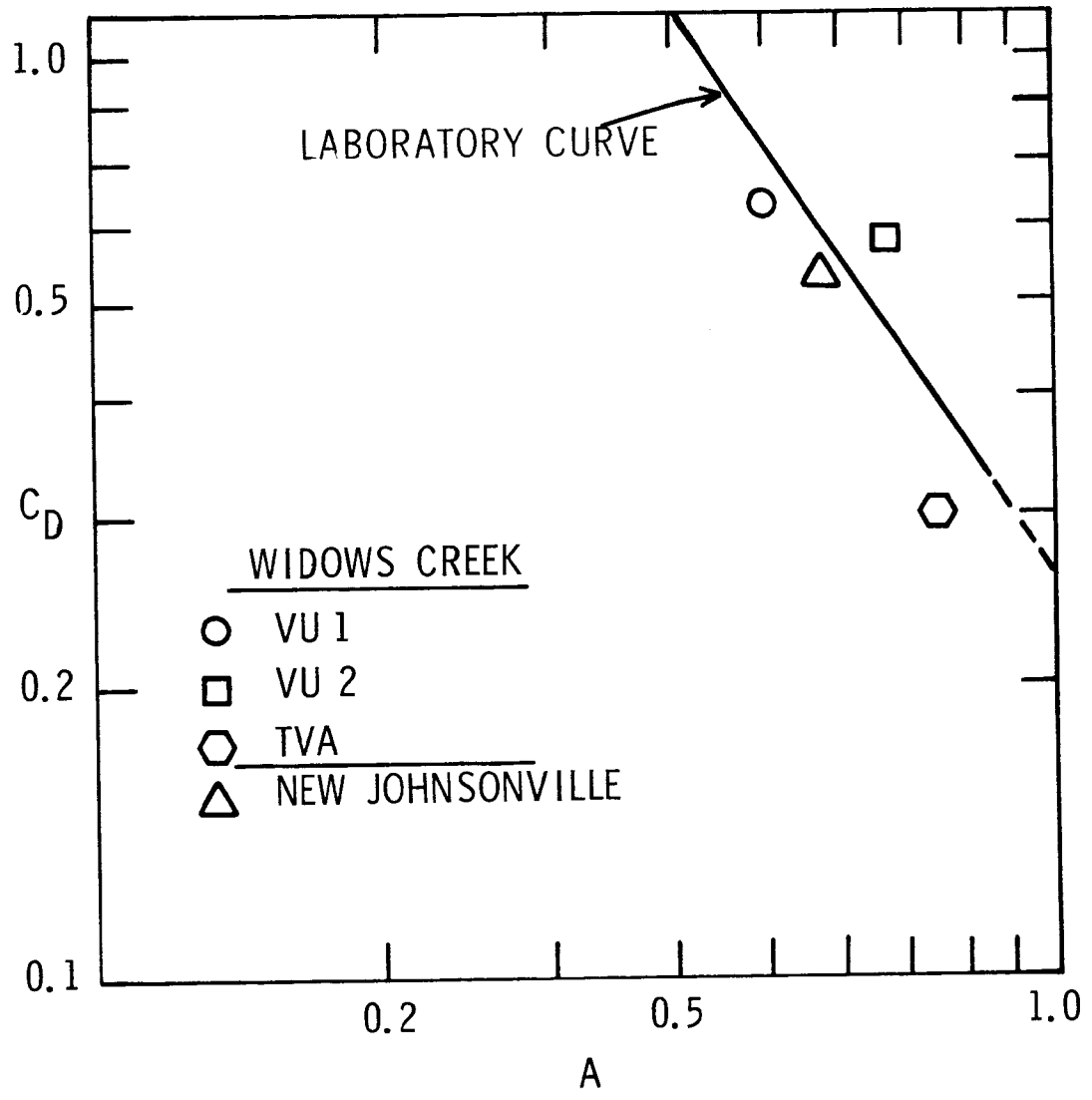

FIGURE 44.--OBSERVED FIELD VALUES OF DRAG COEFFICIENT VERSUS VELOCITY RATIO PLOTTED ON LABORATORY CURVE
(From Figure 21)

A from 0.5 to 0.2 or lower restricts the usefulness of Figure 44 at the present time.

The comparison of the observed field values of C_D with the laboratory-determined curve in Figure 44 implies that C_D is not a function of the Reynolds Number but only a function of A. However, since Reynolds Numbers in the field may be two or more orders of magnitude greater than in the laboratory, it may not be possible to merely extrapolate the C_D vs. A relation from the laboratory to field sites as is done in Figure 44.

Literature references, such as Prandtl and Tietjens (35), present C_D values for solid objects in a moving stream as functions of a Reynolds Number defined in terms of the ambient velocity and viscosity and some characteristic length, or diameter, of the solid body. In the present study, the jet is treated as a solid body in terms of the drag force. Therefore, it is possible to define a Reynolds Number, Re_D, in terms of the ambient velocity and viscosity and the depth of the jet as shown in Equation 75,

$$Re_D = \frac{U_a z}{\nu_a} \tag{75}$$

A plot of C_D vs. Re_D, shown in Figure 45, indicates that C_D may have the same characteristics as the drag coefficient usually associated with flow around solid bodies. The laboratory values of C_D decrease as the Re_D Number increases in the range of $10^2 < Re_D < 10^4$, and the field values of C_D become relatively constant as the Re_D Number approaches values of $Re_D \simeq 10^6$. A quantitative relation between C_D and Re_D in Figure 45 cannot be derived, since there are not enough data points, particularly in the range of $10^4 < Re_D < 10^5$. However, a possible relation

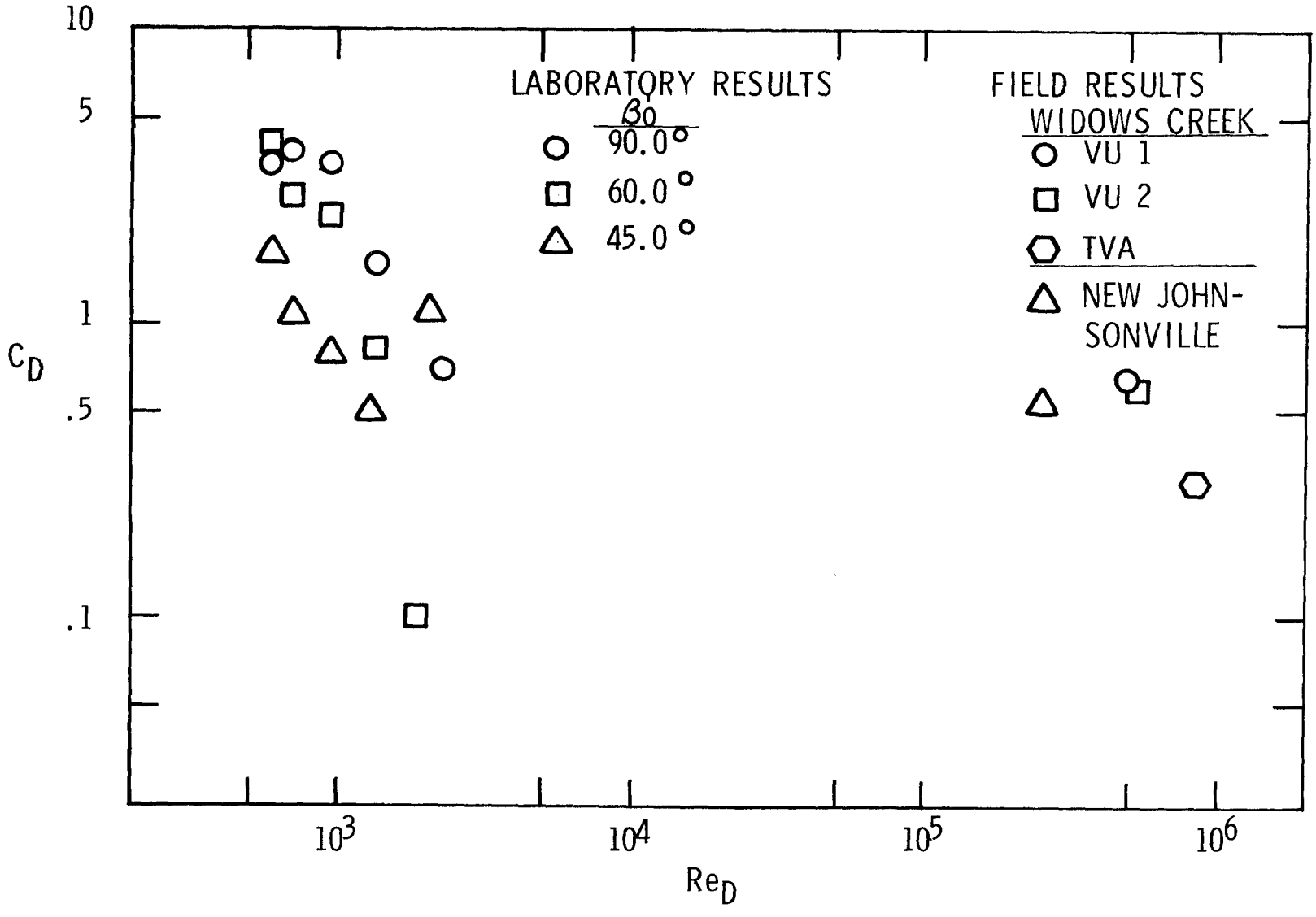

FIGURE 45.--OBSERVED VALUES OF DRAG COEFFICIENT VERSUS REYNOLDS NUMBER

between C_D and Re_D is suggested by Figure 45, and this relation should be studied further.

Possible Sources of Error

Determination of E and C_D

Values of E and C_D were obtained by fitting the theoretical curves to the observed data. Since the solutions were in numerical rather than analytical form, best-fit values were obtained by inspection. Some of the scatter in the reported results may be due to the graphical method of solution, but it is felt that this source of error is negligible when reasonable care is taken in determining E and C_D.

Ambient Turbulence

The effects of mixing due to ambient turbulence are not considered in the analytical model. It is assumed that the decrease in the temperature is due to the entrainment of ambient fluid, which is caused by the difference between the jet and the ambient velocities. As long as the jet velocity is greater than the parallel component of the ambient velocity, the decrease in temperature can be described by the model. However, as the jet velocity approaches the same direction and magnitude as the ambient velocity, the model predicts that entrainment and dilution decrease as the velocity difference decreases. Beyond this point, the observed decrease in the temperature would have to be accounted for by turbulent diffusion in the ambient stream.

Temperature measurements smaller than $T/T_o \simeq 0.10$ were not used in determining the values of the entrainment coefficient. It was felt that the jet velocities beyond this point had approached the same magnitude

and direction as the ambient velocity, and that the temperature decreases beyond this point were caused by the ambient turbulent diffusion.

Density Differences

Changes in density along the jet axis could, in some cases, affect the characteristics of the jet. However, since the maximum density difference was approximately $\Delta\rho/\rho = 0.9\%$ in the laboratory and approximately $\Delta\rho/\rho = 0.1\%$ in the field, changes in density are felt to have been negligible compared to a reference density, ρ_o.

Temperature Losses

Heat losses across the jet surface can be considered negligible, as demonstrated by the following calculations based on the work of Edinger and Geyer (19). The decrease in temperature rise along a stratified stream can be approximated by Equation 76,

$$T/T_o = \exp(-Kx/\rho_o C_p U_o z_o) \tag{76}$$

where K = the thermal exchange coefficient; and

C_p = the heat capacity of water.

Applying this equation to a surface jet actually exaggerates the decrease in temperature rise due to surface heat exchange, since lateral mixing of the jet will also reduce the temperature rise and, consequently, reduce the driving force for surface heat exchange.

Selecting representative values of K = 200 Btu/ft^2-day-°F (=2.32 x 10^{-3} Btu/ft^2-sec-°F), ρ_o = 62.4 lb/ft^3, and C_p = 1.0 Btu/lb °F, then values of T/T_o versus x/z_o can be computed for laboratory and field conditions from Equation 76. For example, using the laboratory value of U_a = 0.5 ft/sec, Equation 76 predicts $T/T_o = 0.98$ at $x/z_o = 200$. In the

laboratory, values on the order of $T/T_o = 0.10$ were measured at $x/z_o = 200$. The observed decrease in T/T_o due to both lateral mixing and surface heat exchange was therefore on the order of 0.90, while the predicted decrease in T/T_o due to surface heat exchange alone from Equation 76 is only about 0.02. Thus, the decrease in T/T_o due to lateral mixing and surface heat exchange is more than an order of magnitude greater than the decrease due to surface heat exchange alone.

Using the field value of $U_a = 1.06$ ft/sec, Equation 76 predicts $T/T_o = 0.965$ at $x/z_o = 1000$, or $x/b_o = 40$. In the field, values on the order of $T/T_o = 0.32$ were measured at $x/b_o = 40$. The observed decrease in T/T_o due to lateral mixing and surface heat exchange was therefore on the order of 0.7, while the predicted decrease due to surface heat exchange alone from Equation 76 is about 0.04. Therefore, since the decrease in T/T_o due to lateral mixing and surface heat exchange is more than an order of magnitude greater than the decrease due to surface heat exchange alone in the laboratory and in the field, then the effects of surface heat exchange can reasonably be neglected in the present study.

Application

The usefulness of the two-dimensional surface jet model in analyzing field data appears to be dependent on the velocity ratio and the discharge angle, the value of the initial Richardson Number, and the intensity of the ambient turbulence.

Velocity Ratio and Discharge Angle

For the ranges of A and β_o' considered in the laboratory and in the field, the results of the present study indicate that, even when the

discharge velocity is on the same order of magnitude as the ambient velocity, the effects of the discharge velocity should be considered, as long as the initial direction of the discharge velocity is significantly different from the direction of the ambient current. The effect of changes in the discharge velocity on the spatial temperature distribution can be seen by examining the observed laboratory and field trajectories. As the velocity ratio is changed, the location of the trajectory is also changed. The analytical model, which considers the non-uniform velocity field caused by the surface jet, can be used to describe how these changes in the velocity ratio affect the temperature distribution.

Initial Richardson Number

The value of the initial Ri Number can be used to indicate whether or not the jet will be two-dimensional. Jen et al. (29) report that the rate of lateral mixing is only twice the vertical rate for the range of $5.0 \times 10^{-5} \leq Ri_o \leq 3.0 \times 10^{-3}$, while the results of Tamai et al. (43) indicate that the lateral rate is somewhat greater when the Ri_o Number is in the range of $1.0 \times 10^{-2} \leq Ri_o \leq 2.0 \times 10^{-1}$. The results of the present study indicate that the two-dimensional assumption is valid when the Ri_o Number is as low as $Ri_o = 0.22$, which is the lowest of the values determined at Widows Creek, where the rate of lateral mixing was found to be about 8.0 times the vertical rate. This is reasonable, since Ellison and Turner (21) and Zeller (48) have all reported for the case of a surface jet that the value of the Ri Number along the jet axis rapidly increases to 1.0 or greater, and that vertical mixing becomes negligible.

The two-dimensional assumption also appears to be valid at even lower values of the Ri_o Number in cases where vertical entrainment is inhibited by shallow depths.

Ambient Turbulence

The effects of ambient turbulence have not been investigated in the present study. Based on the laboratory and field results, the analytical model seems adequate to describe the decrease in the temperature rise to values as low as $T/T_o \approx 0.10$ as far downstream as $x/b_o \approx 100$. In highly turbulent streams, the temperature decrease may be even more dependent on the intensity of the ambient turbulence.

Usefulness of the Proposed Model

When a heated discharge has the characteristics of a two-dimensional surface jet, then the location of the jet trajectory and the changes in temperature and width along the trajectory can be determined by the model developed in the present study. The model developed by Zeller (48) does not consider the pressure gradient across the jet. The importance of the pressure gradient on the location of the jet can be seen by considering the magnitude of the C_D values determined in the present study. The model developed by Carter (12) cannot predict the change in the jet width along the jet trajectory.

It is felt that the present study represents an advance in the analysis and prediction of temperature distributions. The usefulness of the proposed model should increase as more cases of field data are analyzed to determine the values of the entrainment and drag coefficients over a wide range of field conditions.

CHAPTER VIII

SUMMARY AND CONCLUSIONS

A survey of the literature indicated that further study of surface jets was justified. Previous work did not contain a completely suitable method for quantitatively describing the spatial temperature distribution in the vicinity of power plants located on rivers where the discharge and the ambient velocities should both be considered. The analytical and experimental studies performed by Jen, Wiegel, and Mobarek (29), Tamai, Wiegel, and Tornberg (43), and Hayashi and Shuto (28) are applicable primarily to jets discharging into ambient water bodies that have no appreciable velocity. The two-dimensional surface jet model developed by Zeller (48) does not consider the pressure gradient that exists across the surface jet parallel to the ambient current, while the model developed by Carter (12) cannot predict the change in the width of the jet along the axis. Therefore, a model is developed which is able to better describe certain cases of heated power plant discharges.

Analytical Development

The present study, which is based on the previous work of Morton (34), Fan (22), and Zeller (48), develops a system of ordinary differential equations, Equations 25, 27, 28, 30, 31, and 32, which, when solved numerically, predicts the jet trajectory, width, velocity, and temperature distribution for the case of a two-dimensional surface jet.

The entrainment mechanism is assumed to represent the turbulent mixing of the jet. The inflow velocity, which is assumed to be proportional to the difference between the centerline velocity of the jet and the parallel component of the ambient velocity, is written as in Equation 12,

$$v_i = E(U - U_a \cos \beta) \tag{12}$$

The coefficient E is defined as the experimentally-determined entrainment coefficient.

The pressure gradient, due to the separation of the ambient flow, is assumed to be represented by the drag force normal to the jet axis, as shown in Equation 17,

$$(\rho_a F_D ds) = \frac{C_D \rho_a U_a^2 (z\ ds) \sin \beta}{2} \tag{17}$$

The coefficient, C_D, is the experimentally-determined drag coefficient. As the jet becomes parallel to the ambient flow, the drag force goes to zero, because the projected area normal to the ambient current, or $(z\ ds \sin \beta)$, goes to zero.

In practical applications, the zone of flow establishment of the jet, illustrated in Figure 8, must be determined. As in previous work on jets in a non-parallel stream, it was necessary to empirically determine how the length of the zone of flow establishment and how the initial angle at the end of the zone are related to the velocity ratio and to the initial angle of the discharge.

Laboratory Experiments

The laboratory experiments were designed to study the entrainment and drag coefficients and the zone of flow establishment. The object was to functionally relate these coefficients and the zone of establishment to the velocity ratio and to the initial angle of discharge. The velocity ratio, $A = U_a/U_o$, was varied from 0.180 to 0.727, and jets with discharge angles of $\beta_o' = 45.0°$, 60.0°, and 90.0° were used.

The values of the entrainment coefficient are presented in Tables 2, 3, and 4. The results indicate that $E = 0.4$ when $\beta_o' = 90.0°$, and that $E = 0.2$ when $\beta_o' = 60.0°$ and 45.0°. Thus, it appears that E is a function of boundary geometry. For the range of A used in the present study, E was not found to be a function of A.

The results presented in Tables 2 and 3 and Figures 21 and 22 show that C_D ranged from 0.1 to 3.8. It appears that C_D varies with the velocity ratio, as shown in Figure 21, and, possibly, with the initial angle of discharge, as shown in Figure 22.

The length of the zone of establishment and the initial angle at the end of the zone were related to the velocity ratio. The empirically-determined relations describing s_e'/b_o vs. A and β_o/β_o' vs. A are shown in Figures 18 and 19, respectively.

Field Surveys

Data obtained from five field surveys at three different steam-electric generating plants were analyzed to see how well the two-dimensional surface jet model describes the observed temperature distributions.

The values of E and C_D from the field surveys are presented in Table 15. The values of E at Widows Creek are consistently equal to 0.16 for three different field surveys with different values of $A = U_a/U_o$. The small value of E = 0.04 at New Johnsonville reflects the influence of the relatively narrow boundaries, which apparently greatly inhibit lateral entrainment. The value of E = 0.4 at Waukegan seems reasonable, since there are no boundaries to inhibit the lateral entrainment of cooler water into the jet. However, this last value may indicate the effects of ambient turbulence and vertical entrainment, the effects of which the analytical model does not consider. The scatter of the data at this site makes it difficult to determine how great these effects are.

The values of C_D are very close to the values that would have been predicted based on the laboratory results, as shown in Figure 44.

The laboratory-derived relations describing the zone of flow establishment were used in analyzing the field data. The laboratory results were used because detailed field measurements of the establishment zone could not be obtained due to time and equipment limitations.

Results of the Laboratory and Field Investigations

Results indicate that the value of the entrainment coefficient is a function of boundary geometry. The results of the laboratory studies indicate that lateral inflow, or dilution, is inhibited along the near boundary when the discharge angle is decreased: the value of E decreased from 0.4 to 0.2 when θ_o' was decreased from 90° to 60° and 45°.

The results of the field studies indicate that lateral inflow on both sides of the jet is inhibited by a narrow channel. It appears that E decreases as the ratio of the channel width to the discharge width decreases, because values of E = 0.16 were determined at Widows Creek, where the ratio is about 7.5, and a smaller value of E = 0.04 was determined at New Johnsonville, where the ratio is about 3.5.

The field values of C_D closely agree with the empirically-determined laboratory curve, as shown in Figure 44. However, the possible dependence of C_D on the Reynolds Number is also considered. A plot of C_D vs. the Reynolds Number, shown in Figure 45, indicates that C_D may have the same characteristics as the drag coefficient usually associated with flow around solid bodies. The laboratory values of C_D decrease as the Re_D Number increases in the range of $10^2 < Re_D < 10^4$, and the field values of C_D become relatively constant and equal to about 0.5 at values of $Re_D \simeq 10^6$. It is felt that this possible relation between C_D and the Re_D Number should be studied further.

Application

The results of the laboratory and field investigations indicate that the application of the two-dimensional surface jet model is dependent on the velocity ratio and the initial angle of discharge, the value of the initial Richardson Number, and, possibly, the intensity of the ambient turbulence.

Even when the jet velocity is on the same order of magnitude as the ambient velocity, it appears that the temperature distribution can still be described in terms of a surface jet, as long as the initial

direction of the discharge velocity is significantly different from the direction of the ambient current.

The two-dimensional assumption appears valid when the initial Richardson Number is as low as 0.22, which is the lowest of the values determined at Widows Creek, where the rate of lateral mixing was found to be about 8.0 times greater than the vertical rate.

The effect of ambient turbulence is not considered in the proposed model. However, the model seems to adequately describe the decrease in the temperature rise as far downstream as $s/b_o \approx 100$, unless the ambient stream is highly turbulent.

Future Work

Entrainment and Drag Coefficients

The accurate prediction of values of E and C_D for design purposes depends upon additional work. More field data should be obtained and compared to the proposed model in order to determine the values of E and C_D at different field sites under widely varying conditions.

The effects of boundary geometry on the temperature distribution are reflected in the empirically-determined values of E. According to Rouse (38), at some distance downstream in a narrow channel, lateral inflow becomes negligible, and the volume flux of the jet becomes constant. Thus, boundary effects could be treated theoretically by modifying the system of equations so that lateral entrainment goes to zero at some point downstream.

The effects of the ratio of the channel width to the discharge width could be studied in the laboratory by varying the width of the

channel or the size of the jet. Also, these effects would have to be considered in modeling a specific field site.

Vertical Entrainment

Future work should consider the effects of vertical entrainment, which causes a greater decrease in the temperature rise that the two-dimensional model predicts. Vertical entrainment occurs when the shearing force of the jet velocity is greater than the opposing buoyancy force, which is due to the density difference between the jet and the heavier ambient fluid. When the initial Richardson Number is very small, the rate of vertical spreading is no longer negligible compared to the lateral rate and must be considered.

It appears that the rate of vertical spreading could be related to the lateral rate in terms of the Richardson Number, which, according to Ellison and Turner (21), increases with distance along the jet axis. Along the jet axis, the vertical rate of spreading would decrease as a function of the increasing Richardson Number. A three-dimensional analytical model would have to be formulated in which the decrease in temperature rise would be greater than that predicted by a two-dimensional model but less than the decrease predicted by an axi-symmetric model. Fietz and Wood (24) have studied the case of a three-dimensional density current along a sloping floor. However, considerable work remains to be done in order to develop a useful model for cases of surface jets.

Ambient Turbulence

Two approaches to the problem of temperature prediction in the mixing zone downstream from a power plant are currently in use. The

first approach, illustrated by the present study, is to assume that the heated discharge can be described in terms of a momentum jet. The second approach, illustrated by the work of Edinger and Polk (20), is to assume that mixing can be determined by considering the diffusion due to ambient turbulence. However, in some cases, as noted by Csanady (16) and others, both jet momentum and ambient turbulence should be considered.

Future investigators should consider combining the two approaches. Pratte and Baines (36) note the importance of the relative size of the turbulent eddies compared to the size of the jet cross-section. Some suggestions are offered by Briggs (8), who has studied plume rise and dispersion in the atmosphere. He feels that the point at which the plume velocity becomes small compared to the ambient velocity can be characterized by the eddy dissipation, which is a measure of the ambient turbulence, and some characteristic radius of the plume. Such an approach might be applied to the case of a surface jet.

Establishment Zone

The present derivation of the establishment zone assumed a uniform temperature and velocity distribution at the point of discharge. However, at many field sites, the temperature and velocity profiles are likely to be non-uniform at the mouth of the discharge channel, and the establishment zone is likely to be shorter than would be predicted by the present relations. More consideration should also be given to predicting the initial jet depth in terms of the cold water wedge that, according to Harleman (26), may intrude into the discharge channel.

Surface Heat Exchange

The effects of surface heat exchange should be considered for cases where a large surface area is available for cooling. To more accurately describe conditions on lakes and wide rivers, the equation for the conservation of heat could be rewritten to include a "sink" term, which would represent the loss of heat across the air-water interface. Based on the work of Edinger and Geyer (19) and Edinger, Duttweiler, and Geyer (18), the heat loss term would be a function of the equilibrium temperature and the thermal exchange coefficient.

Analytical Solution

The present study solves a system of equations by numerical integration and then evaluates the entrainment and drag coefficients by inspection. If an analytical solution describing the location of the jet trajectory and the decrease in the temperature rise could be obtained, then the coefficients could be evaluated, for instance, by a least-squares technique. This would eliminate some of the subjectivity inherent in the present method. At present, however, analytical solutions for all but the simplest cases of jets are limited to cases of irrotational flow. Gordier (25), for instance, studied a two-dimensional slot jet in terms of free streamline analysis and conformal mapping. The usefulness of ideal flow theory would depend on realistically approximating the turbulent entrainment of the jet.

These suggestions for future work should help to further refine the analysis and prediction of the temperature distribution in the vicinity of thermal-electric power plants. It is hoped that the present study is adequate to serve as a base for future research.

APPENDIX A

LABORATORY
LATERAL TEMPERATURE MEASUREMENTS, T'/T_o

Run	y'/b_o / x'/b_o	1.41	4.51	7.61	10.7	13.8	16.9	20.0	23.1	26.2	29.3	32.4	b/b_o
1-90	84.5	0.08	0.08	0.09	0.10	0.04	0.04	0.01	0.00	0.00	0.00	0.00	7.9
1-90	67.7	0.08	0.09	0.10	0.09	0.04	0.04	0.01	0.00	0.00	0.00	0.00	7.4
1-90	50.7	0.10	0.12	0.11	0.07	0.04	0.01	0.00	0.00	0.00	0.00	0.00	6.7
1-90	33.8	0.11	0.16	0.14	0.05	0.00	0.00	0.00	0.00	0.00	0.00	0.00	5.2
1-90	16.9	0.19	0.26	0.07	0.01	0.00	0.00	0.00	0.00	0.00	0.00	0.00	4.2
2-90	84.5	0.04	0.04	0.07	0.09	0.08	0.09	0.06	0.06	0.03	0.04	0.06	12.6
2-90	67.7	0.04	0.05	0.07	0.10	0.11	0.10	0.07	0.07	0.03	0.03	0.04	11.7
2-90	50.7	0.03	0.06	0.10	0.10	0.12	0.02	0.10	0.04	0.01	0.01	0.01	9.8
2-90	33.8	0.03	0.11	0.13	0.15	0.17	0.09	0.05	0.02	0.01	0.00	0.01	8.1
2-90	16.9	0.06	0.23	0.24	0.16	0.10	0.03	0.00	0.00	0.00	0.00	0.00	6.5
3-90	84.5	0.03	0.03	0.05	0.08	0.12	0.09	0.07	0.07	0.05	0.05	0.08	12.5
3-90	67.7	0.02	0.03	0.05	0.10	0.12	0.08	0.07	0.07	0.07	0.05	0.03	11.5
3-90	50.7	0.02	0.04	0.09	0.12	0.13	0.10	0.05	0.05	0.07	0.08	0.01	11.4
3-90	33.8	0.03	0.07	0.13	0.13	0.14	0.11	0.11	0.08	0.08	0.01	0.01	5.0
3-90	16.9	0.05	0.15	0.24	0.19	0.16	0.07	0.00	0.00	0.00	0.00	0.00	3.5

APPENDIX A -- Continued

Run	y'/b_o / x'/b_o	1.41	4.51	7.61	10.7	13.8	16.9	20.0	23.1	26.2	29.3	32.4	b/b_o
4-90	84.5	0.03	0.03	0.03	0.04	0.06	0.09	0.09	0.13	0.12	0.15	0.13	12.2
4-90	50.7	0.01	0.02	0.05	0.06	0.10	0.13	0.11	0.08	0.06	0.06	0.06	11.1
4-90	33.8	0.01	0.04	0.07	0.13	0.15	0.17	0.13	0.11	0.05	0.03	0.01	9.4
4-90	16.9	0.01	0.09	0.17	0.21	0.08	0.02	0.00	0.00	0.00	0.00	0.00	5.8
4-90	8.45	0.02	0.22	0.30	0.24	0.16	0.02	0.01	0.01	0.00	0.00	0.00	6.5
5-90	84.5	0.02	0.02	0.02	0.07	0.07	0.10	0.09	0.10	0.11	0.11	0.11	11.6
5-90	50.7	0.02	0.03	0.07	0.06	0.10	0.10	0.14	0.14	0.13	0.06	0.00	10.2
5-90	33.8	0.01	0.02	0.07	0.11	0.15	0.19	0.17	0.03	0.00	0.01	0.00	7.3
5-90	16.9	0.01	0.04	0.14	0.24	0.20	0.08	0.02	0.00	0.00	0.00	0.00	5.5
5-90	8.45	0.02	0.14	0.25	0.30	0.06	0.01	0.00	0.00	0.00	0.00	0.00	4.4
1-60	84.5	0.09	0.13	0.17	0.09	0.04	0.04	0.01	0.01	0.00	0.00	0.00	7.6
1-60	67.7	0.10	0.18	0.20	0.09	0.04	0.02	0.01	0.00	0.00	0.00	0.00	6.9
1-60	50.7	0.12	0.23	0.17	0.07	0.06	0.01	0.00	0.00	0.00	0.00	0.00	6.9
1-60	33.8	0.18	0.28	0.09	0.03	0.00	0.01	0.00	0.00	0.00	0.00	0.00	6.1
1-60	16.9	0.34	0.20	0.02	0.01	0.00	0.01	0.00	0.00	0.00	0.00	0.00	5.7
1-60	8.45	0.53	0.01	0.00	0.01	0.00	0.01	0.00	0.00	0.00	0.00	0.00	6.1

APPENDIX A -- Continued

Run	x'/b_o \ y'/b_o	1.41	4.51	7.61	10.7	13.8	16.9	20.0	23.1	26.2	29.3	32.4	b/b_o
2-60	84.5	0.06	0.04	0.06	0.13	0.15	0.15	0.10	0.06	0.06	0.04	0.06	11.5
2-60	67.7	0.06	0.04	0.07	0.17	0.20	0.15	0.07	0.07	0.04	0.04	0.01	9.8
2-60	50.7	0.06	0.06	0.14	0.23	0.21	0.12	0.06	0.05	0.02	0.01	0.01	8.6
2-60	33.8	0.04	0.13	0.30	0.24	0.15	0.06	0.01	0.01	0.00	0.00	0.00	6.7
2-60	16.9	0.07	0.37	0.24	0.06	0.01	0.01	0.00	0.00	0.00	0.00	0.00	6.1
3-60	84.5	0.05	0.03	0.04	0.09	0.17	0.15	0.15	0.13	0.06	0.06	0.08	11.3
3-60	67.7	0.04	0.04	0.05	0.15	0.21	0.17	0.11	0.10	0.05	0.03	0.02	9.6
3-60	50.7	0.04	0.06	0.11	0.19	0.25	0.10	0.05	0.03	0.01	0.00	0.01	7.8
3-60	33.8	0.04	0.09	0.22	0.21	0.19	0.08	0.04	0.17	0.00	0.00	0.01	7.5
3-60	16.9	0.03	0.25	0.22	0.05	0.04	0.01	0.00	0.00	0.00	0.00	0.00	---
4-60	84.5	0.07	0.05	0.04	0.07	0.08	0.11	0.11	0.11	0.08	0.07	0.14	13.4
4-60	50.7	0.05	0.04	0.08	0.14	0.18	0.15	0.15	0.07	0.05	0.04	0.03	10.4
4-60	33.8	0.04	0.05	0.15	0.18	0.18	0.12	0.04	0.04	0.01	0.01	0.00	8.2
4-60	16.9	0.03	0.22	0.27	0.08	0.04	0.03	0.00	0.00	0.00	0.01	0.01	6.8
4-60	8.45	0.12	0.40	0.04	0.02	0.01	0.01	0.00	0.00	0.00	0.01	0.01	6.8

APPENDIX A -- Continued

Run	y'/b_o / x'/b_o	1.41	4.51	7.61	10.7	13.8	16.9	20.0	23.1	26.2	29.3	32.4	b/b_o
5-60	84.5	0.05	0.02	0.04	0.05	0.04	0.08	0.11	0.11	0.11	0.11	0.15	12.6
5-60	50.7	0.03	0.04	0.08	0.10	0.15	0.15	0.11	0.08	0.04	0.04	0.03	10.4
5-60	33.8	0.03	0.04	0.08	0.15	0.19	0.19	0.04	0.04	0.01	0.01	0.01	8.1
5-60	16.9	0.02	0.15	0.22	0.19	0.11	0.01	0.01	0.01	0.00	0.00	0.01	7.4
5-60	8.45	0.03	0.22	0.35	0.08	0.01	0.01	0.00	0.00	0.00	0.00	0.01	6.2
1-45	84.5	0.09	0.13	0.18	0.17	0.06	0.07	0.04	0.01	0.01	0.01	0.01	9.2
1-45	67.7	0.09	0.17	0.23	0.16	0.06	0.04	0.01	0.01	0.01	0.01	0.01	8.6
1-45	50.7	0.11	0.25	0.23	0.09	0.04	0.02	0.01	0.01	0.01	0.01	0.01	8.5
1-45	33.8	0.13	0.38	0.09	0.04	0.01	0.01	0.01	0.01	0.01	0.01	0.01	8.6
1-45	16.9	0.38	0.17	0.01	0.01	0.01	0.01	0.01	0.01	0.01	0.01	0.01	9.4
1-45	8.45	0.56	0.02	0.01	0.01	0.01	0.01	0.01	0.01	0.01	0.01	0.01	9.4
2-45	84.5	0.10	0.11	0.09	0.15	0.18	0.19	0.13	0.11	0.08	0.06	0.09	12.3
2-45	67.7	0.12	0.09	0.11	0.20	0.22	0.21	0.13	0.10	0.06	0.06	0.02	10.8
2-45	50.7	0.11	0.11	0.18	0.30	0.25	0.17	0.08	0.06	0.02	0.01	0.01	8.8
2-45	33.8	0.12	0.14	0.34	0.29	0.13	0.07	0.02	0.01	0.00	0.00	0.00	7.0
2-45	16.9	0.15	0.43	0.21	0.07	0.01	0.01	0.00	0.00	0.00	0.00	0.00	6.1

APPENDIX A -- Continued

Run	y'/b_o / x'/b_o	1.41	4.51	7.61	10.7	13.8	16.9	20.0	23.1	26.2	29.3	32.4	b/b_o
3-45	84.5	0.06	0.03	0.05	0.10	0.09	0.14	0.13	0.07	0.06	0.06	0.03	11.5
3-45	67.7	0.07	0.06	0.07	0.14	0.17	0.15	0.12	0.06	0.05	0.03	0.01	10.4
3-45	50.7	0.07	0.07	0.12	0.20	0.16	0.08	0.05	0.02	0.00	0.00	0.01	8.3
3-45	33.8	0.07	0.11	0.25	0.17	0.05	0.03	0.00	0.00	0.00	0.00	0.01	6.9
3-45	16.9	0.11	0.27	0.08	0.05	0.00	0.00	0.00	0.00	0.00	0.00	0.00	6.6
4-45	84.5	0.06	0.05	0.05	0.09	0.09	0.12	0.09	0.09	0.08	0.08	0.10	13.2
4-45	50.7	0.05	0.05	0.08	0.13	0.17	0.17	0.12	0.06	0.02	0.02	0.02	10.0
4-45	33.8	0.05	0.09	0.16	0.24	0.21	0.14	0.05	0.04	0.01	0.00	0.01	7.8
4-45	16.9	0.04	0.21	0.33	0.05	0.01	0.01	0.00	0.00	0.00	0.00	0.00	5.8
4-45	8.45	0.10	0.51	0.02	0.01	0.00	0.00	0.00	0.00	0.00	0.00	0.00	5.8
5-45-	84.5	0.06	0.06	0.04	0.08	0.08	0.11	0.10	0.10	0.10	0.08	0.11	13.2
5-45	50.7	0.04	0.08	0.10	0.11	0.15	0.17	0.11	0.10	0.06	0.04	0.01	10.3
5-45	33.8	0.03	0.06	0.17	0.21	0.13	0.15	0.10	0.08	0.02	0.00	0.01	8.7
5-45	16.9	0.01	0.19	0.29	0.21	0.06	0.08	0.02	0.00	0.00	0.00	0.00	6.6
5-45	8.45	0.04	0.42	0.06	0.02	0.00	0.00	0.00	0.00	0.00	0.00	0.00	4.9

APPENDIX B

LOCATION OF LABORATORY TRAJECTORIES

Run 1-90				Run 2-90				Run 3-90			
x'/b_o	y'/b_o	s'/b_o	T/T_o	x'/b_o	y'/b_o	s'/b_o	T/T_o	x'/b_o	y'/b_o	s'/b_o	T/T_o
0.07	0.28	0.29	1.00	0.01	0.14	0.14	0.97	0.01	0.13	0.13	0.99
0.49	0.63	0.80	1.00	0.01	0.71	0.71	0.97	0.35	0.78	0.85	1.00
0.71	0.99	1.21	0.97	0.14	0.71	0.72	1.00	0.42	0.99	1.07	0.98
1.41	1.41	1.96	0.85	0.28	0.99	1.03	0.98	0.35	1.06	0.12	1.00
2.82	1.97	3.41	0.75	0.71	1.41	1.58	0.97	0.71	1.20	1.39	0.96
4.23	2.26	4.81	0.63	0.71	1.55	1.70	0.97	0.49	1.41	1.49	0.97
5.64	2.26	6.2	0.54	1.41	2.11	2.71	0.83	1.41	2.33	2.65	0.79
7.05	2.93	7.6	0.48	2.82	3.17	4.15	0.67	2.82	2.95	4.15	0.64
8.46	3.03	9.1	0.47	4.23	3.67	5.79	0.57	4.23	3.95	5.85	0.57
8.46	3.03	9.1	0.47	5.64	3.88	7.09	0.47	5.64	4.37	7.25	0.53
12.7	3.81	13.3	0.33	7.05	4.72	8.40	0.41	7.05	4.93	8.65	0.47
16.9	4.09	17.6	0.26	8.46	4.44	9.81	0.37	8.46	4.79	10.1	0.44
16.9	4.09	17.6	0.26	12.7	5.64	14.2	0.27	12.7	5.77	14.4	0.29
33.8	4.51	34.5	0.16	16.9	5.99	18.4	0.22	16.9	6.35	18.5	0.25
50.7	4.51	51.4	0.12	16.9	5.99	18.4	0.24	16.9	6.34	18.5	0.24
67.7	7.61	68.4	0.10	33.8	13.8	35.3	0.17	33.8	13.8	35.3	0.14
84.5	10.7	85.2	0.10	50.7	13.8	52.2	0.12	50.7	13.8	52.3	0.13
				67.7	13.8	69.2	0.11	67.7	13.8	69.3	0.12
				84.5	10.7	86.0	0.09	84.5	13.8	86.1	0.12

APPENDIX B -- Continued

Run 4-90				Run 5-90				Run 1-60			
x'/b_o	y'/b_o	s'/b_o	T/T_o	x'/b_o	y'/b_o	s'/b_o	T/T_o	x'/b_o	y'/b_o	s'/b_o	T/T_o
0.01	0.28	0.28	1.00	0.01	0.07	0.07	1.00	0.07	0.13	0.15	1.00
0.01	0.85	0.85	1.00	0.01	0.56	0.56	1.00	0.42	0.25	0.49	0.98
0.01	1.13	1.13	0.99	0.01	0.99	0.99	0.98	0.71	0.35	0.79	0.96
0.28	1.55	1.57	0.99	0.01	1.13	1.13	0.98	1.41	0.49	1.45	0.85
0.71	1.69	1.83	0.96	0.01	1.55	1.55	0.95	2.82	0.77	2.86	0.67
0.71	2.11	2.22	0.87	0.71	1.97	2.09	0.85	4.23	0.83	4.30	0.59
1.41	3.17	3.35	0.70	1.41	3.38	3.64	0.60	5.64	1.20	5.71	0.57
2.82	4.79	5.10	0.52	2.82	5.78	6.30	0.50	7.05	1.41	7.15	0.57
4.23	4.79	6.55	0.43	4.23	5.99	7.35	0.40	8.46	1.62	8.55	0.55
5.64	5.50	8.09	0.40	5.64	6.91	9.05	0.36	8.46	1.76	8.56	0.55
7.05	6.35	9.4	0.28	7.05	8.11	10.4	0.32	12.7	2.26	12.8	0.51
8.45	7.33	11.4	0.30	8.46	9.16	12.2	0.31	16.9	2.54	17.0	0.41
8.45	7.61	11.4	0.30	12.7	11.1	16.8	0.23	16.9	2.54	17.0	0.41
16.9	10.0	20.2	0.21	16.9	14.2	22.0	0.18	33.8	4.51	33.9	0.28
33.8	16.9	37.1	0.17	33.8	16.9	38.9	0.19	50.7	4.51	50.8	0.23
50.7	16.9	54.0	0.13	50.7	23.1	55.8	0.15	67.7	7.61	67.8	0.20
84.5	29.3	87.8	0.16	84.5	29.3	89.6	0.11	84.5	7.61	84.6	0.17

APPENDIX B -- Continued

Run 2-60				Run 3-60				Run 4-60			
x'/b_o	y'/b_o	s'/b_o	T/T_o	x'/b_o	y'/b_o	s'/b_o	T/T_o	x'/b_o	y'/b_o	s'/b_o	T/T_o
0.71	0.56	0.90	1.00	0.28	0.13	0.31	1.00	0.28	0.23	0.36	1.00
1.20	0.85	1.65	0.99	0.85	0.44	0.96	0.98	0.71	0.69	0.99	1.00
1.41	1.06	1.95	0.90	0.49	0.40	0.63	0.99	1.41	1.10	1.79	0.99
2.82	1.90	3.60	0.84	0.71	0.80	1.07	0.94	1.69	1.49	2.25	0.97
4.23	2.68	5.15	0.80	1.41	1.2	1.79	0.91	2.82	2.61	3.80	0.75
5.64	2.82	6.60	0.73	2.82	2.1	3.55	0.77	4.23	3.07	5.30	0.55
7.05	3.24	8.05	0.69	4.23	2.8	5.20	0.66	5.64	3.98	6.90	0.53
8.46	3.67	9.50	0.65	5.64	3.5	6.65	0.53	7.05	4.09	8.25	0.43
12.7	5.36	13.9	0.57	7.05	3.9	8.15	0.49	8.45	5.23	9.90	0.46
16.9	6.35	18.3	0.50	8.46	4.0	9.51	0.38	8.45	4.51	9.90	0.40
16.9	4.51	18.3	0.37	12.7	5.5	13.9	0.34	16.9	7.47	18.7	0.30
33.8	7.61	35.2	0.31	16.9	6.3	18.4	0.27	16.9	7.61	18.7	0.28
50.7	10.7	52.1	0.23	16.9	6.3	18.4	0.31	33.8	12.3	35.6	0.18
67.7	13.8	69.1	0.21	16.9	4.5	18.4	0.25	50.7	13.8	52.5	0.18
84.5	13.8	85.9	0.16	33.8	7.6	35.3	0.22	84.5	20.0	86.3	0.14
				50.7	13.8	52.2	0.25				
				67.7	13.8	69.2	0.21				
				84.5	13.8	86.0	0.17				

APPENDIX B -- Continued

Run 5-60				Run 1-45				Run 2-45			
x'/b_o	y'/b_o	s'/b_o	T/T_o	x'/b_o	y'/b_o	s'/b_o	T/T_o	x'/b_o	y'/b_o	s'/b_o	T/T_o
0.01	0.13	0.13	0.98	0.01	0.13	0.13	1.00	0.28	0.14	0.31	1.00
0.71	1.01	1.23	1.00	0.14	0.17	0.20	0.98	0.71	0.42	0.82	1.00
0.71	1.16	1.36	0.99	0.71	0.42	0.82	0.88	1.41	0.85	1.60	0.90
1.41	1.96	2.35	1.00	1.41	0.63	1.45	0.76	2.82	1.55	3.15	0.82
2.82	3.10	4.10	0.60	2.82	0.85	2.85	0.67	4.23	1.83	4.55	0.78
4.23	4.02	5.90	0.45	4.23	1.13	4.30	0.65	5.64	2.40	6.10	0.72
5.64	4.51	7.35	0.44	5.64	1.27	5.72	0.61	7.05	2.68	7.50	0.69
7.05	5.64	9.10	0.39	7.05	1.34	7.10	0.57	8.46	3.10	8.95	0.63
8.46	5.91	10.5	0.37	8.45	1.41	8.49	0.56	12.7	3.95	13.2	0.53
8.45	7.61	10.5	0.35	8.46	1.41	8.50	0.52	16.9	4.79	17.5	0.46
12.7	7.47	15.0	0.29	12.7	1.83	12.8	0.50	16.9	4.79	17.5	0.49
16.9	8.32	19.2	0.24	16.9	2.68	17.1	0.49	16.9	4.51	17.5	0.43
16.9	7.61	19.2	0.22	16.9	1.41	17.1	0.38	33.8	7.61	34.4	0.34
33.8	15.5	36.1	0.19	33.8	4.51	34.0	0.38	50.7	10.7	51.3	0.30
50.7	15.5	53.0	0.15	50.7	4.51	50.9	0.25	67.7	13.8	68.3	0.22
84.5	20.0	86.8	0.15	67.7	7.61	67.9	0.23				
				84.5	7.61	84.7	0.18				

APPENDIX B -- *Continued*

Run 3-45				Run 4-45				Run 5-45			
x'/b_o	y'/b_o	s'/b_o	T/T_o	x'/b_o	y'/b_o	s'/b_o	T/T_o	x'/b_o	y'/b_o	s'/b_o	T/T_o
0.71	0.30	0.77	1.00	0.71	0.41	0.81	1.00	0.21	0.07	0.22	0.98
1.41	0.90	1.69	0.92	1.41	0.97	1.75	0.99	0.49	0.13	0.51	1.00
1.62	0.70	1.80	0.98	1.41	1.00	1.75	0.97	0.71	0.44	0.83	1.00
2.82	1.41	3.25	0.90	2.12	1.25	2.75	0.97	0.63	0.63	0.89	0.94
4.23	2.0	4.75	0.66	2.82	1.83	3.65	0.92	1.41	1.11	1.85	0.98
5.64	2.7	6.30	0.58	4.23	2.95	5.35	0.72	2.82	2.11	3.60	0.91
7.05	3.1	7.75	0.51	5.64	3.52	6.90	0.57	4.23	2.82	5.25	0.78
8.46	3.4	9.20	0.46	7.05	3.95	8.40	0.51	5.64	3.38	6.70	0.63
12.7	5.1	13.7	0.40	8.45	4.51	9.90	0.51	7.05	4.51	8.50	0.56
16.9	5.5	17.9	0.34	8.46	4.65	9.80	0.44	8.45	4.94	9.90	0.42
16.9	5.5	17.9	0.33	12.7	6.49	14.5	0.36	8.46	4.51	9.90	0.49
16.9	4.5	17.9	0.27	16.9	6.63	18.8	0.31	12.7	6.63	14.4	0.42
33.8	7.6	3.48	0.25	16.9	6.63	18.8	0.33	16.9	7.61	18.7	0.34
50.7	10.7	51.7	0.20	33.8	35.7	35.7	0.24	16.9	7.61	18.7	0.29
67.7	13.8	68.7	0.17	50.7	52.6	52.6	0.17	33.8	10.7	35.6	0.21
84.5	16.9	85.5	0.14	94.5	96.4	96.4	0.12	50.7	16.9	52.5	0.15
								84.5	16.9	86.5	0.11

APPENDIX C

FIGURES 46 - 73

TRAJECTORIES AND TEMPERATURE AND WIDTH PLOTS

FOR LABORATORY EXPERIMENTS

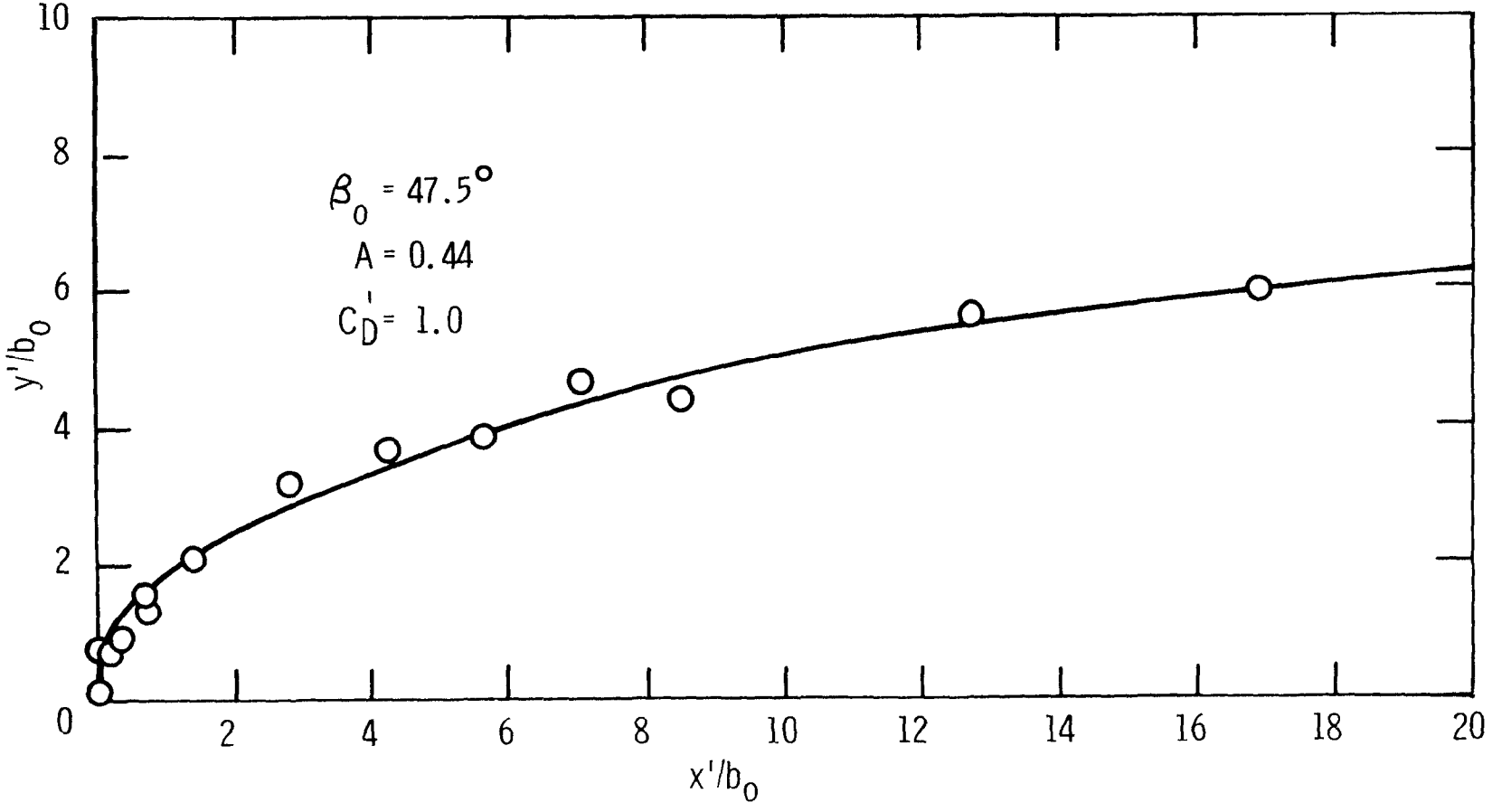

FIGURE 46.--OBSERVED AND FITTED TRAJECTORIES, RUN 2-90

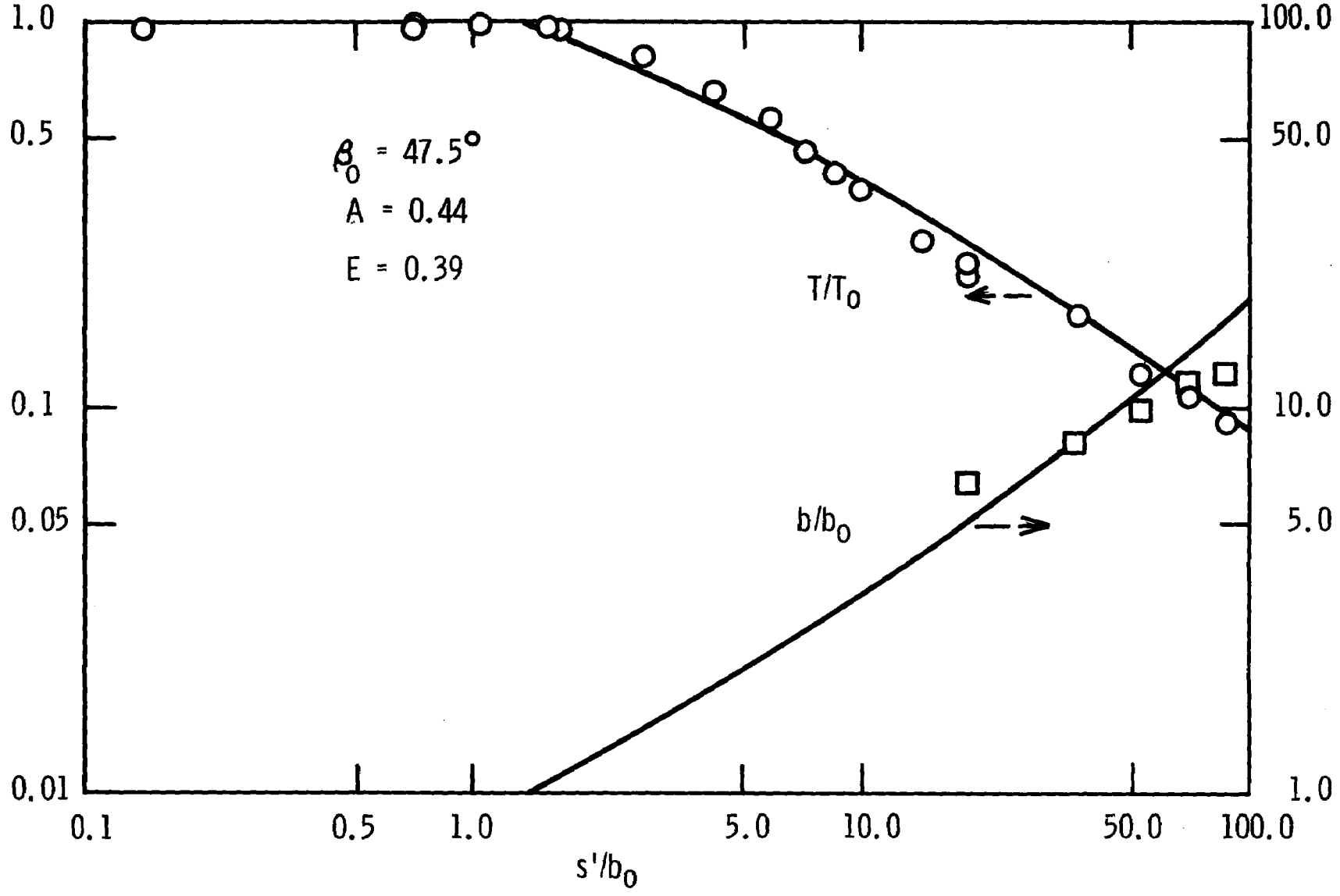

FIGURE 47.--OBSERVED VALUES AND FITTED CURVES FOR TEMPERATURE AND WIDTH, RUN 2-90

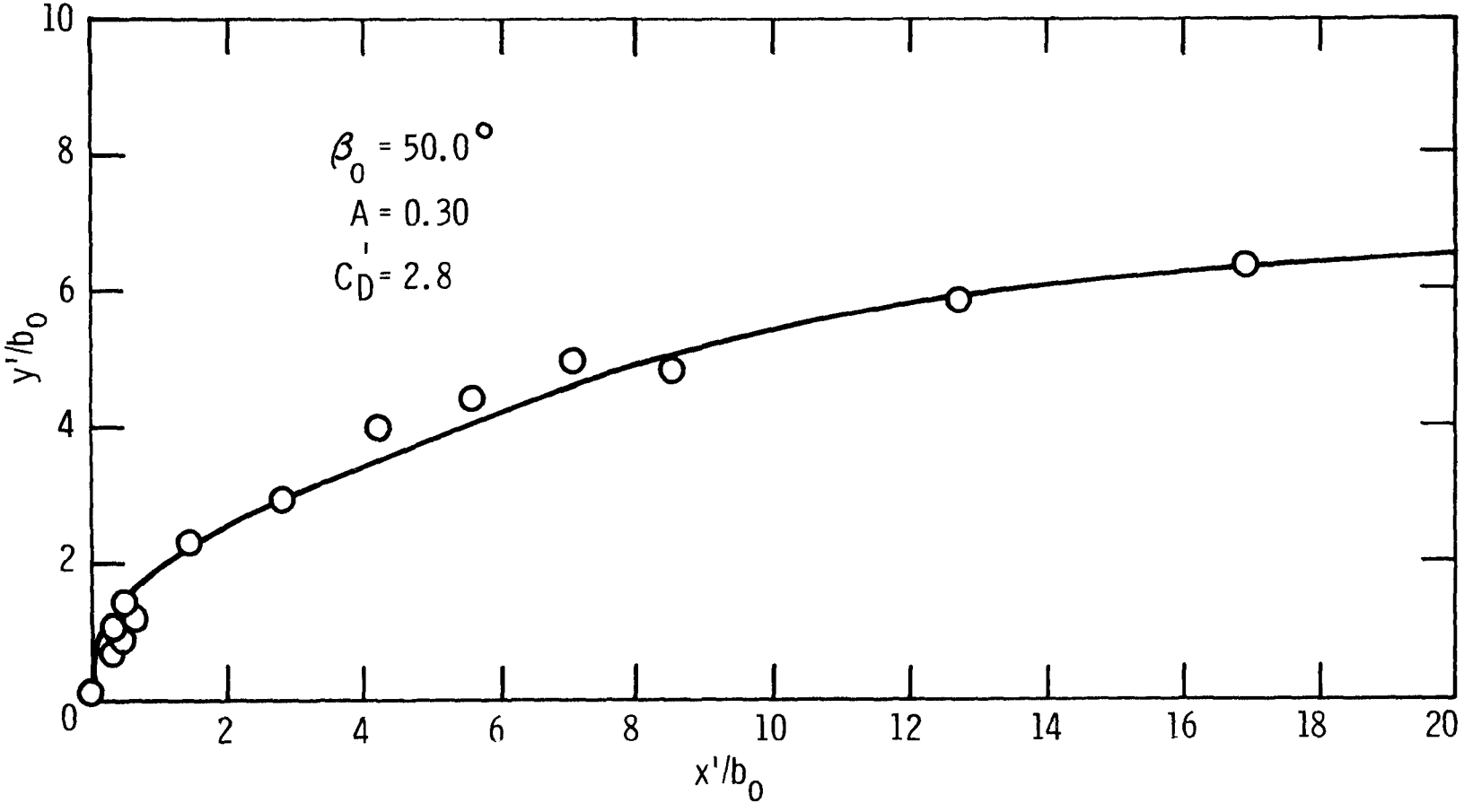

FIGURE 48.--OBSERVED AND FITTED TRAJECTORIES, RUN 3-90

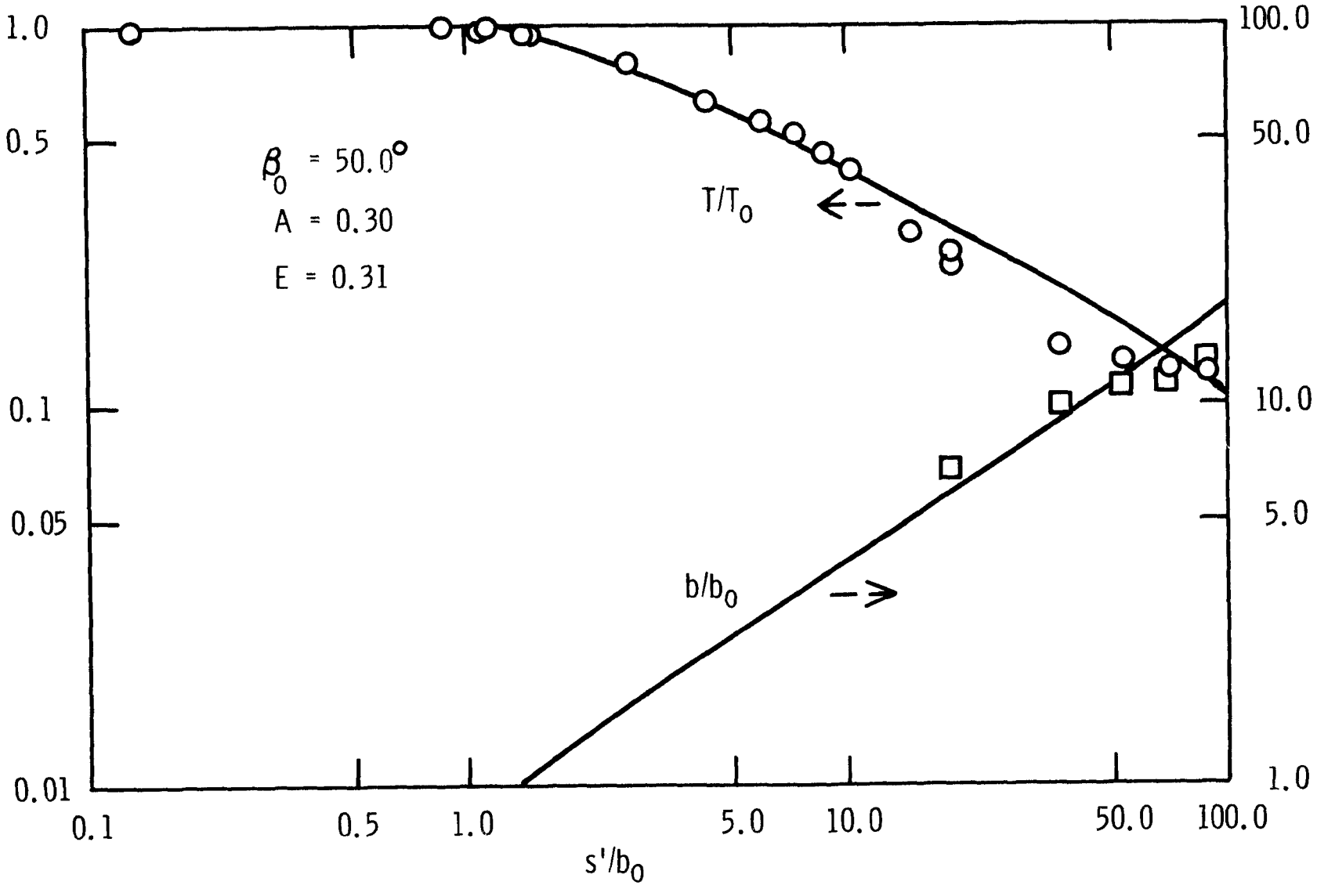

FIGURE 49.--OBSERVED VALUES AND FITTED CURVES FOR TEMPERATURE AND WIDTH, RUN 3-90

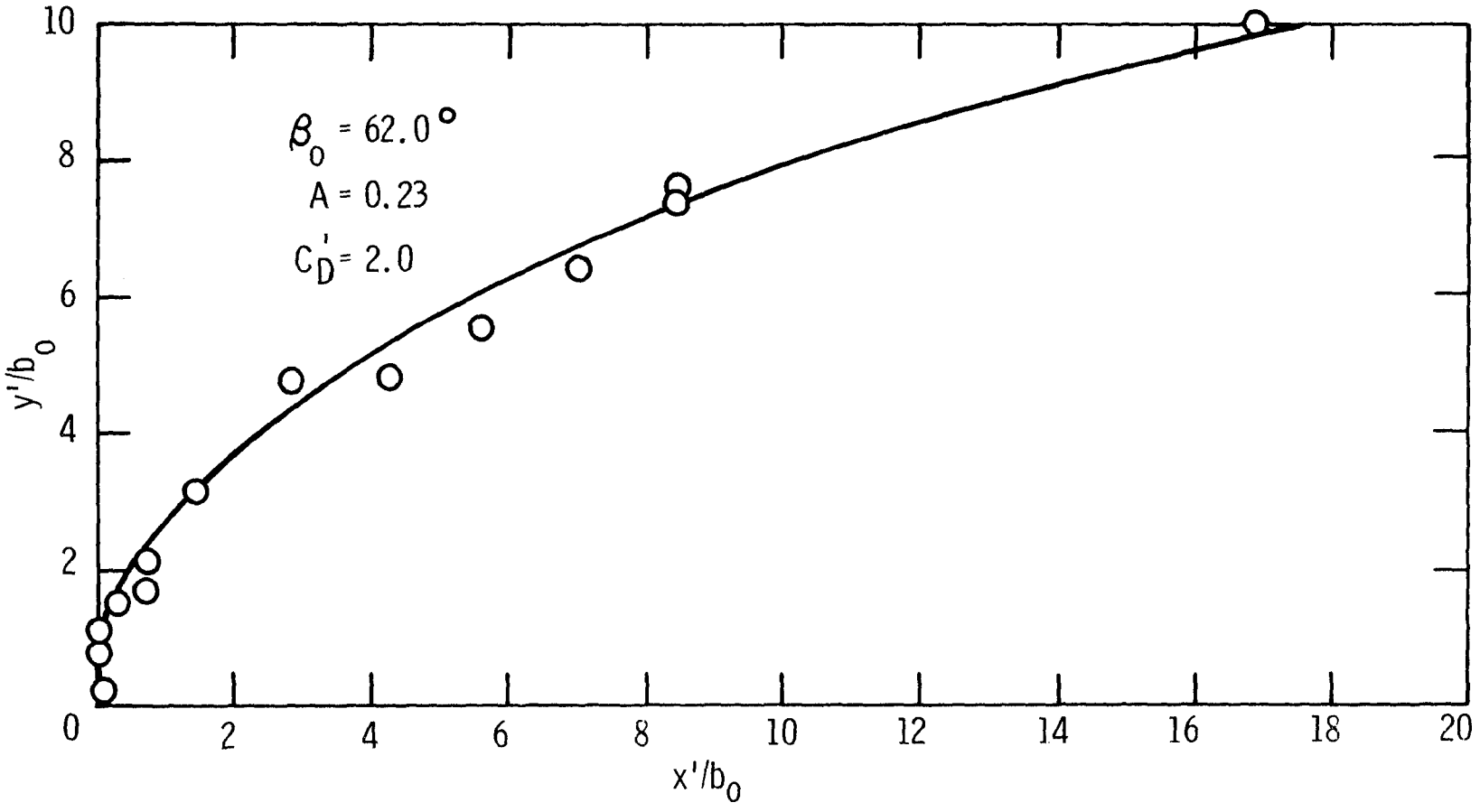

FIGURE 50.--OBSERVED AND FITTED TRAJECTORIES, RUN 4-90

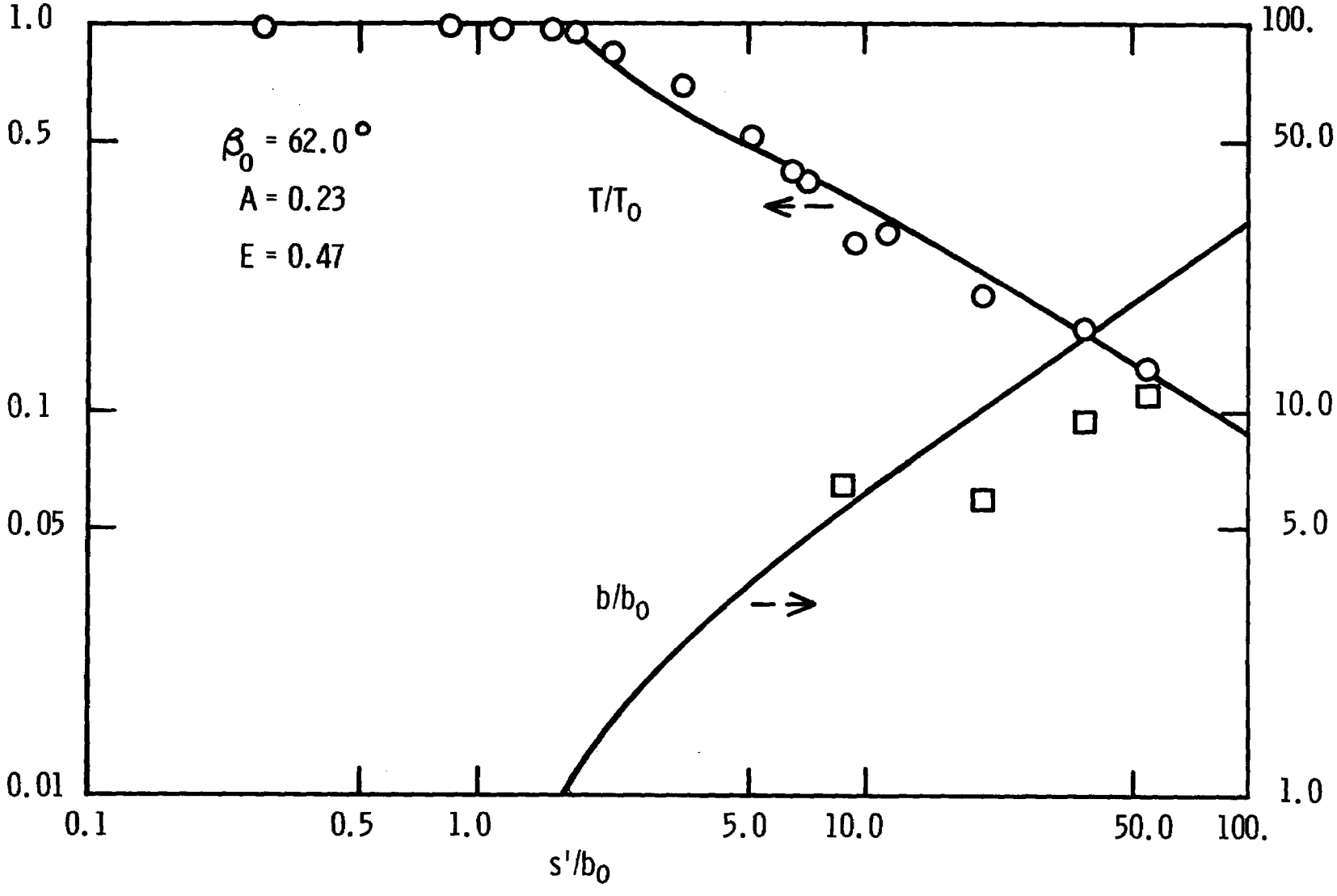

FIGURE 51.--OBSERVED VALUES AND FITTED CURVES FOR TEMPERATURE AND WIDTH, RUN 4-90

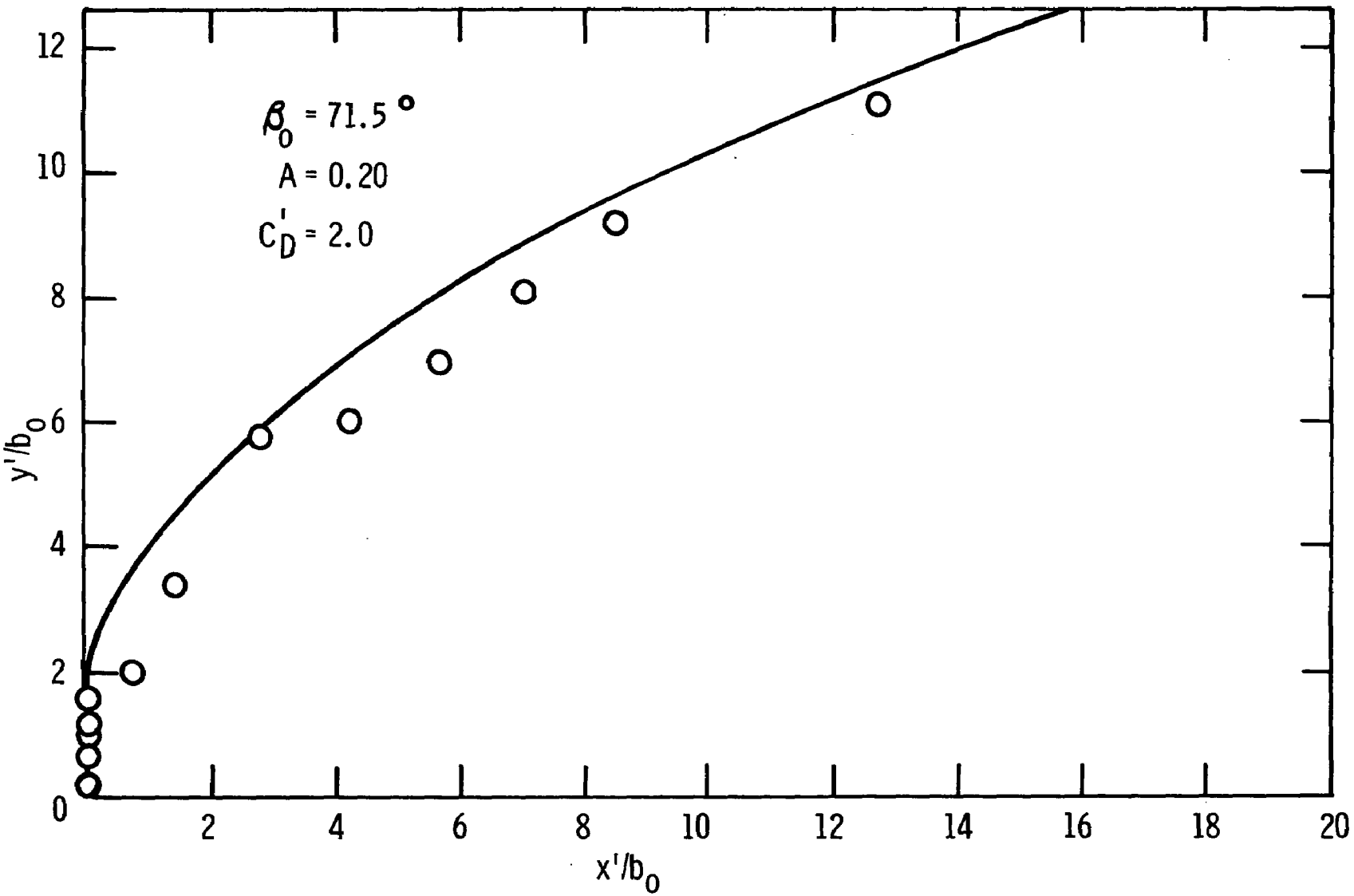

FIGURE 52.--OBSERVED AND FITTED TRAJECTORIES, RUN 5-90

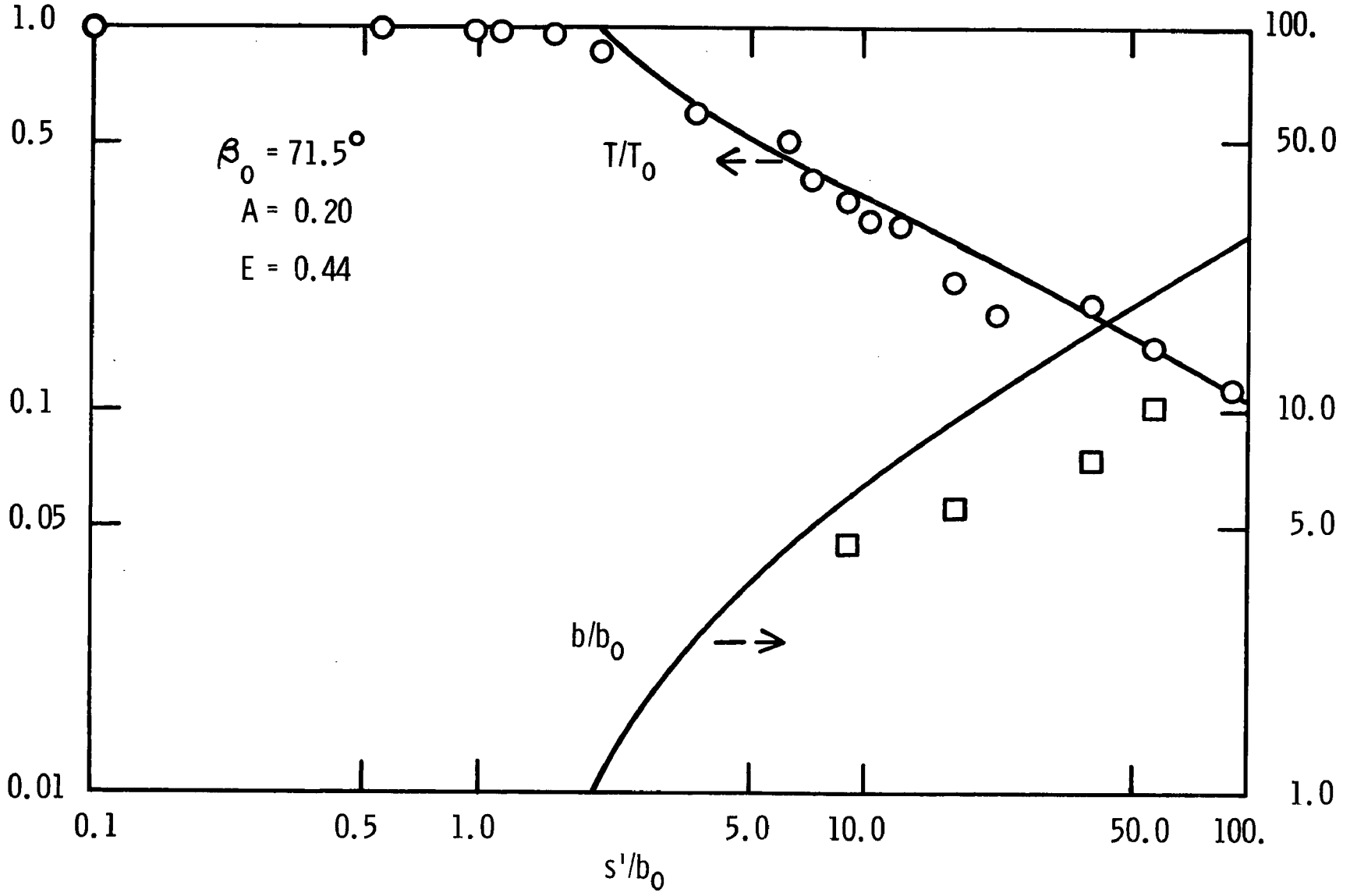

FIGURE 53.--OBSERVED VALUES AND FITTED CURVES FOR TEMPERATURE AND WIDTH, RUN 5-90

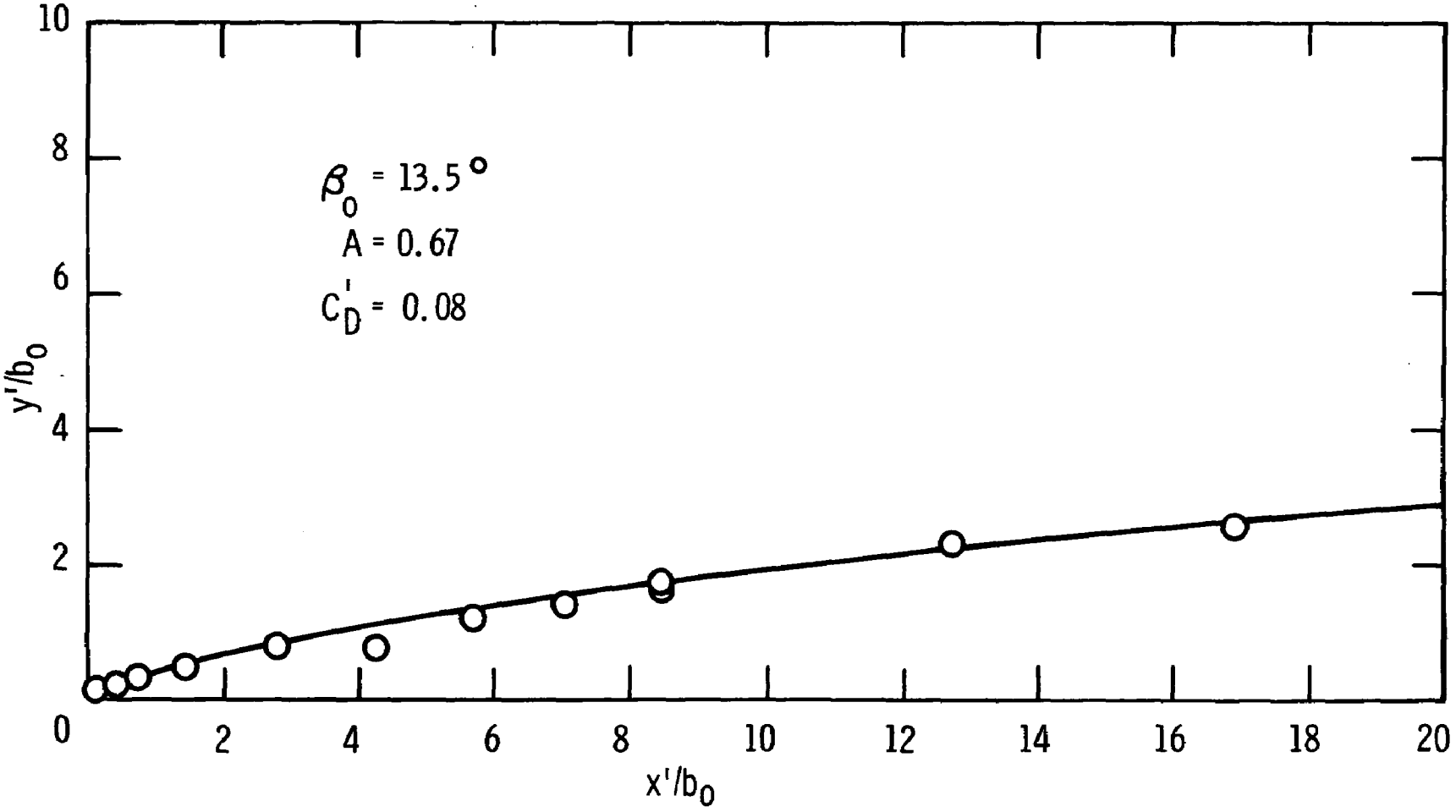

FIGURE 54.--OBSERVED AND FITTED TRAJECTORIES, RUN 1-60

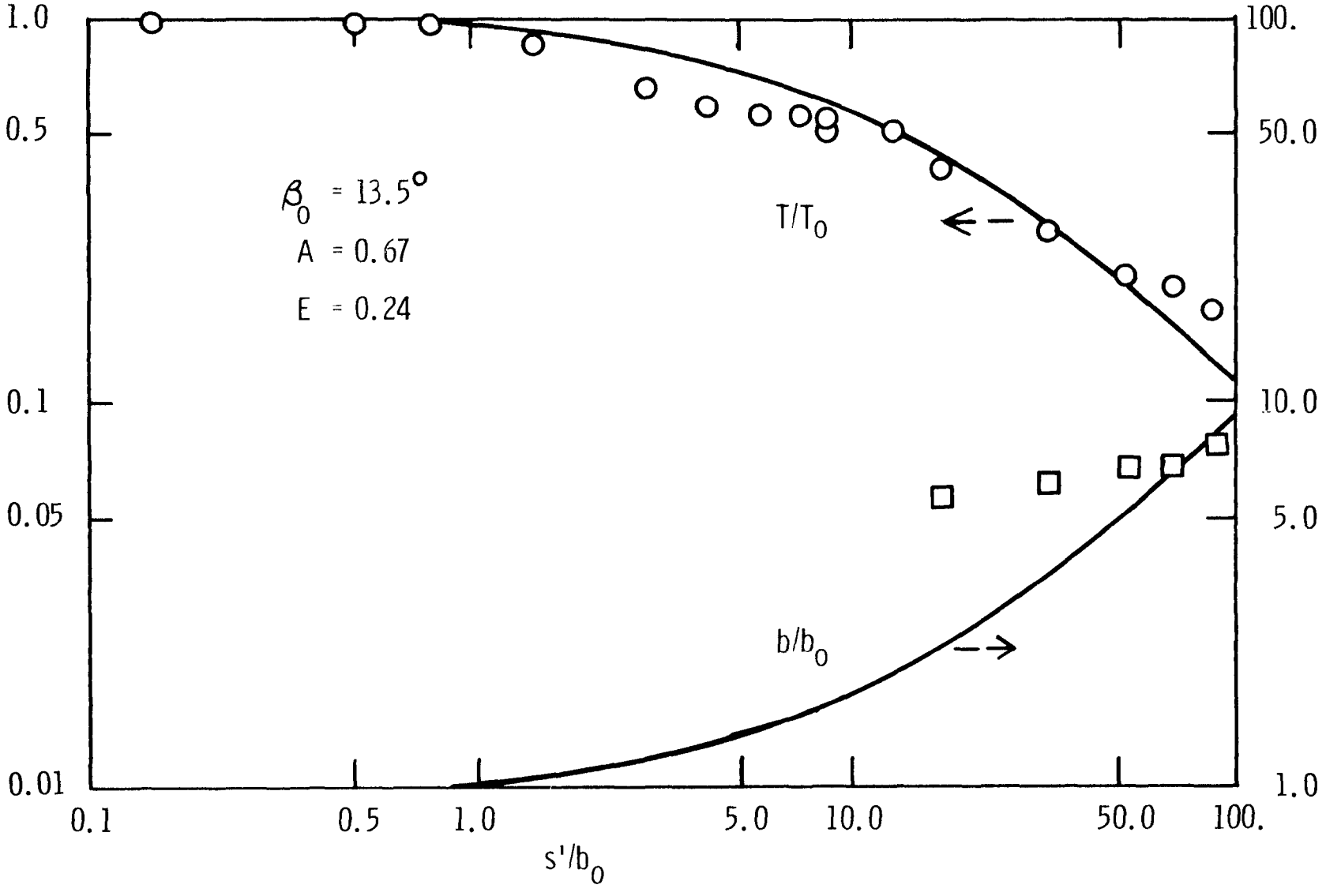

FIGURE 55.--OBSERVED VALUES AND FITTED CURVES FOR TEMPERATURE AND WIDTH, RUN 1-60

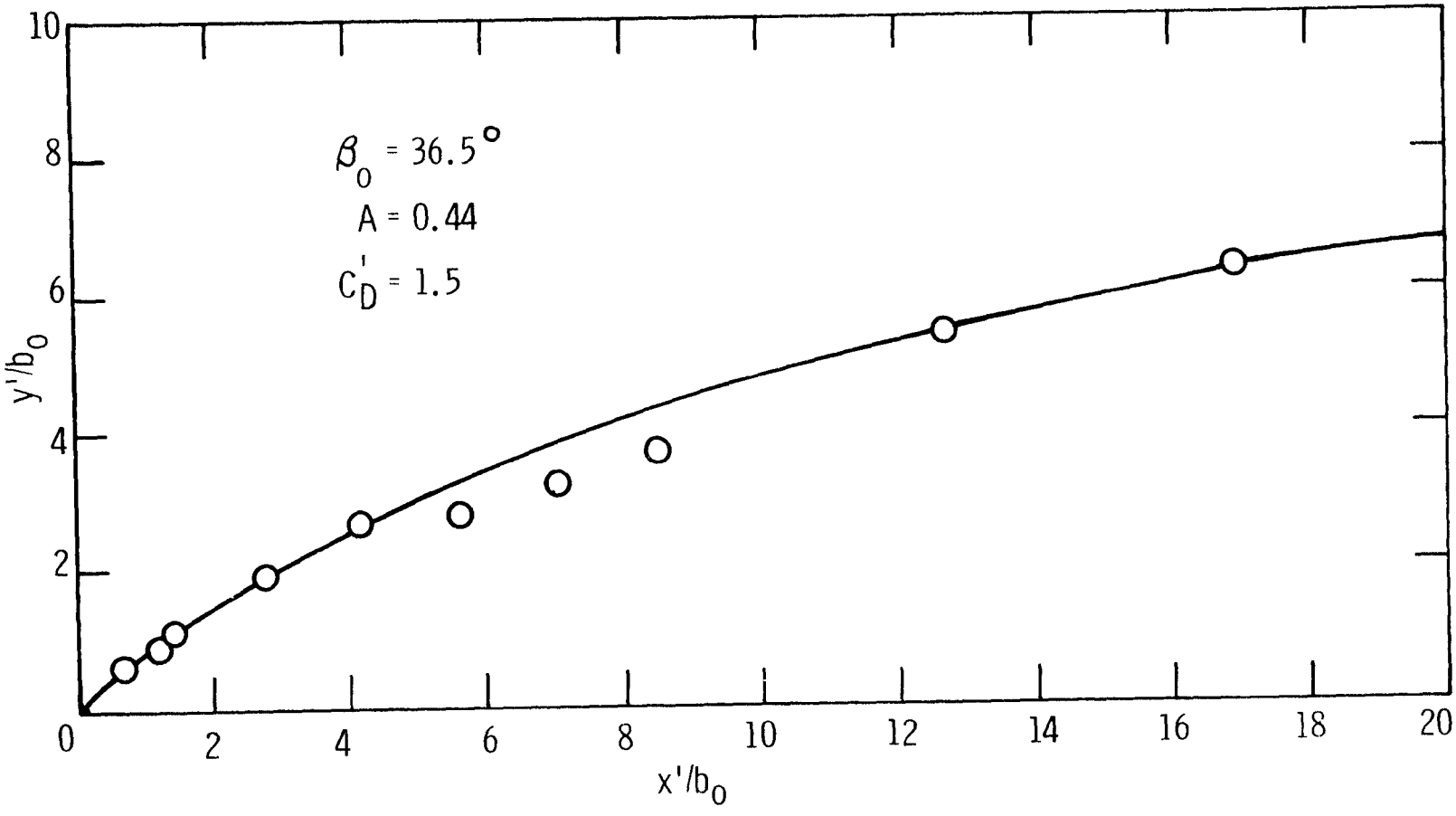

FIGURE 56.--OBSERVED AND FITTED TRAJECTORIES, RUN 2-60

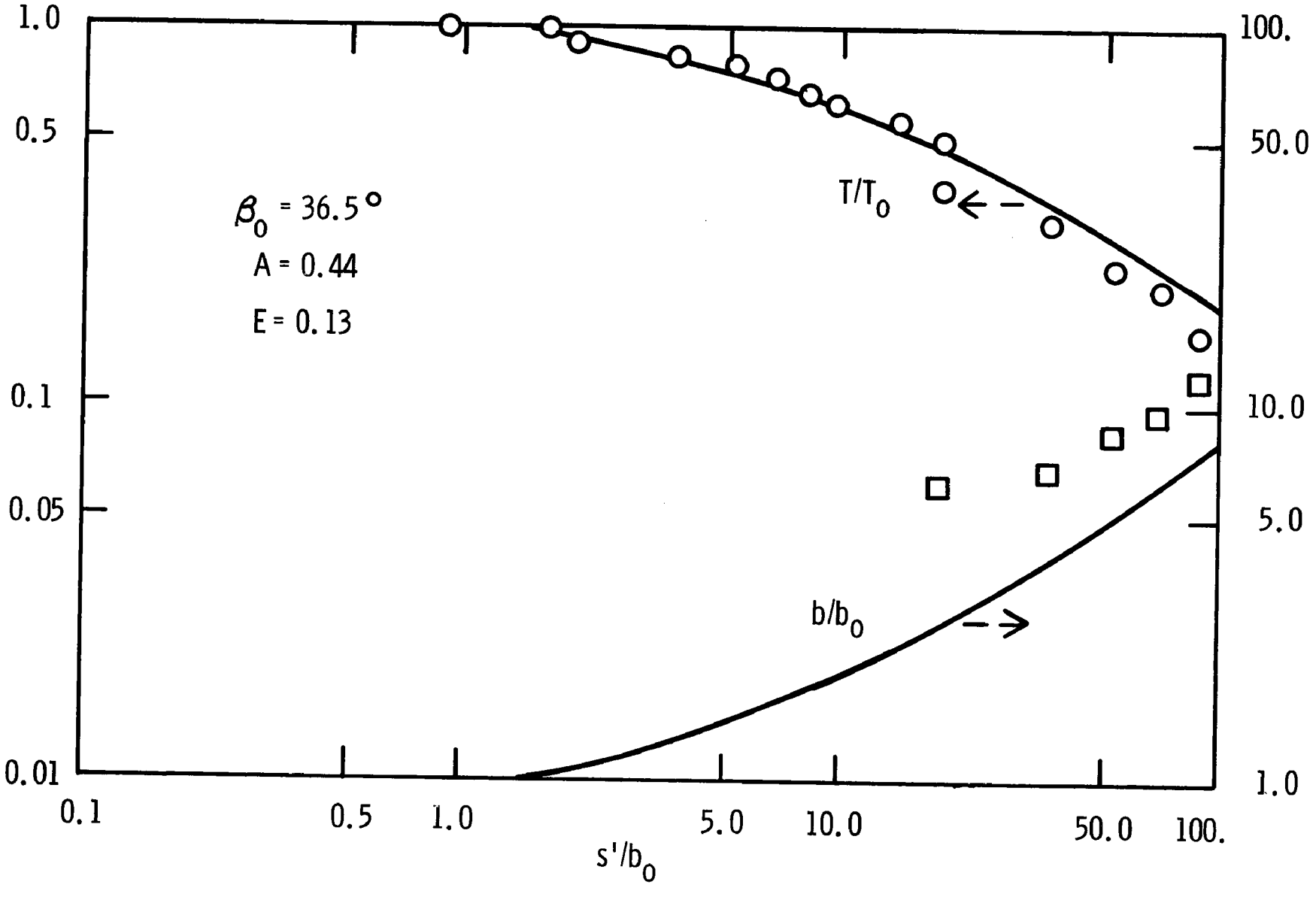

FIGURE 57.--OBSERVED VALUES AND FITTED CURVES FOR TEMPERATURE AND WIDTH, RUN 2-60

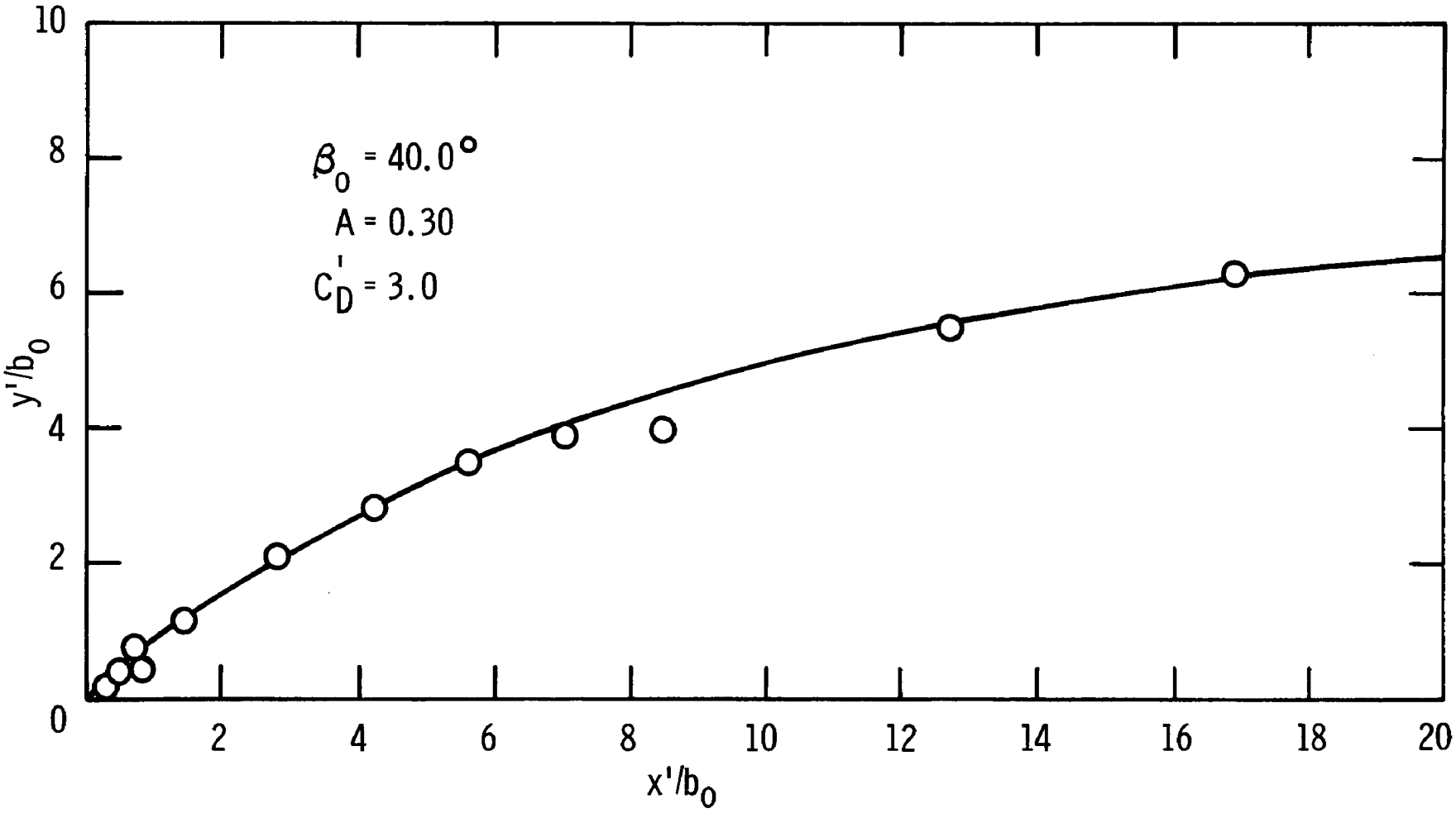

FIGUR E 58.--OBSERVED AND FITTED TRAJECTORIES, RUN 3-60

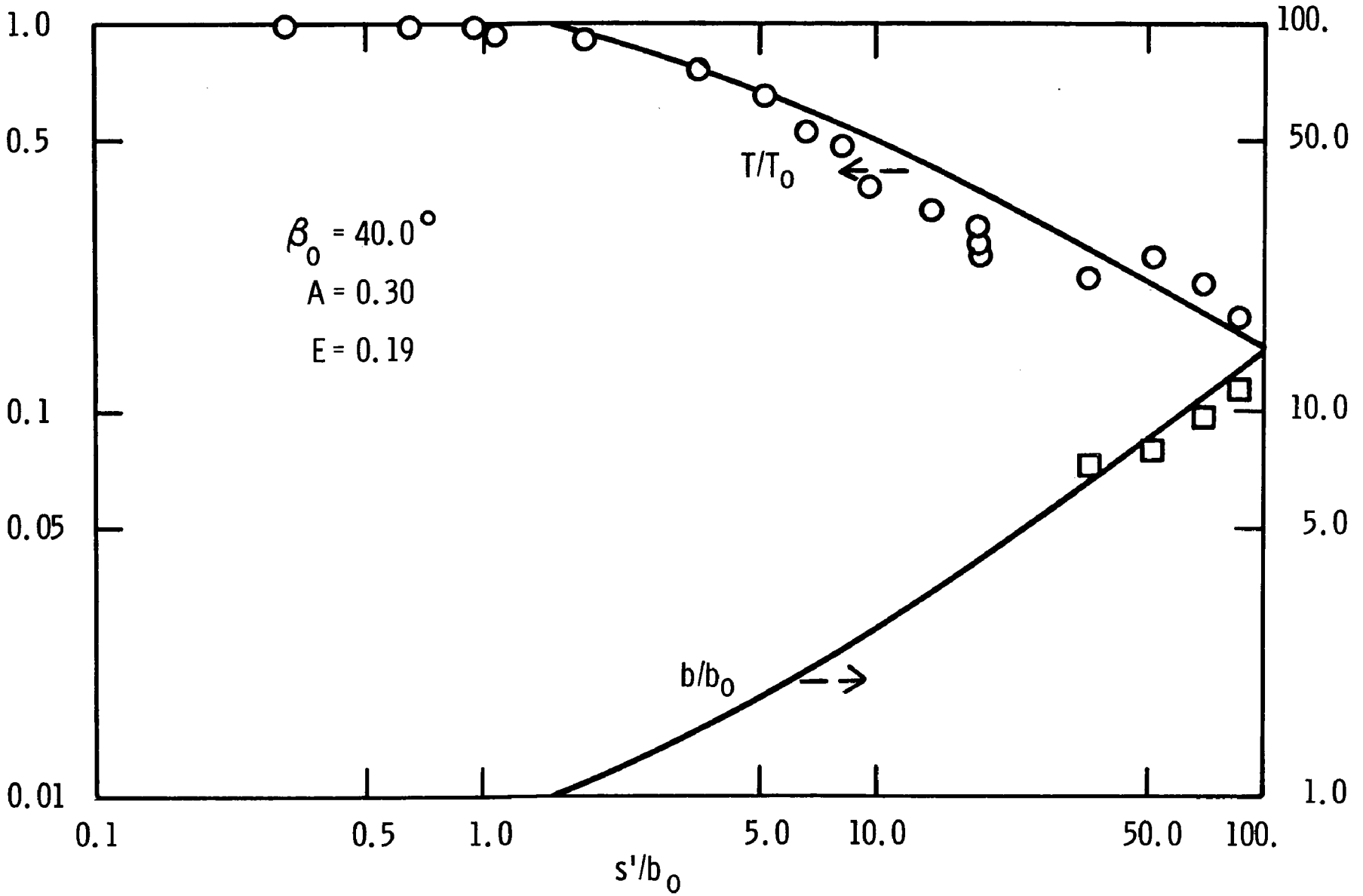

FIGURE 59.--OBSERVED VALUES AND FITTED CURVES FOR TEMPERATURE AND WIDTH, RUN 3-60

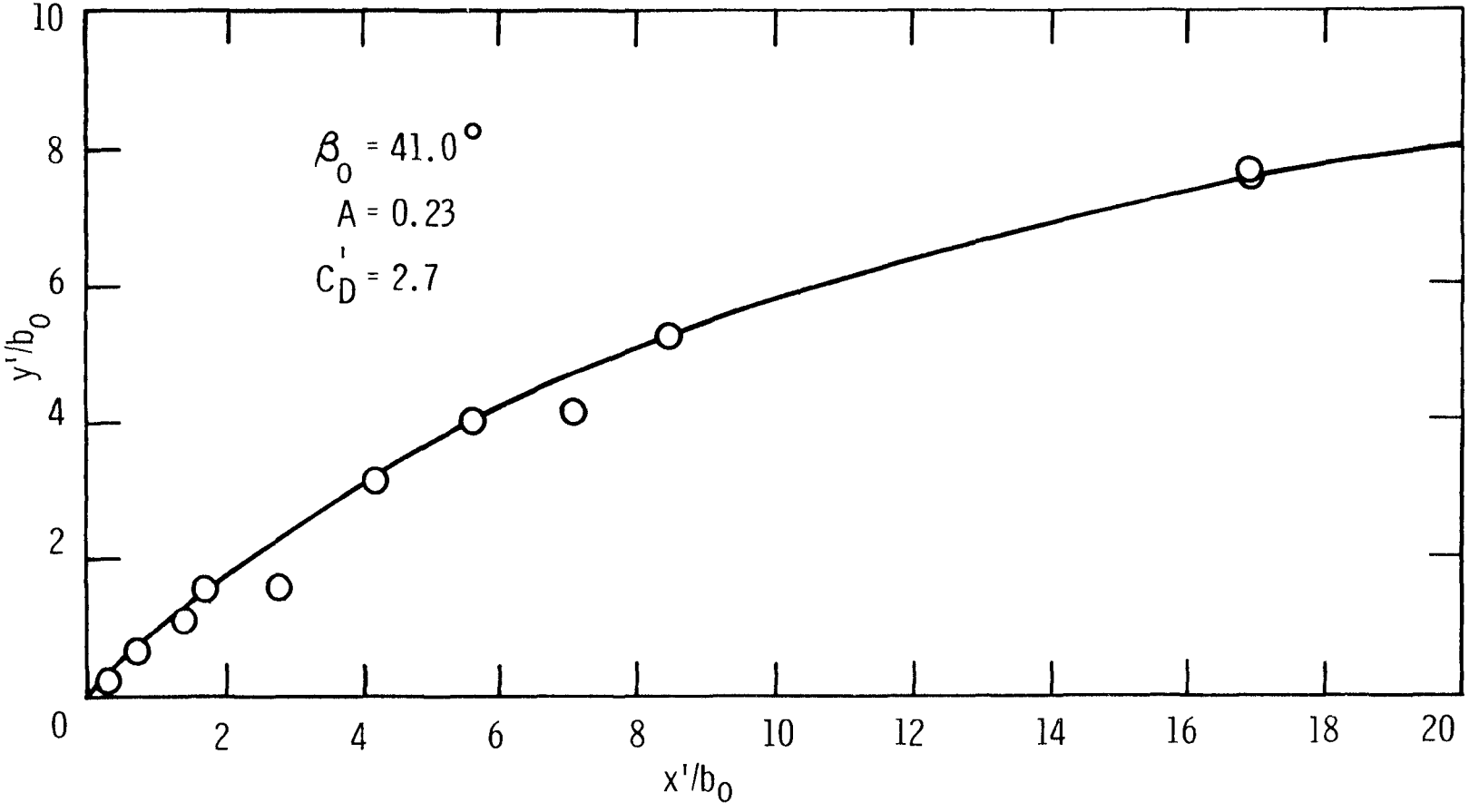

FIGURE 60.--OBSERVED AND FITTED TRAJECTORIES, RUN 4-60

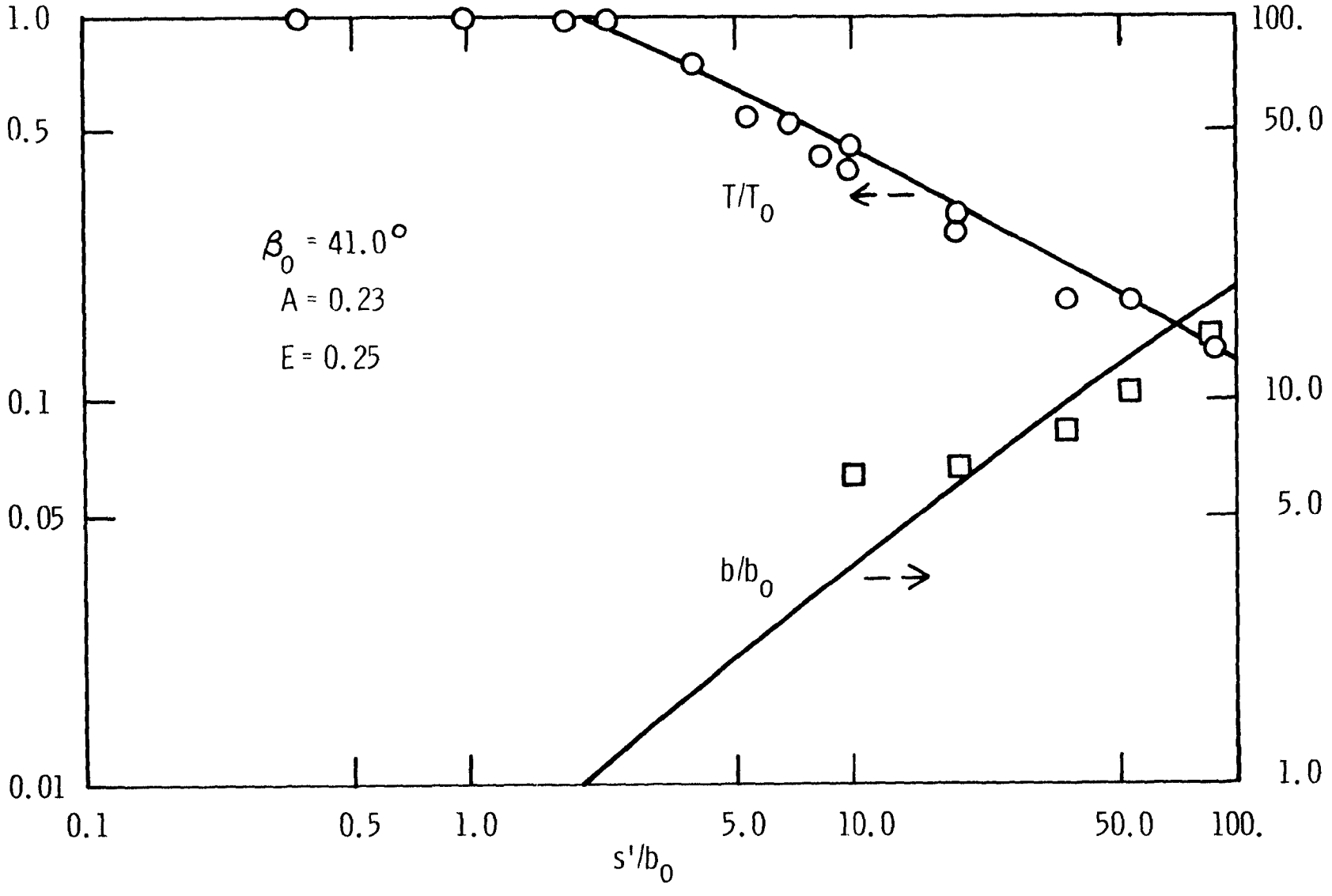

FIGURE 61.--OBSERVED VALUES AND FITTED CURVES FOR TEMPERATURE AND WIDTH, RUN 4-60

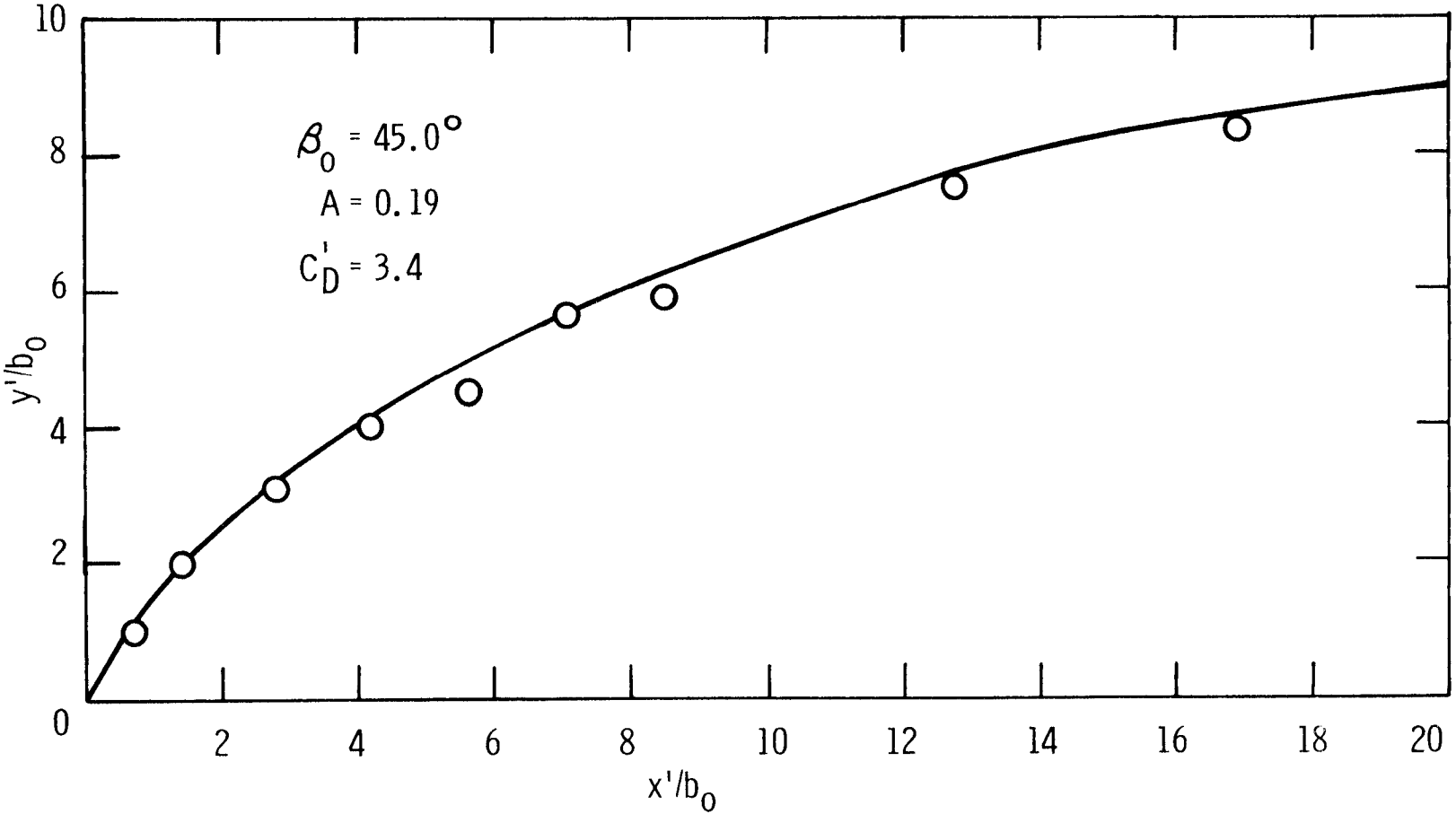

FIGURE 62.--OBSERVED AND FITTED TRAJECTORIES, RUN 5-60

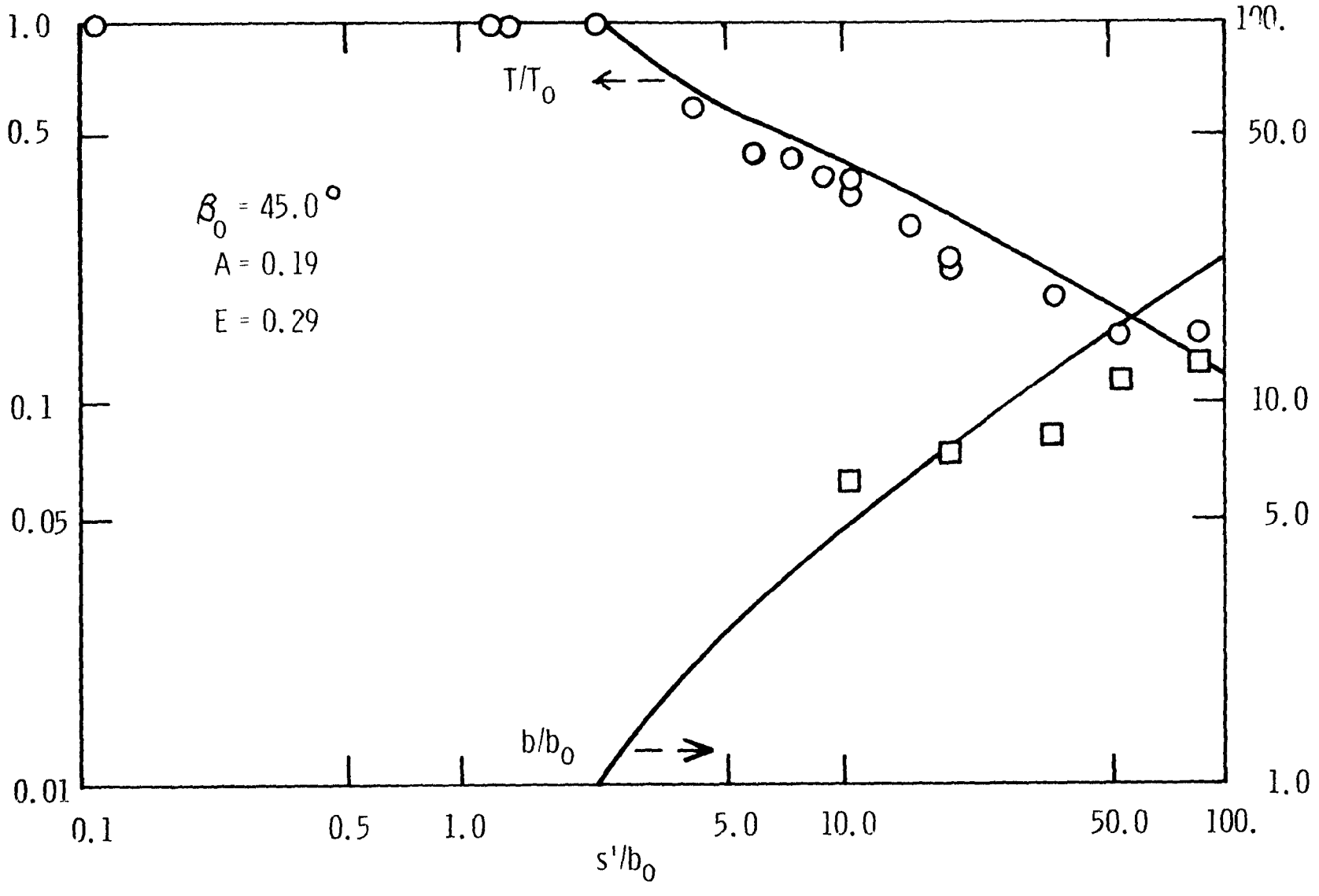

FIGURE 63.--OBSERVED VALUES AND FITTED CURVES FOR TEMPERATURE AND WIDTH, RUN 5-60

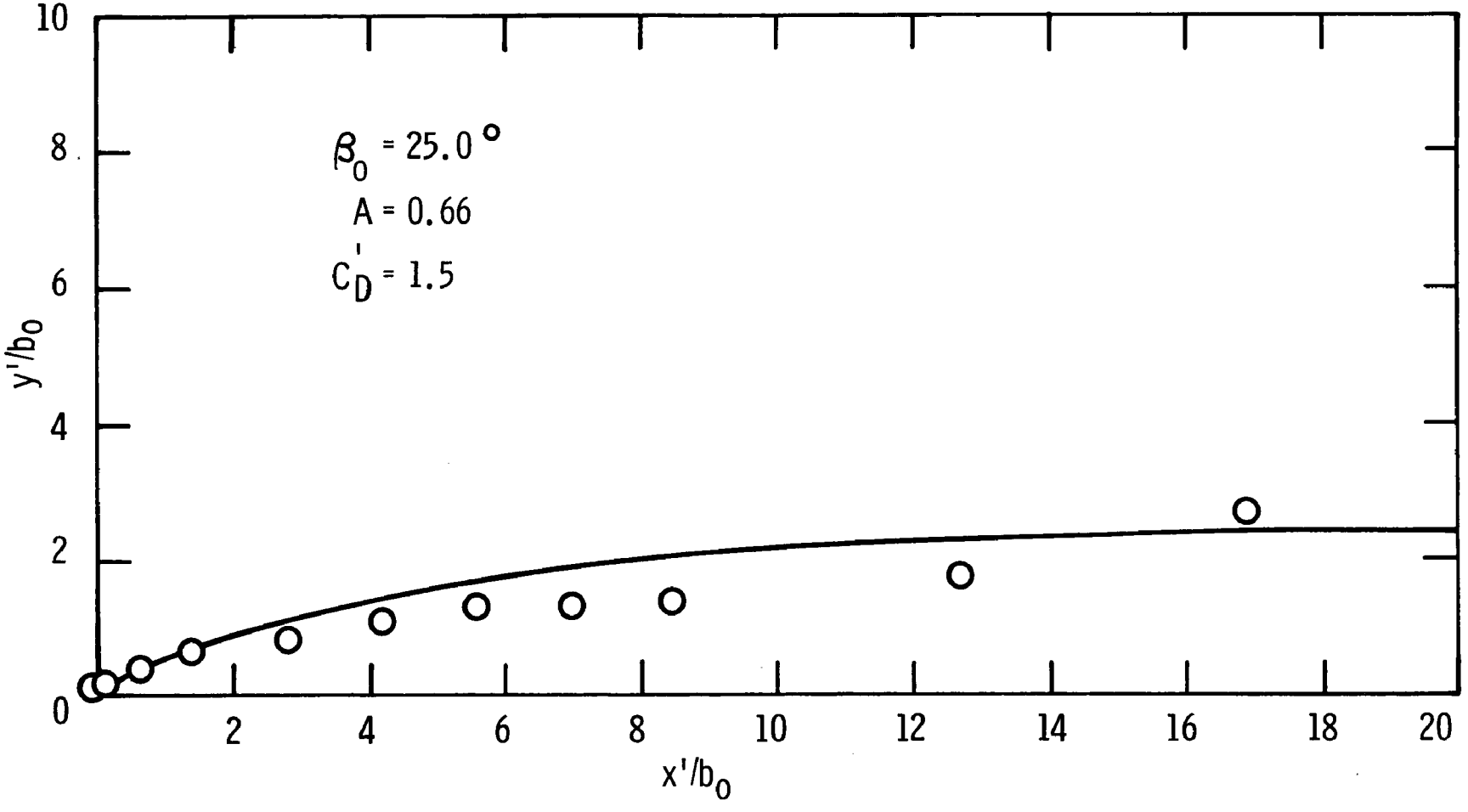

FIGURE 64.--OBSERVED AND FITTED TRAJECTORIES, RUN 1-45

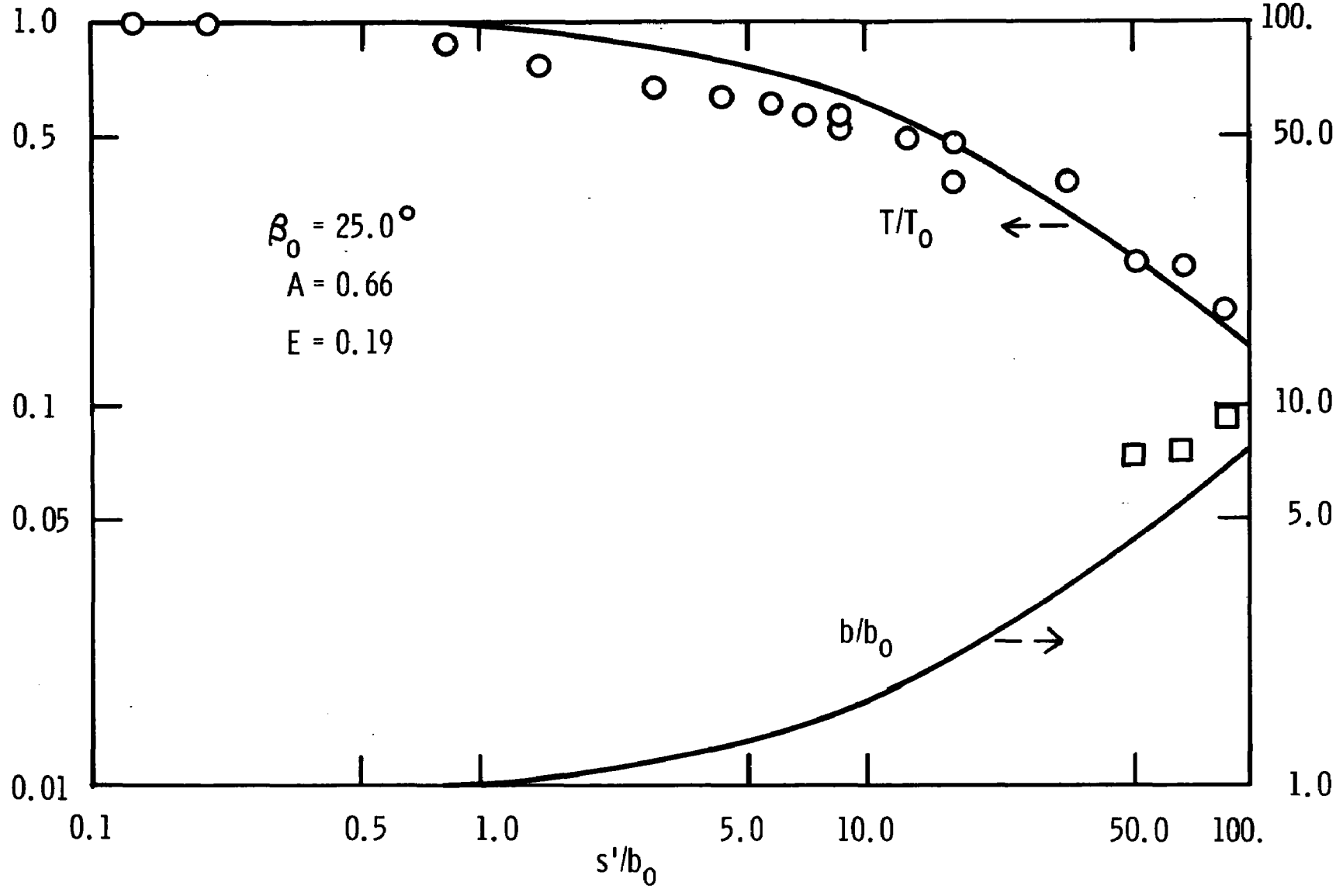

FIGURE 65.--OBSERVED VALUES AND FITTED CURVES FOR TEMPERATURE AND WIDTH, RUN 1-45

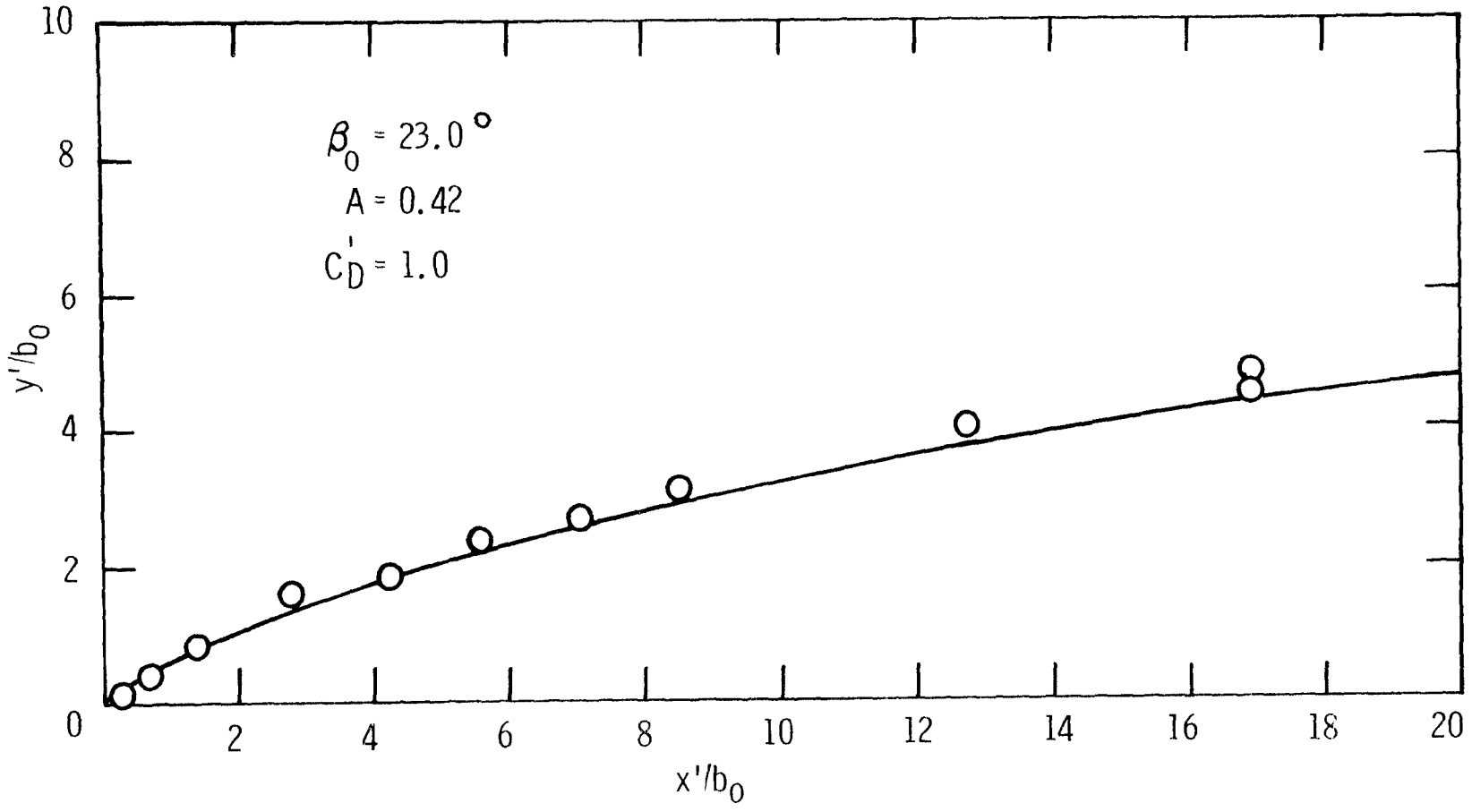

FIGURE 66.--OBSERVED AND FITTED TRAJECTORIES, RUN 2-45

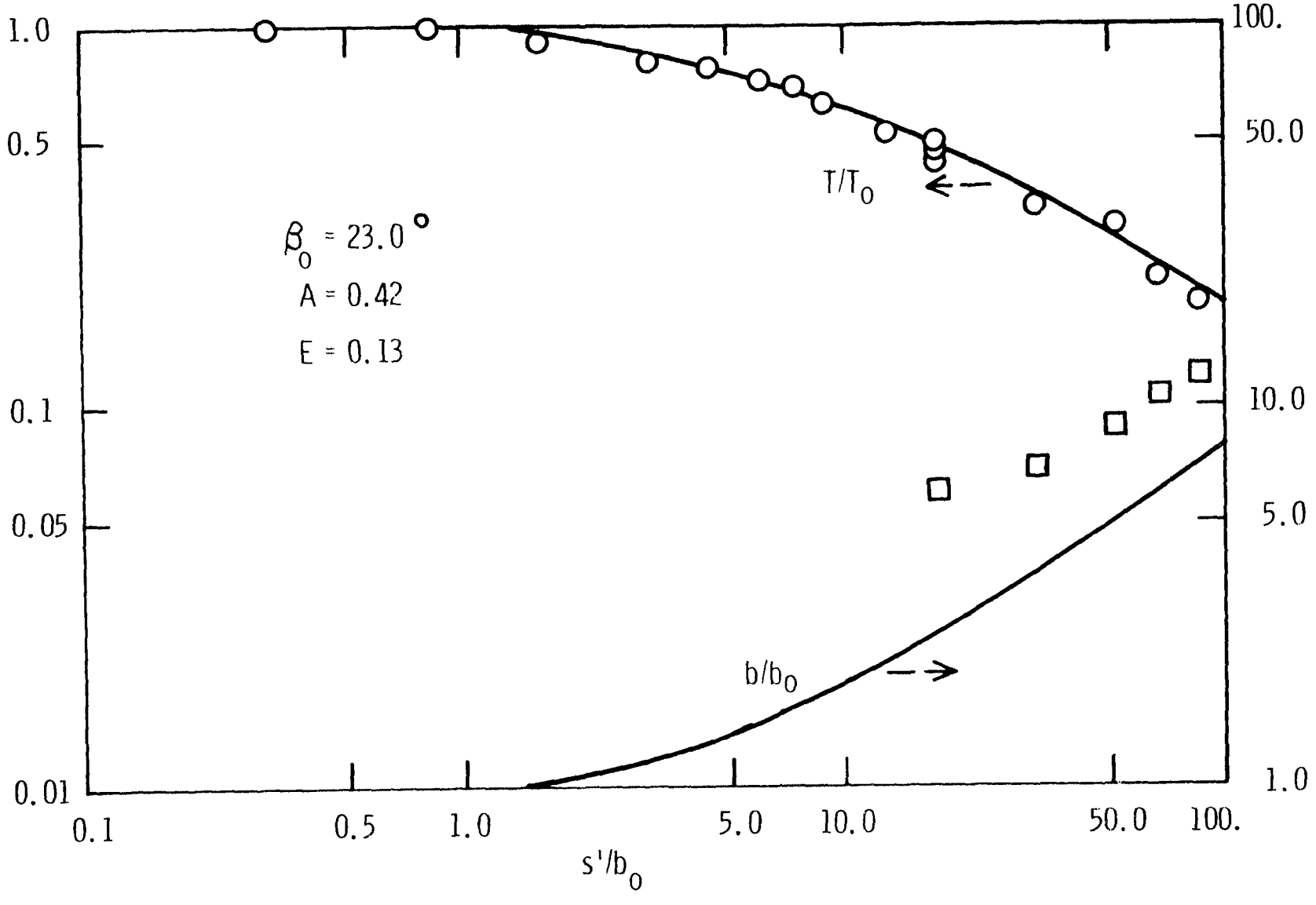

FIGURE 67.--OBSERVED VALUES AND FITTED CURVES FOR TEMPERATURE AND WIDTH, RUN 2-45

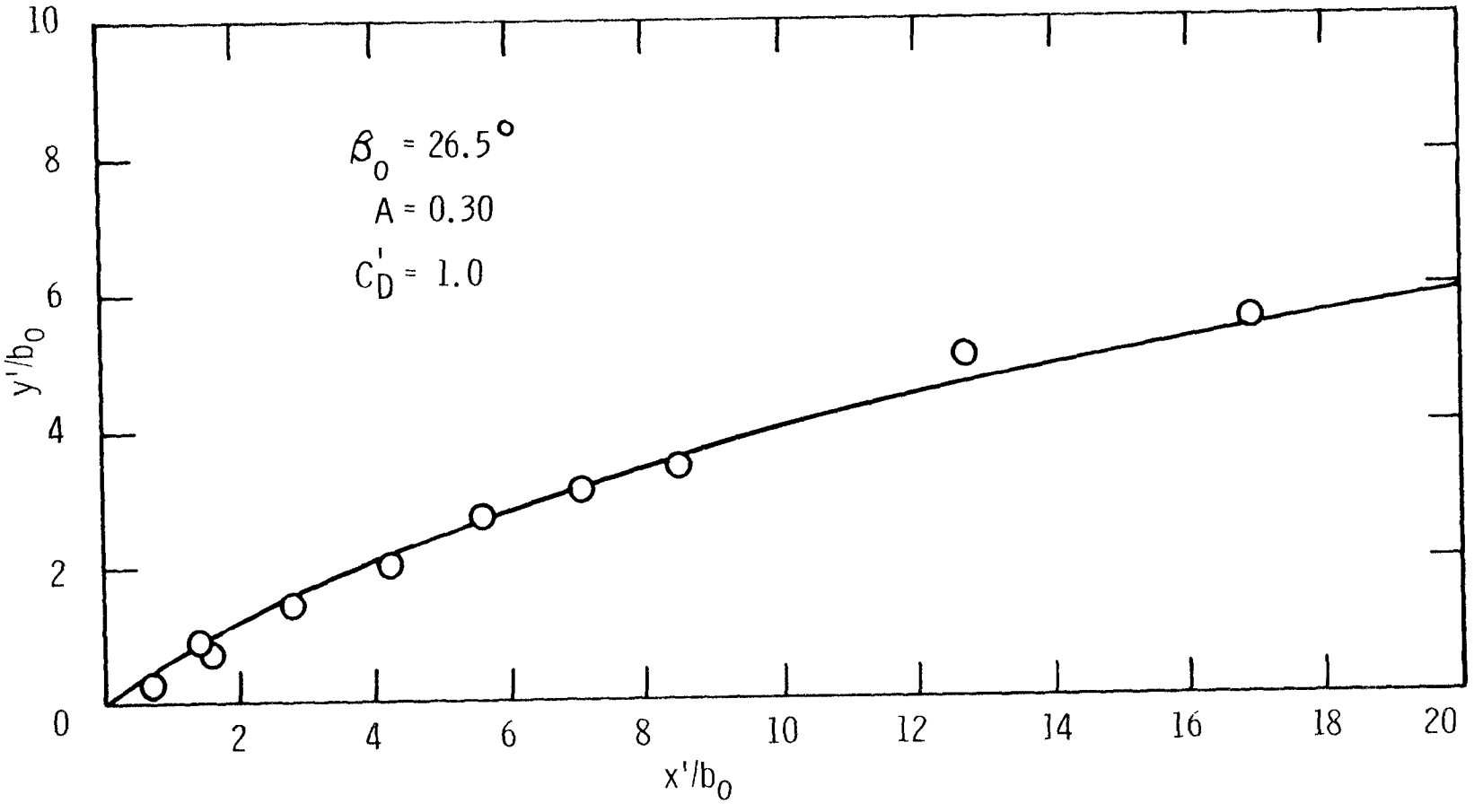

FIGURE 68.--OBSERVED AND FITTED TRAJECTORIES, RUN 3-45

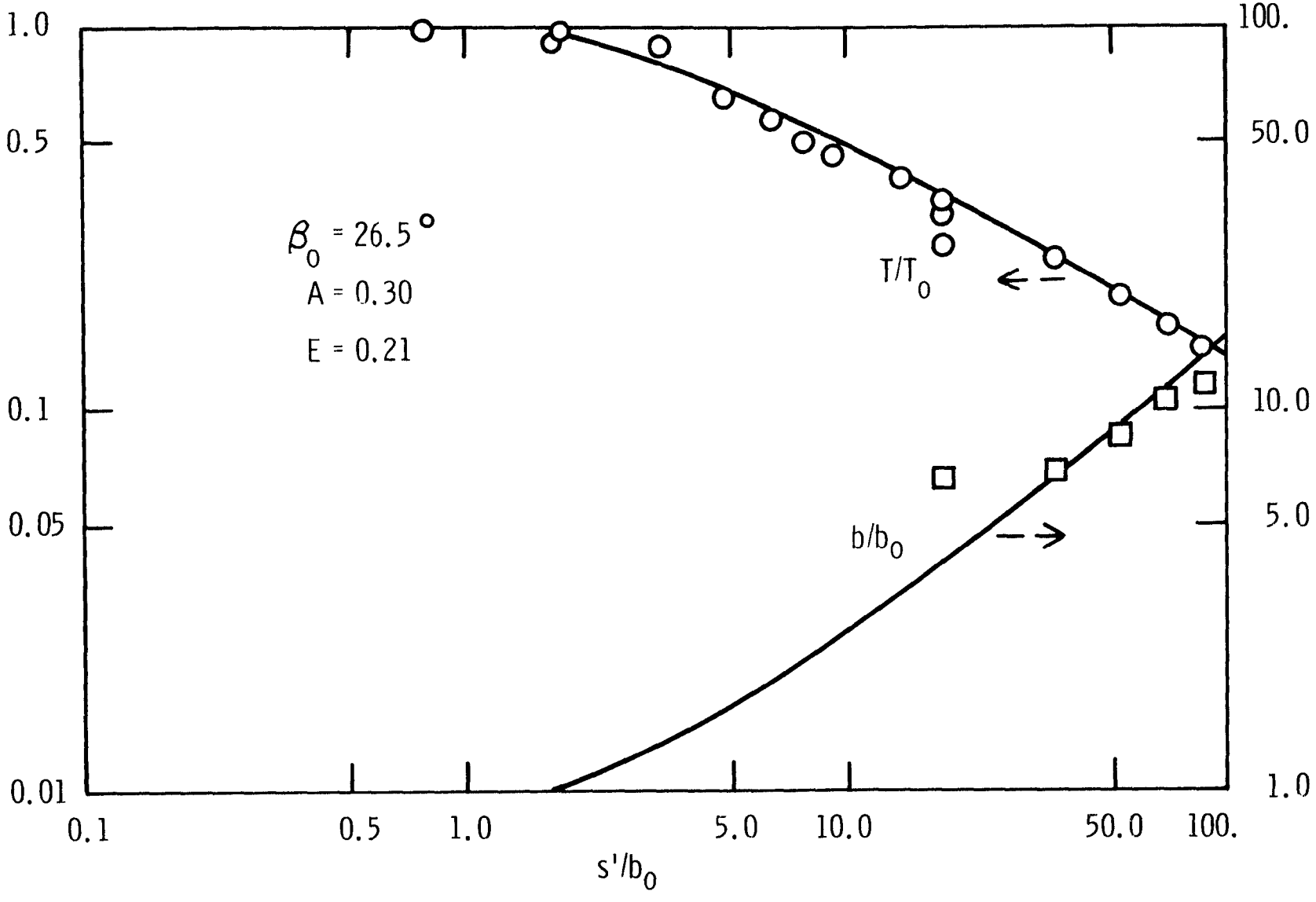

FIGURE 69.--OBSERVED VALUES AND FITTED CURVES FOR TEMPERATURE AND WIDTH, RUN 3-45

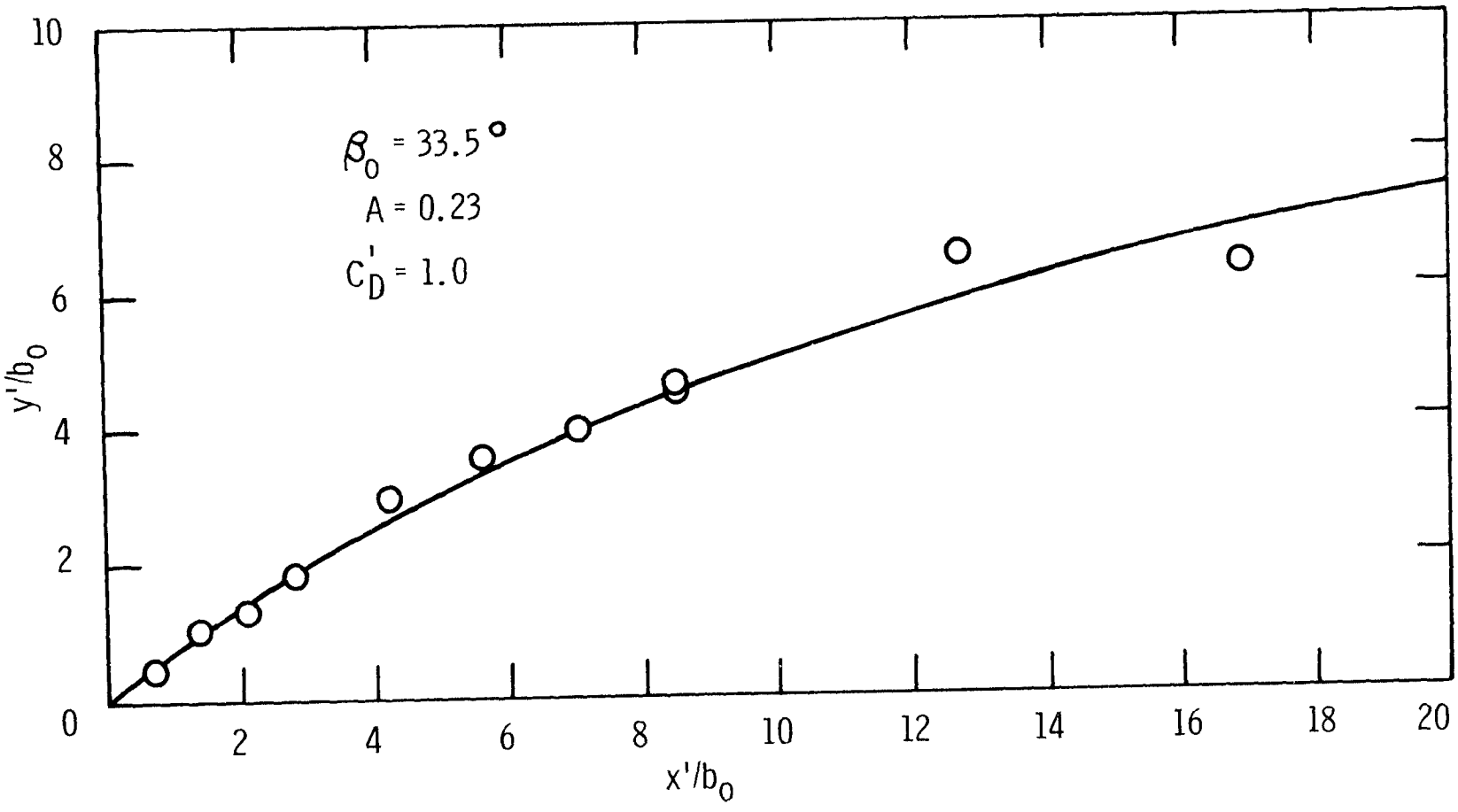

FIGURE 70.--OBSERVED AND FITTED TRAJECTORIES, RUN 4-45

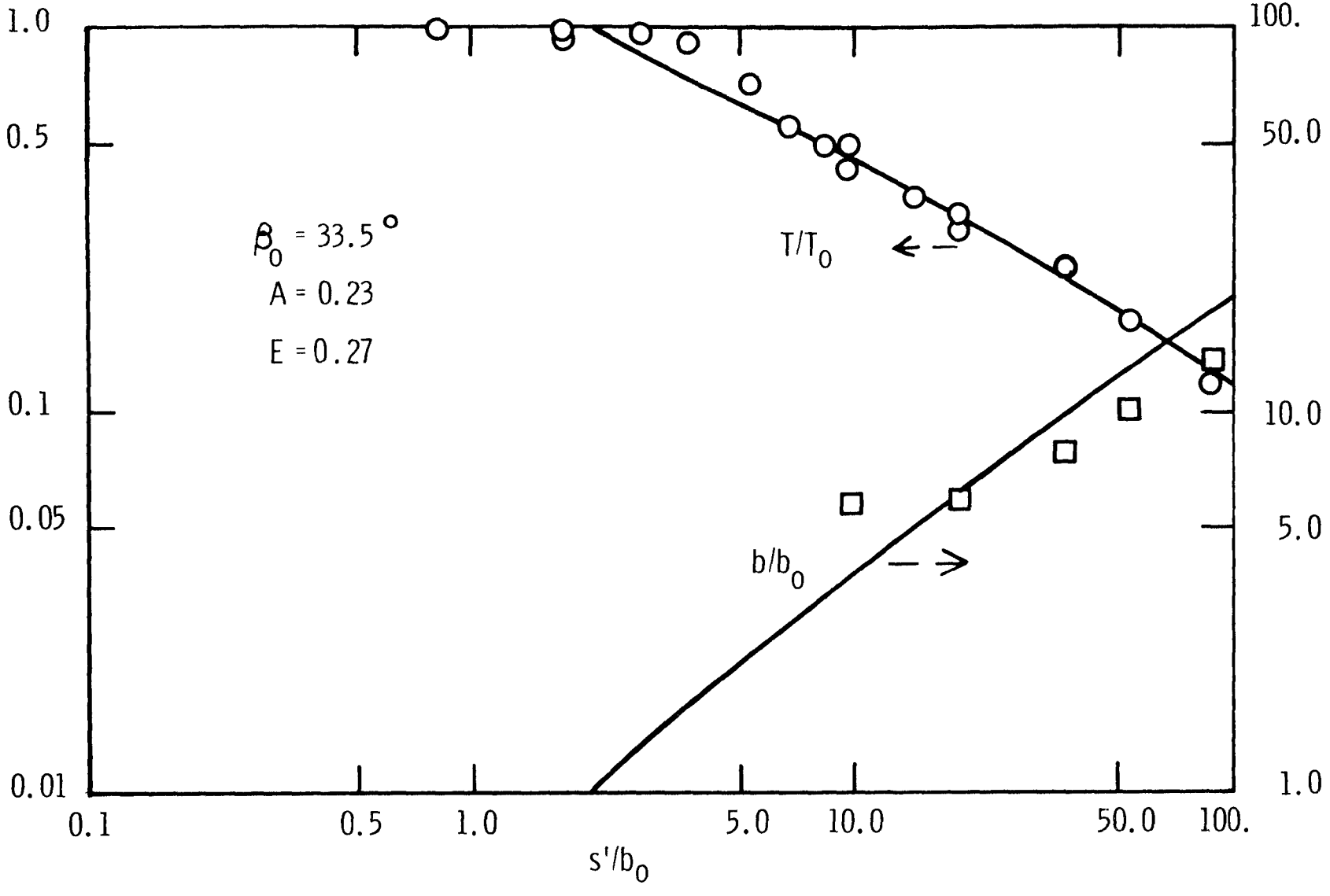

FIGURE 71.--OBSERVED VALUES AND FITTED CURVES FOR TEMPERATURE AND WIDTH, RUN 4-45

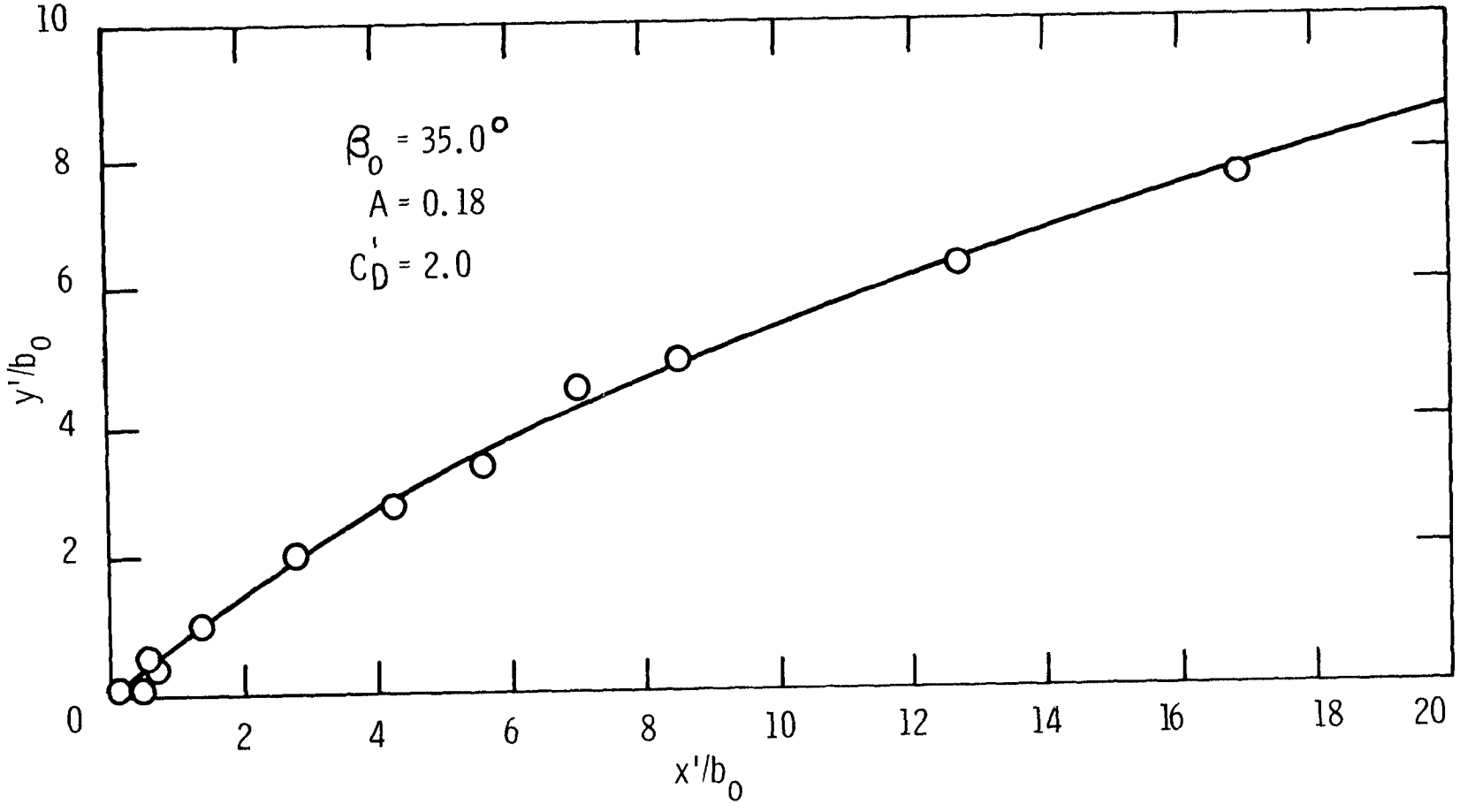

FIGURE 72.--OBSERVED AND FITTED TRAJECTORIES, RUN 5-45

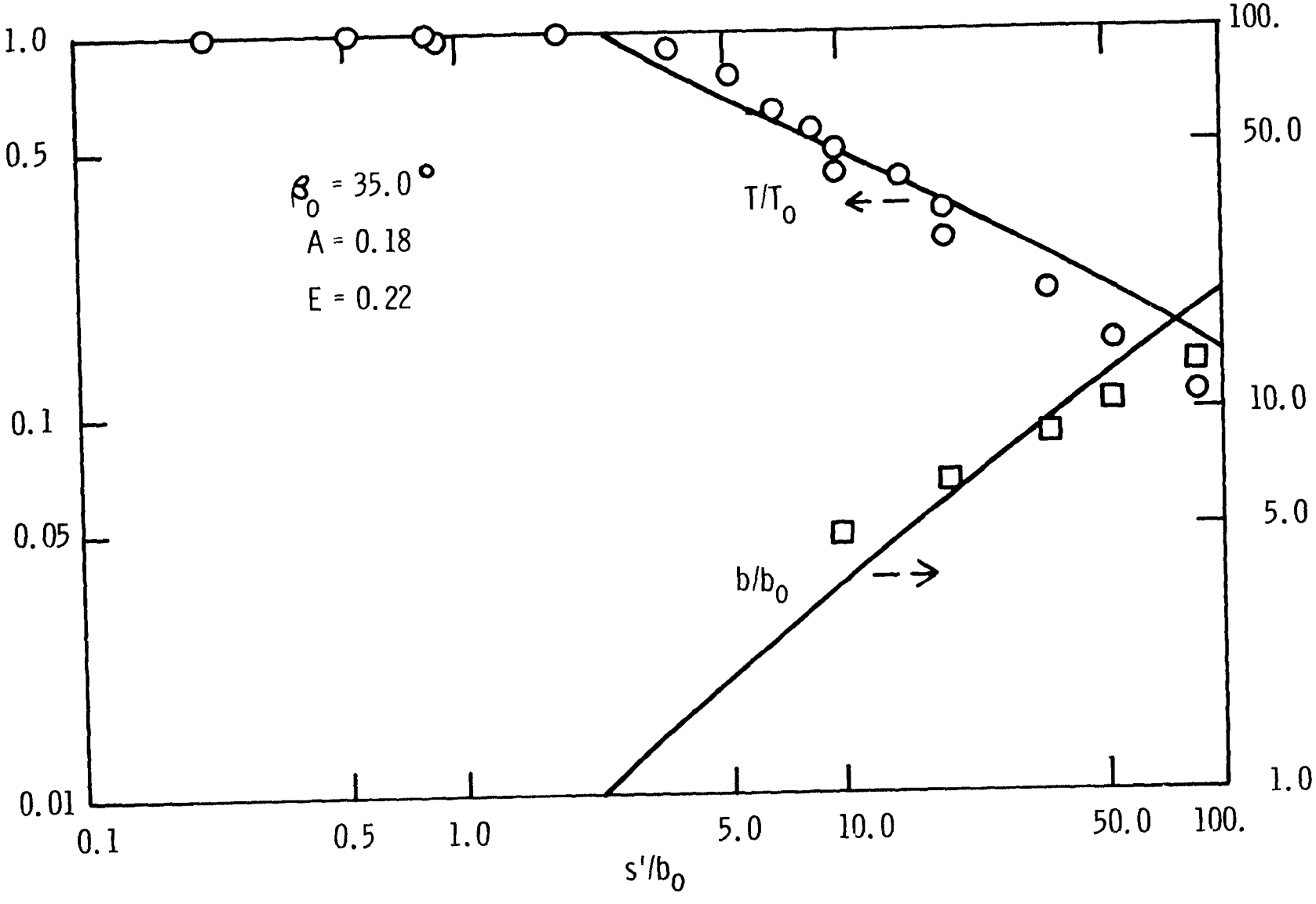

FIGURE 73.--OBSERVED VALUES AND FITTED CURVES FOR TEMPERATURE AND WIDTH, RUN 5-45

APPENDIX D

PRACTICAL APPLICATION EXAMPLE

Representative values of field parameters have been chosen to illustrate the practical application of the model developed in the present study.

The assumed values of the parameters are summarized in Table 16. The assumed plant flowrate, Q_o = 2600 ft^3/sec, is subtracted from the assumed river flowrate, Q_r = 31,900 ft^3/sec, to obtain the ambient flowrate, Q_a = 29.300 ft^3/sec. The ambient width is assumed to be 2000 feet, and the ambient depth is assumed to be 15 feet, giving a cross-sectional area of 30,000 ft^2. Dividing the ambient flowrate by the area gives the ambient velocity, U_a = 0.98 ft/sec.

The jet discharge is assumed to have a flowrate of Q_o = 2600 ft^3/sec, a half-width of b_o' = 100 feet, and a depth of 10 feet. Dividing the value of Q_o by the cross-sectional area, or 2000 ft^2, gives the initial jet velocity, U_o = 1.3 ft/sec. The value of b_o, the initial half-width at the beginning of the zone of established jet flow, is calculated to be b_o = 160 feet from Equation 65,

$$b_o = 1.60\, b_o' \tag{65}$$

The value of the velocity ratio is found to be A = 0.75, using U_a = 0.98 ft/sec and U_o = 1.3 ft/sec and Equation 38,

$$A = U_a/U_o \tag{38}$$

TABLE 16

ASSUMED VALUES FOR DESIGN PROBLEM

Parameter	Value
Q_r, River Flowrate, ft^3/sec	31,900
Q_o, Plant Flowrate, ft^3/sec	2,600
Q_a, Ambient Flowrate, ft^3/sec	29,300
Ambient Width, feet	2,000
Ambient Depth, feet	15.0
Ambient Cross-sectional Area, ft^2	30,000
U_a, Ambient Velocity, ft/sec	0.98
b_o', Discharge Half-Width, feet	100.0
z_o, Discharge Depth, feet	10.0
Discharge Cross-sectional Area, ft^2	2,000
U_o, Initial Jet Velocity, ft/sec	1.3
b_o, Initial Jet Half-Width, feet	160.0
A, Velocity Ratio	0.75
β_o', Initial Discharge Angle, °	90.0
E, Entrainment Coefficient	0.25
C_D, Drag Coefficient	0.5
C_D', Reduced Drag Coefficient	0.5
T_o, Initial Temperature Rise, °F	15.0
Ri_o, Initial Richardson Number	>1.0

The initial angle of discharge is assumed to be $\beta_o' = 90.0°$. From Figure 18, the length of the zone of flow establishment is estimated to be $s_e'/b_o = 0.75$, using A = 0.75. From Figure 19, the initial angle at the beginning of the zone of established jet flow is estimated to be $\beta_o = 34.2°$, using A = 0.75 and $\beta_o' = 90.0°$.

Values of the entrainment and drag coefficients are chosen based on the laboratory and the limited field results of the present study. The entrainment coefficient is assumed to be E = 0.25, since the discharge width is one-tenth as large as the ambient width, while the drag coefficient is assumed to be $C_D = 0.5$, based upon the field results shown in Figures 44 and 45. The value of the reduced drag coefficient is found to be $C_D' = 0.5$ from Equation 39,

$$C_D' = C_D/4E \tag{39}$$

A numerical solution for T/T_o and b/b_o vs. S and for X and Y can be computed, using the values of A = 0.75, $\beta_o = 34.2°$, and $C_D' = 0.5$.

Using the values $s_e'/b_o = 0.75$ and E = 0.25, the value of S_e' is found to be equal to 0.2 from Equation 67,

$$S_e' = (2E/\sqrt{\pi}\, b_o)\, s_e' \tag{67}$$

The values of T/T_o and b/b_o are then referenced to the discharge in terms of S', using the value of S_e' and Equation 68,

$$S' = S_e' + S \tag{68}$$

Using the value of E = 0.25 and solving Equation 69 for s'/b_o,

$$s'/b_o = (\sqrt{\pi}\ S'/2E) \tag{69}$$

then, the predicted values of T/T_o and b/b_o vs. s'/b_o can be plotted as shown in Figure 74.

Using the value of $E = 0.25$ and solving Equation 42 for x/b_o and y/b_o,

$$x/b_o = (\sqrt{\pi}\ X/2E) \quad ; \quad y/b_o = (\sqrt{\pi}\ Y/2E) \tag{42}$$

then, the predicted location of the trajectory can be plotted as shown in Figure 75. The width of the surface jet in terms of b/b_o is also shown in Figure 75. It is assumed that $x'/b_o = x/b_o$, and $y'/b_o = y/b_o$, since the values of x'_e/b_o and y'_e/b_o were considered to be negligible when compared to the values of x/b_o and y/b_o in the field cases of the present study.

The application of the model depends on the magnitude of the initial Richardson Number, accurate prediction of the initial jet depth, and the intensity of the ambient turbulence.

Assuming a 15°F initial temperature rise from 70°F to 85°F, the initial Richardson Number is found to be greater than 1.0, using the values $\Delta\rho/\rho = 2.6 \times 10^{-3}$, $U_o = 1.3$ ft/sec, $U_a = 0.98$ ft/sec, and $z_o = 10.0$ feet. Thus, the two-dimensional model should be applicable, since the value of the Ri_o Number > 1.0 indicates a lack of vertical mixing.

Since the initial jet velocity is calculated from the value of the initial jet depth, accurate prediction of the depth is necessary before the proposed model can be used. At present, this depth is

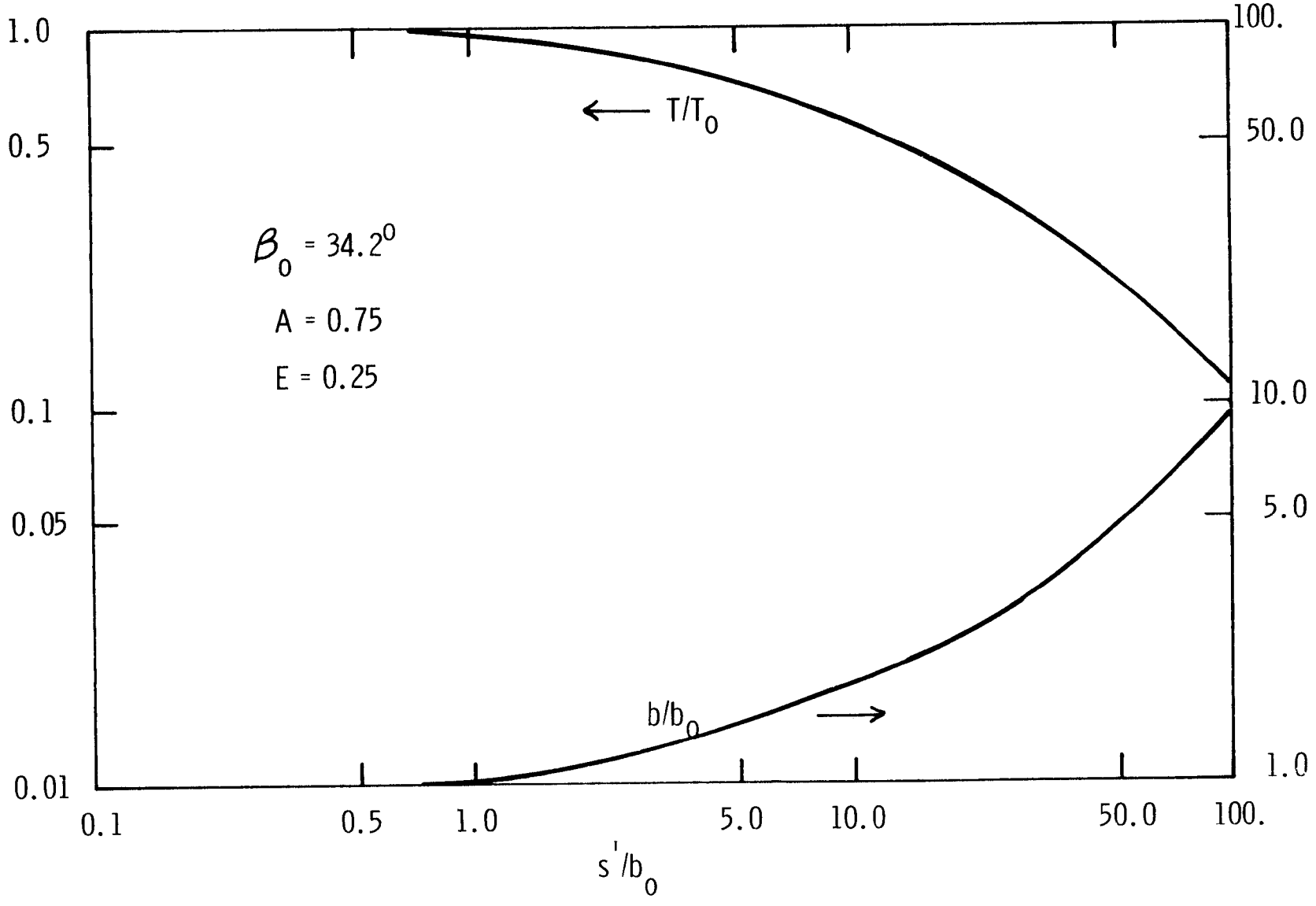

FIGURE 74.-- PREDICTED VALUES OF TEMPERATURE AND WIDTH

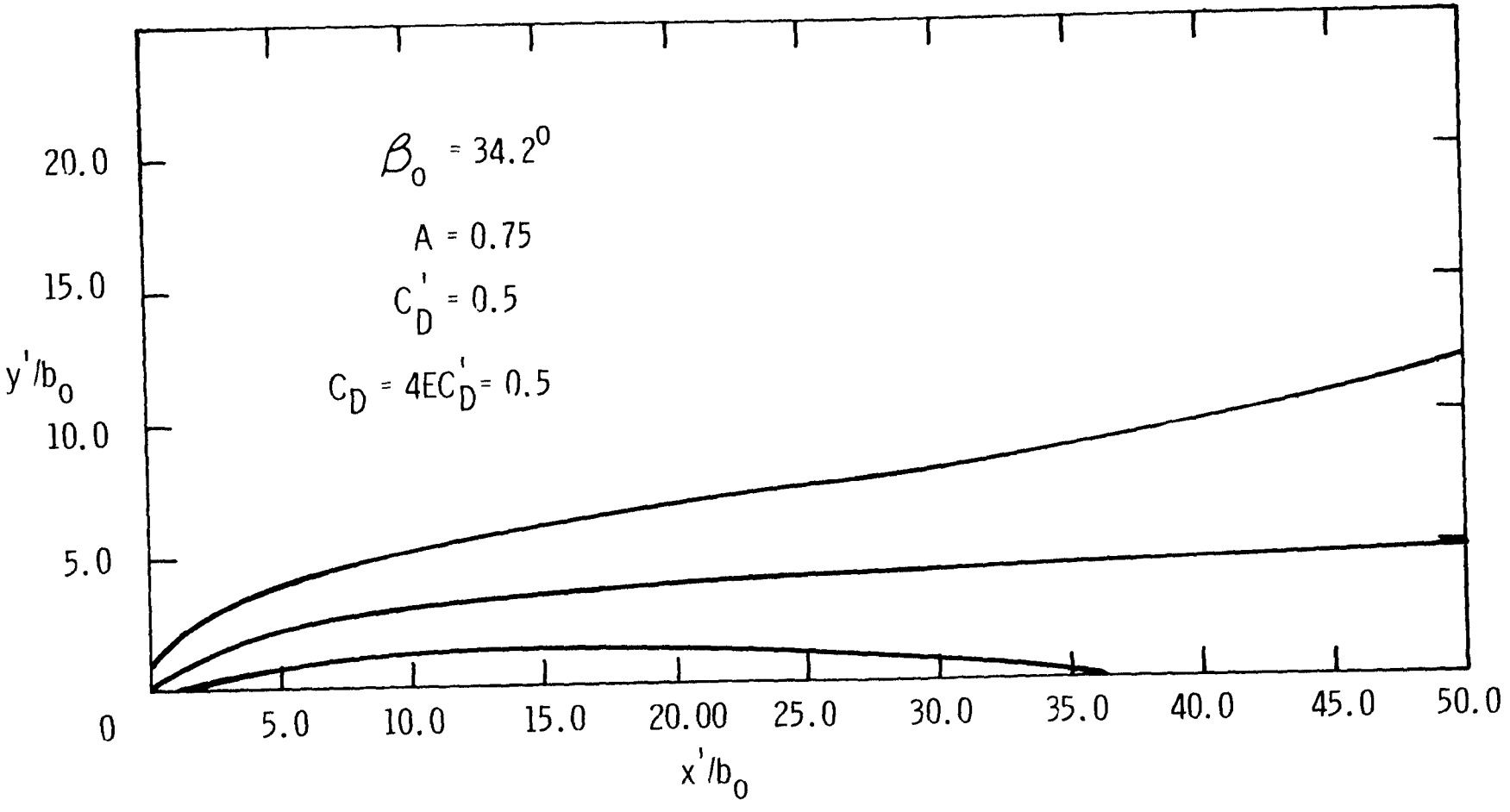

FIGURE 75.-- PREDICTED TRAJECTORY AND WIDTH

difficult to predict, particularly at field sites where a cold water wedge would be expected to intrude into the discharge channel. Harleman's work (26) could be used as a guide, but more research must be done concerning those field sites where the conditions necessary to apply Harleman's two-layer stratified flow theory are not met.

In some cases, ambient turbulence can be expected to cause a greater decrease in the temperature rise than the two-dimensional jet model predicts. Vertical mixing due to ambient turbulence was noted at some of the field sites in the present study. The effects of ambient turbulence must be studied further before they can be quantitatively included in the surface jet model.

APPENDIX E

LIST OF SYMBOLS

a - Subscript pertaining to ambient fluid

A - Ratio of the ambient velocity to the initial jet velocity, U_a/U_o, $M^\circ L^\circ T^\circ$

b - Half-width of jet, L

C - Circumference through which entrainment takes place, L

C_D - Drag coefficient, $M^\circ L^\circ T^\circ$

C'_D - Reduced drag coefficient, $M^\circ L^\circ T^\circ$

dA - Differential area of jet cross-section, L^2

d'_o - Initial jet diameter, L

e - Subscript pertaining to establishment zone

E - Entrainment coefficient, $M^\circ L^\circ T^\circ$

exp - Exponential function

F_D - Drag term, L^3T^{-2}

Fr - Froude Number, $M^\circ L^\circ T^\circ$

g - Acceleration of gravity, LT^{-2}

M - Non-dimensional momentum flux

o - Subscript denoting initial values

O - Origin of the coordinate system (x,y), beginning of zone of established flow

O' - Origin of the coordinate system (x',y'), point of jet discharge

Q - Flowrate, L^3T^{-1}

r - Subscript pertaining to river flow

Re - Reynolds Number, $M^\circ L^\circ T^\circ$

APPENDIX E--Continued

Ri - Richardson Number, $M^{\circ}L^{\circ}T^{\circ}$

s - Coordinate axis of jet referenced to beginning of zone of established flow, L

s' - Coordinate axis of jet referenced to point of jet discharge, L

s'_e - Length of zone of flow establishment, L

S - Non-dimensional distance along jet axis referenced to beginning of zone of established flow

S' - Non-dimensional distance along axis referenced to point of jet discharge

S'_e - Non-dimensional length of zone of flow establishment

T - Centerline temperature rise, °F

T' - Temperature rise at any point in the jet cross-section, °F

u - Velocity along the jet axis, LT^{-1}

U - Centerline jet velocity, LT^{-1}

U_a - Ambient velocity, LT^{-1}

U_o - Initial jet velocity, LT^{-2}

V - Non-dimensional volume flux

v_i - Inflow velocity, LT^{-1}

x - Longitudinal axis referenced to beginning of zone of established flow, L

x' - Longitudinal axis referenced to point of discharge, L

x'_e - Longitudinal length of establishment zone, L

X - Non-dimensional longitudinal axis referenced to beginning of zone of established flow

X' - Non-dimensional longitudinal axis referenced to point of discharge

X'_e - Non-dimensional longitudinal length of establishment zone

APPENDIX E--Continued

y - Lateral axis referenced to beginning of zone of established flow, L

y' - Lateral axis referenced to point of discharge, L

y'_e - Lateral length of establishment zone, L

Y - Non-dimensional lateral axis referenced to beginning of zone of established flow

Y' - Non-dimensional lateral axis referenced to point of discharge

Y'_e - Non-dimensional lateral length of establishment zone

z - Depth of jet, L, subscript pertaining to vertical coordinate

β - Angle between jet and ambient current, degrees

η - Distance along axis perpendicular to s axis, L

ν - Kinematic viscosity, L^2T^{-1}

ρ - Density, FT^2L^{-4}

σ - Standard deviation, L

LIST OF REFERENCES

1. Abraham, G., "Horizontal Jets in Stagnant Fluid of Other Density," Journal of the Hydraulics Division, Am. Soc. of Civil Eng., Vol. 91, No. HY4, Proc. Paper 4411, July, 1965, pp. 139-154.

2. Abramovich, G. N., The Theory of Turbulent Jets, M.I.T. Press, Cambridge, Mass., 1963.

3. Ackers, P., "Modeling of Heated-Water Discharges," Engineering Aspects of Thermal Pollution, edited by F. L. Parker and P. A. Krenkel, Vanderbilt Univ. Press, Nashville, Tenn., 1969, pp. 172-212.

4. Albertson, M. L., Dai, Y. B., Jensen, R. A., and Rouse, H., "Diffusion of Submerged Jets," Transactions, Am. Soc. of Civil Eng., Vol. 115, 1950, pp. 639-697.

5. Bata, G. L., "Recirculation of Cooling Water in Rivers and Canals," Journal of the Hydraulics Division, Am. Soc. of Civil Eng., Vol. 93, No. HY3, Proc. Paper 1265, June, 1967.

6. Beer, L. P., and Pipes, W. O., "Environmental Effects of Condenser Water Discharge in Southwest Lake Michigan," Consulting Engineering Report, Environmental Sciences Industrial Bio-Test Laboratory, Inc., 106 pp.

7. Bosanquet, C. H., Horn, G., and Thring, M. W., "The Effect of Density Differences on the Paths of Jets," Proceedings, Royal Soc. of London, Vol. 263A, No. 263, September, 1961, pp. 340-352.

8. Briggs, G. A., "Plume Rise," Air Resources Atmospheric Turbulence and Diffusion Laboratory, Environmental Science Services Administration, Oak Ridge, Tenn., September, 1969, 81 pp.

9. Brooks, N. H., Discussion of "Mechanics of Condenser-Water Discharge from Thermal-Power Plants, " by D. R. F. Harleman, Engineering Aspects of Thermal Pollution, edited by F. L. Parker and P. A. Krenkel, Vanderbilt Univ. Press, Nashville, Tenn., 1969, pp. 165-172.

10. Burdick, J. C. III, and Krenkel, P. A., "Jet Diffusion Under Stratified Flow Conditions," Tech. Report No. 11, Sanitary and Water Resources Engineering, Vanderbilt Univ., Nashville, Tenn., 1967, 100 pp.

11. Cairns, John, Jr., "Effects of Heat on Fish," Industrial Wastes, Vol. 1, No. 5, May-June, 1956, pp. 180-183.

12. Carter, H. H., "A Preliminary Report on the Characteristics of a Heated Jet Discharged Horizontally into a Transverse Current, Part I - Constant Depth," Tech. Report No. 61, Chesapeake Bay Institute, The Johns Hopkins Univ., Baltimore, Md.; November, 1969, 38 pp.

13. Cederwall, K., "Jet Diffusion: Review of Model Testing and Comparison with Theory," Hydraulics Division, Chalmers Institute of Technology, Goteborg, Sweden, February, 1967, 28 pp.

14. Churchill, M. A., "Effects of Density Currents in Reservoirs on Water Quality," Water and Sewage Works, Reference No. 1965, November, 1965.

15. Clark, J. R., "Thermal Pollution and Aquatic Life," Scientific American, Vol. 220, No. 3, March, 1969, pp. 19-26.

16. Csanady, G. T., "The Buoyant Motion Within a Hot Gas Plume in a Horizontal Wind," Journal of Fluid Mechanics, Vol. 22, 1965, pp. 225-239.

17. Edinger, J. E., Discussion of "The Cooling of Riverside Thermal-Power Plants," by Andre Goubet, Engineering Aspects of Thermal Pollution, edited by F. L. Parker and P. A. Krenkel, Vanderbilt Univ. Press, Nashville, Tenn., 1969, pp. 124-132.

18. Edinger, J. E., Duttweiler, D. W., and Geyer, J. C., "The Response of Water Temperature to Meteorological Conditions," Water Resources Research, Vol. 4, No. 5, October, 1968, pp. 1137-1143.

19. Edinger, J. E., and Geyer, J. C., "Heat Exchange in the Environment," Publication 65-902, Edison Electric Institute, New York, N. Y., June, 1965.

20. Edinger, J. E., and Polk, E. M., Jr., "Initial Mixing of Thermal Discharge into a Uniform Current," Report No. 1, National Center for Research and Training in the Hydrologic and Hydraulic Aspects of Water Pollution Control, Vanderbilt Univ., Nashville, Tenn., October, 1969, 45 pp.

21. Ellison, T. H., and Turner, J. S., "Turbulent Entrainment in Stratified Flows," Journal of Fluid Mechanics, Vol. 6, 1959, pp. 423-448.

22. Fan, Loh-Nien, "Turbulent Buoyant Jets into Stratified or Flowing Ambient Fluids," Tech. Report No. KH-R-15, W. M. Keck Lab. of Hydraulics and Water Resources, California Inst. of Tech., Pasadena, Calif., June, 1967, 196 pp.

23. Federal Water Pollution Control Administration, "Industrial Waste Guide on Thermal Pollution," Pacific Northwest Water Laboratory, Corvallis, Ore., September, 1968, 112 pp.

24. Fietz, T. R., and Wood, I. R., "Three-Dimensional Density Current," Journal of the Hydraulics Division, Am. Soc. of Civil Eng., Vol. 93, No. HY6, Proc. Paper 5549, November, 1967, pp. 1-23.

25. Gordier, R. L., "Studies on Fluid Jets Discharging Normally into Moving Fluid," Tech. Paper No. 28, Series B, St. Anthony Falls Hydraulic Laboratory, Univ. of Minnesota, Minneapolis, Minn., August, 1959, 48 pp.

26. Harleman, D. R. F., "Mechanics of Condenser-Water Discharge from Thermal-Power Plants," Engineering Aspects of Thermal Pollution, edited by F. L. Parker and P. A. Krenkel, Vanderbilt Univ. Press, Nashville, Tenn., 1969, pp. 144-164.

27. Harlemann, D. R. F., and Elder, R. A., "Withdrawal from Two-Layer Stratified Flows," Journal of the Hydraulics Division, Am. Soc. of Civil Eng., Vol. 91, No. HY4, Proc. Paper 4398, July, 1965, pp. 43-58.

28. Hayashi, T., and Shuto, N., "Diffusion of Warm Water Jets Discharged Horizontally at the Water Surface," Proceedings, Twelfth Congress of the International Association for Hydraulic Research, Colorado State University, Ft. Collins, Colo., 1967, pp. 47-59.

29. Jen, Y., Wiegel, R. L., and Mobarek, I., "Surface Discharge of Horizontal Warm Water Jets," Tech. Report HEL 3-3, Hydraulic Engineering Laboratory, Institute of Engineering Research, Univ. of Calif., Berkeley, Calif., December, 1964, 44 pp.

30. Keffer, J. F., and Baines, W. D., "The Round Turbulent Jet in a Cross-Wind," Journal of Fluid Mechanics, Vol. 15, 1963, pp. 481-496.

31. Krenkel, P. A., and Parker, F. L., "Thermal Pollution: Status of the Art," Report No. 3, National Center for Research and Training in the Hydrologic and Hydraulic Aspects of Water Pollution Control, Vanderbilt Univ., Nashville, Tenn., December, 1969.

32. Krenkel, P. A., Thackston, E. L., and Parker, F. L., "Impoundment and Temperature Effect on Waste Assimilation," Journal of the Sanitary Engineering Division, Am. Soc. of Civil Eng., Vol. 95, No. SA1, Proc. Paper 6406, February, 1969, pp. 37-64.

33. Morton, B. R., "On a Momentum-Mass Flux Diagram for Turbulent Jets, Plumes, and Wakes," Journal of Fluid Mechanics, Vol. 10, 1961, pp. 101-112.

34. Morton, B. R., Taylor, G. I., and Turner, J. S., "Turbulent Gravitational Convection from Maintained and Instantaneous Sources," Proceedings, Royal Soc. of London, Vol. 234A, No. 1196, January, 1956, pp. 1-23.

35. Prandtl, L., and Tietjens, O. G., Applied Hydro- and Aeromechanics, Dover Publications, New York, N. Y., 1957, 311 pp.

36. Pratte, B. D., and Baines, W. D., "Profiles of the Round Turbulent Jet in a Cross Flow," Journal of the Hydraulics Division, Am. Soc. of Civil Eng., Vol. 93, No. HY6, Proc. Paper 5556, November, 1967, pp. 53-64.

37. Polk, E. M., Jr., Unpublished Data, National Center for Research and Training in the Hydrologic and Hydraulic Aspects of Water Pollution Control, Vanderbilt Univ., Nashville, Tenn.

38. Rouse, H., editor, Advanced Mechanics of Fluids, John Wiley and Sons, Inc., New York, N. Y., 1965, 444 pp.

39. Rouse, H., Yih, C. S., and Humphreys, H. W., "Gravitational Convection from a Boundary Source," Tellus, Vol. 4, 1952, pp. 201-210.

40. Samai, S., "Space Correlations in Round Turbulent Jet," Journal of the Hydraulics Division, Am. Soc. of Civil Eng., Vol. 95, No. HY3, Proc. Paper 6565, May, 1969, pp. 907-917.

41. Schlichting, H., Boundary-Layer Theory, translated by J. Kestin, 6th edition, McGraw-Hill, Inc., New York, N. Y., 747 pp.

42. Stafan, H., "Modeling Spread of Heated Water over Lake," Journal of the Power Division, Am. Soc. of Civil Eng., Vol. 96, No. PO3, Proc. Paper 7375, June, 1970, pp. 469-482.

43. Tamai, N., Wiegel, R. L., and Tornberg, G. F., "Horizontal Surface Discharge of Warm Water Jets," Journal of the Power Division, Am. Soc. of Civil Eng., Vol. 95, No. PO2, Proc. Paper 6847, October, 1969, pp. 258-276.

44. Taylor, G. I., "Dynamics of a Mass of Hot Gas Rising in Air," U. S. Atomic Energy Commission, MDDC 919, LADC 276, 1945.

45. Tennessee Valley Authority, "Temperature Survey on the Tennessee River in the Vicinity of TVA Widows Creek Steam Plant, August 30-31, 1967," Division of Health and Safety, Water Quality Branch, Chattanooga, Tenn.

46. Wiegel, R. L., Mobarek, I., and Jen, Y., "Discharge of Warm Water Jet Over Sloping Bottom," Tech. Report HEL 3-4, Hydraulic Engineering Laboratory, Institute of Engineering Research, Univ. of Calif., Berkeley, Calif., November, 1964, 60 pp.

47. Yevjevich, V. M., "Diffusion of Slot Jets with Finite Orifice Length-Width Ratios," Hydraulics Papers, No. 2, Colorado State Univ., Ft. Collins, Colo., March 1966, 40 pp.

48. Zeller, R. W., "Cooling Water Discharges into Lake Monona," Ph.D. Thesis, University of Wisconsin, May, 1967, 287 pp.

1 Accession Number	2 Subject Field & Group	SELECTED WATER RESOURCES ABSTRACTS INPUT TRANSACTION FORM
W	05D, 02E	

5 Organization

Department of Environmental and Water Resources Engineering, Vanderbilt University, School of Engineering, Nashville, Tennessee

6 Title

HEATED SURFACE JET DISCHARGED INTO A FLOWING AMBIENT STREAM

10 Author(s)

Motz, Louis H.

Benedict, Barry A.

16 Project Designation

FWQA Contract No. 16130FDQ

21 Note

22 Citation

Federal Water Quality Administration Water Pollution Control Research Series, Office of Research and Development, Report based on Contract No. 16130 FDQ, March,1971

23 Descriptors (Starred First)

*Cooling Water, *Thermal Pollution, *Jets, *Turbulent flow, *Heated water *Thermal power plants, Thermal stratification, Diffusion, Water temperature, Heat exchange, Temperature

25 Identifiers (Starred First)

*Heat discharge, Density differences, Buoyant Jets, Ambient Fluids, Temperature profiles, Widows Creek, New Johnsonville, Waukegan Surveys

27 Abstract

The temperature distribution in the water body due to a discharge of waste heat from a thermal-electrical plant, is a function of the hydrodynamic variables of the discharge and the receiving water body. The temperature distribution can be described in terms of a surface jet discharging at some initial angle to the ambient flow and being deflected downstream by the momentum of the ambient velocity. It is assumed that in the vicinity of the surface jet, heat loss to the atmosphere is negligible. It is concluded that the application of the two dimensional surface jet model is dependent on the velocity ratio and the initial angle of discharge, and the value of the initial Richardson number, as low as 0.22. Both laboratory and field data are used for verification of the model which has been developed. Laboratory data is used to evaluate the two needed coefficients, a drag coefficient and an entrainment coefficient, as well as the length of the zone of flow establishment and the angle at the end of that zone.

Abstractor	Institution

WR:102 (REV. JULY 1969) WRSIC

SEND, WITH COPY OF DOCUMENT, TO: WATER RESOURCES SCIENTIFIC INFORMATION CENTER U.S. DEPARTMENT OF THE INTERIOR WASHINGTON, D. C. 20240

*U.S. GOVERNMENT PRINTING OFFICE: 1972- 484-482/29 1-3